The Liquid Phase Hydrogenation of Nitrobenzene over Supported Copper Catalysts

by

David Scott Anderson

A Thesis Presented to

the University of Glasgow

for the Degree of

Doctor of Philosophy

December 1999

ProQuest LLC.
789 East Eisenhower Parkway
P.O. Box 1346
Ann Arbor, MI 48106 – 1346

To those who were concerned...

Summary

A series of silica-supported copper catalysts have been prepared, characterised and used for the hydrogenation of nitrobenzene. The catalysts were prepared using a wet impregnation technique, with three different metal salts (copper nitrate, copper acetate and copper carbonate) deposited onto two different forms of silica (Cab-O-Sil and C-10), with nominal metal loadings of approximately 10 wt%. Although different pretreatments were applied to produce derivatives of the catalyst precursors, the four principal substrates used are referred to as Cu(N)/Cab, Cu(A)/Cab, Cu(C)/Cab and Cu(N)/C-10.

The catalysts have been the subject of numerous characterisation techniques including atomic absorption spectroscopy, BET surface area determination, thermal gravimetric analysis, temperature programmed reduction and nitrous oxide decomposition; with the latter technique used to measure the metal surface areas of the active catalysts. Selected samples were also analysed using differential scanning calorimetry, variable temperature x-ray diffraction and electron microscopy.

The characterisation experiments provided insight into the nature of the catalysts. The choice of metal salt used in the preparation, rather than the choice of support material, was found to be the major factor affecting catalyst performance. The activation procedure applied to the catalysts was optimised with respect to metal surface area.

The apparatus and experimental protocol for liquid phase nitrobenzene hydrogenation over copper/silica catalysts was developed. A batch slurry reactor was found to be preferable over a bubble-phase vessel. Catalyst activation was conducted

in situ, whilst the design allowed control over a range of variables, *e.g.* mass of catalyst, concentration of reactant, reaction temperature, *etc.* The choice of solvent for the reaction was not trivial, and the suitability of various solvents was assessed.

The use of an alcohol solvent led to the formation of unwanted by-products, arising via an alkylation reaction which occurred between the hydrogenation product, aniline, and the solvent itself, hexan-1-ol. A preliminary investigation of this side reaction was conducted, revealing the sequential formation of N-hexylenebenzenamine and N-hexylaniline. It is believed that the alkylation reaction occurs on the silica support, whilst the hydrogenation step occurs on the metal crystallites; in the presence of nitrobenzene the hydrogenation of the nitro group is favoured over that of N-hexylenebenzenamine.

During the assessment of *t*-butyl benzene as a solvent it was found that its history bore marked effect on catalyst activity. It was established that the presence of sulphur within different batches of *t*-butyl benzene was responsible for an observed enhancement of catalyst performance. The overall concentration of sulphur within the solvent samples was determined, and it was found that five different sulphur species were present. A conclusive assignment of their identities, however, did not prove possible.

Dodecane, ethyl benzene and mesitylene were also found to be unsuitable as solvents for this reaction. *n*-Butyl benzene was ultimately adopted as the reaction medium. Comprehensive testing with *n*-butyl benzene did reveal the existence of two minor reactions involving this solvent, but these were not found to affect the major reaction.

The optimised technique, 'benchmarked' against a platinum/silica catalyst, allowed the behaviour of the different copper catalysts to be evaluated with reproducible results. The Cu(N)/Cab catalyst had the greatest activity and the highest metal surface area, which was attributed to the combination of the copper nitrate salt and powdered Cab-O-Sil support used in its preparation. No by-products were observed from the reaction of nitrobenzene; all of the copper catalysts showed complete selectivity to aniline. Following complete consumption of the nitrobenzene, however, it was apparent that the concentration of aniline in solution decreased through time. This was attributed to hydrogenolysis of the aniline product, with the consequent formation of ammonia and a phenyl species. It was believed that whilst the phenyl species (benzene) was not detected in solution, it was still present on the catalyst surface, and that this 'coke precursor' led to the formation of a carbonaceous overlayer. Lifetime measurements revealed substantial deactivation of the catalyst with time. This is attributed to the formation of a polyaromatic layer on the catalyst surface, which formed as a result of aniline hydrogenolysis in the absence of nitrobenzene.

Further aspects of the reaction chemistry of nitrobenzene hydrogenation were explored, such as the effects of catalyst loading, nitrobenzene and aniline concentrations and temperature upon the rates of reaction. Varying the mass of catalyst confirmed that the reaction was not diffusion limited under the conditions studied. Examination of rate of reaction as a function of temperature revealed an activation energy for nitrobenzene hydrogenation of 57.1 ± 10.5 kJ mol^{-1}.

The hydrogenation of nitrosobenzene was conducted, this being the proposed primary intermediate in nitrobenzene hydrogenation. Little formation of aniline was observed, however, whilst these experiments showed a considerable negative carbon mass balance, *i.e.* the disappearance of the nitrosobenzene from solution far exceeded the observed concentration of aniline. It was therefore concluded that the nitrosobenzene was adsorbed on the catalyst surface to such a degree as to block the catalytic sites, thereby inhibiting the rate of reaction.

The reaction was found to be zero order with respect to nitrobenzene concentration. The presence of aniline was shown to marginally inhibit the rate of nitrobenzene hydrogenation, with a fractional reaction order of -0.3. The rate of reaction increased linearly with the surface area of active copper metal, and it is widely accepted that the reaction is first order in dihydrogen.

A nickel/silica catalyst, representative of that used industrially, was also tested for its behaviour towards nitrobenzene hydrogenation, after a procedure for its activation was determined. This substrate displayed remarkable activity in comparison with the copper catalysts.

Finally, a fluidised bed technique was developed, for use during the calcination step of catalyst pretreatment. Samples of the Cu(A)/Cab catalyst prepared using this technique were compared with those obtained via the conventional fixed bed approach. An exotherm, resulting in a temperature jump of 86 °C, was detected during the calcination as a fixed bed, which was not observed during the fluidised bed experiments. Variable temperature x-ray diffraction analyses confirmed that the exotherm arose from

the combustion of copper acetate. Nitrous oxide decomposition experiments revealed that the fluidised bed technique provided a means to improve the ultimate metal surface area of the catalyst, and reaction testing of the different samples showed that this related to improved catalyst activity. The beneficial effect of the fluidised bed method was ascribed to its ability to dissipate the heat output during the calcination stage.

In conclusion, a system was developed for the hydrogenation of nitrobenzene in the liquid phase, which was suitable for the 'screening' of supported copper catalysts. A range of copper catalysts were prepared, and their catalytic behaviour related to the information gained by catalyst characterisation. These catalysts showed modest activity, but with complete selectivity to aniline. A comparison of their performance was then obtained in relation to a nickel/silica catalyst. Furthermore, a fluidised bed calcination technique was developed, and found to provide a means of maintaining catalyst dispersion, with a corresponding improvement in catalyst activity towards nitrobenzene hydrogenation.

ACKNOWLEDGEMENTS

Sincere gratitude is extended to Prof. G. Webb, Dr. S. D. Jackson and Dr. D. Lennon for their guidance, support and faith throughout the course of this project. In particular I would like to thank Dr. Lennon, without whose continual encouragement this work would not have been completed.

Staff at ICI Synetix (formerly ICI Katalco), particularly Dr. N. Young and Dr. G. Kelly, are thanked for assisting with sulphur analysis and BET surface area determination. Thanks are also given to ICI Synetix and EPSRC for funding through the Industrial CASE scheme.

I am indebted to many members of the Chemistry Department's academic and technical staff. I would especially like to thank Dr. John Cole for his patient advice with numerous gas chromatography queries, Dr. David McComb and Jim Gallagher for their help with the electron microscopy and Vicki Thompson for her help with the thermal analysis. Shaun Seebaluck and Andrew Monaghan are thanked for testing the reproducibility of the reaction technique.

I should also thank individually the colleagues that I have enjoyed working with over the past four years, as well as friends, family (esp. Peter) and Antje for their support, but I'm not going to. In this time there have been so many who have helped in one way or another, that I'd end up parodying an 'Oscar' acceptance speech (featuring a cast of thousands). Suffice to say, some of you have touched me deeply, and on the whole, it's been a pleasure!

Summary

Acknowledgements

CONTENTS

Chapter One

Introduction

This chapter provides a brief review of topics pertinent to the project in general. More detailed discussion of the literature is dispersed through the experimental, treatment and results & discussion chapters where appropriate.

1.1 GENERAL INTRODUCTION

1.1.1 Catalysis

The study of catalysis has provided interest and intrigue to researchers for almost two centuries. Its application was founded by Dobereiner in 1823 with the platinum-catalysed reaction between hydrogen and oxygen [1]. This early work was continued by Kirchoff, Davy, Henry, Philips, Faraday and Berzelius [2], and by 1835 the existence of heterogeneous catalysis was established. Indeed, it was Jakob Berzelius who first used the term "catalysis" to describe certain chemical reactions in 1836, defining the power of the catalyst as being that which is able to "awake the affinities, which are asleep at this temperature, by their mere presence and not by their own affinity."

As subsequent studies increased the knowledge and understanding of the field of catalysis this interpretation evolved, but as different approaches to catalysis have developed from various viewpoints, a precise, universally-accepted definition remains elusive. The definition adopted by C. N. Satterfield [3a] is: *A catalyst is a substance that increases the rate of reaction toward equilibrium without being appreciably consumed in the process.*

The importance of catalysis in the modern chemical industry is unquestionable. Most industrial reactions are of a catalytic nature, with catalysts being employed at some

stage in the manufacture of a large percentage of all chemical goods, and the value of goods produced by the United States' chemical industries, for example, exceeds the gross national products of all but a few countries in the world [4]. The application of catalysis is vast, including the petrochemical, pharmaceutical, heavy and fine chemical industries, predominantly utilising heterogeneous catalysts.

1.1.2 Hydrogenation reactions

The addition of hydrogen to a molecule, known as hydrogenation, is of inestimable importance in chemistry. Functional groups can be reduced, and often with good selectivity. Both homogeneous and heterogeneous processes can be applied, but the latter is favoured as the reaction product(s) are more easily separated from the solid catalyst [5].

Industrially, catalytic hydrogenation processes primarily use nickel or palladium catalysts [6a], although other metals such as platinum, zinc and copper are also employed. These catalysts can be employed in various physical forms such as wires, gauzes or finely divided metal powders, but are most commonly prepared when supported on a high surface area oxide.

The three most important factors affecting the choice of catalyst are *activity, selectivity* and *lifetime* [7a]. The activity is the rate at which the catalyst can convert the reactant to product(s), whilst the selectivity reflects the ability of the catalyst to form the desired product. Lifetime is the time period for which the catalyst maintains an acceptable level of activity and/or selectivity. The cost of catalyst manufacture and any associated

toxicity hazards must also be considered. These factors predominantly govern catalyst selection for an industrial process; the ultimate choice is usually made in economic terms.

1.1.3 Copper catalysts

Copper-based catalysts are used in a wide variety of high added value low volume processes, as well as large scale processes such as the water gas shift reaction and methanol synthesis [8, 9, 10]. Copper catalysts have become the catalyst of choice for certain hydrogenation reactions, where high selectivities are of primary importance. This includes the hydrogenation of unsaturated carbonyl compounds which has been studied over copper-chromite catalysts [11, 12], indicating that copper preferentially hydrogenates the carbonyl group [11], in contrast to platinum-based catalysts which favour the hydrogenation of the unsaturated carbon bonds [13].

One of the disadvantages of copper-based catalysts, however, is the tendency of the metal particles to agglomerate, which results in a decrease in the available metal surface area with a corresponding decrease in catalytic activity. The onset of significant surface mobility, the Hüttig temperature, is approximately one third of the metal's melting point in Kelvin. The low boiling point of copper (1083 °C) therefore gives a much lower Hüttig temperature (179 °C) than that experienced by other common metals used as catalysts (*e.g.* nickel 302 °C, palladium 335 °C, platinum 409 °C). In practice it is therefore recommended that copper-based catalysts are kept below 260 °C during reduction, although subsequent reaction temperatures may be higher [7b].

1.2 NITROBENZENE HYDROGENATION

1.2.1 General

The hydrogenation of nitrobenzene to aniline is expressed by Equation 1.1.

$$C_6H_5NO_2 + 3\,H_2 \rightarrow C_6H_5NH_2 + 2\,H_2O \qquad \text{Equation 1.1}$$

The reaction is highly exothermic, and in the liquid phase $\Delta H_f°$ is approximately -550 kJ mol^{-1}. Dean gathered data on the $\Delta G_f°$ of the reaction from which it is possible to estimate the value of the equilibrium constant of the reaction at 1.53×10^{84} at 298 K [14]. In effect, the reduction of nitrobenzene to aniline is irreversible for all practical purposes.

The proposed mechanism of the reaction has changed little since the work of Haber in 1898 [15], as shown by Figure 1.1. However, despite extensive research on nitrobenzene hydrogenation, a mechanism which conforms with experimental results has yet to be devised. It is probable that the true mechanism is more complex, and should consider the phenomena at the surface of the catalyst [16].

Nitrobenzene reduction to aniline using a homogeneous transition metal catalyst has been studied since the work of l'Eplattenier *et al* using $[Ru_3(CO)_{12}]$ [17]. Indeed, this reaction is now used as a means of evaluating new homogeneous catalysts [18-20].

The use of nitrobenzene hydrogenation as a test reaction is repeated for heterogeneous systems. In this way the activity and selectivity of hydrogenation catalysts, such as platinum [21, 22] and palladium [23], have been assessed. The reaction has also been employed to assess novel reactor designs [24, 25], and indeed, under the assumption

that the reaction is structure insensitive, the gas phase hydrogenation of nitrobenzene has even been used as an indirect measure of catalyst dispersion [26].

Figure 1.1

Mechanism of nitrobenzene hydrogenation

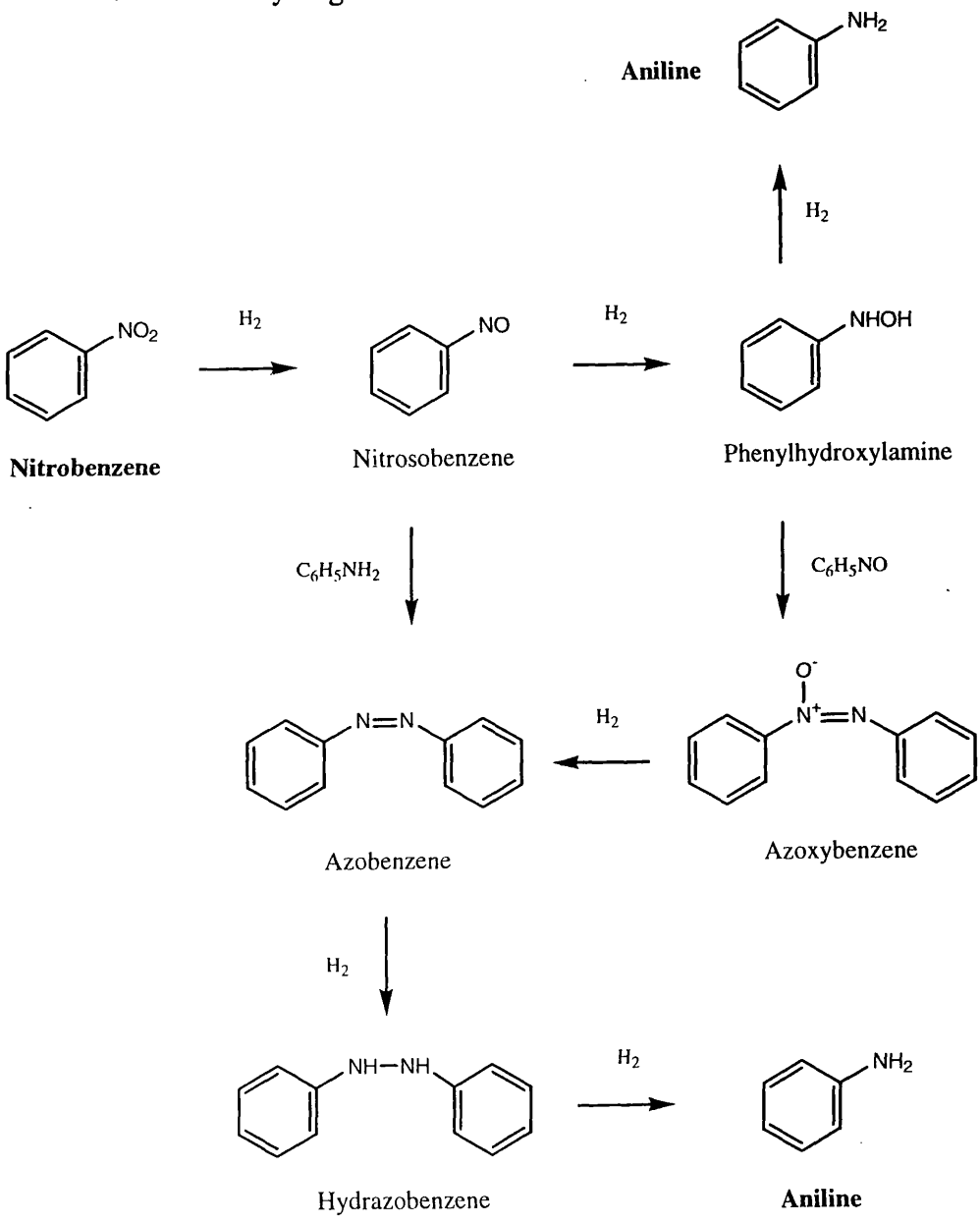

1.2.2 Nitrobenzene hydrogenation - gas and liquid phase

The reduction of nitrobenzene to aniline has been studied in the gas and liquid phases over a variety of catalysts. In the vapour phase attention has focussed on the use of copper catalysts [27-31], whilst nickel [16, 32-35], platinum [21, 24, 36-38] and palladium [39-42] have been used in the liquid phase. The reaction is accepted as being zero order in nitrobenzene [16, 21, 32, 33, 35-37, 39, 41-45] and first order in dihydrogen [16, 24, 33, 35, 37, 41, 42, 45] in both gas and liquid systems.

The use of nickel catalysts has resulted in the formation of nitrosobenzene [34], phenylhydroxylamine [34], azoxybenzene [16, 33-35] and azobenzene [16, 33, 34]. Similarly, nitrosobenzene [38], phenylhydroxylamine [36, 38, 46] and azoxybenzene [36] have been observed as by-products of nitrobenzene hydrogenation over platinum catalysts.

In gas phase studies using iron-substituted $CuCr_2O_4$ catalysts it was found that monovalent copper was more active than metallic copper for nitrobenzene hydrogenation [47, 48]. However, previous attempts to use copper-based catalysts in the liquid phase have been unsuccessful, with Wisniak and Klein observing that 'although copper chromite is unable to hydrogenate nitrobenzene in the liquid phase it will do so in the vapour phase' [16].

The activation energy of the reaction, E_a, has been studied over a variety of catalysts. A range of E_a values have been derived, including 45 kJ mol^{-1} over palladium/alumina [24], 59.0 kJ mol^{-1} over Raney nickel [16] and 69 kJ mol^{-1} over copper and nickel catalysts in the gas phase [30]. With Raney nickel the rate of reaction

was found to increase dramatically from 100 °C, reaching a maximum at 170 °C and decreasing thereafter [16]. This was attributed to a strong influence of temperature upon the adsorption constants of the different components.

In the liquid phase the effect of solvents with different dielectric and thermodynamic properties was studied over platinum/alumina catalysts [49]. It was found that the rate of aniline formation increased in solvents with higher dielectric constants, which indicated that the reduction of nitrobenzene to aniline passes through a transition state with charge separation. This was in agreement with the results of Aramendia *et al* who concluded that dielectric solvents play a role in stabilising the intermediates generated on the catalyst surface [41].

The selection of solvent is clearly important, and on the laboratory scale methanol [33, 50] and ethanol [37, 51, 52] are most commonly employed. Any reaction between the solvent and reactant or product is obviously undesirable, yet alkylation reactions between aniline and alcohols in the presence of a catalyst have been documented since the 1950s [53]. Similar alkylation reactions also occur during dinitrotoluene hydrogenation with Raney nickel catalysts when alcohol solvents are used [54]. The preference for alcohol solvents during nitrobenzene hydrogenation is therefore potentially problematic, although alkylated aniline species are rarely reported in the literature as by-products.

1.2.3 Industrial routes to aniline

As an intermediate to many organic compounds, including isocyanates and hydroquinone, as well as vulcanization accelerators, rubber additives and antioxidants, it is possible to synthesise more than three hundred valuable chemicals from aniline.

Historically, aniline was produced through the Bechamp reduction of nitrobenzene using iron turnings and water in the presence of hydrochloric acid [52]. Although valuable iron oxide pigments could be obtained via this method, the demand for aniline has long reached such levels as to necessitate more efficient methods of manufacture. Detailed information on the industrial synthesis of aniline is held by the companies involved in its production. However, current industrial production utilises several methods, including the ammonolysis of chlorobenzene or phenol, but the predominant route remains the catalytic hydrogenation of nitrobenzene [55]. This is performed in both the vapour and liquid phases.

Gas-phase processes can use fixed or fluidised beds, employing supported copper, cobalt, palladium and nickel catalysts, often in combination [55]. The more active metals require the addition of inhibitors to improve selectivity [52]. Supported copper is the most common choice of catalyst for these gas-phase methods, often with some form of promoter to enhance its activity, such as magnesium, calcium, zirconium, thorium, vanadium or chromium [56, 57]. Reactor conditions range from 270 - 475 °C and 1 - 5 bar. Selectivity to aniline is generally high (up to 99+ %), whilst activity decreases with time [55], and industrial catalysts commonly require regeneration after 10 - 15 days to 3 - 4 months. This is attributed primarily to carbon deposition, the rate of which increases

with increasing nitrobenzene and decreasing hydrogen concentrations. It has been proposed that it is the reaction between nitrobenzene and phenylhydroxylamine, an intermediate, which forms the precursors leading to coke formation [28].

Liquid-phase nitrobenzene hydrogenation methods generally use similar catalysts, or Raney nickel. Surprisingly however, there is a marked absence of publications on the use of copper catalysts in the liquid-phase.

When the reaction is conducted with liquid nitrobenzene heat removal becomes an important factor, owing to the high exothermicity of the reaction (approximately -550 kJ mol^{-1}). A secondary consideration is the volume increase during the conversion of nitrobenzene to aniline (~24 %). These factors, coupled with the fact that nitrobenzene itself can poison some catalysts [42], encourages the use of continuous stirred tank reactors with low concentrations of nitrobenzene operating at high conversion [52]. Mitsui Toatsu, amongst other companies, utilise this heat of reaction by continuously distilling off the aniline product and water, whilst maintaining a low concentration of nitrobenzene [58]. One significant disadvantage of this approach is that the concentration of any high molecular weight by-products will tend to increase through time, with potentially hazardous effects.

1.3 FLUIDISED BEDS

The simplest and most commonly employed method of conducting a heterogeneously catalysed gas phase reaction is to pass the gas mixture over a fixed catalyst bed. Such fixed bed reactors are the standard type of reactor used by the chemical

industry for this type of reaction [59a]. Nevertheless, the operation and optimisation of fixed bed systems is not trivial, and the gas flow, pressure drop and thermal gradients through the catalyst bed must be considered.

A degree of gas flow nonuniformity arises when using nonuniform catalyst pellets, or when the pellets are packed randomly. In certain cases this can lead to reaction runaway [59b]. With regard to the temperature distribution of the catalyst bed, unless the reactor is fitted with a heat transfer medium, heat transfer relies primarily on convection. Thermal gradients, or 'hotspots', which may therefore arise will almost certainly have some effect upon the reaction. Indeed, work by Petrov *et al* has shown that during nitrobenzene hydrogenation as a fixed bed, mass transfer retardation effects leads to thermal oscillations within the catalyst bed [29]. As the temperature rises within the bed the activity of the catalyst increases, but the formation of by-products increases, *i.e.* due to difficulties in mass transfer the selectivity to aniline decreases.

One way to overcome these problems is to employ a 'fluidised' bed technique. At sufficient flow rates, an upward flow of gas passed through an initially stationary bed of catalyst particles leads a state of 'fluidisation'. Advantageous features of such systems as chemical reactors are excellent gas-solid contact in the bed, good gas-particle heat and mass transfer, and high bed-wall and bed-internals heat transfer coefficients [59c]. Fluidised beds are currently applied to specific reactions such as the catalytic cracking of long-chain hydrocarbons [59d] and gas phase polymerisation of ethylene [59e], as well as other gas-solid processes such as cooling-heating, coating and granulation [59c]. With

regard to the treatment of catalysts, fluidised beds have been used to prepare tungsten [60], cobalt [61] and chromium [62] catalysts by controlled and gradual adsorption of the carbonyl-based precursors onto the support material, and to control the conditions required to activate chromium catalysts [63].

The gas flow rate required to achieve fluidisation, or minimum fluidisation point, may be established by measuring the pressure drop across the bed as a function of volume flow rate [59f]. Whereas the pressure drop increases with the flow rate through a fixed bed, the pressure drop through a fluidised bed is effectively constant regardless of the gas throughput. The gas distributor of the reactor must ensure uniform fluidisation over the entire cross-section of the bed, without 'dead spots' where stationary deposits can gather and must not become clogged. In the laboratory scale porous plates of glass, ceramics, *etc.* are used most frequently. In addition, the fluidisation properties can be improved by the use of mechanical equipment *e.g.* agitators, vibrators [59g].

In practice, the catalyst within a fluidised beds will always have a range of particle sizes. Since the solid material essentially behaves as a liquid, particles of greater mass will sink in relation to lighter particles. If the superficial fluid velocity exceeds the free-fall velocity of smaller particles they will be elutriated [64], *i.e.* small particles or 'fines' may be removed from the catalyst bed by the gas flow and 'carried-over'. Such elutriated solids are generally collected by a cyclone.

Whilst fines may be present within the original sample of catalyst, they may be formed as a result of particle attrition. The attrition of solid particles is an unavoidable

consequence of the intense motion of the solids, and may even become the critical economic factor of such processes [59h]. The abrasive forces will also affect the reactor internals themselves.

It should be noted that results observed for fluidised beds at the laboratory scale may not necessarily be reproduced upon scaling up. In general, the scale-up of fluidised bed reactors is a complex process, which requires a large amount of pilot-scale experimentation [59i].

In conclusion, such techniques are not trivial, and fluidised beds are only employed for specific reactions where the advantages of the method outweigh the associated costs. Some of the benefits and drawbacks are summarised as shown:-

Advantages

* Easy handling & transport of solids
* Uniform temperature distribution due to intensive mixing of solids (no hotspots even with strongly exothermic reactions)
* Solid product is uniform, *e.g.* following catalyst treatment as a fluidised bed

Disadvantages

Gas purification/removal of solids expensive

Particle attrition & erosion of reactor materials

Difficulty in scaling up

Chapter Two

Objectives

Objectives of the Present Study

The hydrogenation of nitrobenzene to aniline is a reaction of major industrial importance, as aniline is used as a precursor to many organic compounds. The reaction is generally performed industrially in the liquid phase using nickel catalysts, or in the gas phase using modified copper catalysts.

The selectivities of the nickel catalysts, however, are less than ideal and the disposal of spent catalyst can be expensive in environmental terms. With regard to the use of copper catalysts, vapour phase processes require energy input to maintain the reagents in the gas phase, which adds to the overall costs of aniline manufacture. Earlier attempts at nitrobenzene hydrogenation in the liquid phase using copper-based catalysts were unsuccessful [16], but recent work in these laboratories on the selective hydrogenation of cinnamaldehyde has demonstrated the suitability of copper catalysts towards liquid phase hydrogenation reactions [65].

The central aim of the present study, therefore, was to investigate the catalytic behaviour of supported copper catalysts in the liquid phase hydrogenation of nitrobenzene. Assuming that these catalysts did show affinity towards the reaction, the goals of the project could be subdivided into objectives i) to vi).

i) Develop the necessary experimental apparatus and protocol which would allow an evaluation of the catalytic performance of copper-based catalysts for the liquid phase hydrogenation of nitrobenzene.

ii) Prepare a series of different silica-supported copper catalysts and perform a range of characterisation experiments to enable a correlation between catalyst activity and the nature of the catalysts themselves.

iii) Investigate the reaction chemistry of nitrobenzene hydrogenation, *e.g.* reaction order with respect to reagent and product, activation energy, *etc.*

iv) Evaluate the copper-based catalysts in relation to nickel- and platinum-based catalysts, with respect to catalytic activity and selectivity.

v) Assess the suitability of nitrobenzene hydrogenation as a generic test reaction for screening future copper-based catalysts.

vi) Evaluate the effects of calcination when this stage of catalyst pretreatment is conducted as a fluidised bed.

Chapter Three

Experimental

3.1 INTRODUCTION

A range of silica-supported copper catalysts were prepared, characterised and tested for their activity and selectivity in the hydrogenation of nitrobenzene. The catalysts were prepared using a wet impregnation method, the metal precursors being impregnated onto a silica support. Catalyst treatment before use varied, during which a fluidised bed technique for catalyst calcination was tested.

Several methods were used for the characterisation of these catalysts. Ultraviolet-visible spectroscopy (UV-vis), atomic absorption spectroscopy (AAS), thermal gravimetric analysis (TGA), differential scanning calorimetry (DSC) and temperature programmed reduction (TPR) techniques were carried out at Glasgow University, as were nitrous oxide chemisorption and transmission electron microscopy (TEM) experiments. BET surface area measurements and variable temperature x-ray diffraction (VTXRD) were conducted at ICI Synetix, formerly ICI Katalco.

The catalysts were tested for nitrobenzene hydrogenation in the liquid phase, and the results analysed by gas chromatography (GC) and gas chromatography-mass spectrometry (GC-MS). A stirred batch reactor, or 'slurry vessel', was used for the majority of the reaction testing, and as a comparison for a 'bubble-phase reactor' which was developed. Analysis of sulphur species was conducted at ICI Synetix.

A silica-supported platinum catalyst, previously prepared at Glasgow [66], and a nickel/silica catalyst supplied by ICI Synetix were also employed during the reaction testing.

3.2 PREPARATION OF CATALYSTS

3.2.1 Copper catalysts

A series of silica-supported catalysts were prepared using a wet impregnation method. The metal salts purchased from Aldrich were copper nitrate ($Cu(NO_3)_2.(2.4)H_2O$, 99.999% purity), copper acetate ($Cu(CH_3COO)_2.H_20$, 99.99+% purity) and copper carbonate ($CuCO_3.Cu(OH)_2$). The supports used were M5 Cab-O-Sil and a pelleted Cariact C-10 silica (obtained from Fuji-Davidson Chemical Ltd). These silicas have surface areas of 200 and 307 $m^2 g^{-1}$ respectively.

Different copper salts were chosen to vary the nature of the metal precursors. The copper nitrate, copper acetate and copper carbonate present a range of acidities. The use of the C-10 silica allowed a similar evaluation of the effects of silica pellets versus powdered silica. Pelleted silica allows easier handling, and avoids the hazards associated with finely-powdered silica. However, it has been reported that metal catalysts prepared using C-10 pellets can experience ageing problems, which arises through encapsulation of the metal particles by the silica itself [67].

Details of the preparation are given by a) to d), shown below:-

a) Copper nitrate/Cab-O-Sil

A slurry of Cab-O-Sil (100g of silica and 560 ml of water) was placed in a round bottomed flask, and a copper nitrate solution (36.2 g of $Cu(NO_3)_2.2.4H_2O$ (0.157 moles) in 80 ml of water) was added, to give a nominal metal loading of 9.1 %. The flask was connected to a rotary evaporator and the excess water removed at 80 °C, until a free-

flowing powder was obtained. The water removed was collected in fractions, whose pH values were monitored and kept for analysis by UV-vis spectroscopy. The dried catalyst was then ground and graded by particle size; retaining the fraction between 180 and 250 μm.

b) Copper acetate/Cab-O-Sil

Copper acetate (34.9 g of $Cu(CH_3COO)_2.H_2O$, 0.175 moles) was impregnated on Cab-O-Sil (100g) as in (a), to give a nominal metal loading of 10.0 %.

c) Copper carbonate/Cab-O-Sil

Copper carbonate (19.8 g of $CuCO_3.Cu(OH)_2$, 8.95 $x10^{-2}$ moles) was dissolved in 136 ml of ammonia solution (17.5% wt NH_3), to form copper tetra-ammine $[Cu(NH_3)_4(H_2O)_2]^{2-}$. This would give a metal loading of 10.2 % when impregnated onto a Cab-O-Sil slurry composed of 100 g of silica in 504 ml of water. However, it was necessary to filter the metal salt solution prior to the impregnation step with a consequent loss of metal salt; the nominal metal loading was calculated at 8.8% wt Cu. Subsequent treatment was as per (a).

d) Copper nitrate/C-10

Copper nitrate (40.3 g of $Cu(NO_3)_2.2.4H_2O$, 0.175 moles) was impregnated on C-10 (100g) as in (a), to give a nominal metal loading of 10.0 %. This pelleted catalyst did not require grading however, simply the removal of dust and fines.

The subsequent treatment of the catalyst precursors was varied as required. The calcination step was performed under a flow of air (whether as fixed or fluidised beds), raising the applied temperature at 3 °C min^{-1} to 300 °C, this temperature being maintained for 60 minutes. Alternatively, the catalyst precursors were simply reduced directly *i.e.* without prior calcination. Reduction of the catalysts was performed *in situ*, immediately before use.

A full list of all the catalysts used in this study, along with their precursors, pretreatment and nominal metal loadings, is shown in Table 3.1. It is appreciated that dissolution of copper carbonate in ammonia produces copper tetra-ammine, but this sample is referred to as Cu(C)/Cab. Furthermore, although the active catalysts were in reduced form, for convenience they are referred to as shown in Table 3.1.

Table 3.1 Copper catalysts

Catalyst	Metal Precursor	Type of Silica	Calcined	Nominal Metal Loading (wt %)
Cu(N)/Cab	nitrate	Cab-O-Sil	no	9.1
Cu(A)/Cab	acetate	Cab-O-Sil	no	10.0
Cu(C)/Cab	carbonate	Cab-O-Sil	no	8.8
Cu(N)/C-10	nitrate	C-10	no	10.0
CuO(N)/Cab	nitrate	Cab-O-Sil	yes	9.1
CuO(A)/Cab	acetate	Cab-O-Sil	yes	10.0
CuO(C)/Cab	carbonate	Cab-O-Sil	yes	8.8
CuO(N)/C-10	nitrate	C-10	yes	10.0

3.2.2 Platinum catalysts

This catalyst was prepared at Glasgow University by D. Kennedy, and extensive information on its preparation, characterisation and catalytic activity towards the selective hydrogenation of acetylenes is available [66]. In summary, it was prepared by a wet impregnation technique with hexachloroplatinic acid and M5 Cab-O-Sil. The metal loading, as determined by atomic absorption spectroscopy, was 1.14 wt%. As regards this study, the catalyst was reduced *in situ* prior to reaction testing, ramping from room temperature to 300 °C at 5 °C min^{-1} under flowing 10 % H_2/N_2. This temperature was maintained for 120 mins under the reductive mixture, 60 mins under dihydrogen and a further 60 mins under helium. The active catalyst has a dispersion of 52.8 %, as determined by dissociative O_2 chemisorption experiments [66], which corresponds to 2.06×10^{19} surface platinum atoms per gram of catalyst.

3.2.3 Nickel catalysts

A batch of W2 Raney nickel was prepared, following a standard preparative method [68]. 150g of Ni/Al alloy powder were added to a solution of sodium hydroxide (190g of NaOH in 750ml of water). The addition was controlled to allow the reaction to proceed slowly; the evolution of hydrogen ceasing after twelve hours. The solution was decanted and a fresh alkali solution added, before washing the catalyst suspension repeatedly in water. Ethanol was then used for a further six washes, and the catalyst stored under ethanol.

A nickel/silica catalyst, representative of that employed in the industrial hydrogenation of nitrobenzene, was supplied by ICI Synetix. The silica used was kieselguhr, and the nickel loading 55 wt%; the catalyst's metal surface area is 39 m^2 g^{-1}. Following its preparation by ICI Synetix, the catalyst was partially oxidised. The resultant oxide layer is stable under normal conditions and allows ease of handling without the occurrence of bulk metal oxidation. The metal surface area quoted was determined by ICI Synetix through hydrogen chemisorption, performed in static mode (volumetric adsorption isotherm). Prior to reaction testing in this work, the catalyst was immersed in the reactant mixture and the vessel raised to the desired temperature. Catalyst activation was then performed *in situ* upon the addition of flowing hydrogen; this procedure is comparable to that used industrially.

3.3 CHARACTERISATION OF CATALYSTS

3.3.1 Ultraviolet-visible spectroscopy

As described in Section 3.2.1, the aqueous solution removed during the drying stage of the copper catalyst preparations was collected in fractions. These were analysed using a Perkin Elmer 3101PC UV spectrometer, between the range 190 to 1000 nm. This was performed to identify, and approximately quantify, any species distilled over during the drying stage of copper catalyst preparation, as has been previously conducted for platinum catalysts [69].

3.3.2 Atomic absorption spectroscopy

The copper metal content of each catalyst precursor was determined by atomic absorption spectrometry using a Perkin Elmer 1100B Spectrophotometer fitted with a hollow cathode lamp (supplied by Cathodean Ltd.) suitable for detecting copper.

A calibration curve for copper was constructed by preparing standard solutions containing 1, 2, 3, 4 and 5 parts per million (ppm) of the metal being studied from a 1000 ppm standard solution (BDH Spectrosol). Actual sample solutions were prepared as follows. Having calcined a batch of the catalyst overnight in a muffle furnace at 450 °C, a known weight (ca. 0.1g) of catalyst was placed in concentrated nitric acid (5 ml) and left overnight. This solution was then filtered from the support under reduced pressure, transferred with washings to a 100 ml volumetric flask and diluted up to 100.00 ml with water. This gave a 1000 ppm solution of catalyst at approximately 100 ppm of copper metal, assuming the nominal metal loadings. This solution was then further diluted to

give a final concentration of approximately 2.5 ppm metal, to ensure that the sample was within the linear region of the technique.

The metal content of the standard solutions were measured first, before analysing the copper content of the sample solutions.

3.3.3 Surface area determination

A sample of each copper catalyst was calcined overnight at 500 °C to remove any volatile components. The surface area determination was performed at ICI Synetix using dinitrogen as the adsorbate, with sample sizes of approximately 0.5 g. Data for BET total surface area, total pore volume and pore size distribution was obtained.

3.3.4 Thermal analysis

Thermal gravimetric analysis was performed on each of the catalyst precursors, with approximately 10 mg samples. This was conducted on a Du Pont 951 Thermogravimetric analyser at a ramp rate of 10 °C min^{-1} from ambient temperature to 1000°C, under a 50 ml min^{-1} flow of 6 % H_2/N_2.

Differential scanning calorimetry was performed on the Cu(A)/Cab catalyst, using a 2010 DSC V4.4D supplied by TA Instruments Ltd. A sample size of approximately 2.5 mg was employed, at a ramp rate of 3 °C min^{-1} under a flow of air.

3.3.5 Variable temperature X-ray diffraction

Samples of the Cu(N)/Cab and Cu(A)/Cab catalysts were prepared for variable temperature X-ray diffraction by grinding the powders and compressing them into 1.5 mm thick discs, which were supported by perforated ceramic discs. These specimens were examined using a Siemens D5000 Diffractometer D7 with Anton Parr HTK 16 hot stage. The analyses were conducted at a ramp rate of 3 °C min^{-1} with a flow of 30 ml min^{-1} gas supplied to the sample.

The gas used with the Cu(N)/Cab catalyst was 4 % H_2/N_2, under two different thermal treatments. Initially, a sample was ramped from ambient temperature, with the diffraction patterns recorded at 190, 215, 240, 265, 290, 315, 340, 400, 500 and 600 °C. The second sample was ramped to 290 °C and held at this temperature for 240 mins, recording the diffraction patterns at room temperature, upon reaching 290 °C, and after 30, 60, 90, 120, 180 and 240 mins at this T_{max}.

The Cu(A)/Cab catalyst was analysed under a flow of air, and the sample ramped to 500 °C. The diffraction patterns were recorded at ambient temperature, and at 150, 200, 225, 250, 275, 300, 325, 350, 400 and 500 °C.

3.3.6 Temperature programmed reduction

Temperature programmed reduction experiments were shown by S.D. Robertson and co-workers to provide a 'finger print' method for the characterisation of metal catalysts [70, 71]. Much information regarding the nature of the species on a catalyst surface, and the mechanism of their reduction can be gathered using this technique [72].

Temperature programmed reduction (TPR) and chemisorption experiments were performed using the gas apparatus shown schematically in Figure 3.1. The apparatus consisted of mass flow controllers, a thermal conductivity detector (TCD) and a reaction vessel which were all connected using stainless steel tubing.

The helium gas and the 6 % hydrogen/nitrogen mixture obtained from BOC were purified further before use by consecutive passage through a deoxygenating catalyst and a molecular sieve. The deoxygenating catalyst was prepared as follows. A known weight of palladium chloride (0.34 g) was dissolved in water (100 ml) and impregnated onto WO_3 (20g), the water being removed using a rotary evaporator. The resultant 'cake' was broken into 1 to 2 mm fragments, installed in a small glass vessel and activated by an overnight flow of hydrogen gas. After passage through the deoxygenator the inlet gases were dried using Linde 5Å molecular sieve contained in a brass cylinder, which was reactivated *in situ* by heating to 200 °C under a flow of hydrogen gas.

Brooks Control Ltd. mass flow controllers were used to regulate the gas flow rates. As they measure the number of molecules in the gas process (utilising a bridge circuit amongst other components) rather than simply measuring the volume of gas, they provide a constant flow of gas at the desired rate, unaffected by environmental factors such as temperature and pressure. A bubble flow meter attached to the reactor effluent was used to calibrate the flows of helium and hydrogen/nitrogen mixture.

Figure 3.1 Schematic diagram of the TPR apparatus

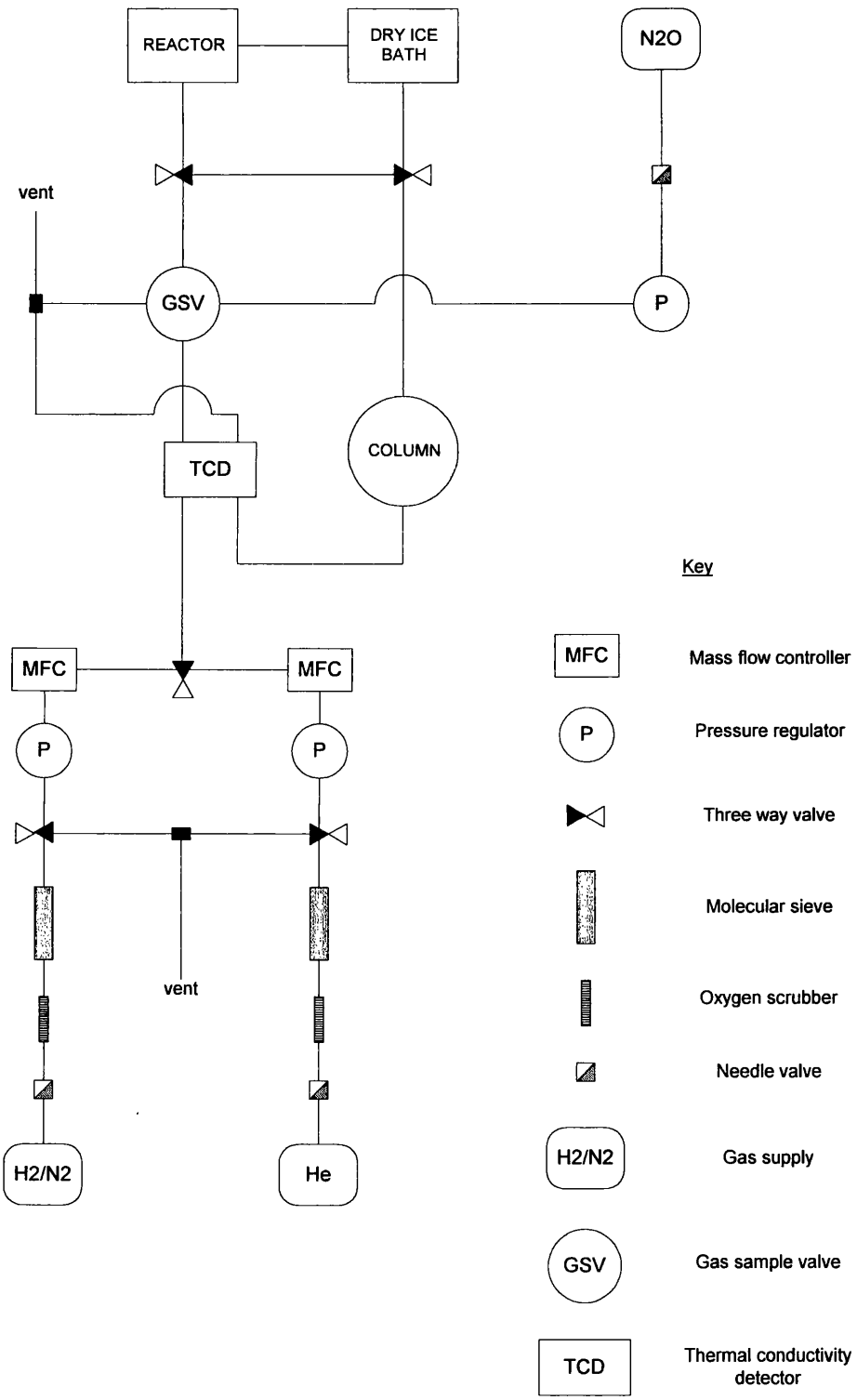

The thermal conductivity detector (TCD) consisted of a set of two twin filaments which were axially mounted, with one set in contact with the stream of reference gas, and the second in contact with the gas flow to be analysed. Heat is transferred from these hot wires at a rate proportional to the thermal conductivity of the gases, which is governed by their composition. Through the use of a Wheatstone Bridge circuit any difference between reference and sample gases can be measured and amplified, and any change in gas composition can be recorded and measured as a peak on an ancillary integrator. The filaments of the TCD were protected from potentially harmful reduction products by a cold trap fitted downstream of the reactor, which consisted of coiled tubing contained within a Dewar flask containing dry ice and acetone.

The reactor vessel itself was of simple design, as shown by Figure 3.2. The applied temperature was governed by a temperature programmer attached to a ceramic furnace and a thermocouple. Specifications of the sample valve and chromatographic column are outlined later in Section 3.5.4. The temperature programmer was supplied by Eurotherm, the furnace by Watlow and the amplifier by Gow-Mac Ltd. Mass flow controllers were obtained from Brooks Control Ltd and the integrator from Hewlett Packard Ltd.

In a typical TPR experiment the sample mass was approximately 0.2 g, and the flows of hydrogen/nitrogen and helium were 50 ml min^{-1}. The experimental procedure was as follows. Having placed a known weight of catalyst in the reactor, the line was purged with helium at ambient temperature, until a steady baseline was achieved on the integrator. The reducing gas was then selected, and the temperature ramped at the desired

rate once the baseline had restabilised. As the reduction of the catalyst progressed, the uptake of hydrogen was plotted, and the temperature recorded at regular intervals to obtain a TPR profile for each of the catalysts.

Figure 3.2 Schematic Diagram of the TPR Reactor Vessel

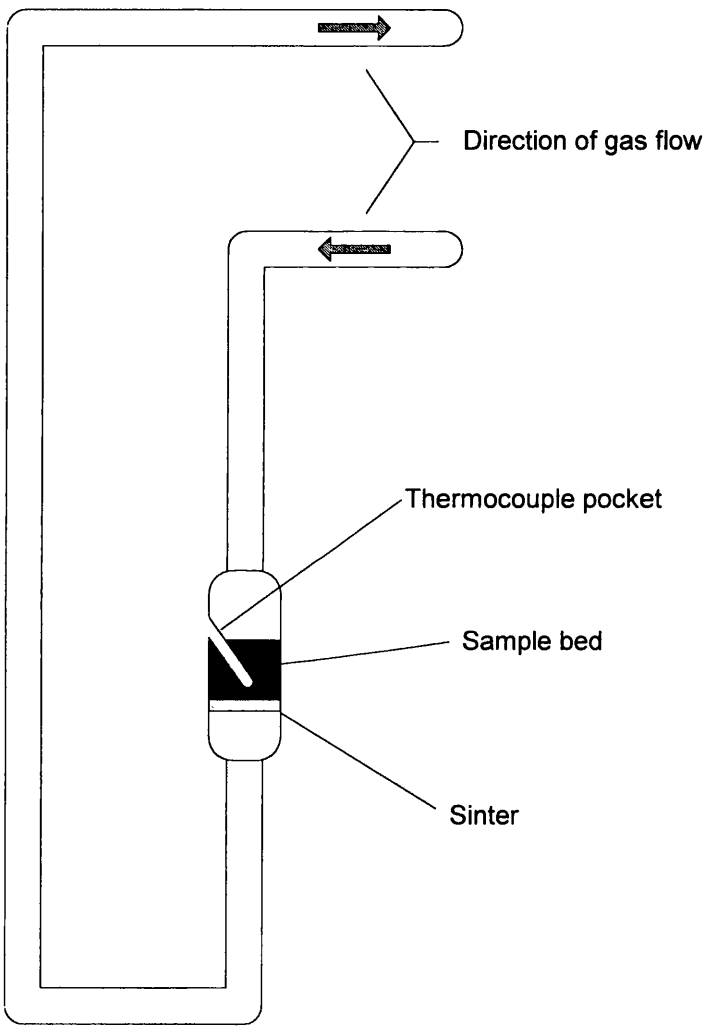

3.3.7 Nitrous oxide decomposition

There are various possible routes to assess the metal surface areas of copper catalysts. The use of carbon monoxide chemisorption to derive such data has been reported [73, 74], but this method is problematic as the results are unreliable due to extensive physical adsorption on the support, and the uncertainty of the CO/Cu_s stoichiometry. Chemisorption experiments utilising molecular oxygen can provide valid measurements of the copper metal surface area [75], but careful experimentation is required as bulk oxidation of the copper crystallites can occur at ambient temperatures [76]. The method of greatest reliability in determining such metal surface areas uses the decomposition of nitrous oxide, and this has been the focus of attention in recent years [77-82]. The reaction between nitrous oxide and the metal surface is shown by Equation 3.1.

$$2\,Cu^{0}_{(surf)} + N_2O_{(g)} \rightarrow N_{2\,(g)} + Cu_2O_{(surf)} \qquad \text{Equation 3.1}$$

The goal of experiments using nitrous oxide decomposition in this manner is to achieve complete surface oxidation of the copper whilst preventing bulk oxidation of the metal. There is some disagreement concerning the appropriate temperature at which this can be accomplished. Some authors favour the range 90 - 100 °C, observing that bulk oxidation occurs significantly above 120 °C [81, 83]. Others have found that the onset of bulk oxidation starts around 67 °C [84]. The majority however concluded that the uptake of nitrous oxide does not change substantially between the range 20 - 80 °C [85-87].

Several experimental techniques can be applied, such as pulse chromatographic N_2O titration [81] and reactive frontal chromatography developed by Chinchen *et al* [88]. Furthermore, quantitative temperature programmed reduction as used by Bond and Namijo [79] and Soerensen and Cant [78] has been shown to provide a relatively simple and accurate means of determining the metal surface area of copper catalysts. The apparatus shown by Figure 3.1 (Section 3.3.6) allows the use of both the pulse chromatographic and quantitative TPR methods; this study uses the latter technique as the same degree of accuracy and precision could be gained with less operator input.

The experimental procedure comprises three stages. During the initial reduction step the catalyst is activated. Having allowed the system to cool the surface of the metal particles are then oxidised through the decomposition of nitrous oxide. The final stage is the re-reduction of the catalyst. This latter process is effectively a quantitative temperature programmed reduction. The overall uptake of dihydrogen can be established, and assuming the ratio of 1 H_2 : 1 $O_{(surf)}$ (Equation 3.2) the number of surface oxygen atoms can be calculated. Hence, using the stoichiometry shown in Equation 3.1, the number of surface copper atoms can be determined.

$$Cu_2O_{(surf.)} + H_{2(g)} \rightarrow 2Cu^0_{(surf.)} + H_2O_{(g)} \qquad \text{Equation 3.2}$$

The experimental procedure was as follows. A known mass of catalyst, typically 0.2 g was reduced using the apparatus described in Section 3.3.6. The vessel was allowed to cool to 60 °C prior to the oxidation, in agreement with other authors [78, 79]. At this

temperature the oxidation step is thermodynamic, *i.e.* surface oxidation of the copper atoms occurs to completion, whilst oxidation of the crystallite bulk is negligible. A 50 ml min^{-1} flow of 5 % N_2O/He was then passed over the catalyst for 15 minutes, at which point the flow was diverted through the bypass and switched to 10 % H_2/N_2. Once the TCD has restabilised, the gas flow was switched back through the reactor, and the temperature of the vessel ramped upwards at 3 °C min^{-1}. The subsequent uptake of hydrogen was followed to completion, and the integrated peak determined.

A calibration line of the hydrogen uptake versus peak area was constructed, via the reduction of cupric oxide. The hydrogen uptake of a particular experiment could therefore be determined, and hence the metal surface area of the sample.

3.3.8 Transmission electron microscopy (TEM)

For studying supported catalysts, TEM is a commonly applied form of electron microscopy. In general, the detection and resolution of the metal particles is possible provided that there is sufficient contrast between metal and support. This contrast depends upon the extent to which the electrons are scattered by the different materials, which is affected by such factors as sample thickness, the identity of the species in question and their crystallinity.

Transmission electron microscopy most frequently uses 'bright-field' techniques, whereby the image is obtained from electrons in the optic axis passing directly through the sample. The electrons which are scattered or diffracted upon passing through the sample material may also be focussed, thereby providing a 'dark-field' image [89]. The

micrographs obtained during the current work were mostly bright-field images which were used to illustrate the nature of the catalyst surface, and to determine metal particle size distributions where appropriate, but dark-field images were also recorded for a number of cases.

Samples of the copper catalysts were prepared by grinding approximately 0.15 g of catalyst into a fine powder, which was then suspended in propanol and ultrasonically dispersed for 20 minutes. A drop of the fine suspension was then placed on a 300 square mesh Cu carbon coated grid. Having dried this impregnated grid overnight at 40 °C, the sample was ready for analysis. The measurements were made on a 002B High Resolution Transmission Electron Microscope, supplied by Topcon.

Energy dispersive x-ray spectroscopy (EDX) analyses were considered to confirm the identity of the copper particles. These were discounted, however, as the grid supporting the sample as well as some components of the microscope itself contain copper, and would prejudice the validity of such experiments.

Particle size distributions were determined for selected samples. The diameters of the particles were measured from a selection of negatives, at different magnifications. Care was taken to ensure that the micrographs analysed in this way provided a representative sample of the catalyst surface.

3.4 FLUIDISED BED PRETREATMENT

3.4.1 Introduction

The pretreatment of catalysts prior to use usually includes a calcination step, whereby the catalyst is heated in the presence of air. This removes the organic material from the metal salts used in most catalyst preparation, leaving the metal in its oxide form. It is possible however to activate some catalysts directly, *i.e.* without prior calcination, if the complexing material can be removed via the reduction step, as has been observed with copper/silica catalysts derived from copper nitrate [90]. Nevertheless, carbon-based salts in general cannot be reduced cleanly, and calcination is required to combust the material which would other wise block the catalyst surface.

The calcination stage is generally conducted as a fixed bed, *i.e.* the catalyst is supported on a porous sinter under a flow of air whilst an external furnace controls the elevated temperature required. The use of a fluidised bed in this stage of catalyst pretreatment was explored, and evaluated in comparison with the conventional fixed bed technique. The attributes of fluidised beds are discussed in Section 1.6, but it is the mass- and heat-transfer properties which are of relevance. These ensure that the temperature is uniform throughout the catalyst bed, in contrast to the sometimes inhomogeneous nature of fixed beds. These have the potential to develop localised 'hotspots', whether derived via poor heat transfer from the external furnace or from the catalyst treatment itself (both the calcination and indeed reduction steps can be considerably exothermic). Figure 3.3 represents an idealised view of fixed and fluidised beds. In addition, the strong flow of gas in a fluidised bed means that any waste products formed during calcination are swiftly

removed from the catalyst surface. This is significant since the presence of water can deactivate metal catalysts [7c, 7d]. In summary, the use of a fluidised bed during the calcination step should increase the dispersion of the catalyst by minimising processes which can lead to sintering of the metal particles.

Figure 3.3 Schematic diagrams of fixed and fluidised beds

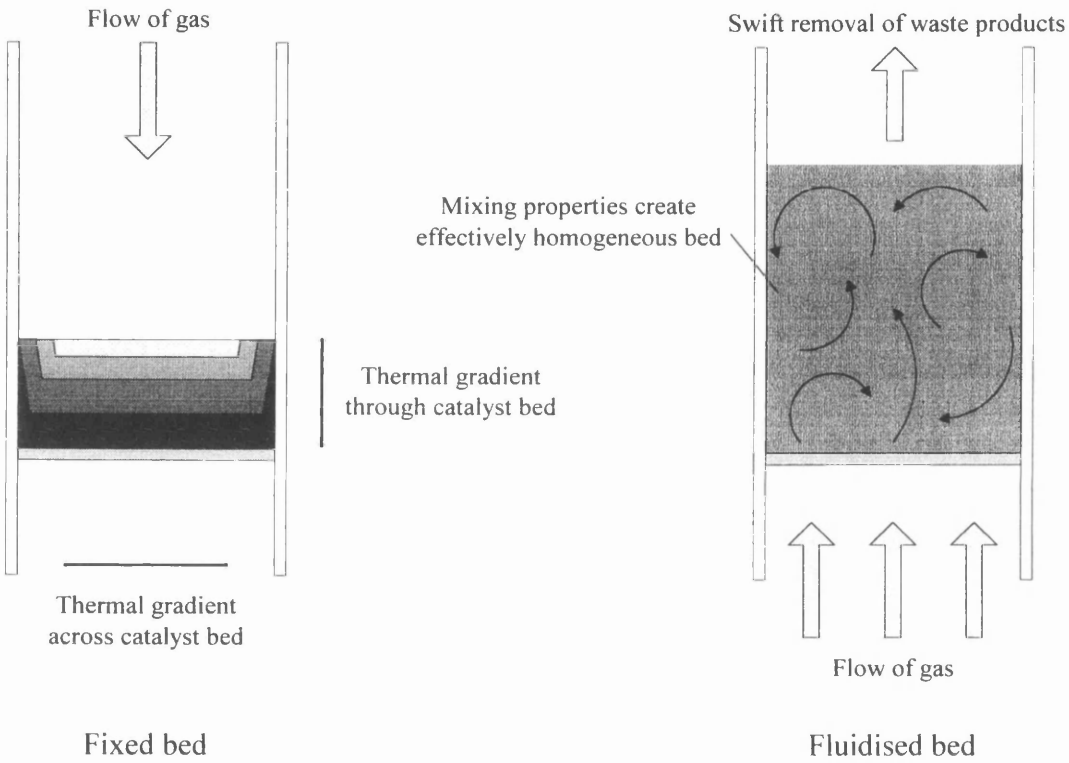

Samples of the four copper catalysts were calcined as fixed beds using the apparatus described in Section 3.4.2. Samples of Cu(A)/Cab were also calcined using a fluidised bed technique to enable an evaluation of the effects of the two different

methods. This catalyst was chosen as it was derived from a carbon-based salt, which generally requires a calcination step before catalyst activation.

The effects of the techniques were determined by measuring the particles of copper oxide directly via transmission electron microscopy, and through nitrous oxide decomposition to quantify the metal surface area of the samples once reduced. These metal surface areas were then correlated with catalyst activity, with samples which had been calcined as fixed and fluidised beds employed for the hydrogenation of nitrobenzene.

3.4.2 Experimental technique

An overwhelming amount of literature has been published on the complex operation of fluidised beds, but the approach adopted in this project was essentially empirical. A simple vessel was tested initially, in which a porous sinter was positioned midway along a linear tube of 1 cm diameter. It was found that fluidisation of the bed could be achieved, but that the high flow of gas required preheating to maintain an even temperature throughout the bed. A coil was therefore added around the central section of the reactor, so that the air flow was directed through the furnace before reaching the catalyst bed. It was also observed that although the catalyst particles had been graded to between 180 and 250 μm, the spillover of fines was observed (possibly produced via attrition), so a disengagement section was added. Finally, a thermocouple pocket was positioned within the catalyst bed. This inevitably retarded the flow rate in some areas of the bed, leading to a degree of inhomogeneity. The presence of this pocket was required,

however, and the relatively small scale of the vessel precluded a less intrusive positioning. It was found that the addition of a mechanical vibrator, attached loosely to the top of the disengagement section agitated the catalyst particles throughout the system, preventing the catalyst from 'sticking' under the thermocouple pocket. An additional effect of the vibrator was to dislodge any fines which had collected on the uppermost sinter, allowing them to return to the bed proper. The final vessel design, with the additional incorporation of a second thermocouple pocket below the sinter is shown by Figure 3.4.

The overall apparatus is shown by Figure 3.5. This arrangement allowed the calcination of catalyst precursors as either fixed or fluidised beds. In addition, the versatility of the design allowed the vessel to be inverted for further variations of the experiment.

The gas flow rate was controlled using the pressure gauge and flowmeter, and the temperature by a Watlow furnace connected to a Eurotherm temperature programmer. The catalyst mass installed for a typical experiment was 1.2 g, the flow rates for fixed and fluidised beds were 50 and 500 ml min^{-1} respectively.

Figure 3.4

Schematic diagram of the calcination reactor

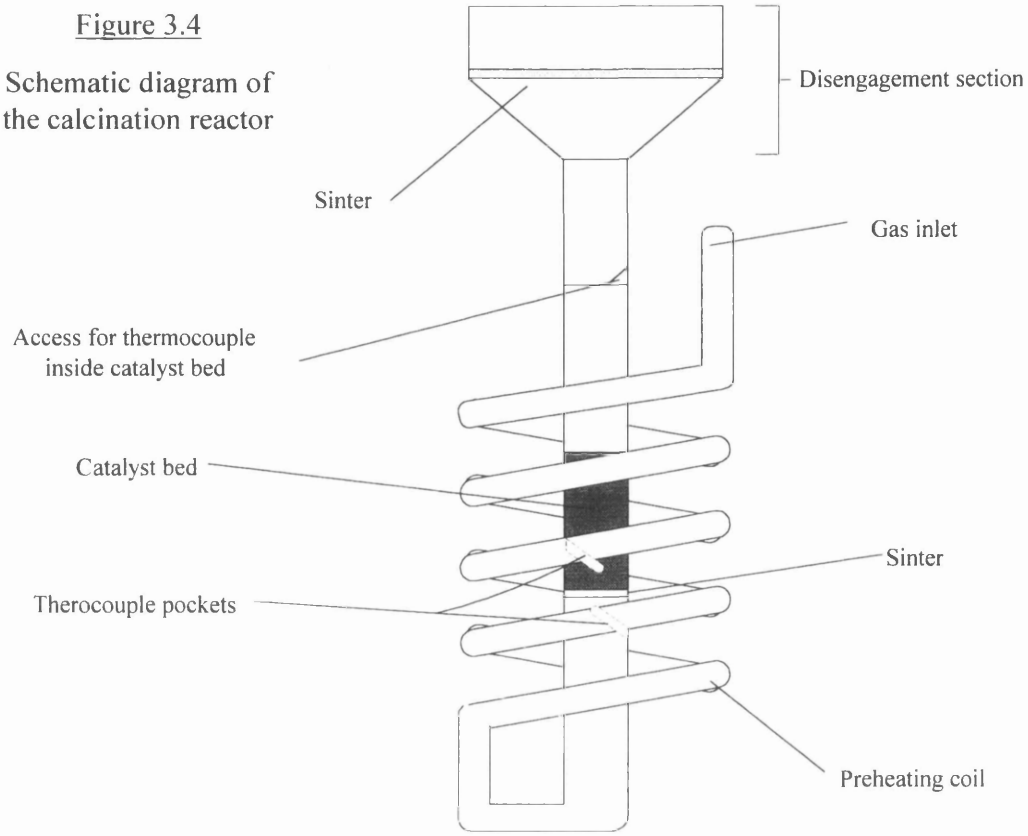

Figure 3.5

Schematic diagram of the calcination apparatus

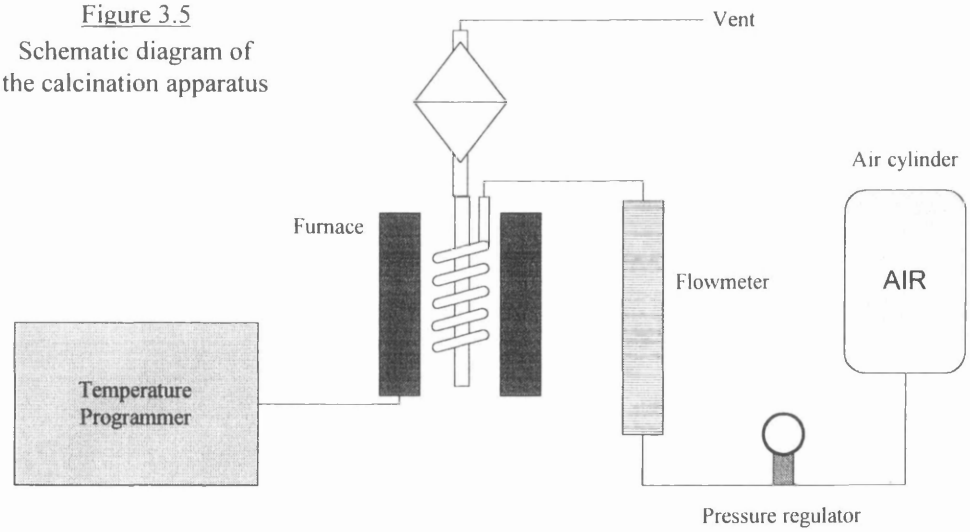

3.5 HYDROGENATION REACTIONS

3.5.1 Materials

Chemicals were purchased from Aldrich, with the purities shown by Table 3.2.

Table 3.2 Purity of chemicals used during reaction testing

Chemical	Purity (%)
Nitrobenzene	99.5
Aniline	99
Dodecane	99+
Ethyl benzene	99
Mesitylene	98
Hexan-1-ol	98
n-Butyl benzene	99+
t-Butyl benzene	99

Chemicals were normally used as supplied, without further purification, bar reaction mixtures which were degassed under reduced pressure prior to use. The exception was *t*-butyl benzene which was purified as required, using Raney nickel with subsequent distillation and degassing.

Gases supplied by BOC were dihydrogen, helium and a 10 % dihydrogen / dinitrogen mixture. These were purified further before use, using deoxygenating catalysts and molecular sieves installed to the TPR and reaction lines.

3.5.2 Reactor system

Liquid-phase hydrogenations of nitrobenzene were carried out in a fume cupboard using the apparatus shown in Figure 3.6. This was developed to allow the use of two different glass vessels; a slurry reactor and a bubble-phase vessel (Figures 3.7 and 3.8 respectively). In this way the catalyst could be reduced *in situ* with either vessel, using the 10 % hydrogen/nitrogen mix and helium, before introduction of the degassed reaction mixture. The reaction was then conducted at the desired temperature under flowing hydrogen.

The temperature programmer was supplied by Eurotherm, the ceramic furnace by Watlow, and the RCT Basic oil bath/magnetic stirrer and ETS-D4 thermostat by IKA Labortechnik.

3.5.3 Experimental conditions

The operation of the slurry vessel was as follows. The catalyst precursor was introduced and supported by the sinter of the reactor when inverted. The system was then purged with helium, before switching to the reductive mixture as temperature ramping was commenced as required, using the temperature programmer and thermocouple attachment to control the temperature of the catalyst bed. After reduction the catalyst was purged with helium at the reduction temperature, and then allowed to cool to room temperature. At this point the vessel was rotated through 180° permitting the active catalyst to fall to the bottom of the reaction vessel. The degassed reaction mixture was then admitted under a high flow of gas, a magnetic stirring bar added and the condenser

Figure 3.6 Schematic diagram of the hydrogenation apparatus

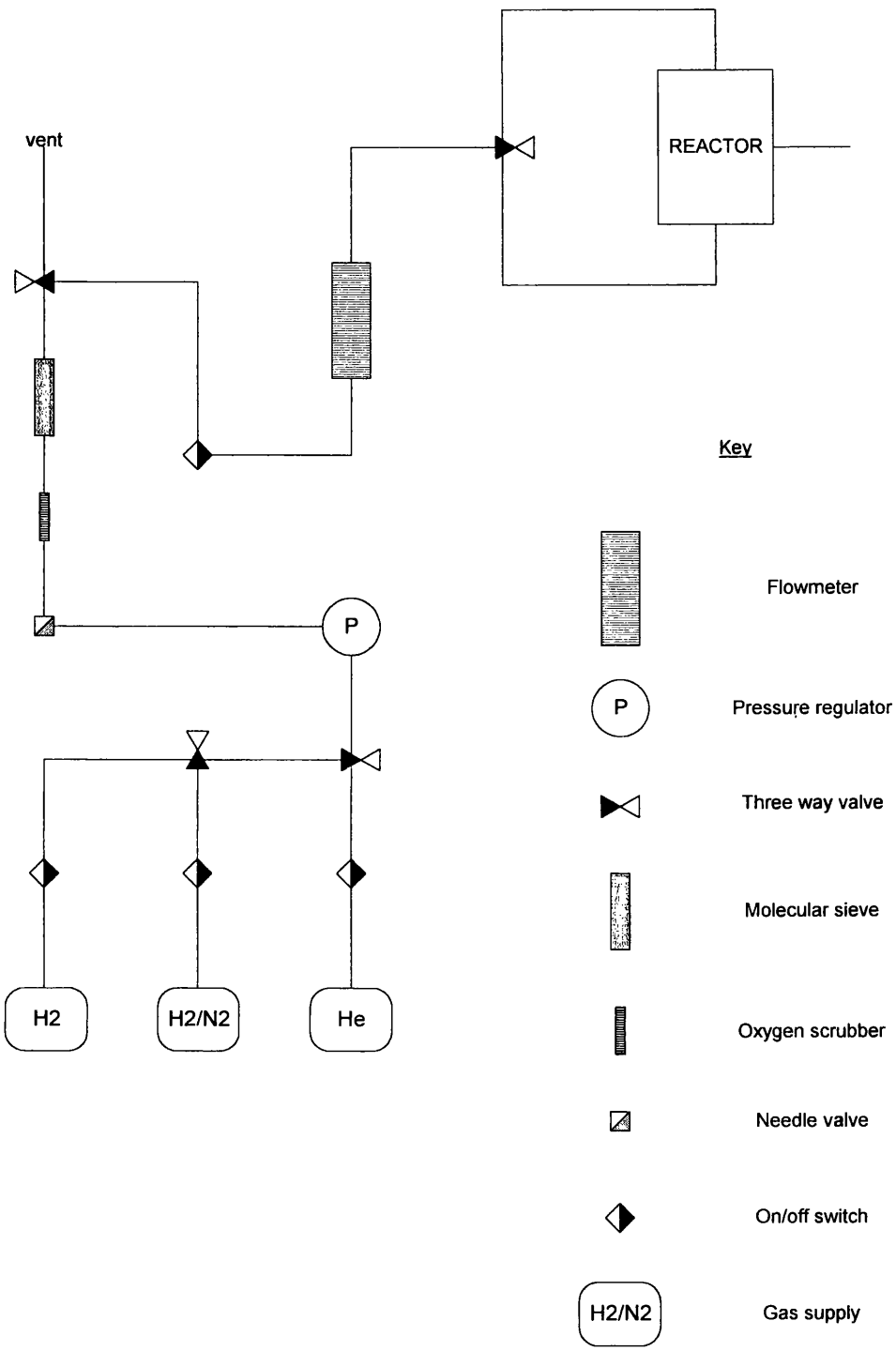

Figure 3.7

Schematic diagram of the slurry reactor

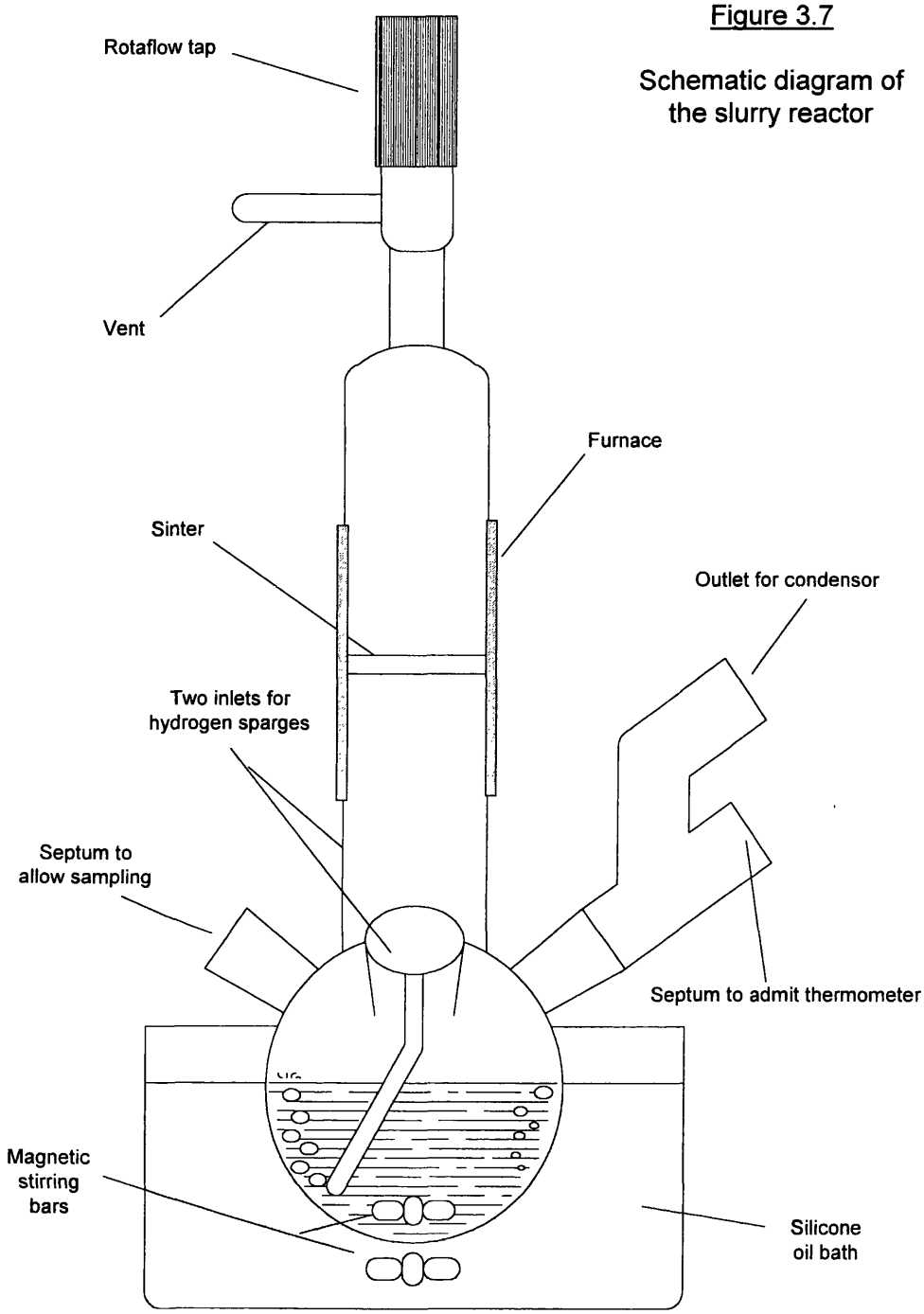

Figure 3.8

Schematic diagram of the bubble-phase reactor

[Note: labels in italics are applicable during catalyst activation only]

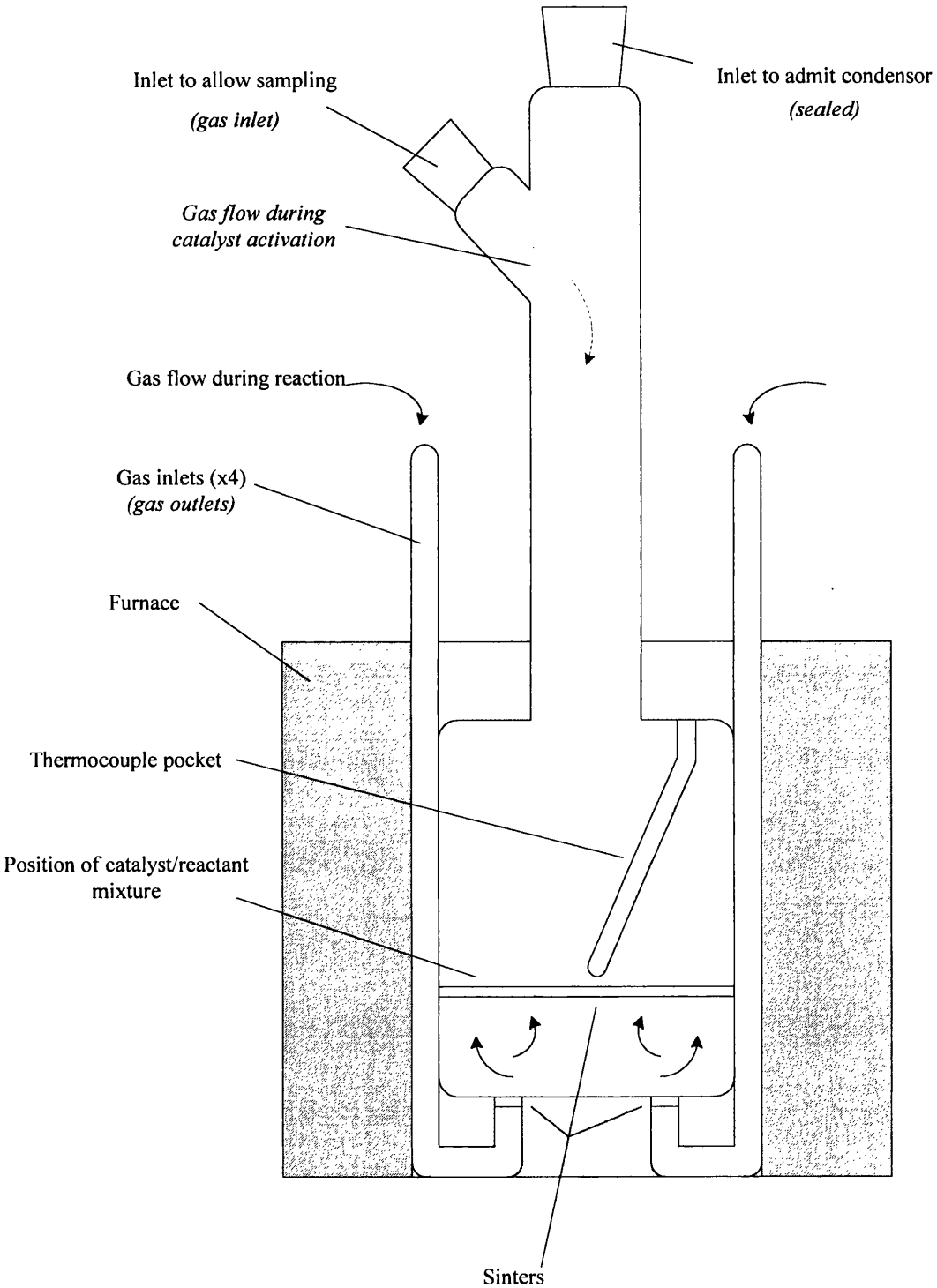

fitted. The reactor was immersed in the oil bath, and the gas changed to hydrogen once the correct temperature had been attained. Approximately 0.3 ml aliquots of the reaction mixture were withdrawn via the septum by a 5 ml glass syringe at appropriate intervals, for subsequent analysis (Section 3.5.4).

Use of the bubble-phase reactor followed the same procedure, but the vessel did not require inversion after the catalyst activation step. The temperatures applied during the reduction and reaction steps were controlled by a temperature programmer and thermocouple attached to a furnace.

Various experimental conditions were applied during the course of the project. The ranges are shown in Table 3.3.

Table 3.3 Range of experimental conditions used during reaction testing

Active Catalyst Mass	0.4 - 0.8 g
Gas Flow during Reduction	50 - 200 ml min^{-1}
Gas Flow during Reaction	200 - 250 ml min^{-1}
Reaction Temperature	60 - 170 °C

3.5.4 Analysis of the reaction samples

Identification of the reaction products was obtained by gas chromatography-mass spectrometry (GC-MS), by comparison of their retention times through the column against known standards, and in some cases by infra-red spectroscopy. Quantitative analysis of the reaction products was performed by gas chromatography.

Primary identification of the species observed was obtained via GC-MS, on a Hewlett Packard 5890 Series II gas chromatograph interfaced with a Hewlett Packard

5971 Series mass selective detector, which was in turn interfaced with a Vectra QS 165 computer. Two columns were used for this stage of analysis, either an HP1 non-polar capillary column (15 m x 0.2 mm x 0.3 μm), or a polar BP20 capillary column (30m x 0.25 mm x 0.25 μm).

Verification of the identities' of the species present during reaction testing was obtained by gas chromatography, comparing their column retention times against those of known standards. Two gas chromatographs (GC) were used during the course of the project, a Chrompack 9000 attached to an electronic integrator supplied by Hewlett Packard, and a Hewlett Packard 5880A Gas Chromatograph attached to a 5880A Series GC Terminal. Integration of the component peaks was performed automatically by the former instrument, and manually using the Hewlett Packard 5880A Gas Chromatograph. The latter technique was done by determining the height of a peak, and multiplying this by the measured half-height peak width to determine the area of the peak. Calibration lines were constructed from known concentration standards for both gas chromatographs to enable quantitative analysis. Both gas chromatographs used capillary columns and were fitted with flame ionisation detectors (FID).

Table 3.4 and Figure 3.9 illustrate the typical reproducibility which was attained using the two systems. The standard solution used in this example was an equimolar amount of nitrobenzene and aniline (0.0489 M) in *n*-butyl benzene. In this diagram the results obtained using the Chrompack GC are plotted on the left-hand scale, and those from the Hewlett Packard GC on the right; the results are plotted in groups. Each group of

data was collected consecutively, whilst the time scale between each set of three results ranged from days and weeks.

These results show that good reproducibility for the injection technique and subsequent integration of the peak area, at any one time, although some variance occurred when using the Hewlett Packard GC. Great care was taken during manual measurement of the gas chromatograms obtained with this instrument, and despite the seeming crudeness of the technique the results are satisfactory. The greatest differences arise when comparing groups of data. Many factors affect the sensitivity of the FID, such as carbon build up and variations in gas flow, and slight changes over a period of time are to be expected. To ensure precision during each analysis, the sensitivity of the GC was calibrated with a standard solution before commencing the injection of reaction samples (Figure 3.9 actually shows six sets of such calibration data).

Table 3.4 Reproducibility of analysis by gas chromatography

	Sample	Chrompack (peak area, $x10^4$)		Hewlett Packard (area, mm^2)	
Series	injection	AN	NB	AN	NB
1	1	321	315	85	87
1	2	320	317	88	88
1	3	317	316	85	85
2	6	290	290	88	88
2	7	290	288	89	90
2	8	283	280	89	90
3	11	284	290	87	88
3	12	290	293	86	86
3	13	287	290	88	88

Figure 3.9 Reproducibility of analysis by gas chromatography

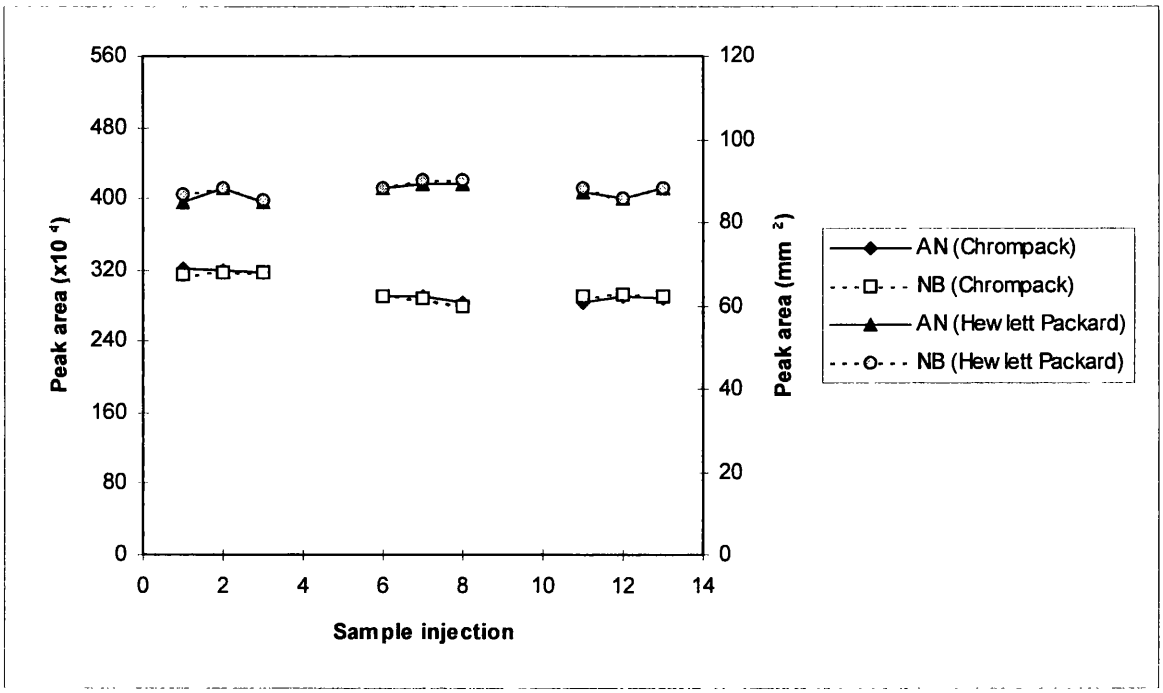

Two columns were used to quantify the components of a reaction sample during the course of the project, a mildly polar J&W Scientific DB-225 column and a non-polar SE-30 column. Choice between the columns was determined by the species under analysis. In general, resolution between the components of a given reaction mixture could be accomplished with one column, but in a limited number of cases (Sections 5.2.5 and 5.3.4) the reaction samples were analysed using both columns individually, to obtain the desired resolution of the various peaks. The columns were of equivalent dimensions (30 m x 0.32 mm x 0.25 μm), and were reconditioned by overnight heating at 200 °C under flowing helium.

The temperature profile of the gas chromatograph's oven was varied as required, in order to obtain satisfactory resolution in the minimum time. Typical oven profiles used

for the DB-225 and SE-30 columns are shown in Figure 3.10. The injection and detector ports were set at 260 °C.

Figure 3.10 Typical oven profiles for gas chromatography

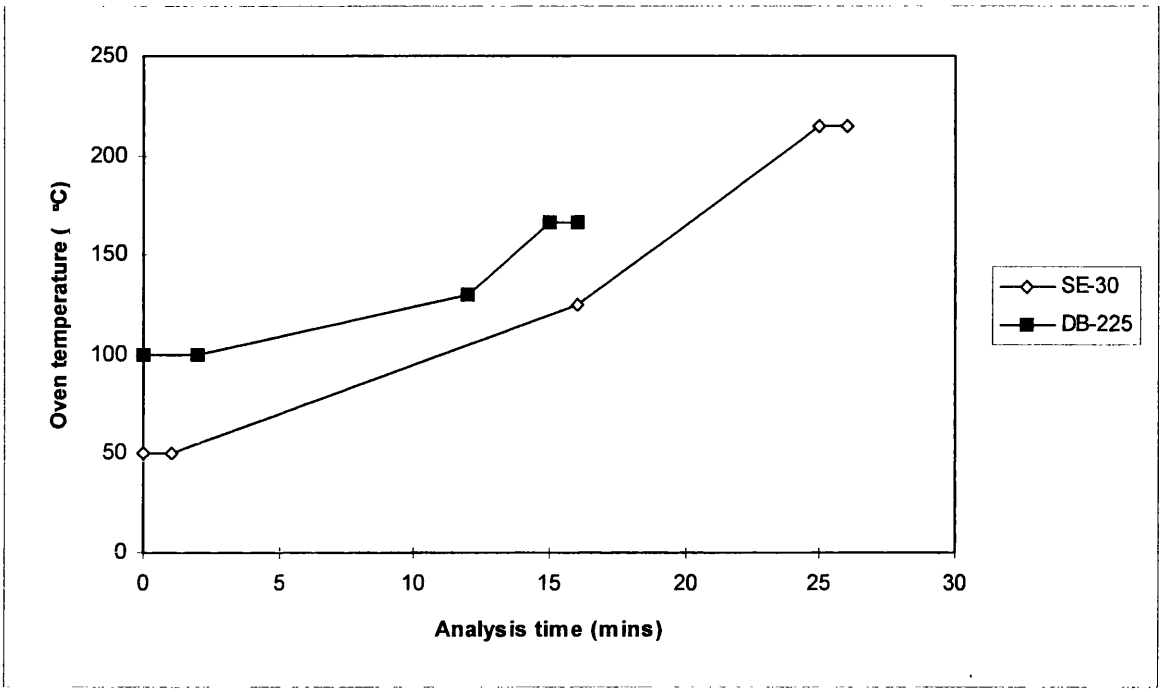

3.5.5 Analysis of sulphur species

As catalyst performance was found to be sensitive to the presence of sulphur within certain solvents, the total sulphur content of these was determined. An attempt at the identification of these sulphur species was then attempted. This section of the project was conducted at ICI Synetix.

The total sulphur content of various key reactant mixtures was determined using a Houston Atlas Model XVI analyser. This apparatus injects a known volume of sample into a stream of hydrogen gas. The sample is vapourised and fed through a furnace, which at 1423 K reduces all sulphur present, regardless of source, to H_2S. This is carried

through a 5 % acetic acid solution to moisturise the gaseous hydrogen sulphide, which is then passed over a section of lead acetate tape. A reflectometer can then establish the total amount of sulphur present, down to parts per billion, by detecting the degree of colour change of the tape. This is done in comparison with a calibration line constructed from standards of known sulphur concentration. Sample sizes were 30 μl, at an injection rate of 30 μl min^{-1} into a hydrogen flow at 200 ml min^{-1}.

The identity of the sulphur species was analysed by gas chromatography using programmed splitless / split injection with flame ionisation and pulse flame photometric detectors in parallel (FID and PFPD respectively). The sample was eluted using a combination of temperature and carrier flow programming from a 100 % methyl silicone column (DB1, 30 m x 0.53 mm x 5 μm). A solution of ca. 100 ppm *n*-alkanes was injected under the same conditions to assess the observed retention times in terms of boiling points. In this way the different components present in a sample can be resolved chromatographically, whilst the PFPD reveals which of the components contain sulphur. Comparison with the standard solution of *n*-alkanes then allows a determination of the approximate boiling points of the sulphur-based species and their probable identities.

Chapter Four

Treatment of Results

4.1 Nitrous oxide decomposition

The dispersions and metal surface areas of the catalysts were determined via nitrous oxide decomposition, using the method described in Section 3.3.7. The number of surface copper atoms was calculated from the peak area of the reduction of $Cu_2O_{surface}$ in comparison with a calibration line of peak area versus hydrogen uptake. The number of molecules of hydrogen reacted during this reduction was established, and hence, the number of active surface copper atoms.

The total mass of copper in the experimental samples was deduced from the initial sample mass, the metal loading (as determined by atomic absorption spectroscopy, Section 5.1.2) and the percentage mass remaining after reduction (determined by thermal gravimetric analysis, Section 5.1.4). The dispersion of the catalyst is defined by Equation 4.1.

$$\text{Dispersion (D)} = \frac{\text{No. of surface copper atoms}}{\text{Total no. of atoms of copper present}} \times 100\ \%$$

Equation 4.1

The metal surface area of the catalysts can be calculated from the number of surface copper atoms; the average areas of the Cu(100), Cu(110) and Cu(111) crystal planes being 0.065, 0.092 and 0.0563 nm^2 per copper atom respectively [75]. Values of 1×10^{19} to 1.7×10^{19} copper atoms per m^2 have been reported in the literature [75, 79, 80, 88], depending on the relative contribution of crystal plane. Parris and Klier [75], assuming that these three planes were present in equal amount, calculated that 1.41×10^{19}

surface copper atoms were equivalent to 1 m^2, and this has been adopted for the present study.

Mean particle sizes can also be obtained from chemisorption experiments, if assumptions are made concerning particle shape, *e.g.* if the supported metal particles are assumed to be spheres of equal diameter (d). The dispersion of a metal (D) varies as the reciprocal of the average particle size, and the larger the dispersion, the smaller the average particle size [91]. The equation used by Smith, Thrower and Vannice [92] is as shown:-

$$\% \text{ Dispersion} = \frac{A \times 6}{\rho \times S_a \times N_a \times d} \times 100$$

where for copper

A	= atomic weight	(63.546 g mol^{-1})
ρ	= density of metal	(8.92 x10^{-21} g nm^{-3})
S_a	= average surface area occupied by one active atom	(0.0709 nm^2)
N_a	= Avogadro's number	(6.022 x10^{23})
Therefore, d, average particle diameter =		100.1 / D

Special attention should be made to the presentation of the results in terms of the active catalyst masses. Thermal gravimetric analysis experiments (Section 5.1.4) showed total mass losses of between 1.6 and 33.6 % for the different catalysts, depending on the nature of the precursor. The conditions used in these experiments were comparable to

those of the activation procedure adopted for the catalysts. Whilst catalyst masses are conventionally reported in terms of the original weight used for the experiments, it was felt that due to the wide variance of mass lost during the reduction, this approach would misrepresent the relative performance of the catalysts in this study. The calculated weights of the copper catalyst *once active* are therefore presented for each experiment reported. Table 4.1 shows the percentage mass losses experienced during reduction, and the scaling factor required to calculate the original mass of copper catalyst used for an experiment.

Table 4.1 Percentage ratios of catalyst mass prior to and following reduction

Catalyst	Mass loss during reduction (%)	Scaling factor (%)
Cu(N)/Cab	31.7	146.4
Cu(A)/Cab	18.3	122.4
Cu(C)/Cab	5.5	105.8
Cu(N)/C-10	33.6	150.6
CuO(N)/Cab	2.1	102.1
CuO(A)/Cab	2.4	102.5
CuO(C)/Cab	1.6	101.6
Cu)(N)/C-10	2.3	102.4

For example, the mass of Cu(N)/Cab catalyst quoted in Figure 5.3.1 (Section 5.3.1) is 0.5473 g. The actual mass of catalyst installed prior to reduction, therefore, is 146.4 % of 0.5473 g *i.e.* 0.8012 g.

The masses of the platinum- and nickel-based catalysts used in the study, however, are reported conventionally as their original weights.

4.2 Reaction testing

Reaction testing results are generally plotted as the number of moles of reactant consumed / product formed versus reaction time. The number of moles of nitrobenzene (NB), aniline (AN) and nitrosobenzene for each sample were calculated from calibration lines of the gas chromatograph's detector response factor for these species, which were produced using known volume standards. The detector response factor (DRF) of the gas chromatograph is defined as the change in signal which is produced by a unit change in the concentration of the carrier gas [93a]. The detector response factors for N-hex-1-ene aniline and N-hexylaniline proved difficult to obtain directly, as pure samples of these materials were not available commercially. The procedure used to quantify their response factors was as follows.

The signal registered by the flame ionisation detector (FID) of the gas chromatograph depends on the ion current as each component is combusted; the actual signal depending upon the number of molecules detected, the number of combustible atoms in each molecule, and the degree of 'completeness' with which they are burnt [93b] For example, assuming equal moles, octane produces a higher signal than hexane due to the higher number of carbon atoms, whilst the detector response factor to hexane is higher than that of benzene, which does not undergo as full a degree of combustion. Making this assumption, the detector response factors for N-hexylaniline, for example, were estimated by summing the individual responses to hexane and aniline. This may be justified by considering Figure 4.1, which shows that the number and approximate structure of the carbon and nitrogen atoms are comparable. The different number of hydrogen atoms will

have no effect, as the FID relies on the combustion of hydrogen to maintain the flame; only the combustion of carbon and nitrogen will contribute to the signal. Although it is realised that this method is only an approximation, it is recognised that such techniques can provide useful analysis [93b].

Figure 4.1 Comparison of hexane, aniline and N-hexylaniline

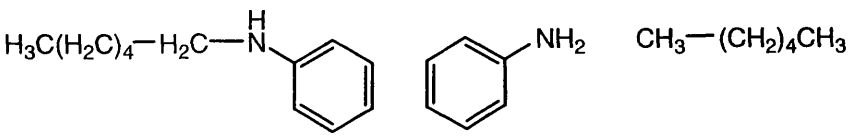

Hexylaniline Aniline Hexane

Besides N-hex-1-ene aniline and N-hexylaniline, which were observed only when using hexan-1-ol as a solvent, no other by-products were detected during reaction testing over the copper catalysts. Several other by-products were observed when using the platinum- and nickel-based catalysts. Given the inevitable time constraints on the project it was decided to investigate the reaction chemistry, rather than accurately quantify the production of minor by-products. These components therefore, have been quantified using the calibration line for nitrobenzene. To avoid ambiguity this is pointed out where appropriate.

Finally, it is emphasized that the masses of copper-based catalyst reported for reaction testing are the weights once active, as explained in Section 4.2.

The results of reaction testing have been presented using the following definitions:-

$$\text{Selectivity} = \frac{\text{No. of moles of aniline formed}}{\text{No. of moles of nitrobenzene consumed}} \times 100\ \%$$

Equation 4.2

$$\text{Conversion} = \frac{\text{No. of moles of NB reacted}}{\text{No. of moles NB present initially}} \times 100\ \%$$

Equation 4.3

It should be noted that the selectivity values reported are only meaningful at reasonable high conversion levels. At very low conversion levels, the degree of error of the sample injections is sufficient to produce wildly erratic selectivity results.

Comparisons between reactions which are expressed as percentage conversion have been normalised to equivalent masses of catalyst and initial concentrations of nitrobenzene.

Reaction rates have been calculated from the rate of aniline formation over the initial linear region of the reactions. The rates have been normalised to 1.0 g of active catalyst and expressed per second. Throughout the report the derived rates are presented to four significant figures, as 'moles $\underline{x10^{-7}}$ s^{-1}', in order to simplify comparisons between different catalysts. The values expressed were calculated using linear lines of best fit derived via a computer graphing program (Excel). Errors reported on such rates are

standard errors, and were obtained using the computer program Origin 4.1 (supplied by MicroCal Inc.).

Turnover frequency has been defined as the number of molecules reacting per second, per active site [7a], assuming that every surface copper atom behaves as an active site.

Chapter Five

Results & Discussion

5.1 CATALYST CHARACTERISATION

5.1.1 Ultraviolet-visible spectroscopy

As outlined in Section 3.2.1 the condensate evolved during the drying step of catalyst preparation was collected in fractions. The present chapter reports the subsequent UV-vis spectroscopy analyses of these fractions, as well as their measured pH values. The pH values of the various fractions collected for each catalyst precursor are shown in Table 5.1.1, along with those measured for the copper salt solutions before impregnation, and the subsequent salt/silica slurry. This data is displayed by Figure 5.1.1, where the points plotted for fraction number zero are the pH values of the salt/slurry mixtures.

Progressive changes in the appearances of the fractions were also noticed. The nitrate-derived fractions were initially clear and colourless, but an opaque white colour developed with the later samples. This pattern was repeated with the acetate-based precursor, although the later fractions displayed a slight blue tinge, and the precipitate was more evident. The initial samples collected whilst drying the carbonate-based precursor were clear and slightly blue in appearance. This colour faded with successive fractions, the final sample being slightly opaque with a white colour.

The peaks observed during UV-vis spectroscopy, and their assignments, are summarised by Table 5.1.2. In addition, all of the samples showed strong absorbance peaks around 200 nm, which are attributable to water. The results for each of the catalysts reveal the presence of copper complexes.

The observance of the various copper species by UV-vis spectroscopy, and the measured pH values of the condensate fractions, indicate the transport of the metal salts during this step of catalyst preparation. In addition, the opaque appearance of the later fractions themselves suggests that fine particles of silica have also been carried over by the vacuum. The transport of the copper salts and the silica do not necessarily occur independently, however, and it is likely that the removal of fine, dry catalyst particles accounts for all of the observed phenomenom. In summary, the results of this chapter show that the dynamic vacuum applied by the rotary evaporator is sufficient to remove solid material during the drying stage. This provides one explanation why nominal and actual catalyst metal loadings do not generally agree.

Table 5.1.1 pH values of original salt solutions and condensate fractions

	pH value		
Sample	Cu(N)/Cab	Cu(A)/Cab	Cu(C)/Cab
salt solution	2.3	2.3	13.6
salt/silica slurry	-	5.0	10.8
1	3.9	3.3	11.2
2	3.6	3.3	10.8
3	2.9	3.3	10.3
4	3.2	3.3	10.6
5	3.2	3.0	10.6
6	3.5	3.4	10.8
7	3.5	3.4	10.9

Figure 5.1.1 pH values of the Condensate Fractions

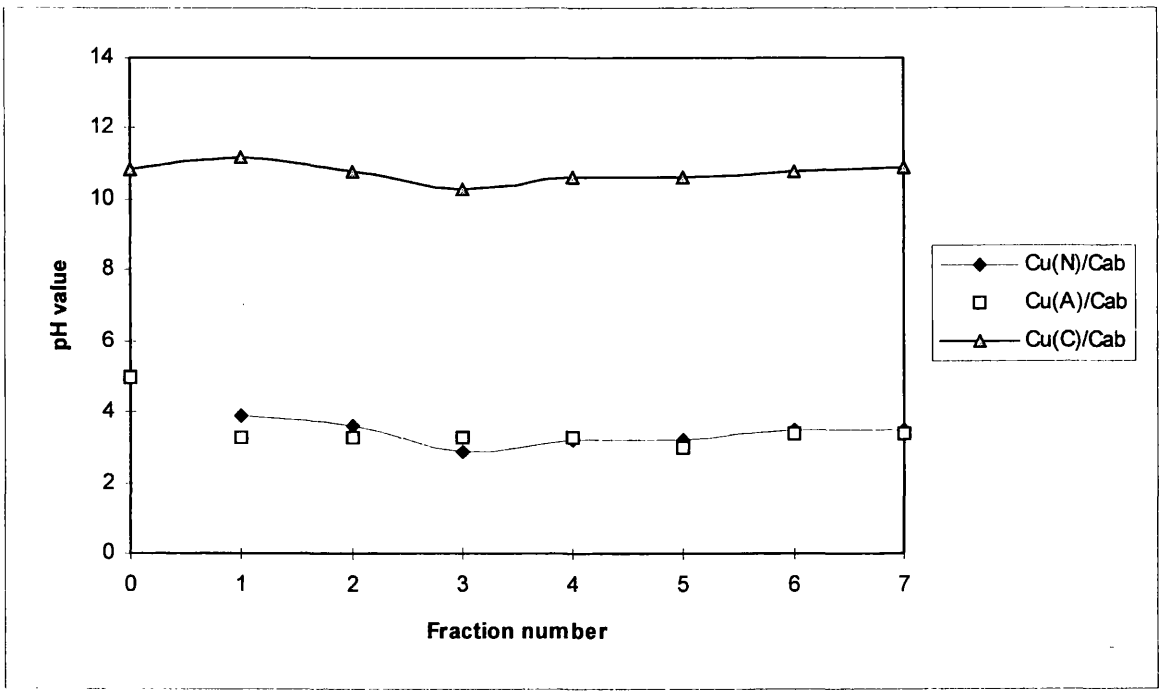

Table 5.1.2 Summary of UV-vis spectroscopy analyses

Catalyst	λ (nm)	Assignment
Cu(N)/Cab	307	NO_3^- $n \rightarrow \pi^*$
	805	$[Cu(H_2O)_6]^{2+}$
Cu(A)/Cab	265	$Cu_2(CH_3COO)_4(H_2O)_2$
	790	$[Cu(H_2O)_6]^{2+}$
Cu(C)/Cab	620	$[Cu(NH_3)_4(H_2O)_2]^{2+}$
	800	$[Cu(H_2O)_6]^{2+}$

5.1.2 Atomic absorption spectroscopy

Copper loadings for each of the catalysts were determined by atomic absorption spectroscopy (AAS) as described in Section 3.3.2. A full list of the calcined catalyst precursors and their metal loadings is shown in Table 5.1.3.

Table 5.1.3 Metal loadings of the copper catalysts

Catalyst	Metal Precursor	Type of Silica	Nominal Metal Loading (wt %)	Metal Loadings by AAS (wt %)
CuO(N)/Cab	nitrate	Cab-O-Sil	9.1	8.59
CuO(A)/Cab	acetate	Cab-O-Sil	10.0	9.68
CuO(C)/Cab	carbonate	Cab-O-Sil	8.8	6.31
CuO(N)/C-10	nitrate	C-10	10.0	9.18

It is evident that for the Cu(C)/Cab catalyst has lost ca. 28% of its nominal metal loading; this is attributed to precipitation of $CuCO_3.Cu(OH)_2$ from the ammonia solution during the preparation. The other three precursors display a slight drop between nominal and actual metal loadings (5.6, 3.2 and 8.2 % for the Cu(N)/Cab, Cu(A)/Cab and Cu(N)/C-10 catalysts respectively), as usually occurs during catalyst preparation.

This may be partially accounted for by the results presented in Section 5.1.1, which proved that some of the metal salt is removed from the slurry mixture during the evaporative drying stage.

5.1.3 Surface area measurements (BET)

The BET surface areas and porosities for the silicas and the calcined catalyst precursors are given in Table 5.1.4.

Table 5.1.4 Surface areas and porosities of the catalysts

Catalyst	N_2 Surface Area ($m^2\ g^{-1}$)	Total Pore Volume ($cm^3\ g^{-1}$)	Average Pore Diameter (nm)
Cab-O-Sil	200	-	-
C-10	307	1.02	9.9
CuO(N)/Cab	174	1.02	22.0
CuO(A)/Cab	120	0.41	29.4
CuO(C)/Cab	242	0.67	17.4
CuO(N)/C-10	240	0.90	15.0

These results show that all four catalysts have total surface areas in excess of 120 $m^2\ g^{-1}$, the support therefore providing a large surface area to separate the metal particles. It is apparent that the nitrate and acetate forms of the Cab-O-Sil-supported catalyst have lower surface areas than the original Cab-O-Sil material.

What is perhaps more interesting is that the copper carbonate-based precursor has a higher surface area than that of Cab-O-Sil alone. This indicates that the relatively high pH value (10.84) of the cupric tetraammine solution was sufficient to induce restructuring of the silica. Dissolution of the copper carbonate in ammonia solution, to form cupric tetraammine, required a strongly alkaline solution. The pH of the salt solution was 13.6, with 10.8 recorded for the final salt/silica slurry, as shown in Table 5.1.1 (Section 5.1.1). Silica undergoes reconstruction at alkaline pH values, with complete dissolution

occurring around pH 10.7 [94]. This catalyst preparation was essentially a compromise between achieving a high metal loading (ideally about 10 wt%), whilst minimising the effect of the alkaline solution upon the silica. The results indicate although an 6.31 wt% metal loading was achieved, which is comparable with the other three copper catalysts, a degree of reconstruction of the silica did occur.

5.1.4 Thermal analysis of catalysts

Details of the conditions applied during the thermal gravimetric analysis and differential scanning calorimetry experiments are given in Section 3.3.4. In summary, the former experiments were performed in a flow of 6 % H_2/N_2, whilst the latter were performed in flowing air. The results obtained by thermal gravimetric analysis for the four catalysts are summarised in Table 5.1.5. In addition to the figures reported, all of the samples exhibited a slow gradual weight loss above 250 °C. This may be attributable to dehydroxylation of the silica support or possibly baseline drift of the analytical technique, but was not deemed to be significant.

The decrease in mass below 150 °C is attributed to the loss of water from the catalysts; Cu(N)/Cab and Cu(N)/C-10 retain significant amounts of water following preparation, far more than is observed with the Cu(A)/Cab and Cu(C)/Cab catalysts. Mass losses recorded above 150 °C are attributed to the removal of the salts themselves. The overall decrease in the masses of these uncalcined catalysts is considerable. Table 5.1.6 shows the theoretical weight loss which is observed assuming that the salt material is completely removed during the treatment, and the actual percentage losses observed.

Table 5.1.5 Mass losses observed during thermal gravimetric analysis

Sample	Range of mass loss (°C)	Mass loss (%)	Total mass loss (%)
Cu(N)/Cab	50 - 150	24.2	
	150 - 200	2.8	
	200 - 250	4.7	31.7
Cu(A)/Cab	75 - 125	4.0	
	125 - 185	5.5	
	185 - 255	8.8	18.3
Cu(C)/Cab	50 - 150	3.2	
	150 - 265	2.3	5.5
Cu(N)/C-10	50 - 150	23.6	
	150 - 200	4.7	
	200 - 265	5.3	33.6
CuO(N)/Cab	180 - 260	2.1	2.1
CuO(A)/Cab	160 - 245	2.4	2.4
CuO(C)/Cab	190 - 270	1.6	1.6
CuO(N)/C-10	165 - 265	2.3	2.3

Table 5.1.6 Mass loss from removal of salt for the uncalcined catalysts

Catalyst	Actual weight loss (%)	Theoretical mass loss (%)
Cu(N)/Cab	7.5	14.4
Cu(A)/Cab	14.3	15.2
Cu(C)/Cab	2.3	6.3
Cu(N)/C-10	10.0	15.2

These results show that in each case the observed mass losses are lower than would be expected. This implies that reduction performed without prior calcination may leave organic residues on the catalyst surface. In addition, the Cu(C)/Cab should display an even greater decrease in weight, assuming that the carbonate ligands are also removed.

This has been observed previously by Jackson *et al*, using similar copper/silica catalysts prepared from cupric tetra-ammine [90]. They interpreted this lower than expected mass loss as indication that either the metal complex was incompletely reduced, or that the gas phase species formed on reduction were readsorbed on another component of the catalyst such as the support.

The data obtained with the calcined catalysts is less complex. No significant loss of mass was observed for any of these four samples, indicating that the calcination step effectively dries the catalyst as would be expected. The decreases in the sample masses above 160 °C are attributed to the reduction of copper oxide to copper metal, and the observed values correlate with the metal loadings of the different catalysts.

Samples of the Cu(A)/Cab catalyst were analysed using differential scanning calorimetry. The results are shown by Figure 5.1.2. The endothermic peak around 100 °C is assigned as the removal of water from the catalyst. The second endothermic transition between 181 and 191 °C is believed to be the loss of water from copper acetate hydrate to copper acetate *i.e.* $Cu(CH_3COO)_2.H_2O \rightarrow Cu(CH_3COO)_2$. Of greatest interest is the large exothermic peak around 260 °C, which is attributed to the combustion of the copper acetate to copper oxide, this feature showing a heat output of 170.7 J g^{-1}. These assignments have been made in conjunction with the results obtained via VTXRD (Section 5.1.5).

Figure 5.1.2 Differential scanning calorimetry of Cu(A)/Cab

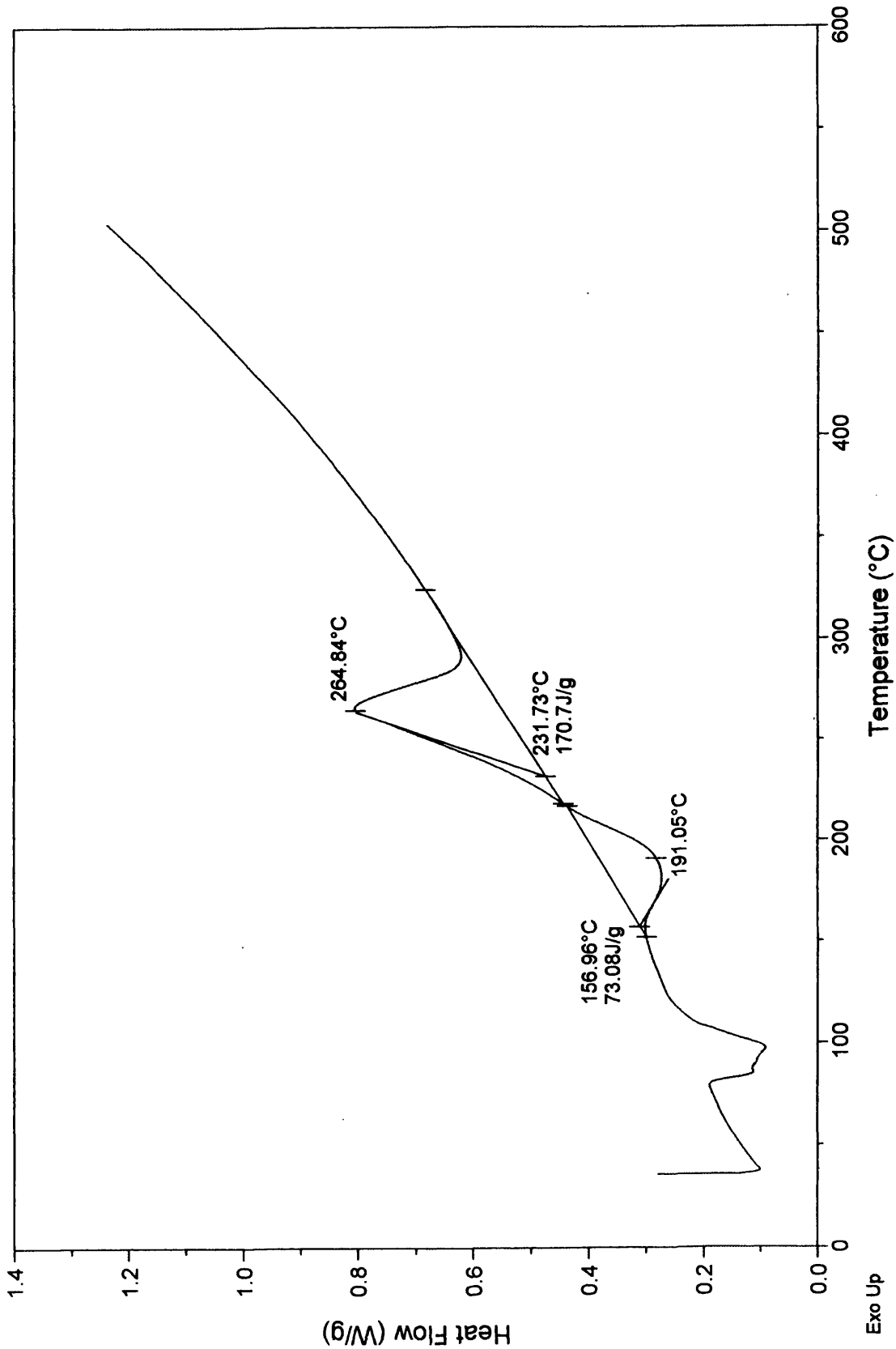

5.1.5 Variable Temperature X-Ray Diffraction (VTXRD)

The samples and applied conditions pertaining to the VTXRD studies are described in Section 3.3.5. Table 5.1.7 summarises the samples studied, the applied conditions and the figures which correspond to the results thereby obtained.

Table 5.1.7 Samples, conditions and results of VTXRD

Catalyst	Gas	Thermal treatment	Figures
(1) Cu(N)/Cab	4 % H_2/N_2	Ambient to 600 °C	5.1.3 (a, b, c)
(2) Cu(N)/Cab	4 % H_2/N_2	Ambient to 290 °C (held for 240 mins)	5.1.4 (a, b)
(3) Cu(A)/Cab	Air	Ambient to 500 °C	5.1.5 (a, b)

i) Cu(N)/Cab at 3° min^{-1} to 600 °C under 4 % H_2/N_2 (Figures 5.1.3 a, b & c)

At room temperature the sample was amorphous, presumably a mixture of silica and hydrated copper nitrate $Cu(NO_3)_2.xH_2O$. On heating from ambient to 190 °C the sample changed to a combination of amorphous material assigned as Cab-O-Sil silica and a crystalline phase of copper nitrate hydroxide, $Cu_2(NO_3)(OH)_3$. The amorphous material remained present throughout the experiment. At 215 °C a crystalline phase of tenorite, CuO, was identified, with no evidence of copper nitrate hydroxide. At 240 °C a crystalline phase of copper metal was identified, with some very small peaks of tenorite. These peaks of crystalline copper metal and residual CuO were present for the remainder of the experiment, up to 600 °C. The shift in peak positions is an effect of the elevated temperature; thermal expansion resulting in peak position movement.

ii) Cu(N)/Cab at 3° min^{-1} to 290 °C (held for 240 minutes) under 4 % H_2/N_2

(Figures 5.1.4 a & b)

The same species in the same pattern of evolution were detected as per (i). Crystalline copper metal and a small amount of residual tenorite were observed even after reduction at 290 °C for 240 minutes.

iii) Cu(A)/Cab at 3° min^{-1} to 500 °C, under air (Figures 5.1.5 a & b)

At room temperature the sample contained some amorphous material, assigned as Cab-O-Sil silica, with a crystalline phase identified as copper acetate hydrate, $Cu(CH_3COO)_2.H_2O$. As the sample was heated to 150 °C the hydrated copper acetate changed to copper acetate, $Cu(CH_3COO)_2$. Although the data does not match the reference patterns exactly, this is not unusual for organic type phases. At 200 °C the copper acetate intensity had diminished, but there was only a slight indication of the development of copper oxide, tenorite. By 225 °C the copper acetate had disappeared and the tenorite pattern was clearly strengthening. Further temperature increases saw the tenorite developing in crystallinity, and the peaks gradually becoming more intense and narrower.

One additional point regarding the VTXRD experiments requires highlighting. The diffraction pattern for each scan was collected over a 30 minute period, and so the increases in temperature are effectively conducted in stages. Since the processes occurring on the catalyst may well be kinetic, the transitions between the various species

when determined by VTXRD may appear to occur at relatively low temperatures when compared with other techniques, *e.g.* temperature programmed reduction. The actual nature of these species and the transitions between them, however, will remain constant.

In conclusion, the reduction of the Cu(N)/Cab sample proceeds from hydrated copper nitrate to a crystalline phase of copper nitrate hydroxide, $Cu_2(NO_3)(OH)_3$, this transition occurring by 190 °C. Upon reaching 215 °C this latter species has been converted to tenorite. This is in turn reduced to copper metal around 240 °C. The reduction of the catalyst is complete by 290 °C; higher temperatures or prolonged reduction times do not alter the species on the catalyst. The Cab-O-Sil silica support remains amorphous, up to 600 °C. These results can be summarised by Equation 5.1.1.

Equation 5.1.1

$Cu(NO_3)_2.xH_2O$		$Cu_2(NO_3)(OH)_3$		CuO		Cu^0 + [CuO]
	→		→		→	
Ambient		190 °C		215 °C		240 °C +

Bond *et al* when studying CuO/SiO_2 using temperature programmed reduction observed the existence of two forms of copper oxide on the catalyst surface [95]. The bulk of this metal oxide formed particles which did not interact strongly with the support, and could be reduced around 217 °C. A dispersed Cu^{II} species was also present which required 287 - 337 °C to achieve reduction. The present study observed that the bulk of the copper in the Cu(N)/Cab catalyst was reduced to copper metal by 290 °C, whilst a fraction of residual copper oxide remained on the catalyst regardless of treatment. This

data therefore shows that the applied reduction procedure produces a catalyst that consists predominantly of dispersed Cu^0 particles, but the additional presence of a small quantity of Cu^{II}. The reduced copper metal is believed to be the active phase of the catalysts.

The silica phase of the Cu(A)/Cab catalyst also remains amorphous during the course of the experiment. Initially, this sample features a crystalline phase of hydrated copper acetate which is converted by 150 °C to copper acetate. Upon reaching 200 °C oxidation of this species has commenced with the appearance of tenorite, this process reaching completion by 225 °C; higher temperatures show only the increasing crystallinity of the copper oxide phase. These results are summarised by Equation 5.1.2.

Equation 5.1.2

$Cu(CH_3COO)_2.H_2O$		$Cu(CH_3COO)_2$		$Cu(CH_3COO)_2$ + [CuO]		CuO
	→		→		→	
Ambient		150 °C		200 °C		225 °C +

The VTXRD treatment of the Cu(A)/Cab sample is equivalent to calcination, and is comparable with the DSC analyses of Section 5.1.4. The changes observed during this work indicates that the exotherm observed during DSC is attributable to the oxidation of copper acetate.

Finally, the temperatures reported for the transitions between the phases present on the catalyst, as determined by the VTXRD technique, may not necessarily agree exactly with the findings of other experimental methods, for the reasons described above.

Figure 5.1.3a VTXRD patterns of Cu(N)/Cab (60 - 179 °C)

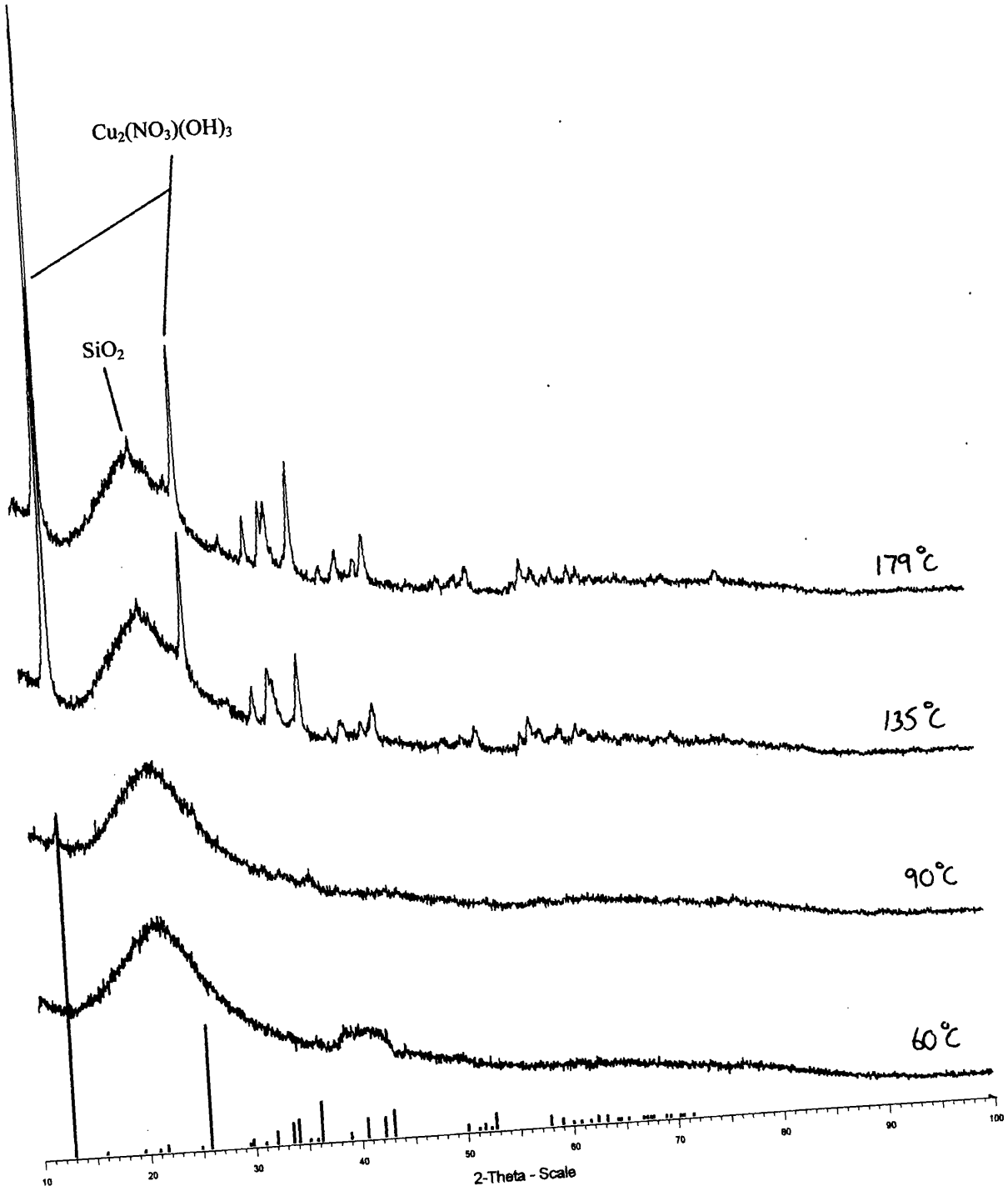

Figure 5.1.3b VTXRD patterns of Cu(N)/Cab (189 - 237 °C)

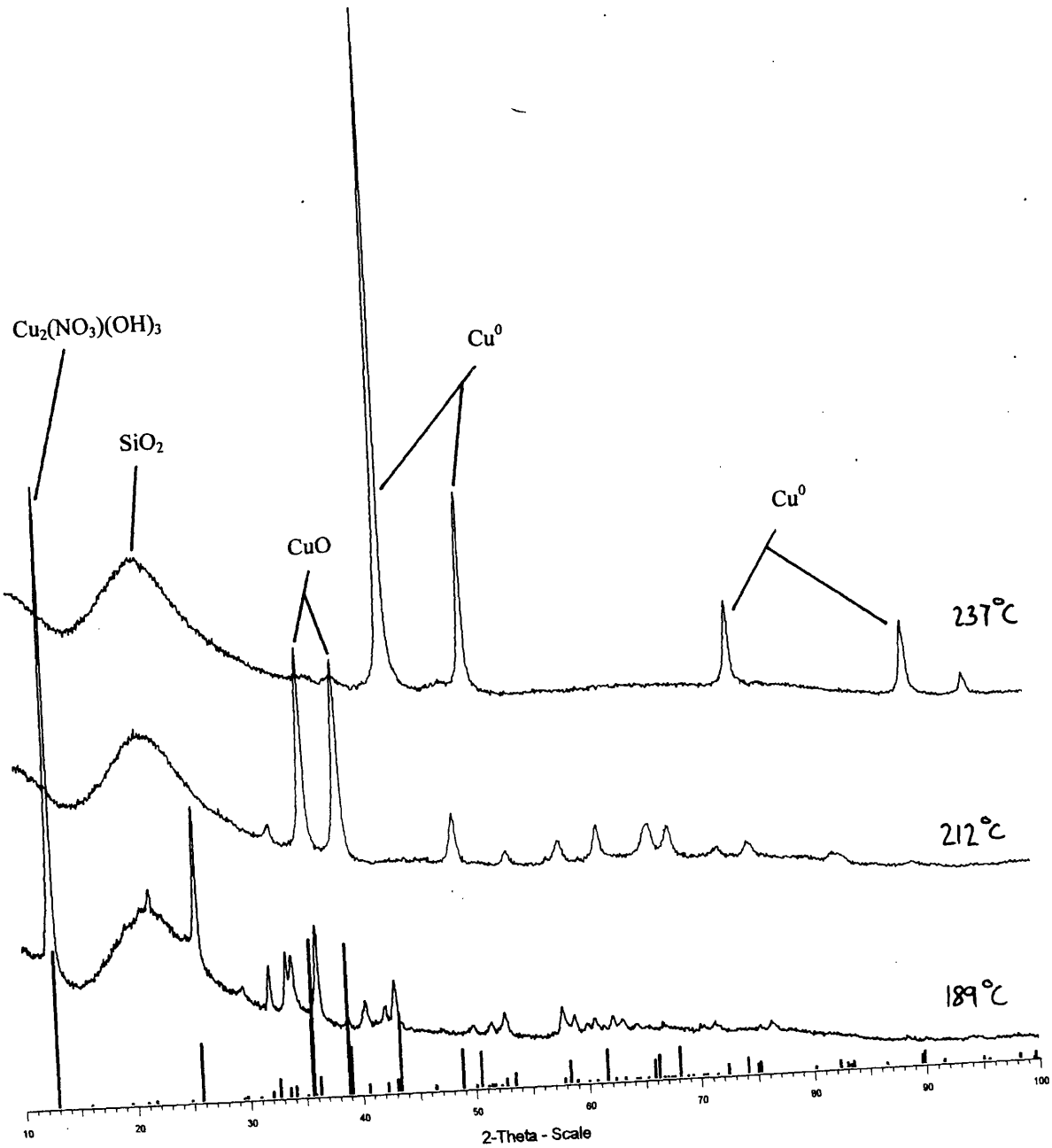

Figure 5.1.3c VTXRD patterns of Cu(N)/Cab (262 - 596 °C)

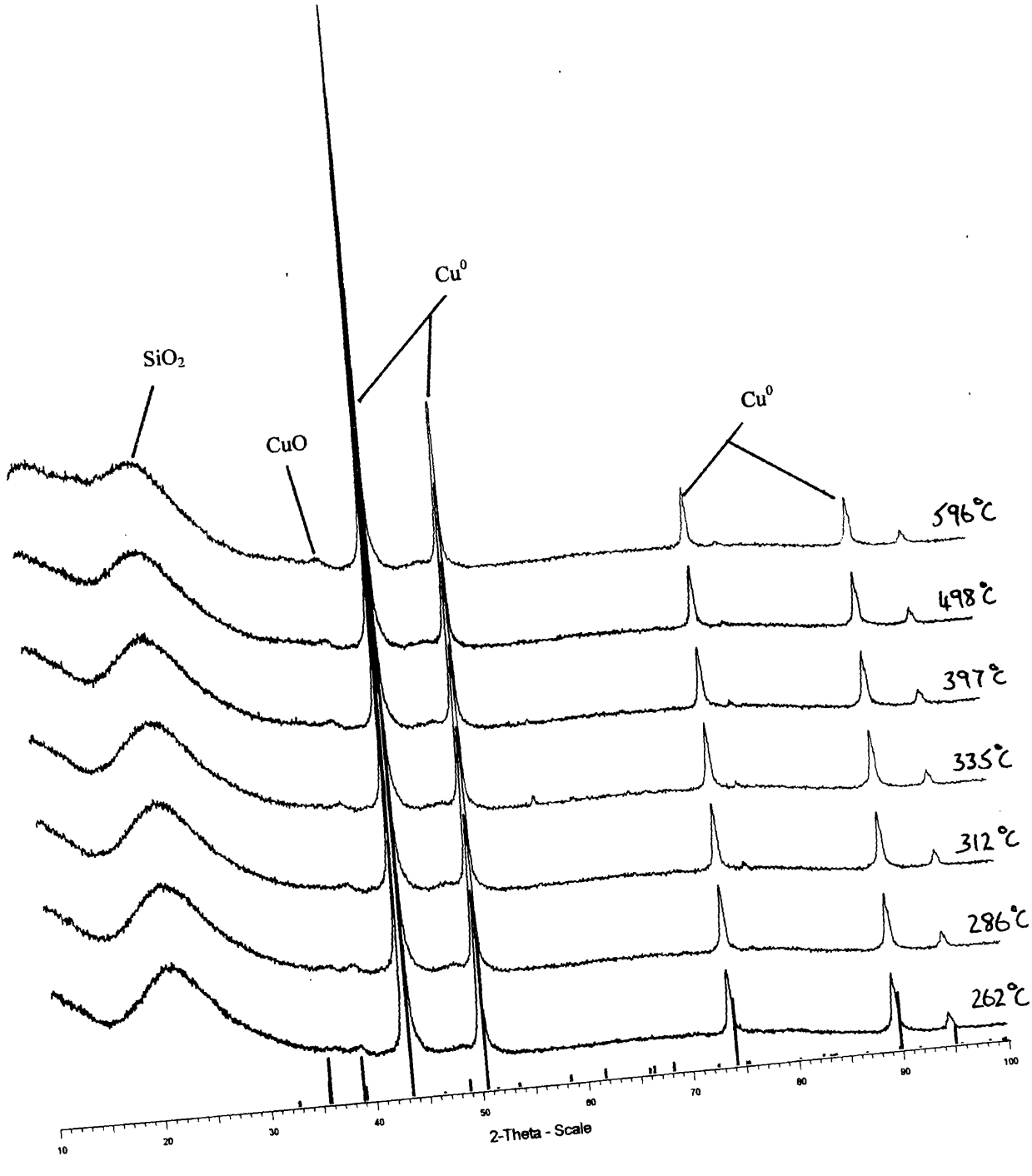

Figure 5.1.4a VTXRD patterns of Cu(N)/Cab (22 - 182 °C)

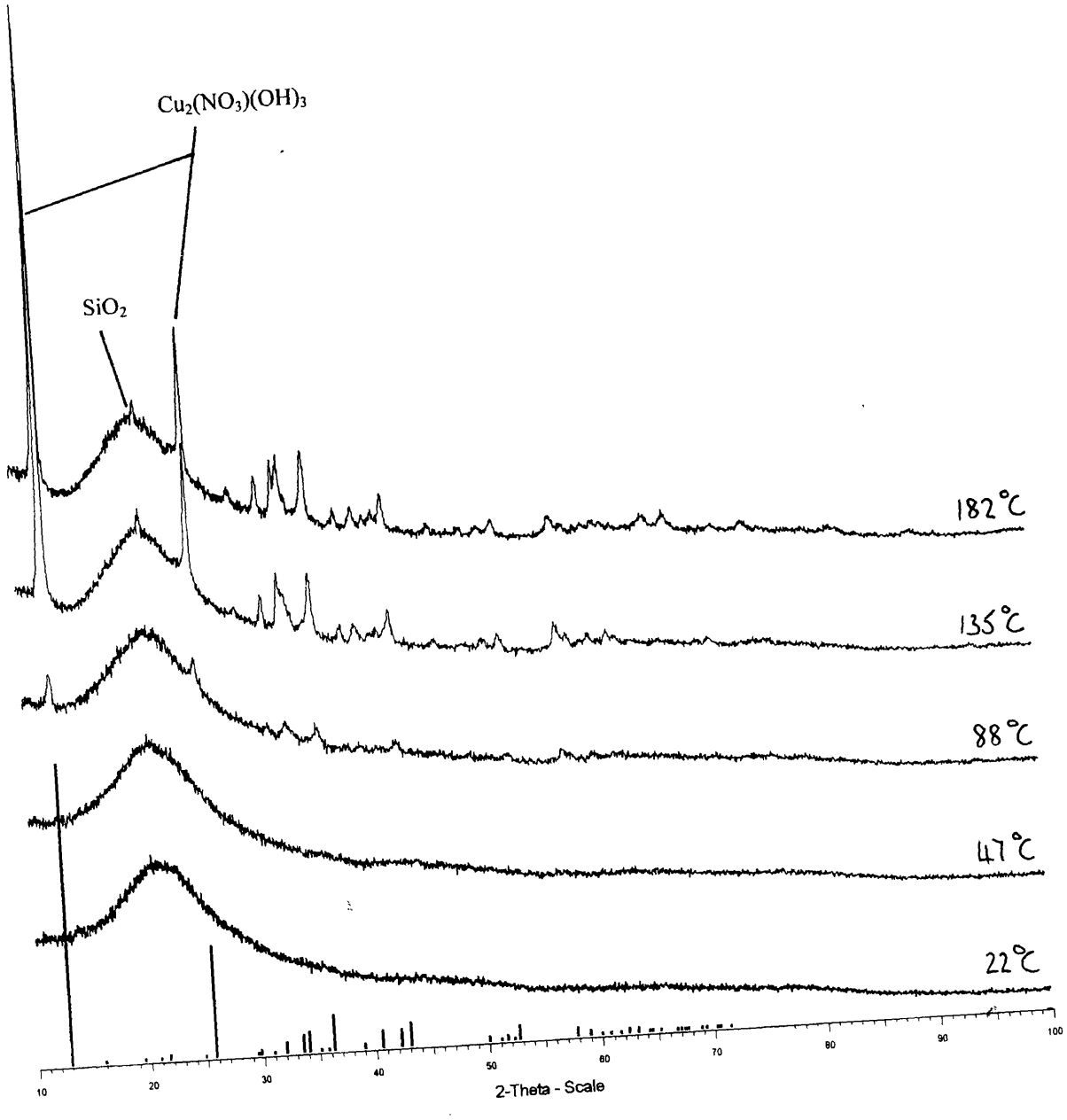

Figure 5.1.4b VTXRD patterns of Cu(N)/Cab (287 - 290 °C, at 0 to 240 minutes)

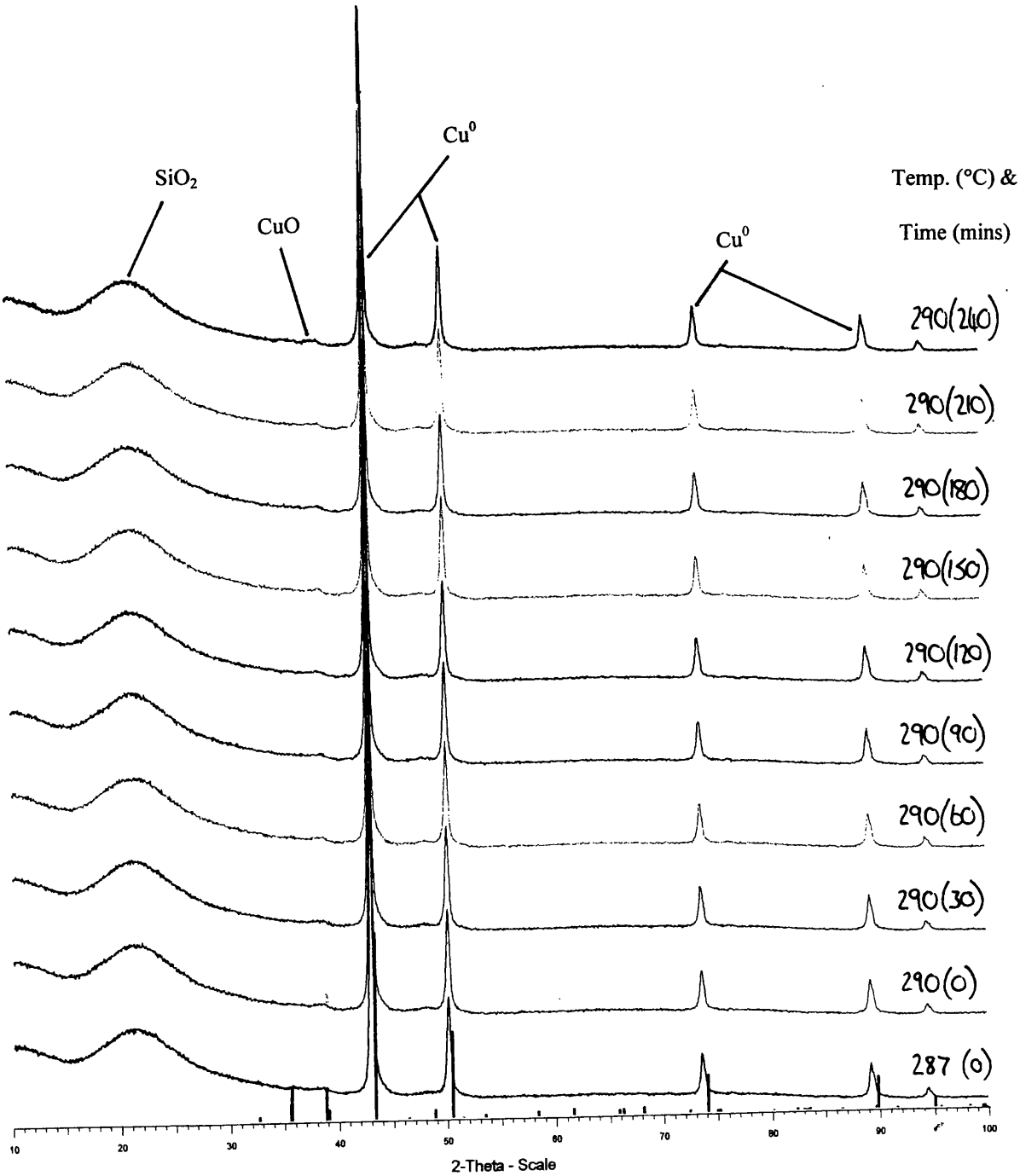

Figure 5.1.5a VTXRD patterns of Cu(A)/Cab (25 - 87 °C)

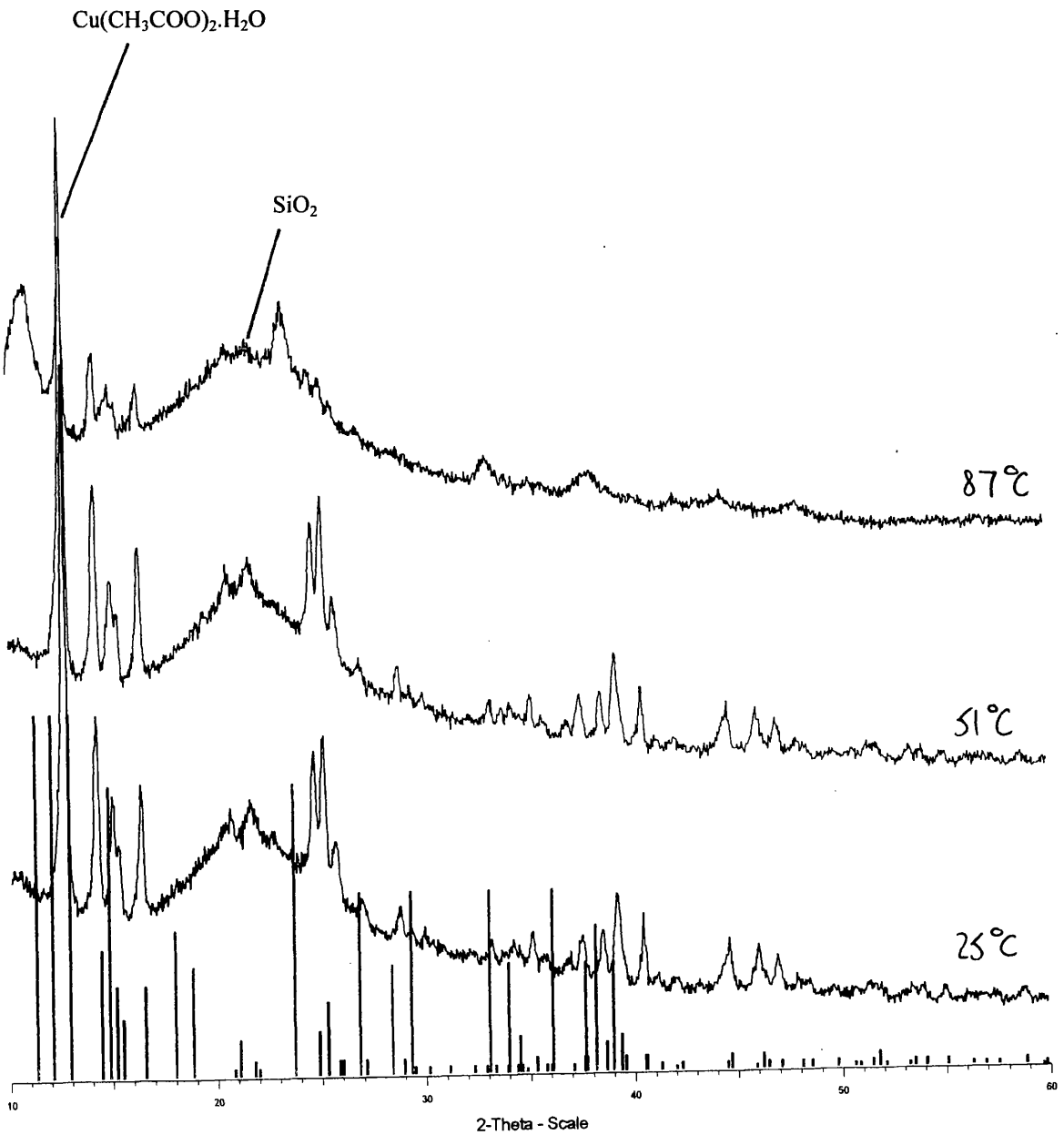

Figure 5.1.5b VTXRD patterns of Cu(A)/Cab (147 - 497 °C)

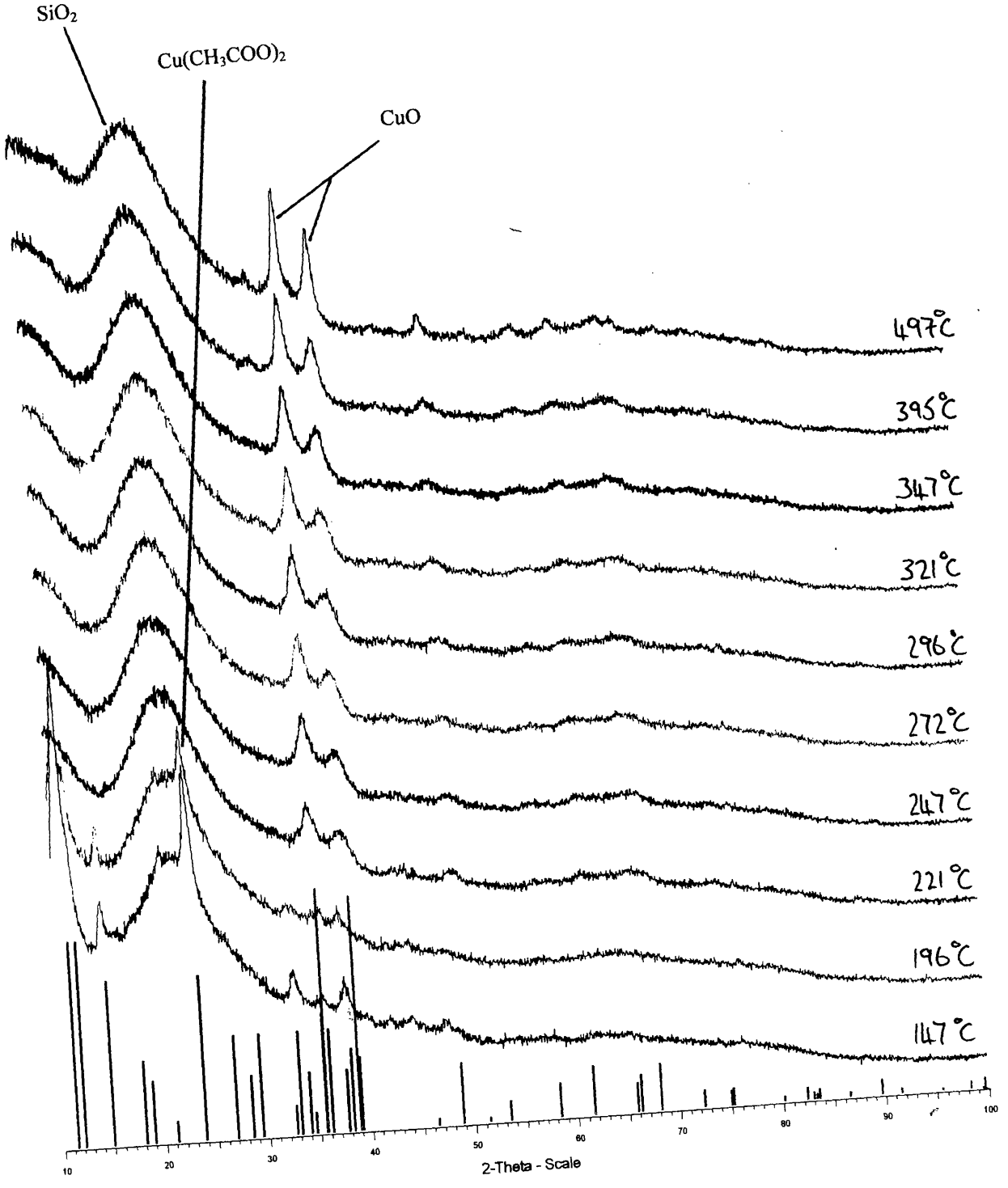

5.1.6 Temperature programmed reduction

Temperature programmed reduction (TPR) experiments were performed using the apparatus and technique described in Section 3.3.6. A summary of results when the catalysts are ramped at 3° min^{-1} is shown by Table 5.1.8, where T_{min}, T_{max} and T_{final} refer to the temperatures at which hydrogen uptake commences, peaks and terminates respectively. Figures 5.1.9 to 5.1.16 represent typical TPR profiles for each of the copper catalysts.

Table 5.1.8 Summary of the TPR profiles of the catalysts

Catalyst	T_{min} (°C)	T_{max} (°C)	T_{final} (°C)
Cu(N)/Cab	167.7	244.7	280.0
Cu(A)/Cab	142.3	232.3	355.3
Cu(C)/Cab	184.8	253.0	371.7
Cu(N)/C-10	172.7	247.3	278.7
CuO(N)/Cab	125.0	239.7	301.3
CuO(A)/Cab	115.7	208.3	298.7
CuO(C)/Cab	143.3	234.6	310.3
CuO(N)/C-10	126.2	233.8	354.0

Both of the nitrate-derived catalysts show the largest hydrogen uptakes, with single peaks centred about 245 °C. The TPR profile of Cu(N)/Cab is essentially symmetrical, and occurs over a narrow temperature range (Figure 5.1.9). The profile of the Cu(N)/-10 catalyst displays a shoulder following the T_{max} (Figure 5.1.12). This is attributed to an effect of the support, the result of diffusion through the pelleted C-10 silica, rather than a difference in the chemistry of the copper nitrate species. The copper

nitrate-derived species which are observed during the reduction step are reported in Section 5.1.5. Analyses by VTXRD showed staged transitions from copper nitrate to copper nitrate hydroxide to copper oxide, which was then reduced to copper metal by 240 °C. As stated previously, however, the ramp rates of the VTXRD experiments were halted in 30 minute stages during the acquisition of the diffraction patterns. TPR results presented in this chapter show only a single narrow maximum of hydrogen uptake over the same catalyst, which occurs at approximately 245 °C. It therefore appears that the reduction of copper nitrate to copper metal, via the various intermediates, occurs rapidly around 245 °C when the applied temperature is ramped continuously at 3 °C min^{-1}.

The TPR profile of the Cu(A)/Cab catalyst shows a relatively broad peak of hydrogen uptake centred around 232 °C (Figure 5.1.10). This is assigned as the reduction of copper acetate to copper metal.

The Cu(C)/Cab catalyst displays two peak maxima, at 253 and 290 °C. The largest peak, at the lower temperature, is assigned to the reduction of copper tetra-ammine, whilst the peak maximum at 290 °C is attributable to the reduction of the carbonate ligands of this complex.

Jackson *et al* conducted a study of copper/silica catalysts with similar precursors [90]. They used a wet impregnation technique to deposit copper nitrate on silica, with a metal loading of 4.2 wt%, and copper tetra-ammine on silica at 3.3 wt%. TPR was applied to study these catalysts without prior calcination. The applied ramp rate was 7 °C min^{-1}, determining the T_{max} values at 272 and 277 °C for the nitrate- and tetra-ammine-derived catalysts respectively. It is clear that the difference between the T_{max}

values of Cu(N)/Cab and Cu(C)/Cab is constant at 5 °C for the two studies, but that transitions observed during the current project occur at significantly lower temperatures. This is ascribed to the different thermal ramp rates applied by the two research groups, as higher ramp rates shift the observed peak maxima to higher temperatures [72].

As highlighted by Bond *et al* [95] comparisons of TPR results with the literature, is difficult for two reasons. Firstly, TPR measurements can vary greatly with the experimental system, and the applied ramp rate, starting temperature and reactor geometry are just a few of the factors which will influence the results. Secondly, the nature of the catalysts themselves may well be different. Different metal salts, supports, preparation methods and pretreatment will all affect TPR measurements. As a consequence, the reduction of CuO/SiO_2 has been reported to occur with one peak [70, 96, 97], two peaks [98, 99] and three peaks [100].

However, Bond [95] also shows that the T_{max} values of CuO/SiO_2 are remarkably similar; with most relevance to the current work were the findings of Robertson and co-workers, who reported a T_{max} value of 230 °C for a 10 wt% CuO/SiO_2 catalyst [70]. The results of Table 5.1.8 and Figures 5.1.13 to 5.1.16 show the TPR profiles of the calcined CuO/SiO_2 catalysts. It is clear that the T_{max} values recorded for the CuO(N)/Cab, CuO(C)/Cab and CuO(N)/C-10 samples at 240, 235 and 234 °C are in accordance with the literature [70]. CuO(A)/Cab exhibits a lower T_{max} value at 208 °C which could suggest that this catalyst has smaller metal particle sizes. This concept is not supported, however, by the electron microscopy results which are reported in Section 5.1.8. The peak maxima of the calcined catalysts are consistent with the reduction of $Cu^{II}O$ to Cu^0.

Figure 5.1.9 TPR profile of Cu(N)/Cab

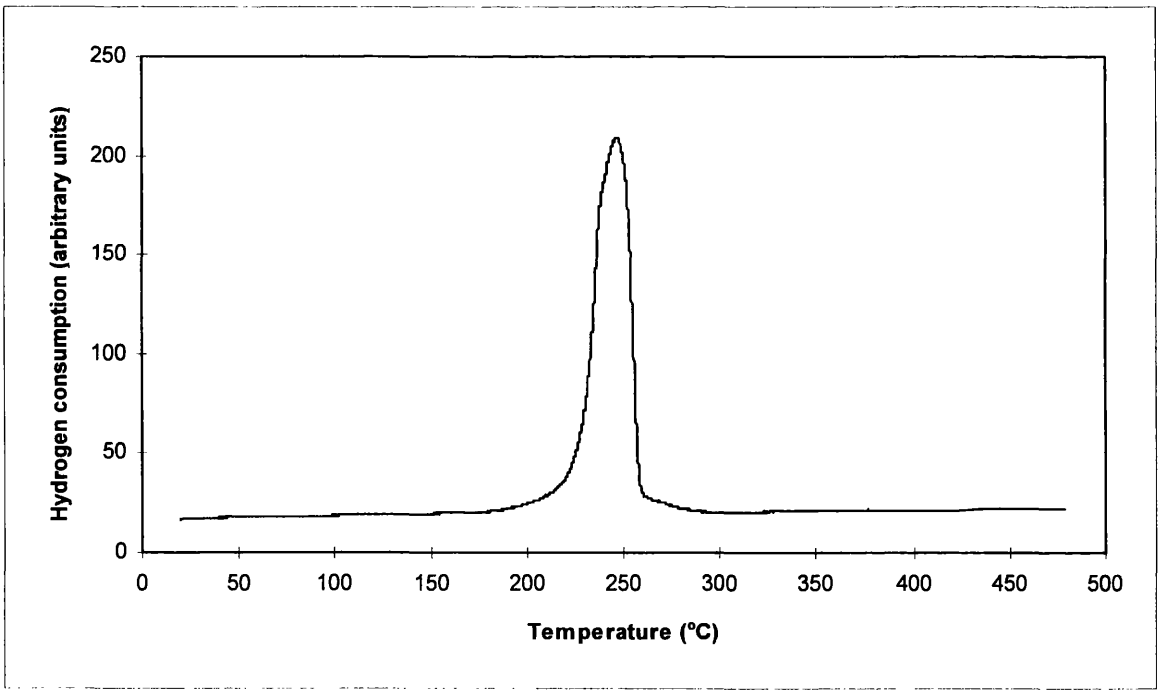

Figure 5.1.10 TPR profile of Cu(A)/Cab

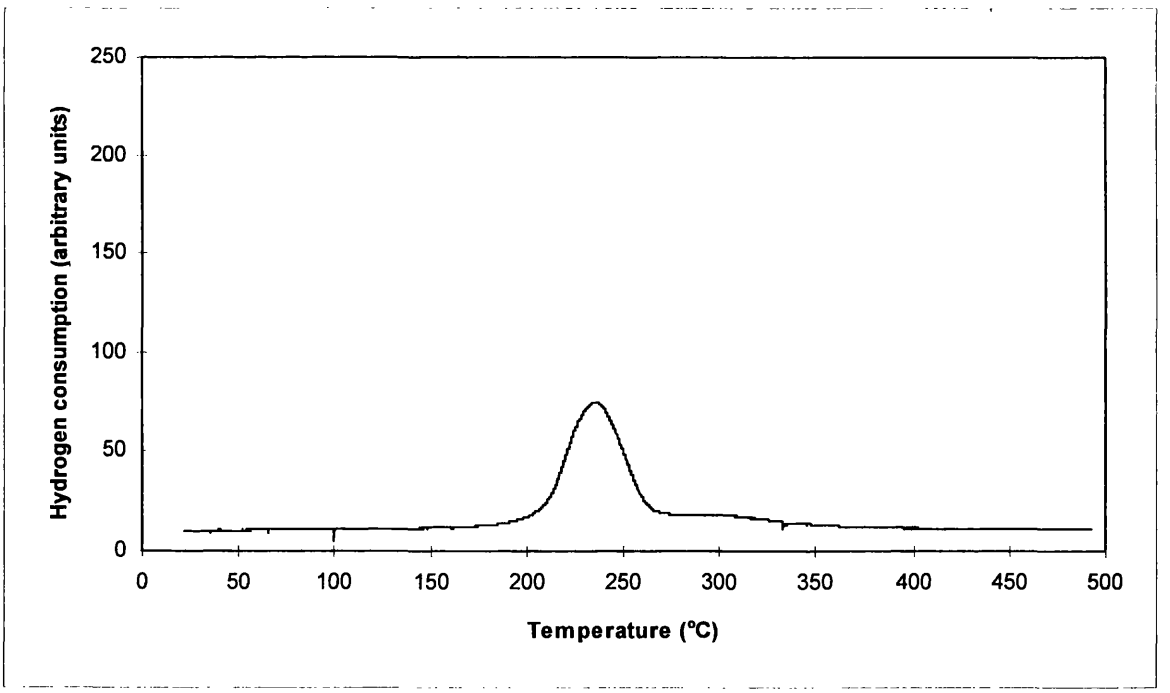

Figure 5.1.11 TPR profile of Cu(C)/Cab

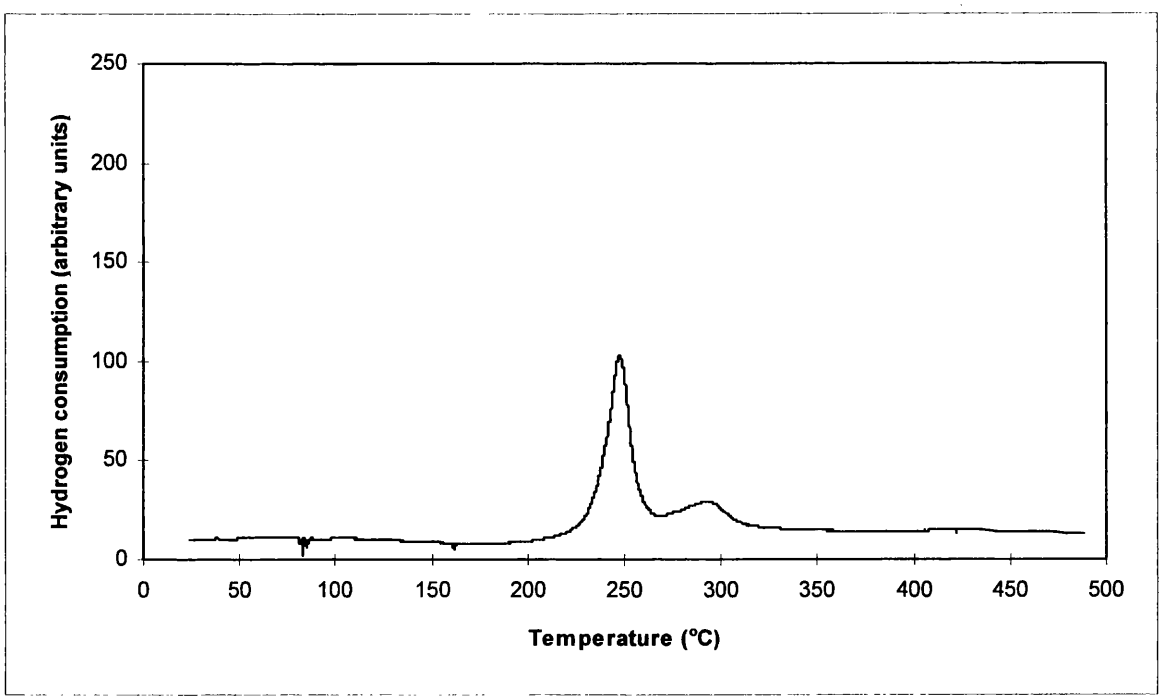

Figure 5.1.12 TPR profile of Cu(N)/C-10

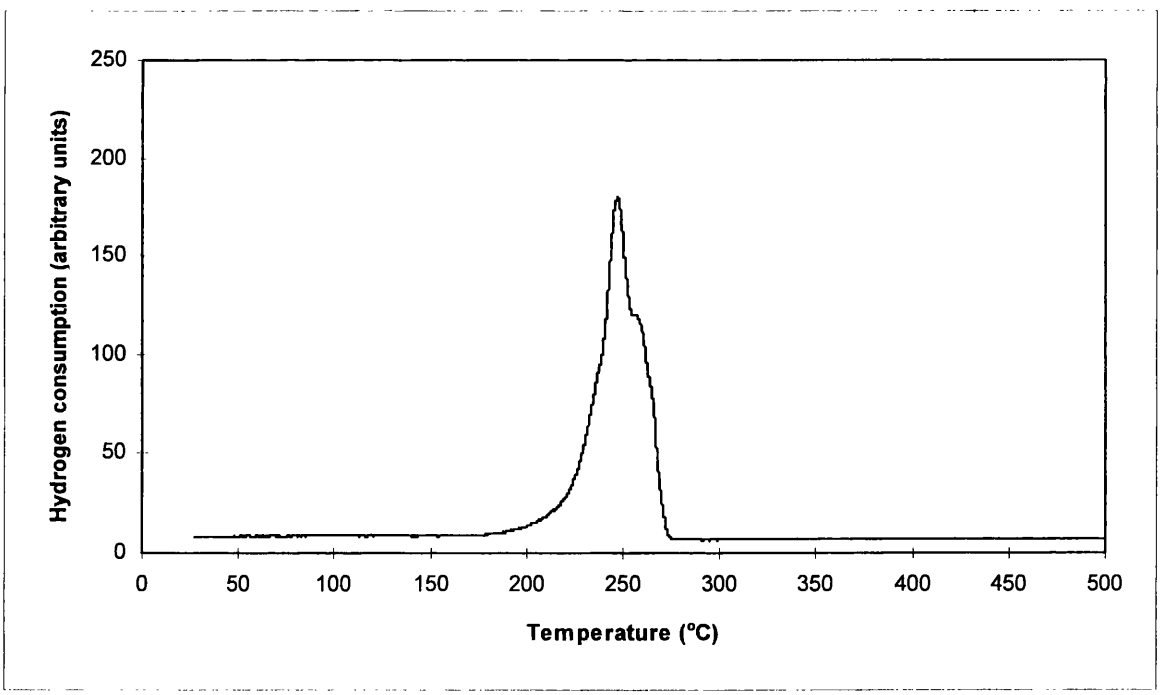

Figure 5.1.13 TPR profile of CuO(N)/Cab

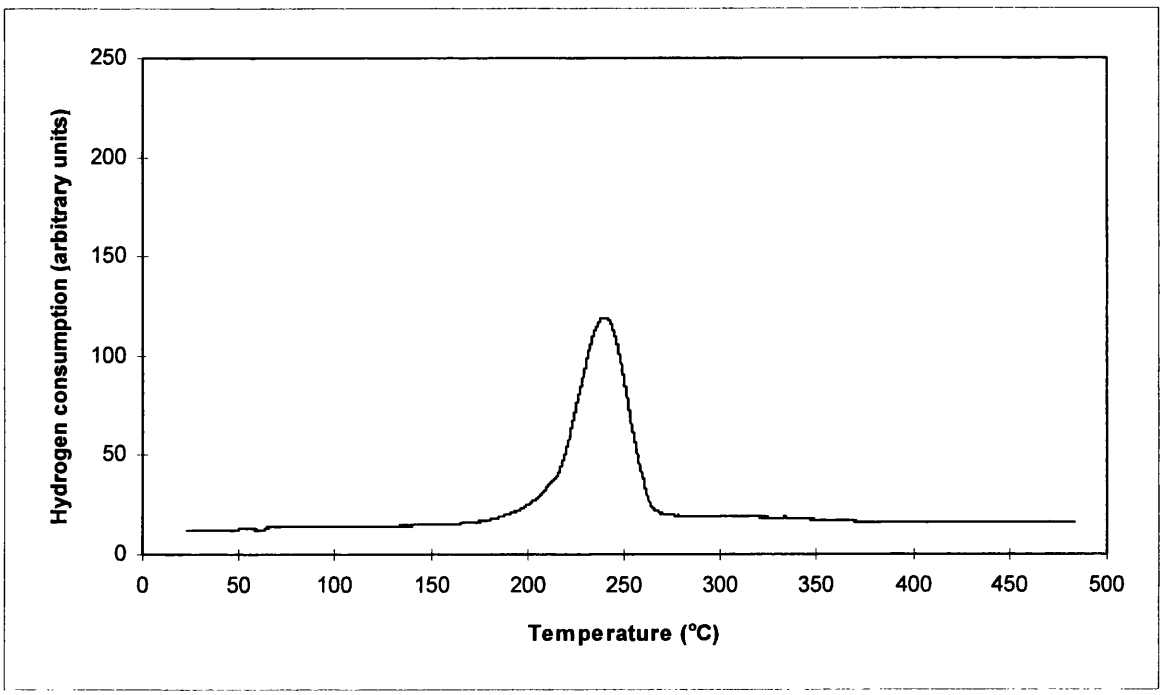

Figure 5.1.14 TPR profile of CuO(A)/Cab

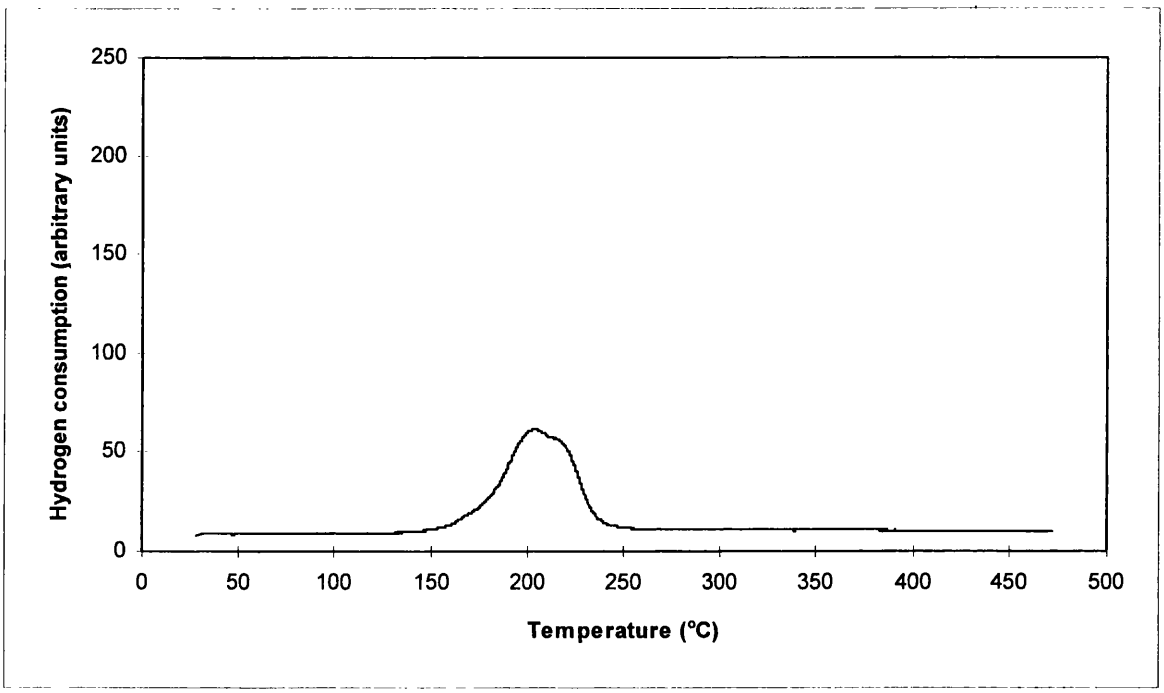

Figure 5.1.15 TPR profile of CuO(C)/Cab

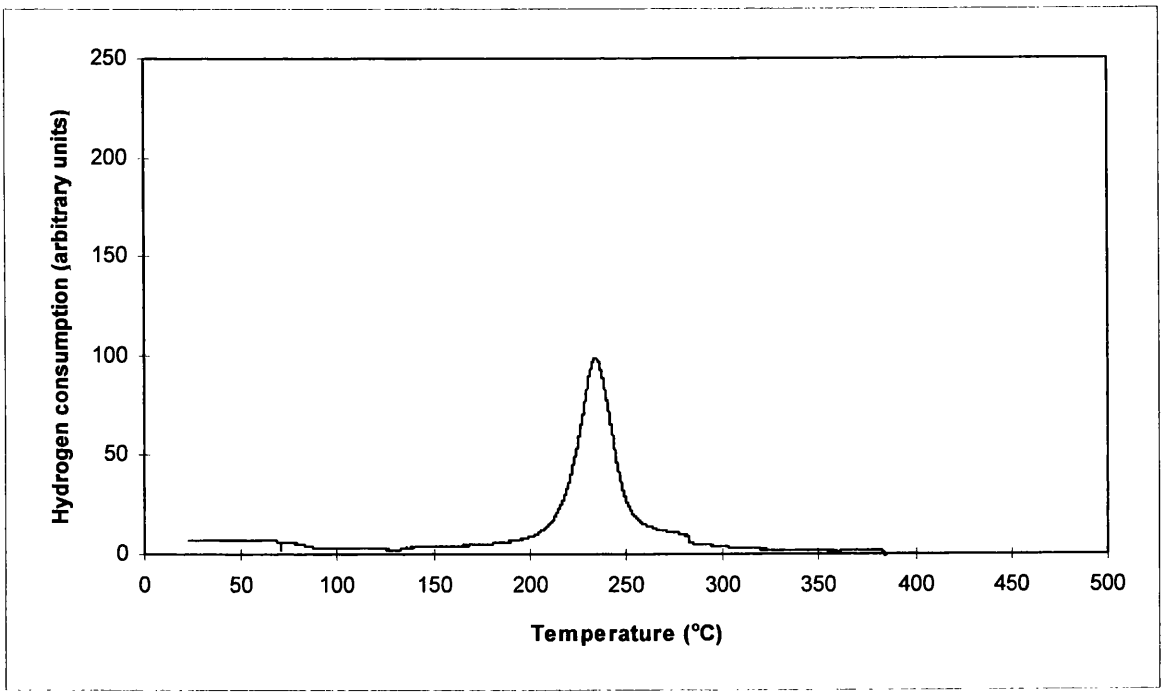

Figure 5.1.16 TPR profile of CuO(N)/C-10

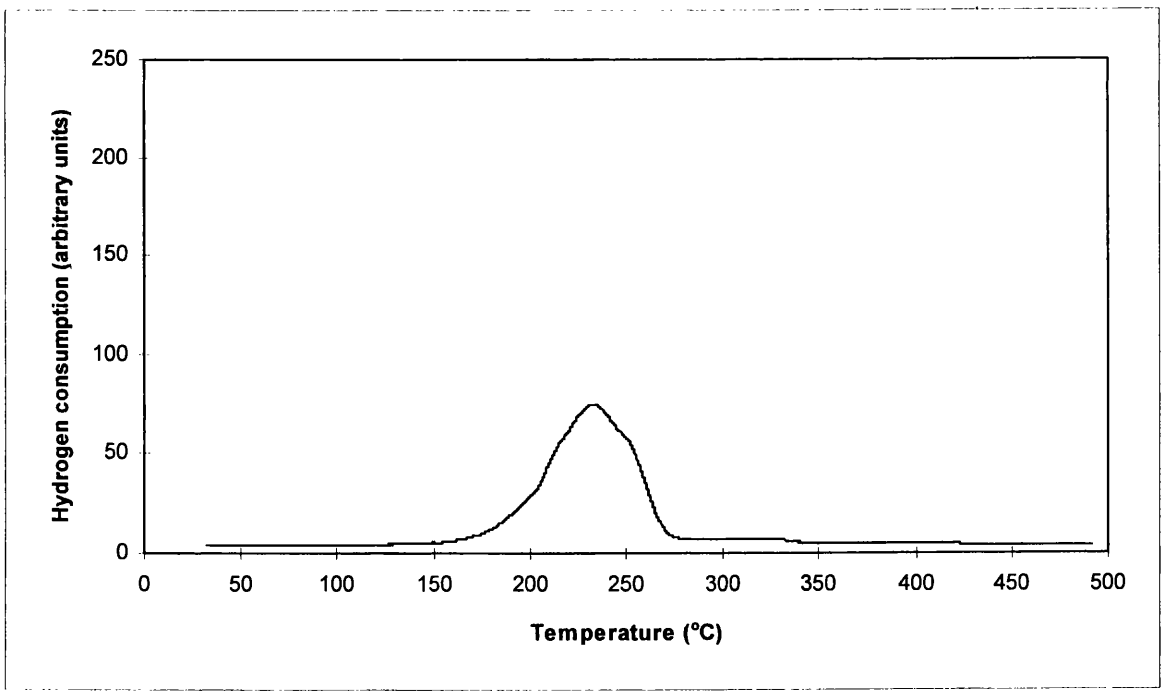

5.1.7 Nitrous oxide decomposition

The dispersion (D) and the copper metal surface area of the catalysts used in this study were measured by following the decomposition of nitrous oxide over the reduced catalysts. The average diameters of the metal crystallites were then calculated as described in Section 4.1. Cu(N)/Cab was selected as the benchmark catalyst of the series, as nitrates are comparatively simple to reduce and this is the precursor most commonly reported in the literature. A series of experiments varying the reduction conditions of this catalyst were conducted to optimise catalyst dispersion within a reasonable time frame (see Table 5.1.9 and Figure 5.1.17).

Table 5.1.9 Dispersion of Cu(N)/Cab catalyst under different reduction conditions

Ramp rate (° min^{-1})	$T_{red.}$ (°C)	Time at $T_{red.}$ under H_2/N_2 (mins)	Time at $T_{red.}$ under He (mins)	Dispersion (%)	Metal surface area (m^2 g^{-1})	Mean particle size (nm)
3	290	30	0	12.80	7.39	7.9
3	290	30	30	11.47	6.62	8.8
3	290	60	30	9.47	5.47	10.6
3	290	120	30	9.44	5.45	10.7
10	290	120	30	6.26	3.61	16.1
10	290	180	30	8.04	4.64	12.5
10	290	240	30	9.69	5.59	10.4
10	400	120	30	6.29	3.63	16.1
10	500	60	30	10.84	6.26	9.2
10	600	60	30	6.10	3.52	16.4

Figure 5.1.17 Metal surface area of Cu(N)/Cab catalyst reduced to 290 °C, varying ramp rates and time at $T_{red.}$

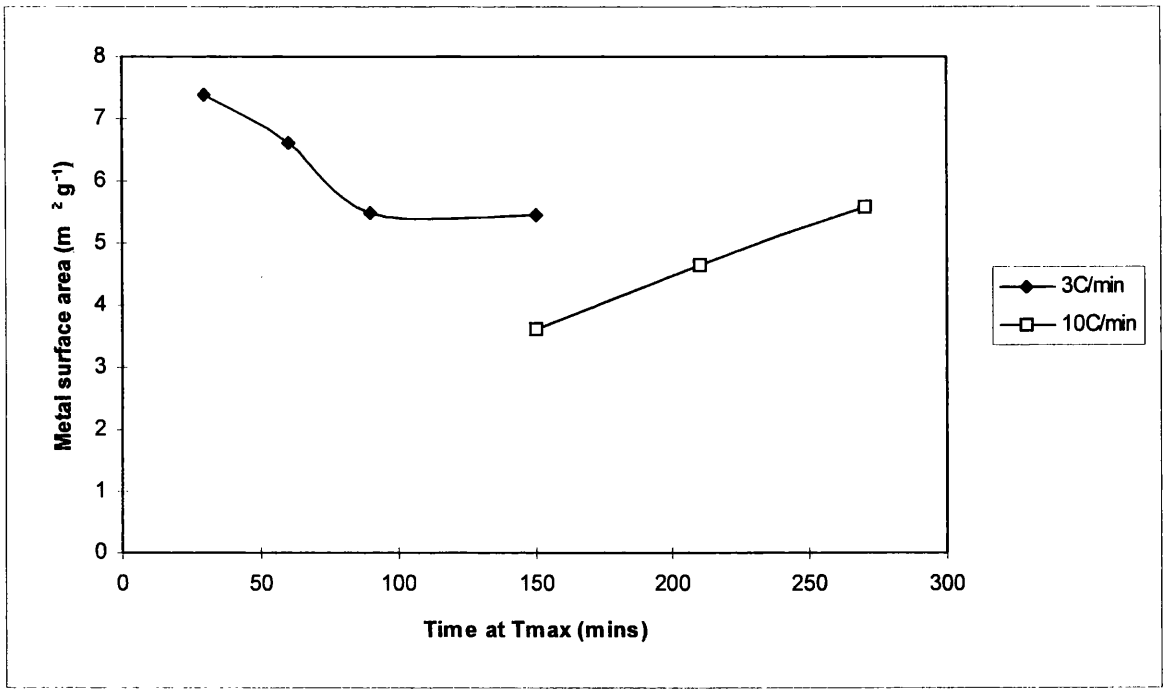

Higher temperatures and longer reduction times ensure a greater degree of catalyst activation, but provide the conditions required for agglomeration of the metal particles. When optimising the metal surface area, the activation step, therefore, is essentially a compromise between the extent of reduction and the degree of sintering. This is illustrated by the results in Table 5.1.9 and Figure 5.1.17.

Considering first the data obtained when ramping the temperature at 3 °C min^{-1} to 290 °C, it is evident that prolonging the time at $T_{red.}$ results in lower metal surface areas as the degree of sintering reduces the catalyst dispersion. The ramp rate itself is also of obvious importance, with the higher rate of 10 °C min^{-1} resulting in significantly lower metal surface areas. The catalyst reduction is exothermic, and as the ramp rate is raised

the resultant exotherm becomes sharper; this heat output is localised around the metal particles and enhances their mobility further.

However, having reduced samples at 10°C min^{-1} to 290 °C it is observed that prolonged reduction times result in improved metal surface areas; the degree of reduction offsets that of the sintering process. This conclusion indicates that complete reduction had yet to be achieved, and the calculated values of mean particle size therefore represent an upper limit; increasing the temperature or time taken for reduction should not, of course, decrease the size of the metal crystallites. Finally, it is apparent that the metal surface area improves substantially if the $T_{red.}$ is raised to 500°C, but that the metal surface area drops once more if this temperature is increased to 600 °C.

It is therefore believed that (at least) two forms of copper exist on the precursor - an 'easily' reducible copper species which comprises the bulk of the metal and will form Cu^0 by 290 °C, and a finely dispersed copper species which requires more extreme conditions to activate. In support of this concept are the results obtained via VTXRD (Section 5.1.5) indicate the presence of copper oxide which resists reduction up to 600 °C.

In view of these factors, and attempting to keep the overall activation time to a minimum, it was decided that the four catalysts would be reduced at 3 °C min^{-1} to 290 °C, and held at this temperature for 60 minutes under the dihydrogen/dinitrogen mixture, and then 30 minutes under helium. The results obtained are shown in Table 5.1.10. This reduction treatment was also adopted for the calcined forms of the catalysts, as nitrous

oxide experiments revealed that the period of time spent at 290 °C under the reductive gas mix made little difference to the ultimate metal surface area (see Table 5.1.11).

Table 5.1.10 Dispersions, metal surface areas & average particle size of the catalysts

Catalyst	Dispersion (%)	Metal surface area ($m^2 g^{-1}$)	Mean particle size (nm)
Cu(N)/Cab	9.47	5.47	10.6
Cu(A)/Cab	2.87	1.87	35.1
Cu(C)/Cab	6.04	2.56	16.6
Cu(N)/C-10	6.12	3.78	16.8

Table 5.1.11 Dispersions, metal surface areas & average particle size of CuO(N)/Cab when varying the time at $T_{red.}$

Time held at $T_{red.}$ under H_2/N_2 (mins)	Dispersion (%)	Metal surface area ($m^2 g^{-1}$)	Mean particle size (nm)
30	1.68	0.97	59.6
60	1.62	0.94	61.6
90	1.71	0.99	58.4
150	1.68	0.97	59.6

As the loading of the four catalysts varied between 6.31 and 9.68 % (see Section 5.1.2), the most appropriate comparison between them is against their dispersions. Many factors will affect the final dispersion of each catalyst, *e.g.* metal loading, type of silica used, precise conditions during preparation, the exotherm magnitude during reduction, *etc.* With regard to the copper nitrate-derived catalysts, Cu(N)/Cab and Cu(N)/C-10 have dispersions of 9.47 and 6.12 % respectively. Use of the pelleted C-10 support, therefore,

resulted in a lower catalyst dispersion. The preparations of these two catalysts were effectively identical, and it is possible that during catalyst preparation the metal salts gather in the pores of the C-10 silica, and consequently form larger copper particles.

However, it seems that the predominant factor is the nature of the metal salt following the drying step. The nitrate-derived catalysts have the largest metal surface area following direct reduction, whilst the catalysts which incorporate carbon on the catalyst surface have the lowest metal surface areas. It was therefore concluded that the ease with which the metal complex is reduced under hydrogen largely determines the final dispersion.

The metal salts which are introduced during the impregnation stage of catalyst preparation can be removed by calcination. In this way the metal complexes can be removed, and conversion to the metal oxide achieved, but care is required to avoid excessive sintering of the metal particles [3b]. This phenomena is illustrated by the results of Table 5.1.11, whereby the approximate metal surface areas of the CuO(N)/Cab samples upon reduction are just 1.0 $m^2 g^{-1}$.

The Cu(N)/Cab catalyst exhibited the largest metal surface area, and hence was chosen as the 'benchmark' catalyst. Furthermore, this catalyst showed increased metal surface area when the time at $T_{red.}$ under dihydrogen/dinitrogen is limited to 30 minutes. For the majority of reaction testing using this precursor, it was advantageous to limit the time at $T_{red.}$ under H_2/N_2 to 30 minutes, thereby obtaining an improved dispersion in less experimental time. In addition, selected reduction profiles shown in Table 5.1.9 would be employed to control the metal surface area of the Cu(N)/Cab catalyst, to determine the

effect of this variable upon reaction rates (see Section 5.3.5). To avoid ambiguity the activation conditions used in any series of experiments have been described as appropriate.

Finally, it is interestingly to compare the copper metal surface areas obtained in the present study with those obtained by other authors. Table 5.1.12 presents a review of such metal surface areas for copper/silica prepared by different methods and at different metal loadings. It is clear that the catalysts prepared by ion-exchange exhibit the largest metal surface areas, and that the catalysts used in this study are respectable in comparison with others prepared by impregnation. In summary, whilst the Cu(N)/Cab catalyst provides a workable metal surface area with regard to the reaction testing, it is quite possible to improve the performance of copper catalysts towards nitrobenzene hydrogenation.

Table 5.1.12 Comparison of copper/silica metal surface areas

Author	Preparation method	Metal loading (wt%)	Metal surface area (m^2 g^{-1})
Kohler *et al* [96]	Ion-exchange	9.5	33.4
Clarke *et al* [101]	Ion-exchange	7.0	18.2
Kohler *et al* [102]	Ion-exchange	6	15
Present study, Cu(N)/Cab	Impregnation	8.6	6.6
Bond & Namijo [79]	Deposition-precipitation	5.6	5.2
Koeppel *et al* [103]	Deposition-precipitation	6.5	4.1
Chambers *et al* [65]	Impregnation	12.4	2.2
Bond & Namijo [79]	Impregnation	4.3	1.4
Chambers *et al* [65]	Impregnation	5.6	0.53

5.1.8 Transmission electron microscopy

Batches of the uncalcined copper catalysts were prepared under different reduction treatments. A summary of the samples analysed by transmission electron microscopy (TEM) is presented in Table 5.1.13. Particle size distributions were calculated for the Cu(N)/Cab catalyst under the reduction treatments which are labelled i), ii) and iii). TEM was similarly employed to assess the effects of the different calcination methods described in Section 3.4.2. The samples of CuO(A)/Cab obtained via these different pretreatments are shown by Table 5.1.14.

Table 5.1.13 Summary of samples analysed by TEM

Catalyst	Ramp rate (°C min^{-1})	$T_{red.}$ (°C)	Time at $T_{red.}$ under H_2/N_2 (mins)	Time at $T_{red.}$ under He (mins)
Cu(N)/Cab (i)	3	290	30	0
	3	290	30	30
	3	290	60	30
	3	290	120	30
(ii)	10	290	120	30
	10	290	180	30
(iii)	10	290	240	30
Cu(A)/Cab	3	290	60	30
Cu(C)/Cab	3	290	60	30
Cu(N)/C-10	3	290	60	30

Table 5.1.14 Samples of CuO(A)/Cab analysed by TEM

Catalyst	Bed type	Flow rate (ml min^{-1})
CuO(A)/Cab	Fixed	50
CuO(A)/Cab	Fixed	500
CuO(A)/Cab	Fluidised	500

All of the samples studied exhibited particles of crystalline copper metal on the amorphous silica supports, both of these species being stable under the electron beam. A large range of particle sizes was observed, from 900 nm down to the resolution of the microscope (< 1 nm).

The presence of material which was not stable under the electron beam was also observed for the samples reduced without prior calcination. This was attributed to metal complex deposited during catalyst preparation, *e.g.* copper nitrate, copper acetate, *etc.*, which was not removed during the activation procedure. The nature of the complex material varied with the thermal treatment experienced by the sample. This phenomenom is displayed by Figure 5.1.18, and by Figure 5.1.19. The former micrograph is of Cu(N)/Cab (i) following the mildest reduction, and the crystalline nature of the copper nitrate complex is clear. This somewhat selective view of the catalyst surface focusses exclusively on the complex material; it should be noted that the majority of this sample displayed a mixture of silica, copper particles and the metal complex. The latter micrograph, Figure 5.1.19, shows the same catalyst under the most severe reduction conditions. Whilst the metal complex is still observed, its structure is less defined and the presence of the metal particles is more apparent. The copper crystallites are located mainly, but not exclusively, on the complex material. In general, longer times at the $T_{red.}$

temperature did decrease the amount of complex present on the catalyst, but the reduction of this material does not reach completion. This is a somewhat surprising result, given the sharp TPR profiles reported in Section 5.1.6, which indicated that reduction proceeded to completion over a narrow temperature range.

All of the uncalcined catalysts displayed regions of metal complex, and with a large range of particle sizes. This is illustrated by Figures 5.1.20 a), b) and c). This sequence of micrographs of the Cu(A)/Cab sample uses dark field as well as bright field techniques. These micrographs show the range of crystallite sizes observed. Figure 5.1.20a also illustrates the presence of the copper acetate complex, as defined by the distinct edges of the large particle/cluster in the central portion of the micrograph.

The presence of these relatively large areas of metal complex suggests that the copper salt was deposited in large clusters during the preparation stage, rather than being uniformly dispersed over the silica support. The metal particles of the catalysts, reduced without prior calcination, were located predominantly on the areas of complex material. The inhomogeneous nature of the catalyst preparations therefore limited the maximum metal surface areas which could be obtained upon catalyst activation. One beneficial avenue of future work, therefore, would be to attempt to disperse the metal salt more evenly across the support material during the slurry stage.

The particle size distributions calculated for the Cu(N)/Cab i), ii) and iii) samples are shown by Figure 5.1.21. In this series, the diameters of the particles were measured in nanometers and summed in 2 nm groups, *i.e.* ≤ 2 nm, >2 - 4 nm, >4 - 6 nm, *etc.* The value

quoted for 30 nm represents the percentage of the observed particles which were 30 nm in diameter or more, and it should be noted that this includes particles up to 900 nm.

It is clear from Figure 5.1.21 that the Cu(N)/Cab catalyst exhibits a large range of particle sizes, but that the different reduction treatments do not significantly affect these distributions. Measured diameters ranged from approximately 1 nm to 862 nm. Whilst the crystallites sizes are predominantly below 10 nm, approximately 5 % of the observed particles are at least 30 nm in diameter. A definitive average value is therefore difficult to obtain. The mode of the three samples is approximately 4 nm, but this approach neglects the larger crystallites which account for a considerable amount of the copper metal loading. The mean value, however, is distorted by the presence of the large crystallites which ultimately bear little effect upon catalyst activity due to the low metal surface area which they provide to adsorbates. The modal and mean values of the Cu(N)/Cab samples with respect to the mean calculated via nitrous oxide decomposition are discussed below.

Samples of Cu(A)/Cab calcined under different conditions were also analysed using TEM. Representative micrographs for the CuO(A)/Cab Fl.Bed^{500} and CuO(A)/Cab Fixed^{50} are shown by Figures 5.1.22 and 5.1.23 respectively. The electron micrographs of the calcined CuO(A)/Cab samples did not reveal the presence of copper acetate. This indicates that the calcination step, regardless of the technique employed, is sufficient to combust the organic material and leave particles of 'clean' copper oxide on the catalyst surface.

The dimensions of these catalyst particles depended on the applied conditions of the calcination treatment. The particle size distributions calculated for these two samples are shown by Figure 5.1.24. As explained previously, the measured particles have been grouped into 2 nm sets, whilst the value quoted at 50 nm represents the percentage of the metal crystallites which were at least 50 nm in diameter; this includes particles up to 700 nm. No obvious concentrations of particles of a given size are apparent within the upper ranges, and so Figure 5.1.24 does provide representative particle size distributions for these samples. It is recognised, however, that the $\geq$ 50 nm group accounts for a significant proportion of the copper present in the catalyst.

It is clear from Figure 5.1.24 that the nature of the calcination step bears marked effect upon the size of the copper crystallites, and that both of the samples display a large range of particle diameters. The modal value of the CuO(A)/Cab Fl.bed^{500} sample, however, is 2 nm whilst that of the fixed bed calcination is 8 nm. The percentage of observed particles larger than 50 nm is also revealing, at 13.3 and 18.0 % for the CuO(A)/Cab Fl.Bed^{500} and CuO(A)/Cab Fixed^{50} samples respectively. As these samples originated from the same batch of Cu(A)/Cab it was concluded that the different particle size distributions arise as metal particle sintering is increased during calcination as a fixed bed. In support of this concept are the micrographs of the two samples, Figures 5.1.22 and 5.1.23, where it is apparent that the larger particles of copper oxide are formed from the agglomeration of smaller crystallites. The mobility of the copper crystallites is therefore assumed to be higher during calcination as the fixed bed, which results in the formation of larger crystallites and an overall loss of metal surface area.

The particle size distributions of all of the catalysts studied exhibited 'tails' out to large diameters. However, no evidence of bimodal distribution was observed, and in all cases the overall picture was one of an approximate Gaussian distribution skewed to higher values.

When comparing the metal particles sizes determined by TEM and chemisorption experiments, the deficiencies of the two techniques should be considered. Using TEM the diameters of the metal particles may be measured accurately down to 1 nm. However, any metal crystallites which are below the level of resolution of the instrument (ca. 1 nm) will remain undetected, and such small particles may provide considerable metal surface area, with a corresponding significance to catalyst activity. Furthermore, the accuracy of a particle size distribution determined by TEM relies on obtaining a representative sample population. Chemisorption experiments measure the actual metal surface area available to an adsorbate, and therefore enable a valid evaluation of a catalyst's catalytic behaviour. However, the mean particle sizes calculated from chemisorption data relies on the assumption that the crystallites are of an idealised shape, and are contained within a narrow size range. This is clearly not the case for the copper catalysts studied in this work.

A comparison of the metal particle sizes determined by TEM and calculated from nitrous oxide chemisorption data is shown by Table 5.1.15.

Table 5.1.15 Metal particle sizes as determined by TEM and N_2O decomposition

Catalyst	Mode via TEM (nm)	Mean via TEM (nm)	Calculated mean via N_2O (nm)
Cu(N)/Cab i)	4	18.8	7.9
Cu(N)/Cab ii)	2	5.8	16.1
Cu(N)/Cab iii)	4	10.4	10.4
CuO(A)/Cab Fixed^{50}	8	33.3	22.6
CuO(A)/Cab Fl.Bed^{500}	2	31.5	13.1

This table displays the discrepancies between the two techniques. The modal values measured by TEM are significantly lower than the calculated average diameters derived from nitrous oxide decomposition data. The mean values calculated from TEM measurements, however, are generally higher than those obtained via nitrous oxide decomposition, which is attributed to the disproportionate effect exercised by the larger particles. In addition, the higher values derived via TEM may arise as this technique fails to account for the smallest particles which are accessible by chemisorption. The two techniques should therefore be considered as complementary but not directly comparable, *i.e.* chemisorption experiments provide accurate information on the metal surface area of a catalyst but unreliable data regarding the sizes of its metal particles, and vice versa for electron microscopy. In essence, during catalyst characterisation the two techniques are 'different pieces of the jigsaw'.

In summary, all of the catalysts studied exhibited a large range of particle sizes, from 1 nm, up to 900 nm in extreme cases. It was found that the metal salt was not

deposited uniformly across the silica support during the preparation stage, which will ultimately limit the metal surface areas which are achievable upon activation. The structure of this complex material changes with more severe reduction treatment, but was not completely removed by reduction alone. The modal value of the Cu(N)/Cab catalyst effectively remains constant at roughly 4 nm regardless of treatment.

Samples of CuO(A)/Cab did not reveal the presence of the copper acetate salt, indicating that the calcination step is effective in removing this material. The dimensions of the copper oxide particles were found to depend upon the nature of the calcination procedure. Calcination as a fluidised bed produced particles with a mode of 2 nm, whilst this value was reduced to 8 nm following a fixed bed calcination. The formation of the larger particles within these samples was attributed to metal particle sintering.

A comparison between average particle dimensions as determined by electron microscopy and nitrous oxide decomposition showed a considerable degree of variation between the results of the two techniques. This was attributed to the assumptions made for each method. It was concluded that whereas nitrous oxide decomposition experiments provide valuable information on the available metal surface areas of the catalysts, transmission electron microscopy provides a more reliable assessment of their particle size distributions.

Figure 5.1.18 Micrograph of Cu(N)/Cab (i)

Figure 5.1.19 Micrograph of Cu(N)/Cab (iii)

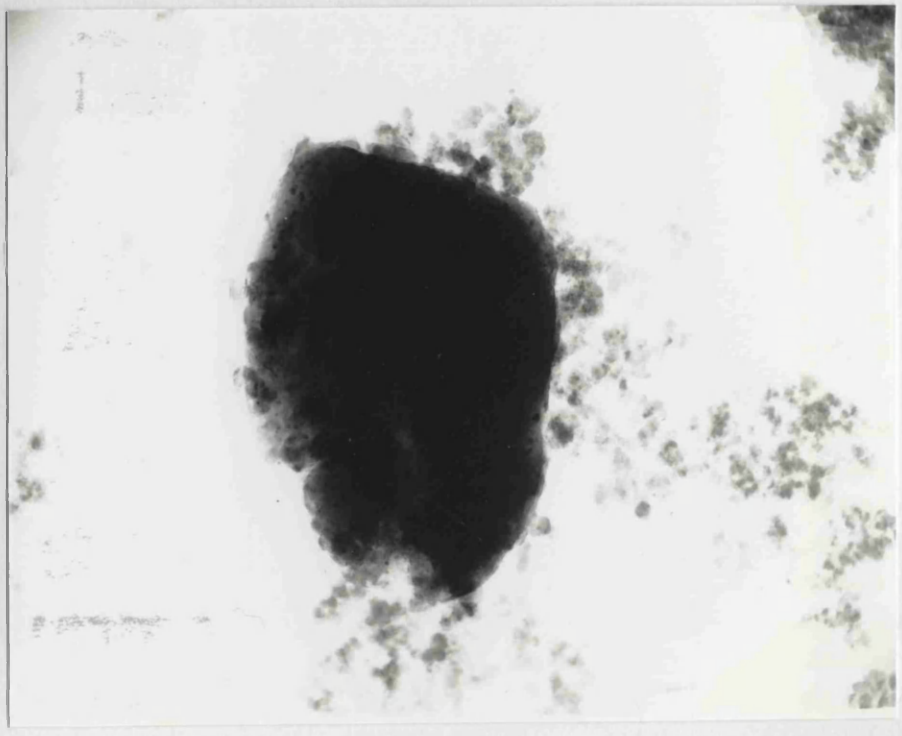

Figure 5.1.20a Bright field image of Cu(A)/Cab

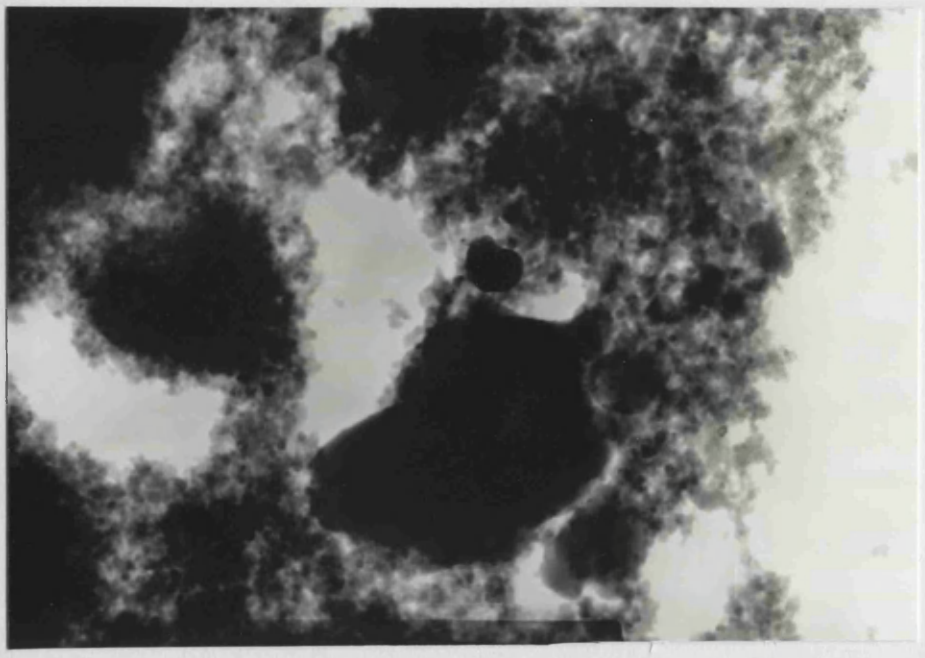

Figure 5.1.20b Dark field image of Cu(A)/Cab

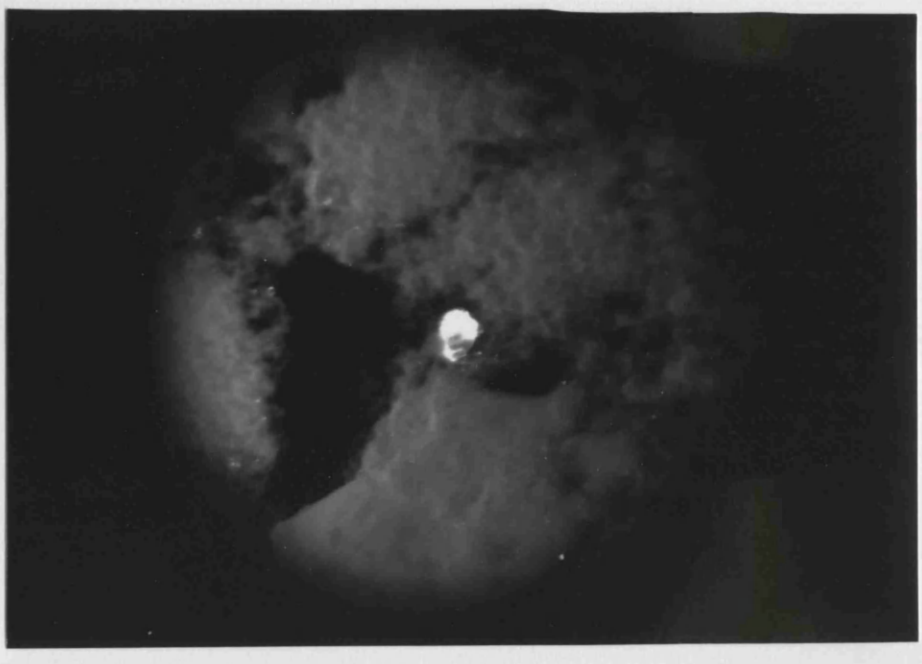

Figure 5.1.20c Dark field image of Cu(A)/Cab

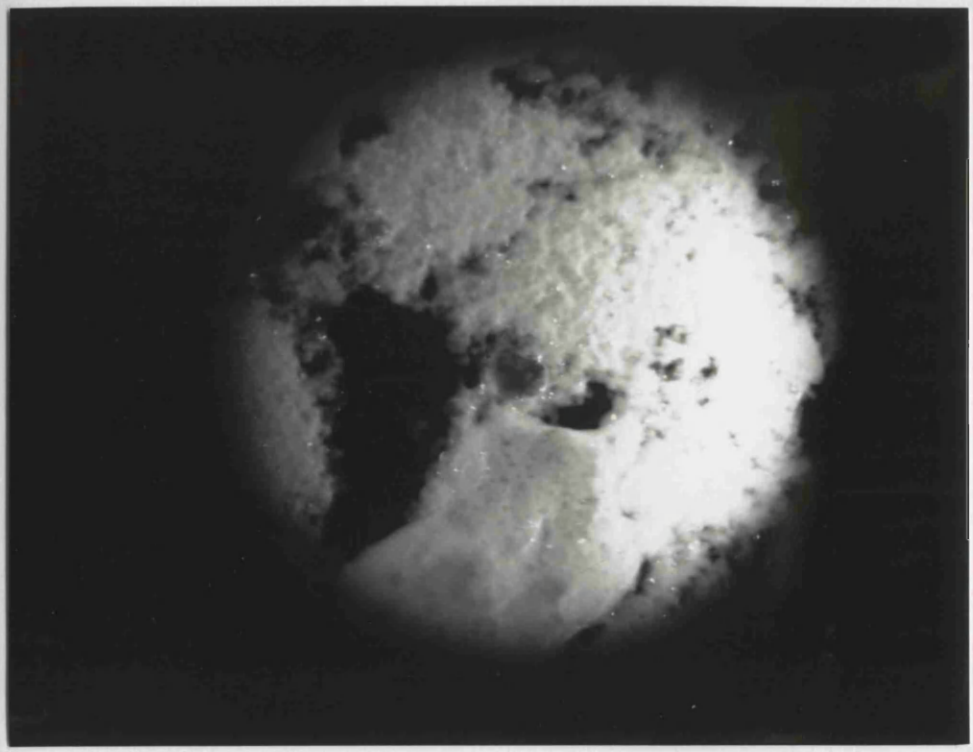

Figure 5.1.21 Particle size distributions for Cu(N)/Cab i), ii) and iii)

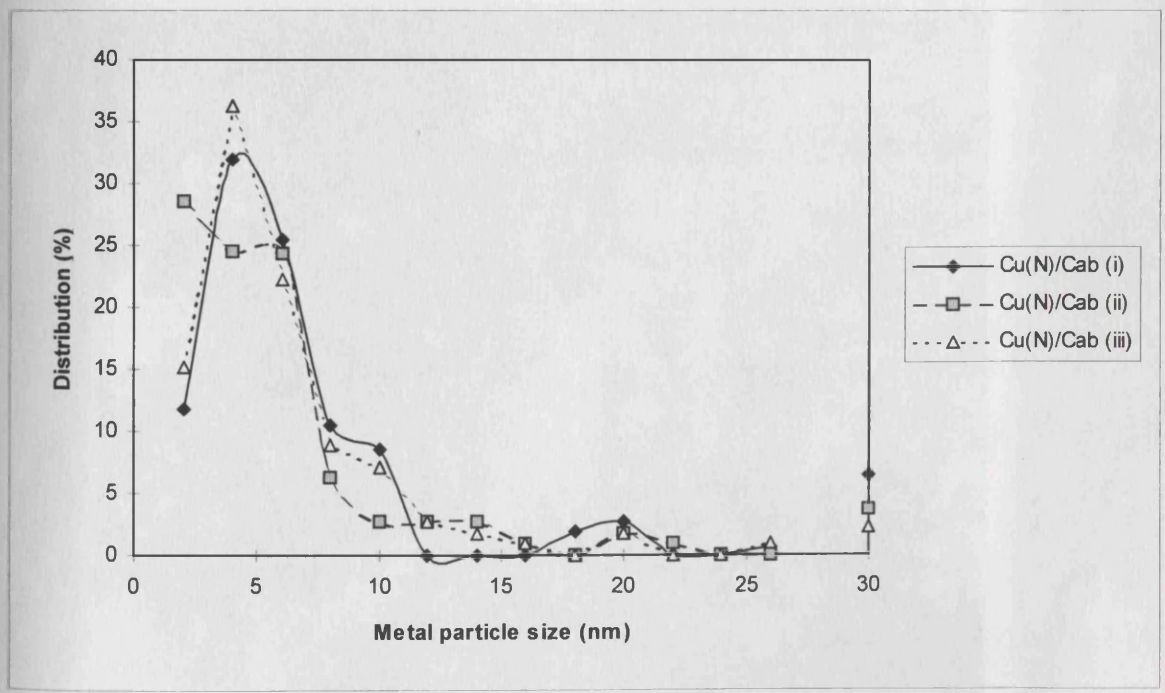

Figure 5.1.22 Typical micrograph of CuO(A)/Cab Fl.bed[500]

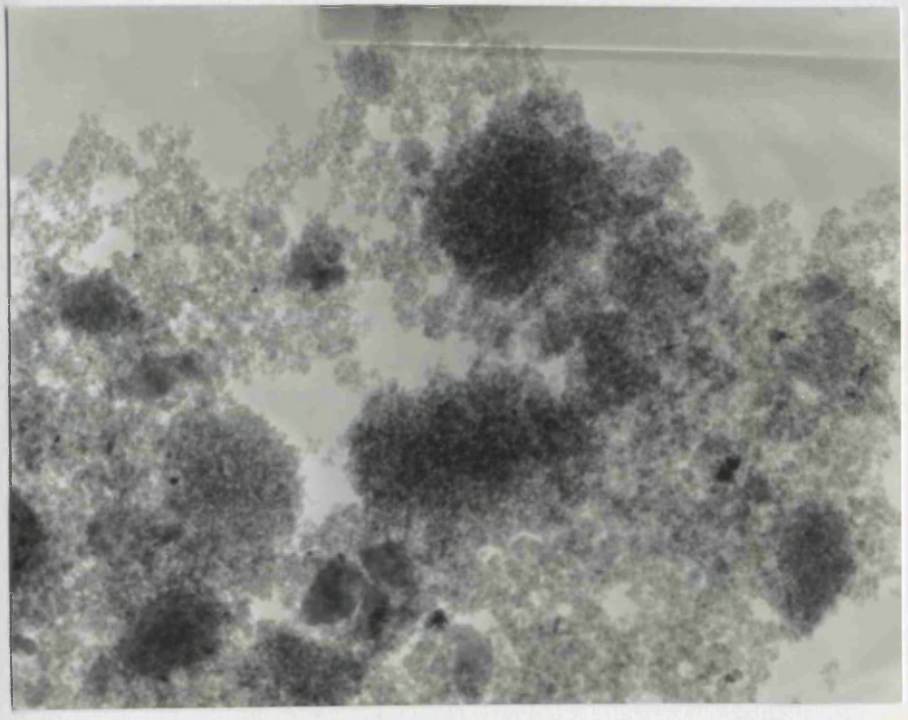

Figure 5.1.23 Typical micrograph of CuO(A)/Cab Fixed[50]

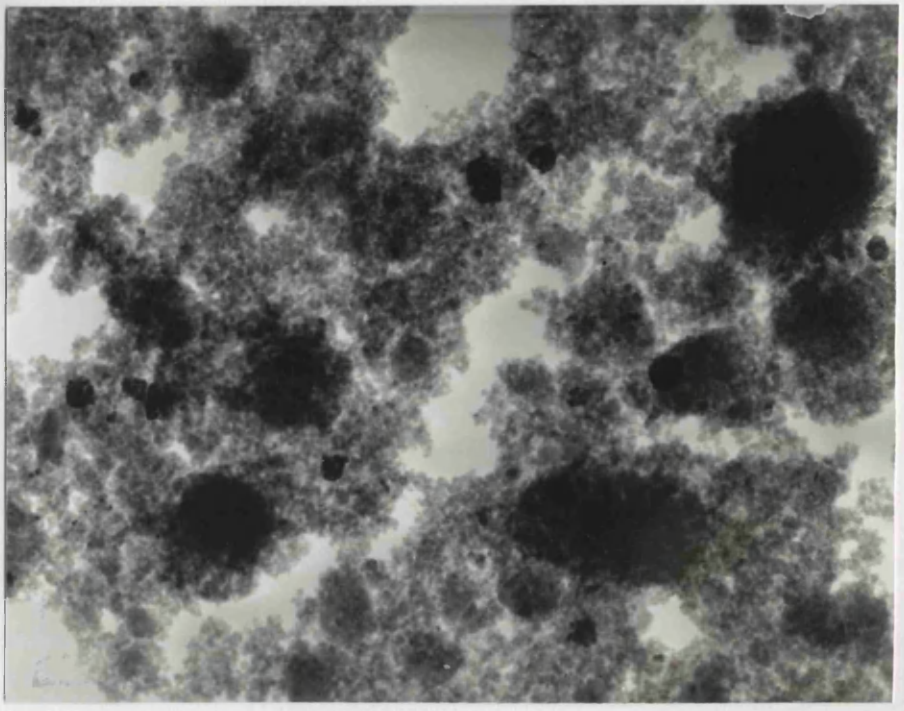

Figure 5.1.24 Particle size distributions of the CuO(A)/Cab samples

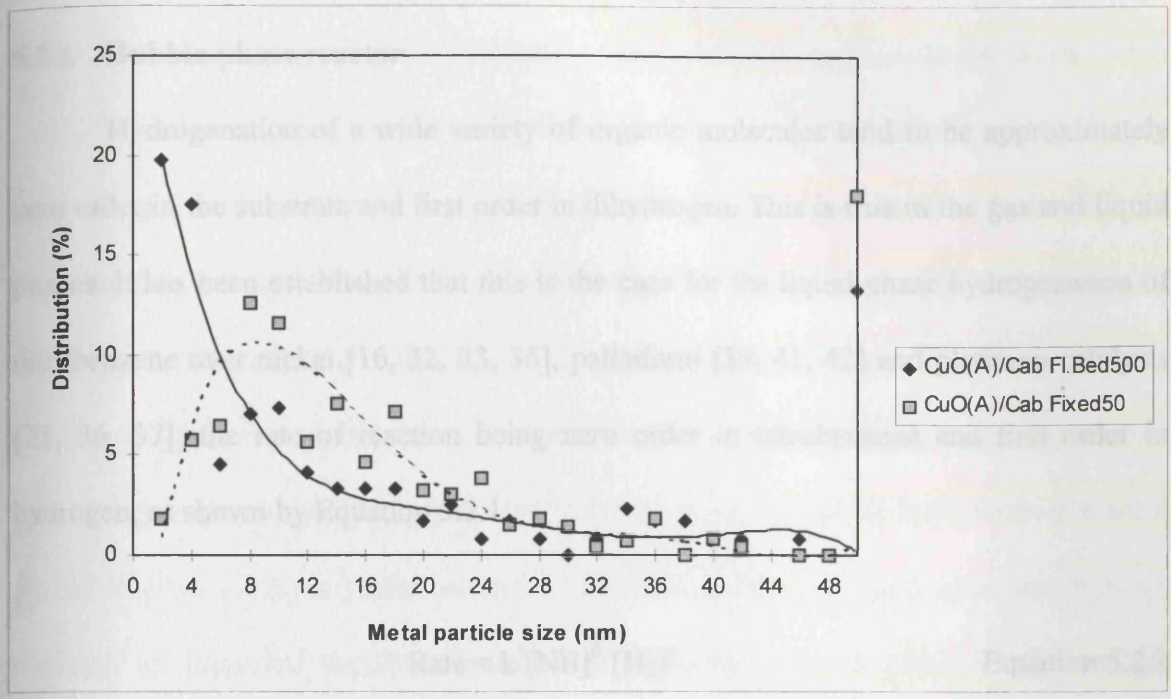

5.2 DEVELOPMENT OF REACTION TESTING

5.2.1 Bubble-phase reactor

Hydrogenation of a wide variety of organic molecules tend to be approximately zero order in the substrate and first order in dihydrogen. This is true in the gas and liquid phases. It has been established that this is the case for the liquid phase hydrogenation of nitrobenzene over nickel [16, 32, 33, 35], palladium [39, 41, 42] and platinum catalysts [21, 36, 37]; the rate of reaction being zero order in nitrobenzene and first order in hydrogen, as shown by Equation 5.2.1.

$$\text{Rate} = k\,[NB]^0\,[H_2]^1 \qquad \text{Equation 5.2.1}$$

where k is a rate coefficient

In the liquid phase, the critical parameter for efficient reaction rates is the solubility of hydrogen in the solvent. Ultimately, this limits the supply of hydrogen to the catalyst, and is governed by Henry's Law. Henry's law states that the mass of gas which is dissolved by a given volume of a liquid is directly proportional to the pressure of the gas, at a constant temperature and assuming no chemical reaction between the phases. The reaction rate of nitrobenzene hydrogenation can then be improved by increasing the applied pressure. However, pressurised batch reactors often rely on an *in situ* activation of the catalyst whereby the catalyst is reduced in the liquid-phase. Whilst this is acceptable for catalysts such as palladium which will reduce at room temperature, it is not trivial to

activate copper-based catalysts in this manner, as they are not amenable to reduction at the modest temperatures (ca. 100 °C) usually encountered in liquid phase hydrogenations.

The aim of this project was to develop a simple method of evaluating copper catalysts in the liquid-phase. Chambers *et al* had proven the viability of copper catalysts for selective hydrogenation of cinnamaldehyde in the liquid-phase [65] using a batch slurry reactor. A variant of this reactor was constructed, and compared against a bubble-phase vessel (see Figures 3.7 and 3.8 respectively). This was designed, built and tested in view of the importance of hydrogen supply. It was believed that the bubble-phase reactor would improve catalyst performance by maximising the gas-liquid interface, thereby ensuring an increased supply of solubilised dihydrogen to the catalyst surface. The operation of these vessels is outlined in Section 3.5.2, whereby the catalyst is reduced *in situ* in the gas phase, before the reaction mixture is admitted and the reaction commenced.

During operation of this vessel it was found that the activation of the catalyst was relatively straightforward, obtaining the desired control over gas flow and applied temperatures. The introduction of the reactant mixture was simple and the subsequent removal of reaction samples achieved using a purpose-built lengthened syringe needle. During the reaction the temperature was maintained at 150 ± 2 °C. Mixing between the gas, liquid and solid phases was satisfactory, as the sinter broke the gas flow down into a steady stream of tiny bubbles, thereby agitating the liquid. A considerable proportion of the catalyst, however, remained attached to the sinter following the activation step. In addition, the relatively high gas flow necessitated proportionately scaled oxygen and water traps, with frequent regeneration.

Perhaps the most significant disadvantage of the design was that the upward flow of gas was not sufficient to prevent a significant proportion of the liquid phase (ca. 20%) passing down through the sinter during the course of the reaction. The applied reaction temperature did provide a mechanism for the return of this material, as the mixture was volatilised and carried back through the sinter by the flow of hydrogen, but a fraction of the reaction mixture was essentially separated from the catalyst at any one time. Table and Figure 5.2.1 display results obtained using the bubble-phase vessel, also including the composition of samples taken from above and below the sinter after terminating the reaction.

It is evident that the hydrogenation of nitrobenzene does indeed proceed to aniline, but that as the reaction seems to proceed to completion the concentration of nitrobenzene then gently rises. This is attributed to the return of nitrobenzene which had sunk below the sinter. The post-reaction samples again illustrate this factor. Although the fraction taken above the sinter corresponds with the concentrations of the last reaction sample as would be expected, the fraction below the sinter shows a considerably higher nitrobenzene concentration. It was concluded that although the applied temperature did provide a mechanism for the return of material which had passed down through the sinter, this was not sufficient to ensure a uniform distribution throughout the flask. In essence, the overall mixing through the system was poor, and the resultant concentration gradient prejudiced reliable determination of reaction profiles.

A comparative evaluation of the bubble-phase vessel was obtained against the slurry reactor, described previously. The reaction results derived are displayed by Table and Figure 5.2.2.

It is apparent from these results that the reaction follows broadly similar patterns to those obtained when using the bubble-phase vessel, although the reaction rate is markedly slower.

It was not possible to obtain a true comparison between the vessels for several reasons. Firstly, the hexan-1-ol solvent was later found to react with the aniline product. This observation is reported in Section 5.2.5, but for simplicity the resultant by-products have been omitted from this series of graphs; at this stage it is the activity, rather than the selectivity, which is of importance. Secondly, the applied temperatures for these reactions differ by 17 °C. However, the effect of temperature upon the reaction rate has been assessed in Section 5.3.3, and the rates obtained from the slurry vessel scaled up accordingly from 133 °C to 150 °C. The resultant qualitative comparison between the vessels has been normalised to an initial nitrobenzene concentration of 0.2 mol l^{-1}, and plotted as percentage conversion per gram of catalyst (shown by Table and Figure 5.2.3).

These results show that the bubble-phase vessel increases the activity of the catalyst. This is attributed to the bubble-phase reactor facilitating the dissolution of dihydrogen, and hence its supply to the active catalyst surface. However, the assumptions made with regard to reaction temperature and by-products must be borne in mind, as must the concentration gradient through the bubble-phase. The bubble-phase reactor certainly

showed potential and merits further study. A change in design, perhaps with the addition of a re-circulation loop, could overcome the problem of poor mixing.

In summary, the bubble-phase reactor design allows the use of copper-based catalysts for liquid-phase hydrogenation reactions, with catalyst activation conducted *in situ* in the gas phase. Catalyst performance appears to be enhanced in comparison to that obtained in a slurry vessel. However, due to the factors outlined above, a direct quantitative comparison cannot be made. In particular, the temporary loss of reaction mixture through the sinter prevents the vessel's use for kinetic studies as the system is not homogeneous. This factor could be overcome through the installation of a pumped re-circulation loop, but this option was not considered practical for this project. Subsequent development focussed on the slurry reactor.

Table 5.2.1 Nitrobenzene hydrogenation in hexan-1-ol, 100 ml, over 0.4977 g Cu(N)/Cab using bubble-phase vessel at 150 °C

Reaction time (mins)	Nitrobenzene (mmols)	Aniline (mmols)	Selectivity to aniline (%)
0	9.75	0.00	0.0
20	8.65	0.86	77.9
43	8.16	1.44	90.8
71	6.85	1.97	68.0
106	4.95	2.65	55.3
164	3.34	3.44	53.6
222	0.56	3.99	43.4
271	1.07	4.74	54.6
325	1.37	5.97	71.3
383	1.39	5.19	62.0
387	1.19	4.27	49.9
479	1.34	4.60	54.8
Sample above sinter after 500 mins	1.20	4.38	51.2
Sample below sinter after 500 mins	2.33	4.59	61.9

Figure 5.2.1 Nitrobenzene hydrogenation in hexan-1-ol, 100 ml, over 0.4977 g Cu(N)/Cab using bubble-phase vessel at 150 °C

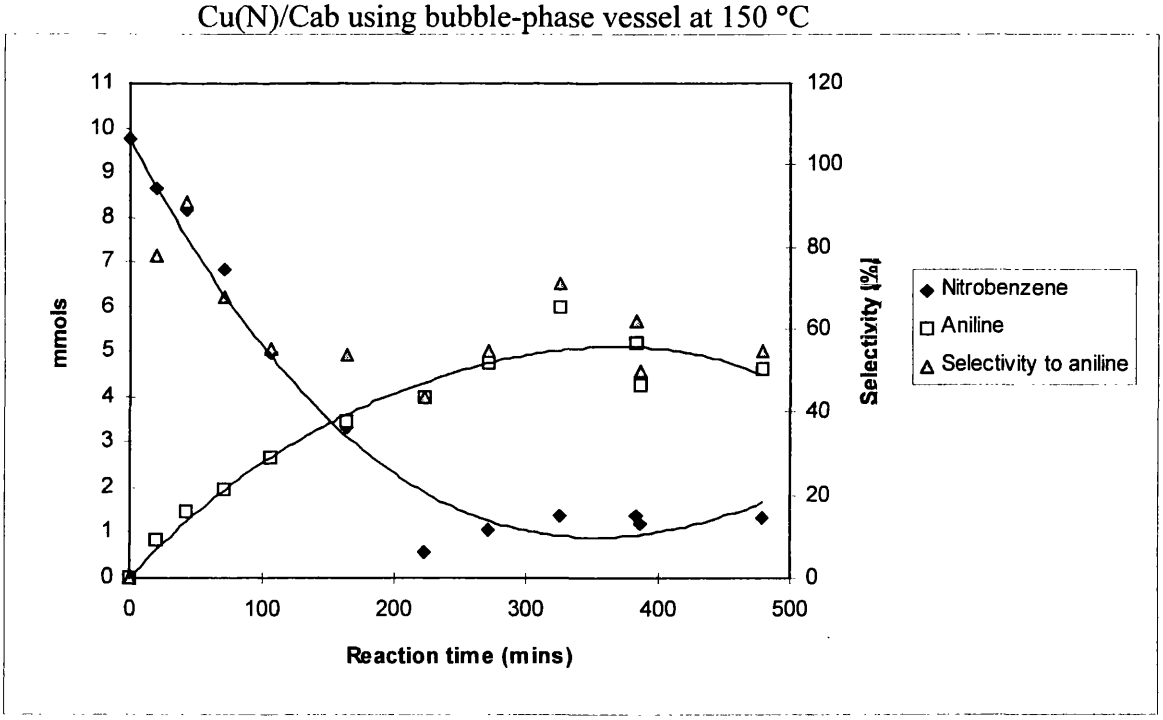

Table 5.2.2 Nitrobenzene hydrogenation in hexan-1-ol, 50 ml, over 0.2540 g Cu(N)/Cab using slurry vessel at 133 °C

Reaction time (mins)	Nitrobenzene (mmols)	Aniline (mmols)	Selectivity to aniline (%)
0	4.797	0.0	0.0
30	4.20	0.13	21.5
63	4.18	0.33	53.2
94	3.75	0.46	43.4
141	3.57	0.70	56.9
199	3.01	0.89	49.5
247	2.60	1.03	46.6
440	1.06	1.26	33.6
541	0.63	1.29	30.9
643	0.32	1.19	26.6
1247	0.0	1.35	28.2

Figure 5.2.2 Nitrobenzene hydrogenation in hexan-1-ol, 50 ml, over 0.2540 g Cu(N)/Cab using slurry vessel at 133 °C

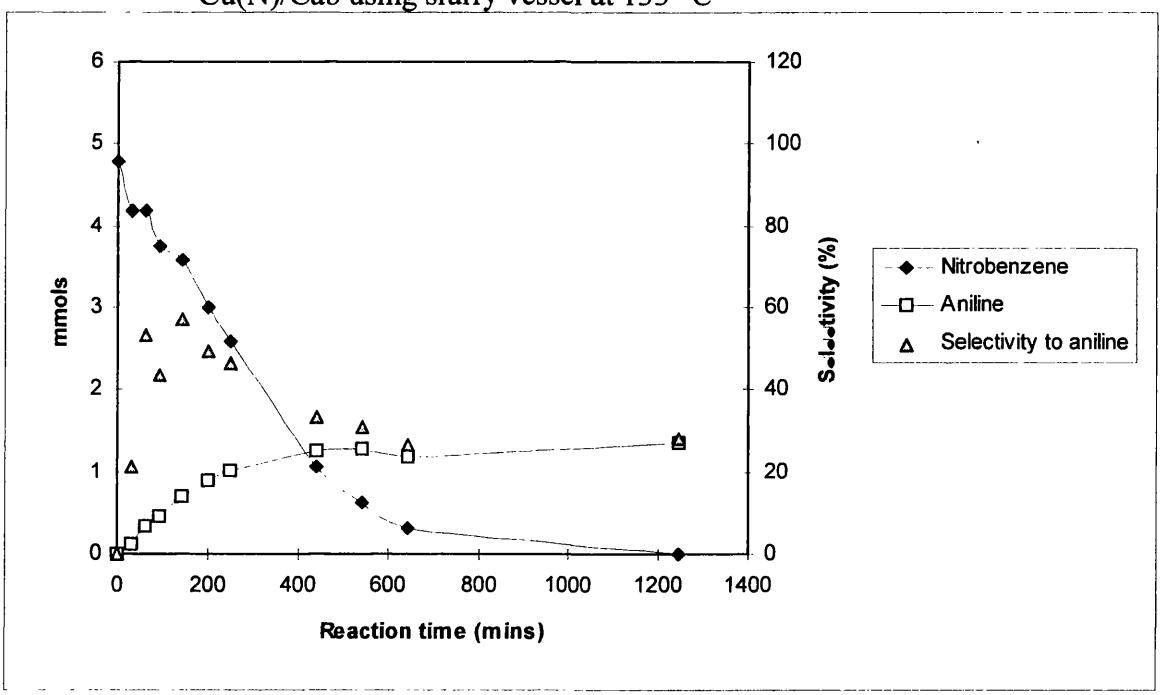

Table 5.2.3 Comparison of catalyst performance between bubble-phase and slurry vessels

Reaction time (mins)	NB (Slurry vessel, %)	AN (Slurry vessel, %)	NB (Bubble-phase vessel, %)	AN (Bubble-phase vessel, %)
0	100.0	0.0	100.0	0.0
20			89.0	8.6
30	84.6	3.3		
43			84.1	14.4
63	84.2	8.4		
71			71.0	19.7
94	73.1	11.7		
106			52.0	26.5
141	68.6	17.9		
164			35.9	34.4
199	54.2	22.7		
222			8.1	39.9
247	43.7	26.3		
271			13.2	47.4
325			16.2	59.7

Figure 5.2.3 Comparison of catalyst performance between bubble-phase and slurry vessels

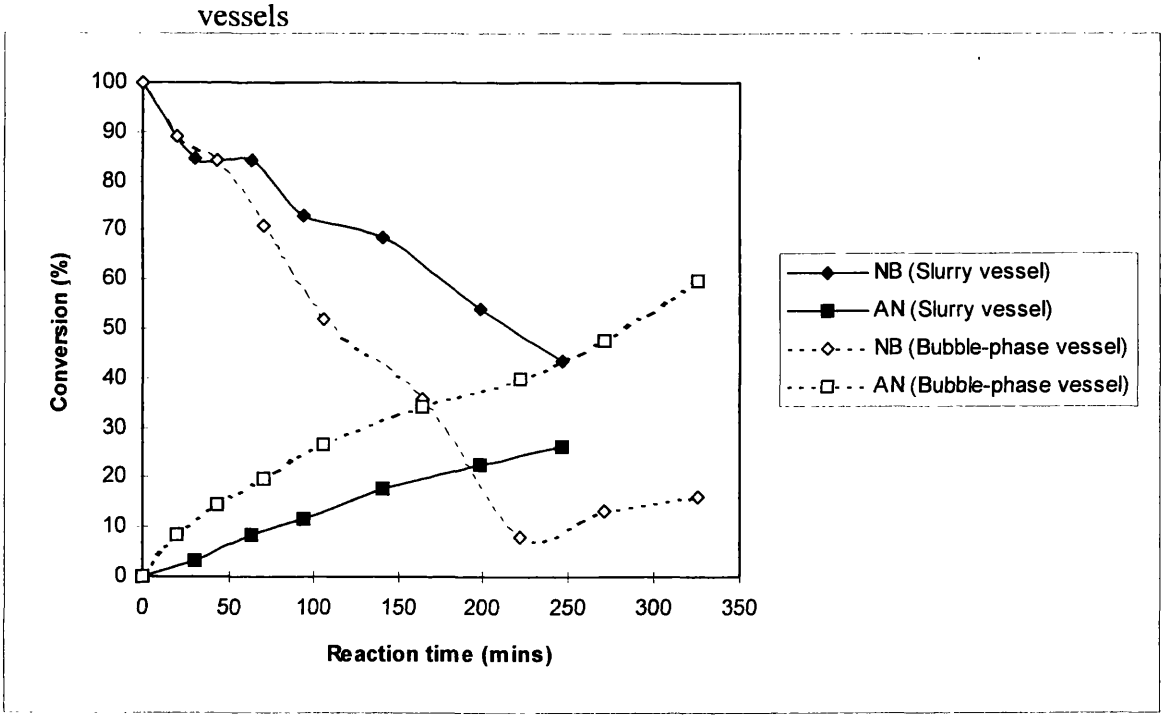

5.2.2 Slurry reactor

The acquisition of valid kinetic data, and the evaluation of different catalysts, requires the fulfilment of several key experimental conditions. The pressure and flow rate of the gas should remain constant, as should the applied temperature. For a batch reactor such as this slurry vessel the system should be closed, *i.e.* matter should neither be gained or lost during the course of the reaction [104]. The apparatus itself should not contribute to the reaction. Mass-transfer and heat-transfer should be considered, to ensure that the measured activities are those of the catalysts themselves, free of any intrusion by these phenomena [7]. Finally, the reproducibility of the experimental technique should be assessed. Mass- and heat-transfer effects are covered in Section 5.3.2. The assessment of the slurry vessel with regard to the remaining factors are discussed in this section. The operation of the apparatus is described in Section 3.5.2.

It had been established that nitrobenzene hydrogenation progressed relatively slowly over the supported copper catalysts, and to ensure an acceptable rate of reaction the applied temperatures were set within 20 °C of the boiling point of the solvent. The gas flow was maintained at 200 ml min^{-1} to ensure an adequate supply of dihydrogen. These conditions produced a fast flow of organic vapour, which necessitated the use of an efficient condenser to maintain a closed system.

Standard Liebig and double surface area condensers proved incapable of preventing the loss of reaction mixture. An adapted double surface area condenser incorporating a sinter, which supported boiling chips was evaluated. This arrangement broke up the flow of gas and provided a large surface area for condensation. The

condensate, however, collected above the sinter, and an improved variant was required. Ultimately it was found that a Liebig condenser packed with glass beads proved to be sufficient; preventing the loss of evaporate whilst allowing it to return to the flask. Table and Figure 5.2.4 illustrate the results of two 'blank' runs, conducted without catalyst.

These results indicate that a closed system had been attained, with no loss of reactant during the course of the reaction. In addition, not only do they prove that the reactor itself does not contribute to the reaction, but that Cab-O-Sil alone has no catalytic effect. The hydrogenation of nitrobenzene, therefore, occurs heterogeneously, and requires the presence of an active metal catalyst.

Incidentally, the removal of liquid samples should not affect the course of the reaction. Samples were withdrawn by syringe, the reactant mixture and suspended catalyst particles being removed in proportion, *i.e.* whilst the total volume is marginally decreased, the overall concentrations of reactant, product, catalyst and solvent are unaffected. This is true of all the experiments conducted, with the exception of the pelleted Cu(N)/C-10 catalyst. In any case, the aliquots were limited to approximately 0.3 ml from a typical volume of 80 ml, to minimise any potential effects.

Inadequate control over the reaction temperature is cited by Twigg [7] as one of the most common factors which hinders the reproducibility of experimental performance. Temperature stability during the reaction testing was critical so that reaction rates between various parameters could be reliably compared. The temperature of the reaction mixture was measured throughout each experiment; a sample of the temperature variance during the course of the experiment is displayed by Table and Figure 5.2.5.

It is clear that the temperature of the vessel remains constant at the desired value of 110 ± 2 °C, which was deemed to be acceptable. This was to be expected as the oilbath was heated by a thermostatted hotplate, both oilbath and reaction mixture were continuously stirred, and all other conditions were constant. In addition, no variation in the pressure or flow of dihydrogen was observed during the course of the experiment. The temperature applied during catalyst activation was similarly monitored, with divergence from the desired value limited to ±2 °C.

The temperature gradient between the oilbath and the vessel interior was determined at different temperatures; the results shown by Table and Figure 5.2.6. Knowledge of this relationship allowed the hotplate thermostat to be pre-programmed, and the desired temperature reached in the minimum of time. The actual temperature inside the reactor was obviously affected by the depth and position of the reactor within the oilbath, as well as the temperature of the oilbath itself. Positioning of the apparatus was standardised as far as possible. The oilbath temperature was then varied if necessary to obtain the desired internal vessel, as measured by the internal thermometer.

A silica-supported platinum catalyst (described in Section 3.2) was used as a means to further evaluate the slurry vessel. The liquid-phase hydrogenation of nitrobenzene over platinum-based catalysts is frequently reported in the literature [21, 36, 37], with relatively rapid reaction rates.

There is general agreement that the reaction proceeds via the formation of phenylhydroxylamine. This molecule, however, is not stable during gas chromatographic analysis, decomposing to nitrosobenzene and aniline [105]. Nevertheless, the formation

of phenylhydroxylamine can be established and quantified as exemplified by Galvagno *et al* [36], who detected nitrosobenzene but not phenylhydroxylamine during gas chromatography. As spectrophotometric studies did not reveal the absorption band of nitrosobenzene, they concluded that its presence during gas chromatographic analysis originated from the decomposition of phenylhydroxylamine. The calculated conversion to phenylhydroxylamine observed by Galvagno and co-workers rose linearly to ca. 70 %, until the complete consumption of nitrobenzene; the concentration decreasing thereafter as the phenylhydroxylamine was reduced to aniline. This pattern is in agreement with other publications [38, 46]. Other authors have reported the presence of by-products in much lower concentrations [37], or have apparently detected only the formation of aniline [21].

The results obtained when using the platinum/silica catalyst are shown by Table and Figure 5.2.7. It should be noted that the concentrations of N-cyclohexylaniline [$C_6H_5NHC_6H_{11}$] and N-dicyclohexylamine [$C_6H_{11}NHC_6H_{11}$] have been calculated using the detector response factor of nitrobenzene, as described in Section 4.2.

The reaction can be divided into two stages. For the first forty minutes the nitrobenzene is hydrogenated to aniline without the detection of by-products. Thereafter, the aniline is hydrogenated to N-cyclohexylaniline, which is reduced in turn to N-dicyclo-hexylamine. The initial selectivity to aniline is consistent with the tendency of platinum to favour the adsorption of nitro-aromatics. Phenylhydroxylamine and more significantly, nitrosobenzene, were not detected during the course of the reaction. This seeming disparity with other authors is attributed to the relatively high temperature applied in this

study, as it has been reported that the selectivity to phenylhydroxylamine over platinum-based catalysts decreased from 70 % at 0 °C, to 60 % at 10 °C and 20 % at 60 °C [36].

Following the complete conversion of the nitrobenzene, the reaction then proceeds as the hydrogenation of aniline. The sequential formation of N-cyclohexylaniline and N-dicyclohexylamine is in accord with the literature. Although cyclohexylamine can also be detected as a precursor to these compounds, in general the major and minor products of aniline hydrogenation are N-cyclohexylaniline and N-dicyclohexylamine respectively [106-108].

It is possible to compare the results in Table and Figure 5.2.7 with those of Li and co-workers [37]. This publication presented data on nitrobenzene hydrogenation over a 1.0 wt% Pt/Al_2O_3 catalyst in a continuous stirred tank reactor at 50 °C and 1 atm. They observed a linear conversion of nitrobenzene to aniline, with catalyst activity per gram calculated at 17.3 $x10^{-7}$ moles s^{-1}. This is comparable with 29.8 $x10^{-7}$ moles s^{-1} per gram of the 1 wt% Pt/SiO_2 used in the present study at 148 °C. Considering the different supports and reaction temperatures, as well as inevitable differences in method, the reaction rates are remarkably similar. This comparison was interpreted as validation of the experimental technique. In addition, the results obtained with the supported platinum catalyst provide a useful benchmark against which the copper-based catalysts can be evaluated, and indicate that the reaction chemistry is not limited by hydrogen supply.

Three nitrobenzene hydrogenation reactions, using the Cu(N)/Cab catalyst at 158 °C and conducted under identical conditions, are displayed in Table and Figure 5.2.8(a) to give an example of the reproducibility of the experimental technique. The

conversions shown have been normalised to 1.0 g of catalyst and an initial nitrobenzene concentration of 0.1 M. Table 5.2.8(a) also presents the rates of aniline formation and error ranges for each of the individual reactions, and the overall reaction rate and error obtained when the three sets of data are grouped together. The rates are presented as the number of moles of aniline formed per second, per gram of catalyst. This data represents the typical reproducibility which was attained during reaction testing of the catalysts. Table and Figure 5.2.8(b) present the selectivity towards aniline derived from these sets of data. Disregarding the spurious values calculated at low conversions, it is evident that the ultimate selectivity to aniline is of the order of 90 - 100 %; no other intermediates or by-products were detected.

In summary the system was closed, and the control of reaction temperature acceptable. The temperature gradient between the oilbath and the vessel was understood. Variation in gas pressure or flow rate could be discounted, and the reaction equipment was inert towards nitrobenzene hydrogenation. The reaction was heterogeneous and required the presence of an active metal catalyst; with the Cu(N)/Cab catalyst demonstrating excellent selectivity towards aniline. The reaction technique had been validated in comparison with published results, and the reproducibility of the protocol proven. It had therefore been established that the reaction equipment and protocol were suitable for the liquid phase hydrogenation of nitrobenzene over supported metal catalysts.

Table 5.2.4 Reactions conducted in *n*-butyl benzene at 158 °C without catalyst and with 0.5513 g Cab-O-Sil support only

Time (mins)	Nitrobenzene (blank) (mmols)	Nitrobenzene (Cab-O-Sil) (mmols)
0	6.43	8.72
60	6.4	8.91
120	6.51	8.68
180	6.28	8.75
240	6.52	8.9
300	6.42	
360	6.48	

Figure 5.2.4 Reactions conducted in *n*-butyl benzene at 158 °C, without catalyst and with 0.5513 g Cab-O-Sil support only

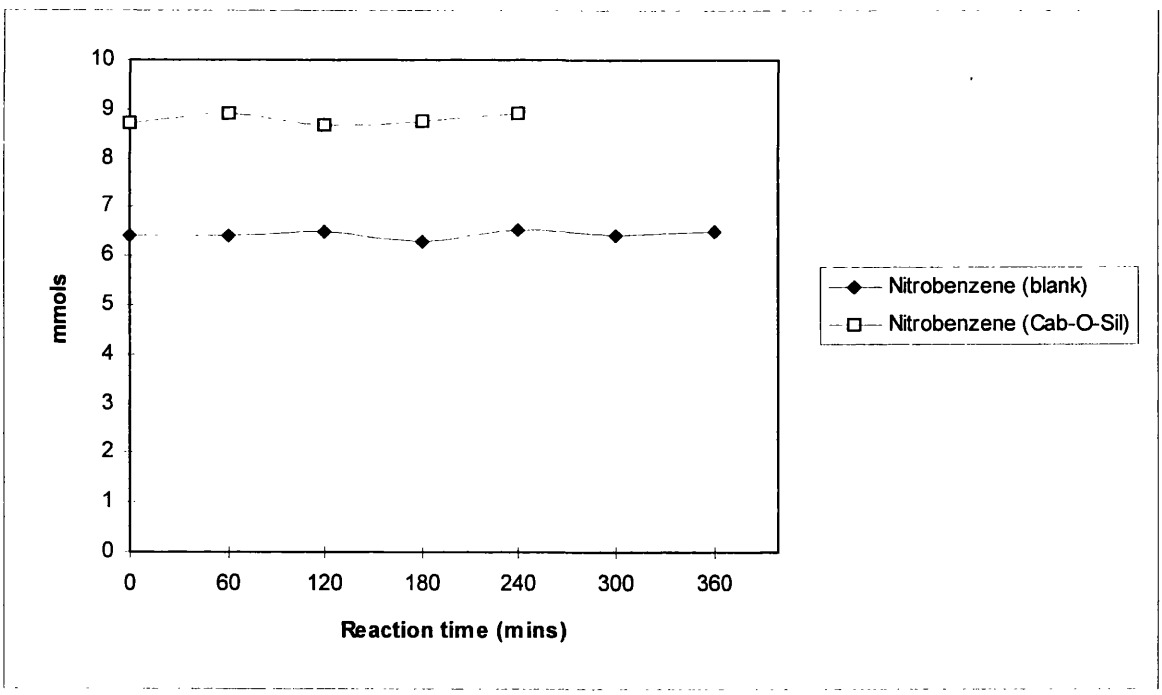

Table 5.2.5 Temperature variance of the oilbath and vessel through time

Reaction time (mins)	Oilbath temperature (°C)	Vessel temperature (°C)
0	122.5	108.5
5	124.5	109.5
15	124.5	110.0
34	125.0	110.5
45	126.0	110.0
60	126.0	110.5
94	126.5	111.0
120	124.5	110.0
152	124.0	110.0

Figure 5.2.5 Temperature variance of the oilbath and vessel through time

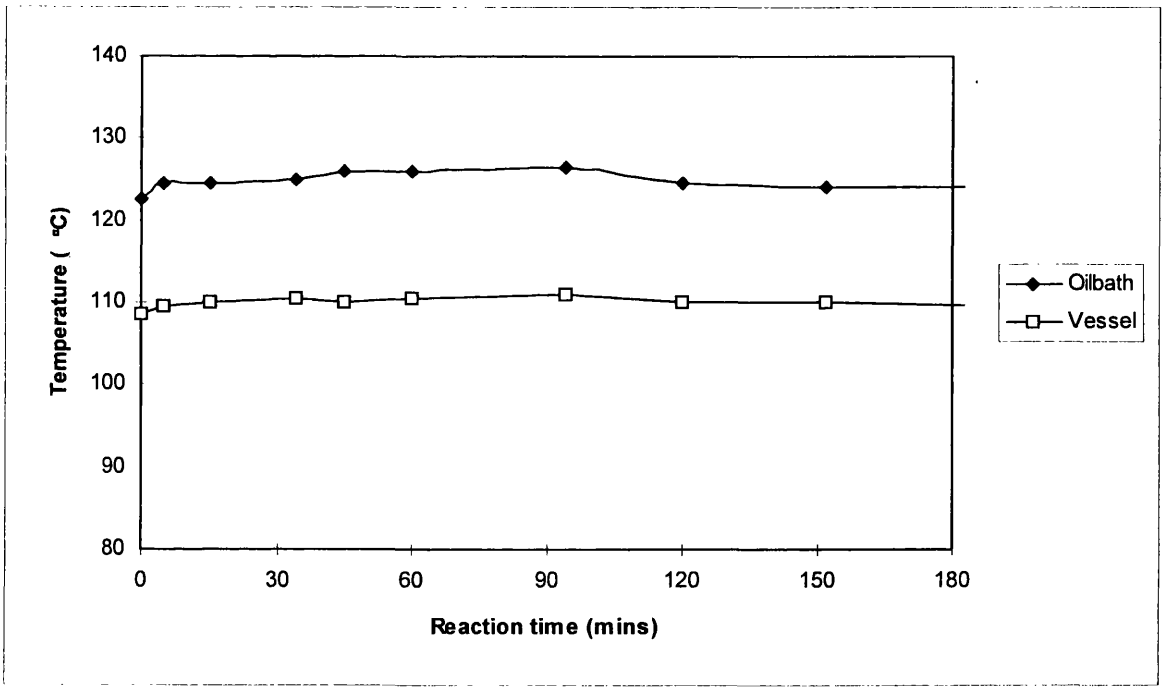

Table 5.2.6 Comparison of oilbath v. vessel temperatures

Vessel temperature (°C)	95	110	125	133	144	148	158	170
Oilbath temperature (°C)	107	122	141	150	162	169	183	200

Figure 5.2.6 Comparison of oilbath v. vessel temperatures

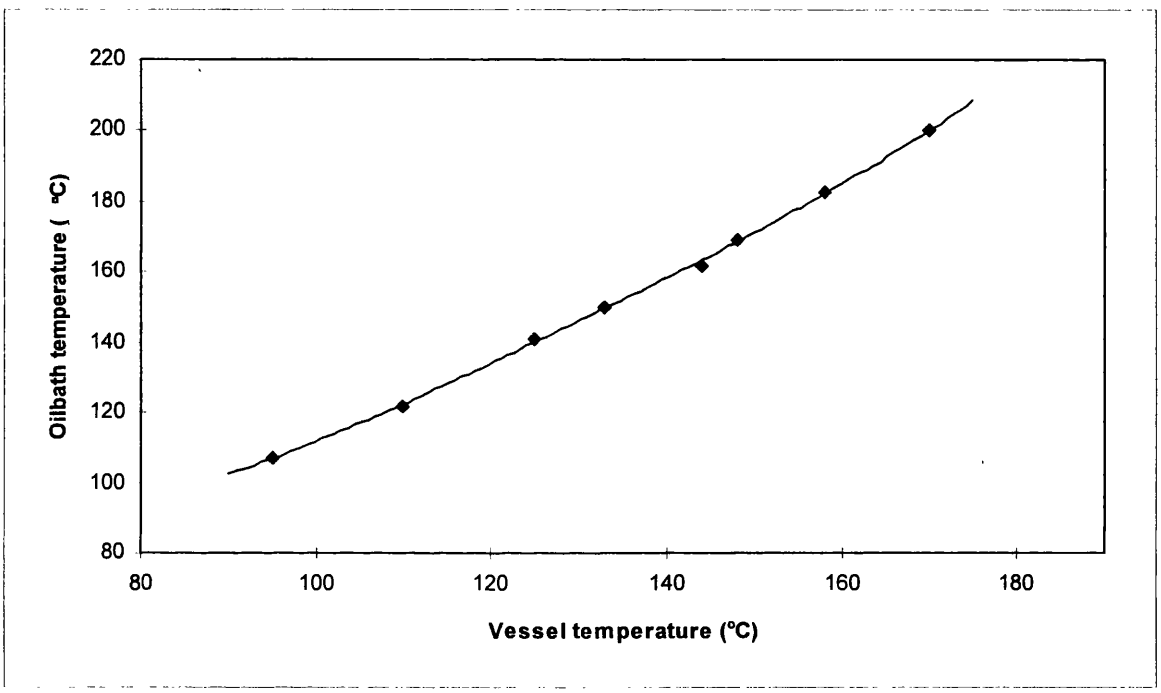

Table 5.2.7 Nitrobenzene hydrogenation in *t*-butyl benzene over 0.3994 g Pt/SiO_2 at 148 °C

Reaction time (mins)	Nitrobenzene (mmols)	Aniline (mmols)	N-Cyclohexyl-aniline (mmols)	N-Dicyclo-hexylamine (mmols)
0	7.49	0.00	0.00	0.00
4	6.87	0.62	0.00	0.00
9	5.93	1.35	0.00	0.00
14	5.16	2.26	0.00	0.00
19	4.07	3.14	0.00	0.00
25	3.27	4.26	0.00	0.00
29	2.28	5.02	0.00	0.00
34	1.47	5.96	0.00	0.00
39	0.66	7.09	0.00	0.00
43	0.00	7.56	0.00	0.00
50	0.00	7.11	0.33	0.00
57	0.00	6.40	0.62	0.00
66	0.00	5.90	0.87	0.00
79	0.00	5.21	1.30	0.36
94	0.00	4.63	1.61	0.51
109	0.00	4.17	1.92	0.72
134	0.00	3.64	2.20	0.94
167	0.00	3.09	2.44	1.19

Figure 5.2.7 Nitrobenzene hydrogenation in *t*-butyl benzene over 0.3994 g Pt/SiO_2 at 148 °C

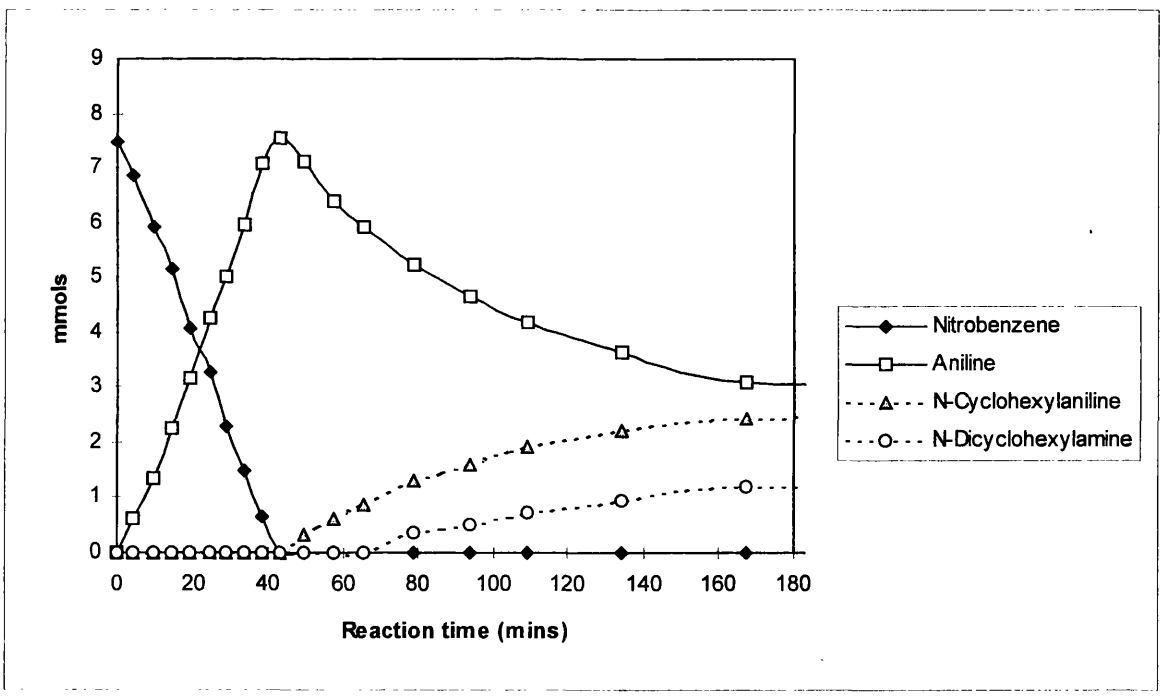

Table 5.2.8(a) Nitrobenzene hydrogenation over Cu(N)/Cab using slurry vessel at 158 °C

	1st		2nd		3rd	
Reaction time (mins)	NB (%)	AN (%)	NB (%)	AN (%)	NB (%)	AN (%)
0	100.0	0.0	100.0	0.0	100.0	0
30	96.8	4.2	85.5	3.6	95.3	5.825
60	91.0	11.7	76.0	10.6	84.5	9.825
90	82.8	21.3	71.0	14.8	79.8	26
120	72.5	27.5	65.3	29.5		
150	62.3	32.5	61.8	32.8	61.5	38.25
180	52.0	39.0	49.8	44.3	49.5	50.75
210	48.8	51.8	42.0	49.0	42.8	61.75
240	39.0	59.3	36.8	53.3	39.3	73
270	31.0	70.8	26.5	59.3		
300	18.5	80.8	16.8	73.3	14.1	87.5
330	6.2	94.5				
345					-0.8	96.25
360	0.2	96.0	-6.7	95.5		
Rate	3.75 ± 0.12		3.43 ± 0.14		3.78 ± 0.16	
Overall rate			3.69 ± 0.10			

Figure 5.2.8(a)Nitrobenzene hydrogenation over Cu(N)/Cab using slurry vessel at 158 °C

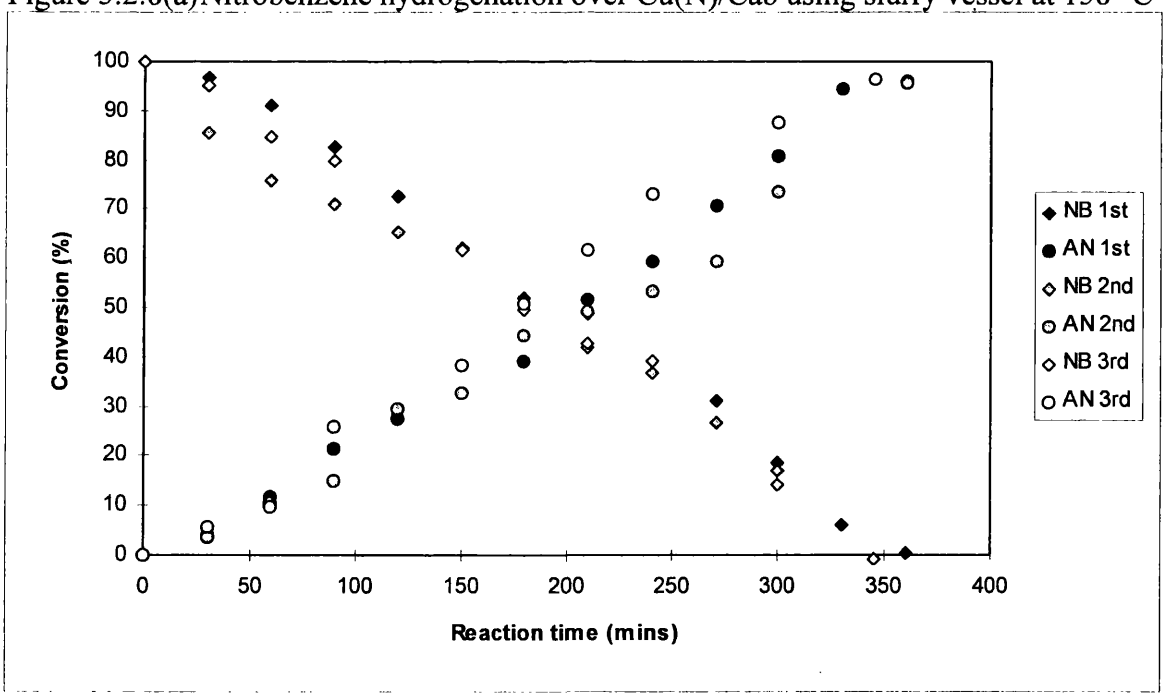

Table 5.2.8(b) Nitrobenzene hydrogenation over Cu(N)/Cab using slurry vessel at 158 °C

Reaction time (mins)	1st	2nd	3rd
0.0	0.0	0.0	0.0
30.0	130.0	24.7	122.6
60.0	129.7	44.2	63.4
90.0	123.2	50.9	128.4
120.0	100.0	84.9	99.4
150.0	86.1	85.6	100.5
180.0	81.3	88.1	107.9
210.0	101.0	84.5	120.2
240.0	97.1	84.2	101.9
270.0	102.5	80.6	95.5
300.0	99.1	88.0	
330.0	100.8	89.5	
360.0	96.2		

Figure 5.2.8(b) Nitrobenzene hydrogenation over Cu(N)/Cab using slurry vessel at 158 °C

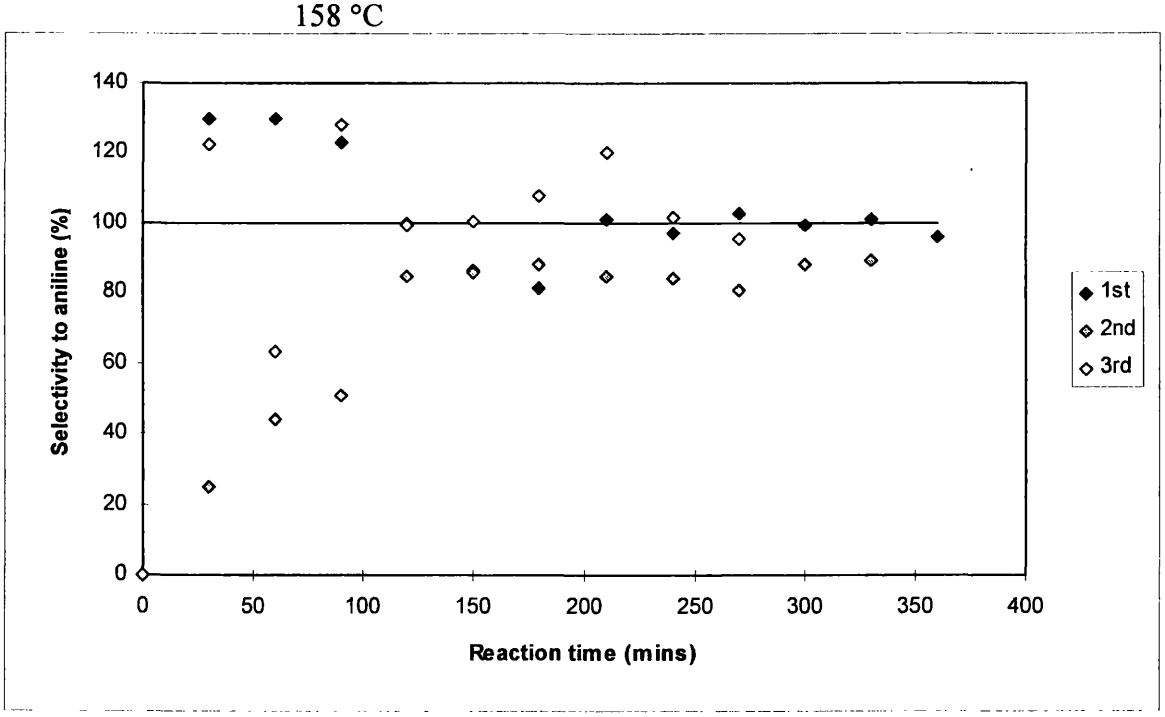

results are given for each of the solvents tested, with the exception of *t*-butyl benzene and hexan-1-ol.

Nitrobenzene hydrogenation to aniline when using hexan-1-ol was observed to occur at reasonable reaction rates, and resolution of the reaction mixture was achieved during analysis by gas chromatography. However, a subsequent alkylation reaction between aniline and hexan-1-ol was detected, as reported in Section 5.2.5.

Similarly, *t*-butyl benzene was evaluated as a possible solvent. A series of reactions and subsequent analysis revealed the presence of sulphur-containing impurities which greatly affected catalyst performance. Although these interesting results are reported in Section 5.2.6, this complication prevented the use of *t*-butyl benzene for catalyst evaluation.

5.2.3.2 Dodecane

Table and Figure 5.2.9 display results obtained when using dodecane. It should be appreciated that at this stage of development the reaction protocol was still being refined. In this experiment the first 87 minutes were conducted under 6 % H_2/N_2 ; the remainder under H_2 as should be the case. Nevertheless, it is clear that the nitrobenzene is successfully hydrogenated, and no other products were detected.

However, doubts arose over dodecane's ability to solubilise aniline at the concentrations which would be required; prepared sample solutions with high concentrations of aniline in dodecane appearing to form two distinct layers. Incidentally, the use of dodecane itself would not be practical as its boiling point of 216 °C is higher

than those of nitrobenzene and aniline, preventing an efficient reflux. Although the use of decane (bp 174 °C) would overcome this simple problem, it would not address the issue of adequate solubilisation.

5.2.3.3 Ethyl benzene

Table and Figure 5.2.10 display results obtained when using ethyl benzene. In this example the relatively high initial nitrobenzene concentration should be noted. These results indicated that ethyl benzene was suitable as a solvent for the reaction. No by-products were detected and the solvent was resolvable from reactant and product during the analysis. The relatively low boiling point of ethyl benzene however, precluded the application of reaction temperatures above 136 °C.

5.2.3.4 Mesitylene

Table and Figure 5.2.11 display results obtained when using mesitylene. It should be noted that it was not possible to resolve aniline from mesitylene during the gas chromatography analysis, with the non-polar column which was available at this time. Solubilisation of reactant and product was satisfactory, and no interaction between mesitylene and these species was observed. These results indicated that mesitylene could be employed, and provided further evidence that substituted aromatics were suitable solvents for nitrobenzene hydrogenation. However, it was desired that the final test reaction could be conducted within a single laboratory period, *i.e.* eight hours. As mesitylene's boils at 165 °C this would limit the range of applied temperatures, and hence reaction rates, and a solvent with higher boiling point was required.

5.2.3.5 *n*-Butyl benzene

Figure 5.2.12 and Table 5.2.12 show results obtained using *n*-butyl benzene, where approximately 8 mmols of nitrobenzene will have been present initially. Hydrogenation of nitrobenzene to aniline proceeded without the formation of by-products. The consumption of nitrobenzene could not be followed at this stage; the *n*-butyl benzene solvent proving to be irresolvable from the nitrobenzene peak during gas chromatographic analysis with the existing non-polar column. This solvent, however, fully solubilised both nitrobenzene and aniline, and as it boils at 183 °C it allows reaction temperatures right up to the boiling point of aniline (184 °C).

5.2.3.6 Summary

A summary of the results obtained during this solvent evaluation is presented by Table 5.2.13.

Table 5.2.13` Summary of solvent testing

Solvent	bp (°C)	Able to solubilise NB & AN	Resolvable during analysis	Comments
Dodecane	216	No	Yes	Solubility problems
Mesitylene	164.7	Yes	No	Irresolvable during gas chromatography
Ethyl benzene	136.2	Yes	Yes	Low boiling point limits reaction temperatures
Hexan-1-ol	158	Yes	Yes	Reacts with aniline
t-Butyl benzene	169	Yes	Yes	Complicated by sulphur-based impurities
n-Butyl benzene	183	Yes	No	Expensive, and difficult to purify and reuse following reaction, but suitable

In conclusion, the use of dodecane was precluded by its inability to fully solubilise aniline. The use of ethyl benzene or mesitylene was considered, but would limit the range of possible reaction temperatures. Hexan-1-ol, despite the predominance of lower alcohol solvents reported in the literature, was found to be unsuitable as it combined with aniline in an alkylation reaction. *t*-Butyl benzene was also discounted as a possible solvent owing to minute traces of sulphur-based contaminants, which greatly affected catalyst performance. *n*-Butyl benzene allowed reaction temperatures up to 183 °C, was not found to interact with the reaction species, and no solubility problems were encountered. It was, however, a relatively expensive chemical, and as the boiling points of aniline and *n*-butyl benzene differed by just one degree it would be problematic to purify and reuse the solvent following reaction. Finally, with the existing non-polar SE-30 capillary column, mesitylene could not be resolved from aniline during gas chromatography, and *n*-butyl benzene could not be separated from nitrobenzene.

In view of these factors, *n*-butyl benzene was chosen as the solvent for subsequent reaction testing. The polar DB-225 capillary column described in Section 3.5.4 was used to separate this solvent from the reactant and product. An example chromatogram is shown by Figure 5.2.13, which identifies the peaks for aniline, nitrobenzene and *n*-butyl benzene. The other peaks present are solvent-derived impurities which were not significant, with the exception of the labelled solvent peaks A and B (see Section 5.2.4).

All reactions reported in later chapters, unless otherwise stated, use the DB-225 capillary column during gas chromatographic analysis and employ *n*-butyl benzene as the solvent.

Table 5.2.9 Nitrobenzene hydrogenation in dodecane over 0.2504 g Cu(N)/Cab at 155 °C

Reaction time (mins)	Nitrobenzene (mmols)	Aniline (mmols)	Selectivity to aniline (%)
0	8.58	0.0	0.0
34	8.25	0.0	0.0
62	7.54	0.0	0.0
87	6.37	0.11	5.0
123	6.83	0.75	43.0
146	5.60	1.38	46.4
168	3.34	1.37	26.2
198	1.62	0.76	11.0
217	1.63	2.67	38.4
252	0.39	2.42	29.6
281	0.00	4.79	55.8
315	0.00	3.98	46.4

Figure 5.2.9 Nitrobenzene hydrogenation in dodecane over 0.2504 g Cu(N)/Cab at 155 °C

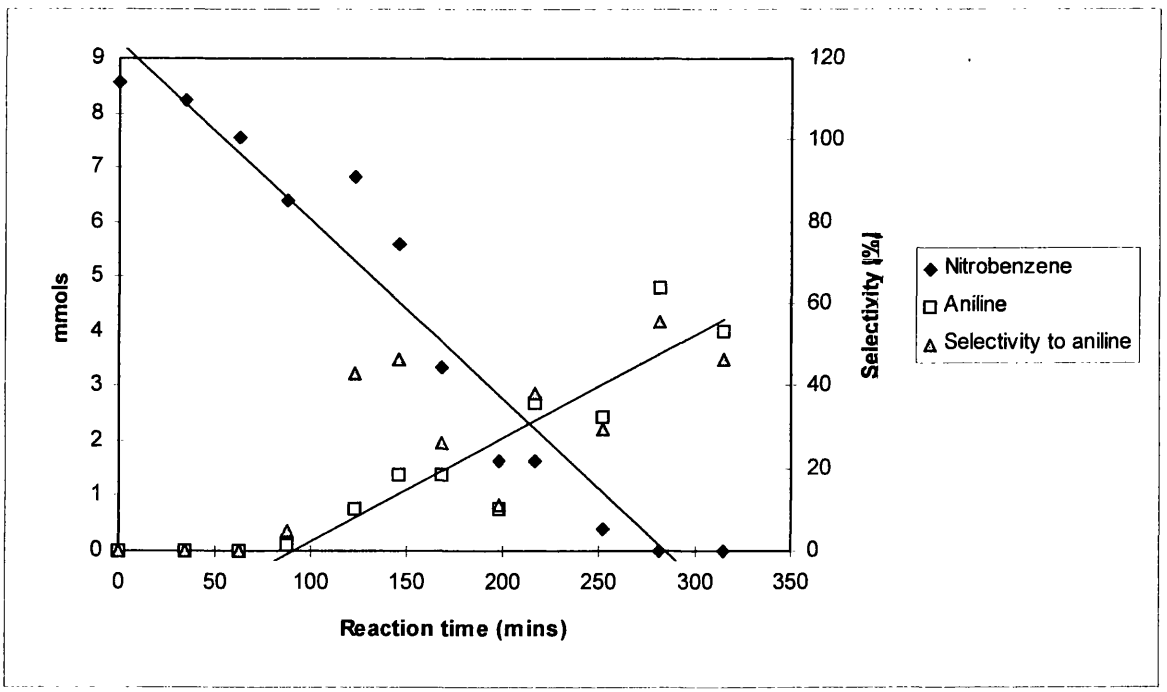

Table 5.2.10 Nitrobenzene hydrogenation in ethyl benzene over 0.2503 g Cu(N)/Cab at 121 °C

Reaction time (mins)	Nitrobenzene (mmols)	Aniline (mmols)	Selectivity to aniline (%)
0	74.75	0.0	0.0
30	69.48	0.0	0.0
60	70.57	0.04	1.0
89	69.74	0.10	2.0
125	73.90	0.23	27.2
169	73.61	0.39	34.0
205	67.42	0.41	5.5
252	74.77	0.66	-4301.6
301	74.79	0.82	-2120.5
344	75.37	0.88	-143.1
404	73.76	1.01	101.4
459	71.29	1.04	30.1

Figure 5.2.10 Nitrobenzene hydrogenation in ethyl benzene over 0.2503 g Cu(N)/Cab at 121 °C

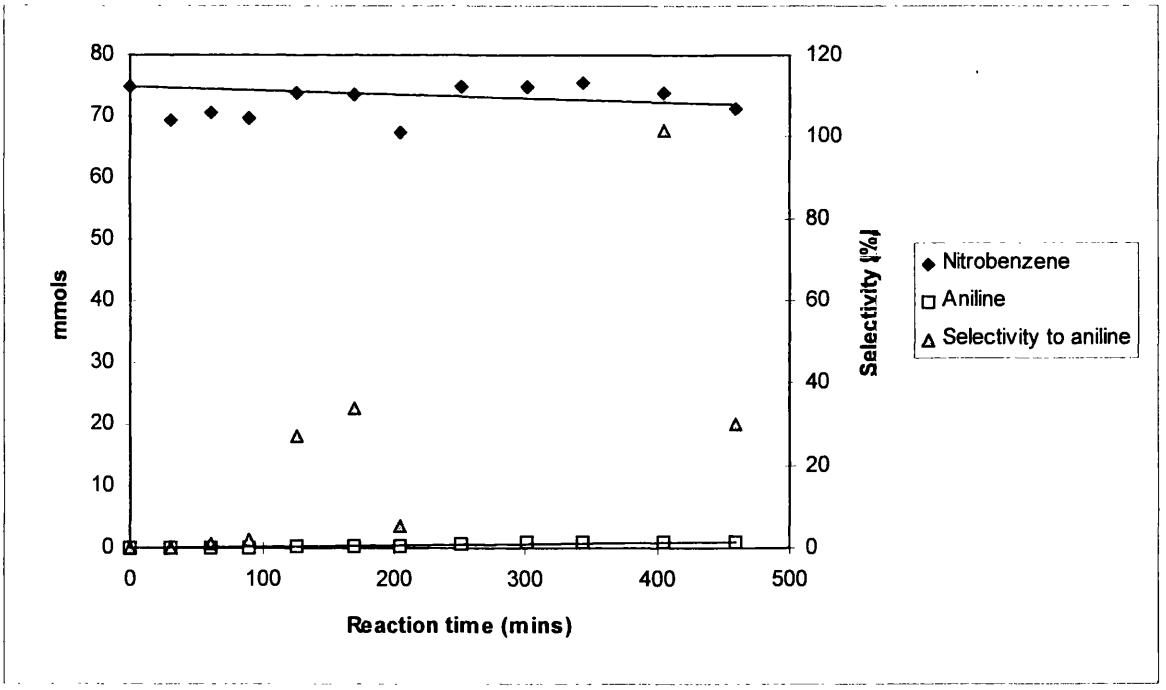

Table 5.2.11 Nitrobenzene hydrogenation in mesitylene over 0.4029 g Cu(N)/Cab at 141 °C

Reaction time (mins)	Nitrobenzene (mmols)
0	7.82
33	7.44
61	7.58
100	9.40
145	5.62
190	7.37
1125	4.58
1128	3.15

Figure 5.2.11 Nitrobenzene hydrogenation in mesitylene over 0.4029 g Cu(N)/Cab at 141 °C

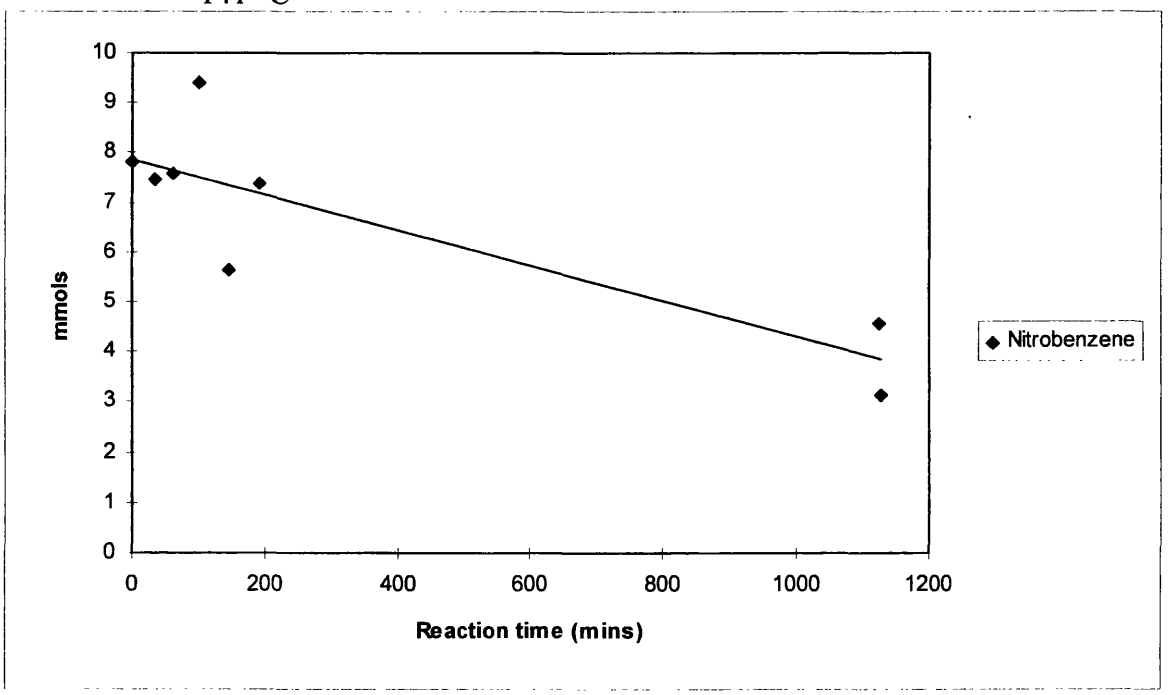

Table 5.2.12 Nitrobenzene hydrogenation in *n*-butyl benzene over 0.4003 g Cu(N)/Cab at 158 °C

Reaction time (mins)	Aniline (mmols)
0	0.00
38	0.59
67	1.06
115	2.02
153	2.44
191	2.84
245	3.24
311	3.84
368	4.02
430	4.64
493	4.79
545	5.03
628	5.42
1211	5.01
1325	4.82
1400	4.68

Figure 5.2.12 Nitrobenzene hydrogenation in *n*-butyl benzene over 0.4003 g Cu(N)/Cab at 158 °C

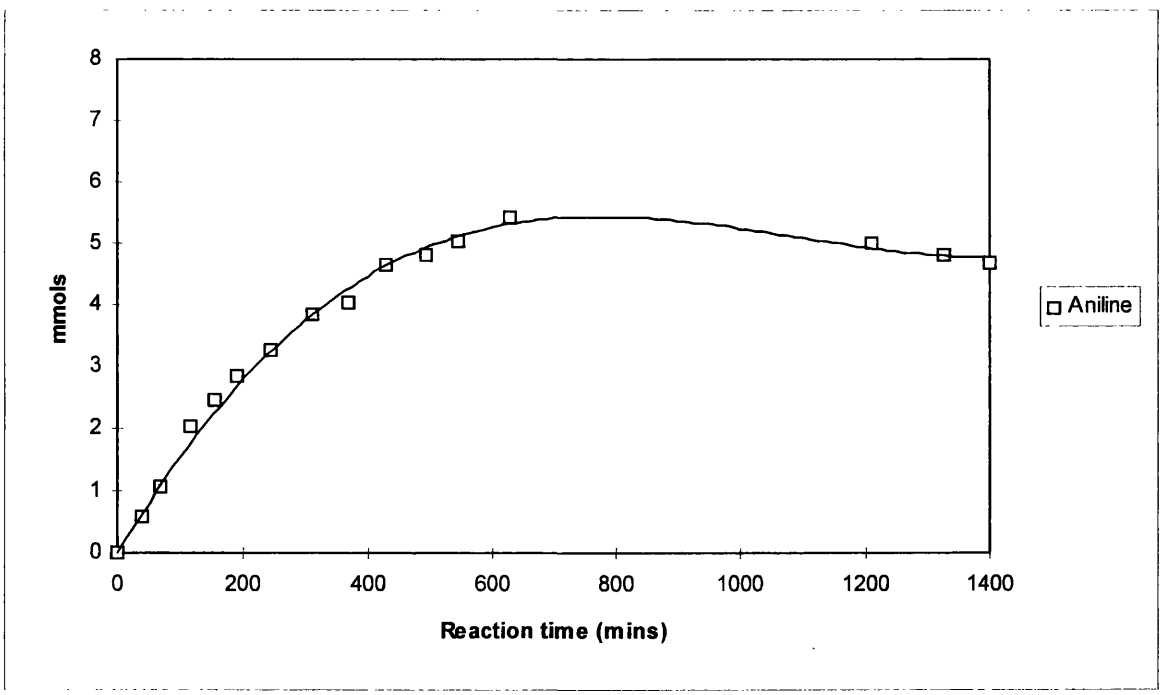

Figure 5.2.13 Representative gas chromatogram using DB-225 capillary column

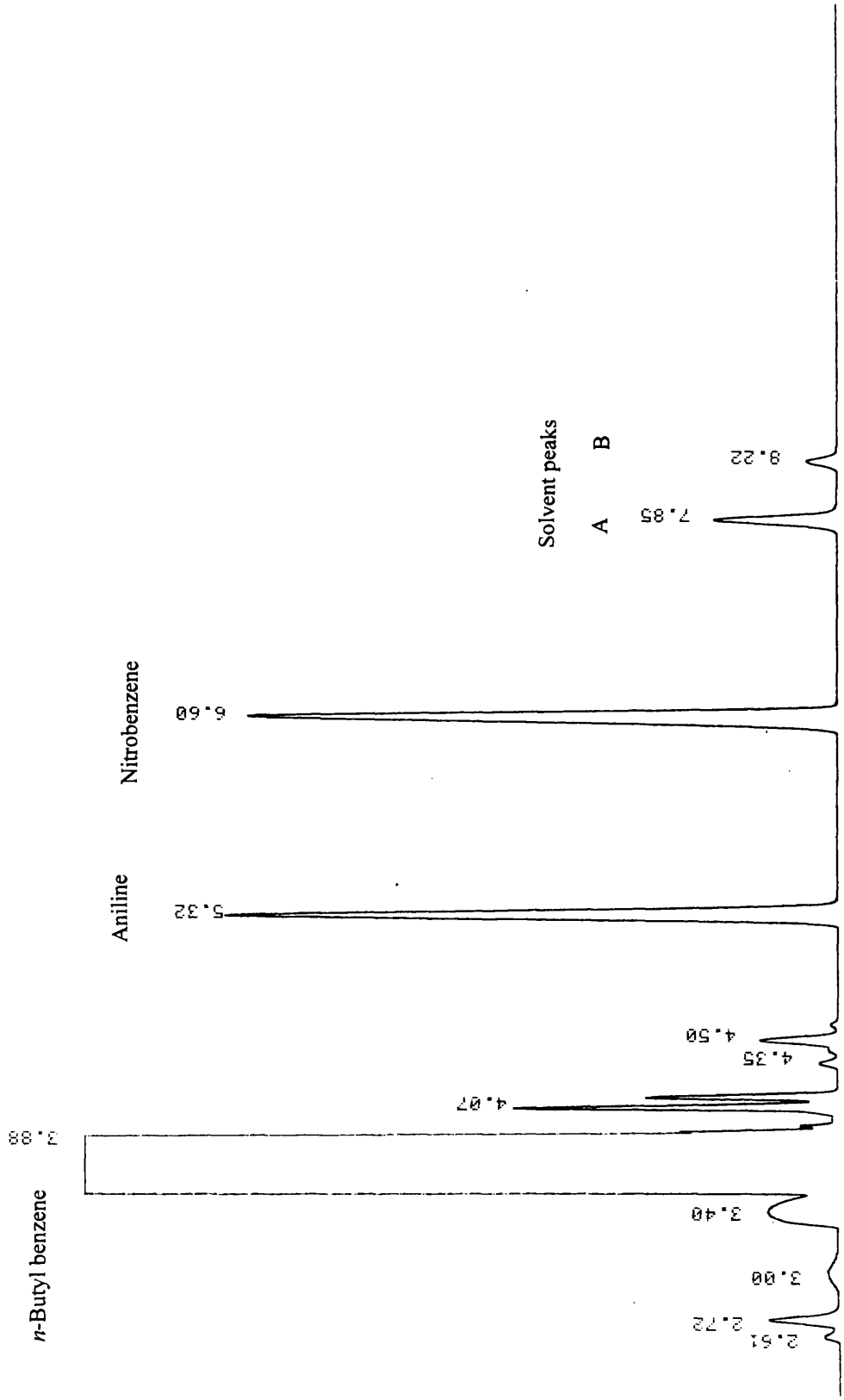

5.2.4 Overview of catalyst performance in *n*-butyl benzene

5.2.4.1 Solvent effects

Having chosen *n*-butyl benzene as the solvent to be used for the reaction testing, a thorough evaluation of its use was conducted. This section details these findings, as well as giving some information on the performance of the copper catalysts themselves.

The first observation was the change in relative peak intensities of two solvent impurities, denoted A and B (see Figure 5.2.13, Section 5.2.3). Table and Figure 5.2.14 display the peak areas of A and B during the course of a typical reaction, *i.e.* in the presence of nitrobenzene. Table and Figure 5.2.15 compare the areas of A and B when the reaction is conducted in the presence and absence of nitrobenzene.

It is apparent that A is converted to B, and that this probable hydrogenation reaction reaches equilibrium after one hour. The relative concentrations at equilibrium are affected by the presence of nitrobenzene, but the sum total of the two components effectively remains constant throughout the reaction. Overall, the concentrations of the solvent impurities are low in comparison with those of nitrobenzene and aniline, and whilst the main reaction occurs over 360 minutes the 'side reaction' between A and B reaches completion after 60 minutes. It was therefore concluded that this solvent effect did not contribute to the major reaction, *i.e.* this phenomena did not directly involve nitrobenzene or its derivatives, and was of no consequence to the hydrogenation of nitrobenzene to aniline.

All analyses of reaction samples when using *n*-butyl benzene as solvent were performed with the polar DB-225 capillary column, to obtain the required resolution of

the various components. It was observed that a small broad peak with a retention time of approximately nine minutes was sometimes observed. The appearance of this peak however was erratic, and would even vary between injections of the same sample. Analysis on the non-polar SE-30 capillary column provided a means to resolve and reliably quantify this component, revealing its development during the reaction sequence. Gas chromatography-mass spectrometry identified the compound as N-phenylmethylenebenzenamine [$C_6H_5N{=}CHC_6H_5$]; Table and Figure 5.2.16 display its peak area, in comparison with that of aniline, during a typical reaction.

The presence of nitrogen in this species suggests the involvement of nitrobenzene. However, Figure 5.2.16 shows that the amount of N-phenylmethylenebenzenamine present in the reactant mixture plateaus after roughly one hour, indicating that its formation requires another component which is available in limited supply. It was concluded, therefore, that the formation N-phenylmethylenebenzenamine resulted from the presence of an unknown solvent impurity. Whilst nitrobenzene was involved in this reaction, the concentration of N-phenylmethylenebenzenamine is small in comparison with that of nitrobenzene, and did not significantly affect the major reaction. The observance of this by-product was deemed to be only an effect of the solvent; no other by-products were detected in solution when using the copper-based catalysts.

In addition, a 'cold-trap' experiment was conducted in which the exit gases were passed through a Dreschel bottle immersed in an ice bath downstream of the condenser. This was performed to verify that no volatile species were formed during the course of

the reaction, and then carried beyond the condenser by the flow of gas; no such species were observed.

5.2.4.2 Carbon mass balance

During reaction testing of the catalysts it was observed that the sum of the aniline and nitrobenzene components did not always correspond to the initial number of moles of nitrobenzene present. The deficit generally increased with time, and was outside the range of experimental error. This loss of material could be accounted for in three ways; the removal of material from the system, the formation of by-products, or carbon deposition onto the catalyst. Blank reactions, as presented in Section 5.2.2, had confirmed that the system was closed, *i.e.* the reagents were contained within the reaction vessel. When using *n*-butyl benzene as the solvent the only by-product detected over the copper catalysts was related to the solvent itself, and not of a significant concentration. The loss of material observed during the reactions was therefore attributed to carbon deposition onto the catalyst. This carbon deposition/laydown has been defined as the difference between the initial number of moles of nitrobenzene present and the sum of the aniline and nitrobenzene components at any given time.

The formation of carbonaceous overlayers is a topic of considerable interest in catalysis. Both the activity and selectivity of a catalyst can be altered by the presence of such residues, and these changes can be positive or negative [109]. It is believed that the effect of overlayers is to restructure the catalyst surface to create new catalyst sites and affect the bonding of reactants, intermediates and products [6b].

The pattern of this mass loss and inferred carbon laydown predominantly followed that shown by Table and Figure 5.2.17; becoming significant only after the nitrobenzene is exhausted. The rate of deposition at this point is relatively rapid, but slows with time.

This evidence implies that the formation of the carbonaceous overlayer arises from the aniline. Carbon laydown is not observed as long as nitrobenzene is present, the greater adsorption strength of the nitro group being favoured over the amine, *i.e.* the nitrobenzene is assumed to have a higher heat of adsorption than the aniline. Upon the exhaustion of nitrobenzene, adsorption of the aniline then occurs, with its subsequent hydrogenolysis to benzene and ammonia. This reaction sequence is shown by Figure 5.2.18. It has been shown that aromatic compounds have a propensity to act as coking agents, polymerizing through a series of dehydrogenation reactions to from polyaromatic compounds [109].

Figure 5.2.18 Reaction sequence leading to formation of carbonaceous overlayer

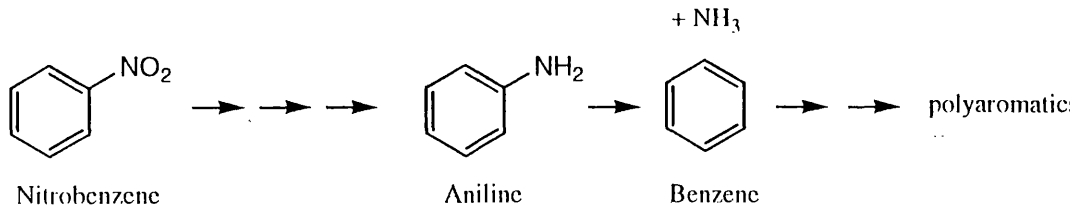

No polyaromatics were detected in solution and the 'cold-trap' experiment did not reveal the presence of ammonia. However, complete hydrogenolysis of the aniline present

would result in the formation of only *ca.* 8 mmols of ammonia. Considering the surface area of the condenser, it is not surprising that the presence of this volume of ammonia (*ca.* 0.58 ml) was not observed. It is assumed that the phenyl moieties, the precursors to polyaromatic formation, were retained by the catalyst surface.

In order to test this hypothesis a catalyst lifetime experiment was performed. Here, the catalyst underwent a typical batch run of conversion of nitrobenzene to aniline. Following complete consumption of the nitrobenzene, an additional aliquot of the reactant was added. The results are presented by Table 5.2.18 and Figure 5.2.19. The results are as expected for the initial volume of nitrobenzene, and on addition of the second aliquot the rate of nitrobenzene consumption was initially consistent with that observed previously. However, after approximately two hours the rate dropped dramatically and minimal activity was observed after this point; this considerable loss of activity suggests that deactivation of the catalyst has occurred.

The carbon mass balance trend shown by Table and Figure 5.2.17 was observed in the overwhelming majority of cases. At an early stage in the project, however, the alternative pattern displayed by Table 5.2.19 and Figure 5.2.20 was produced. It appears in this case that carbon deposition proceeds slowly but steadily throughout the reaction. As stated above, this model was only occasionally observed, and the predominant pattern showed no measurable carbon deposition until the consumption of the nitrobenzene, but becoming significant thereafter. The different temperatures reported for these two

possibilities is not believed to be a factor; the pattern shown by Figure 5.2.17 being produced from 95 to 170 °C.

One further point merits discussion in this section of the report. It will be noticed that the reaction results over the copper catalysts presented from Sections 5.2.1 to 5.2.3 inclusive and Section 5.2.6 show reaction rates which decrease through time. These experiments were conducted during the 'development' phase of the project, whilst the experimental protocol was still under refinement. Subsequent results show that the reaction is zero order in nitrobenzene, which is consistent with the majority of published results. It is unlikely that this was due to some radical change in the reaction chemistry, and it is believed that a flaw in the early experimental technique led to these erroneous results. The gradual loss of catalyst activity observed in this initial work is attributed to ineffective purification of the dihydrogen feed gas, leading to a progressive oxidation of the reduced metal surface.

5.2.4.3 Conclusions

In summary, *n*-butyl benzene had been shown to be a suitable solvent for nitrobenzene hydrogenation. Minor solvent effects are observed but do not appear to affect the course of the reaction. There is evidence of carbon deposition on the copper catalysts, but the mechanism at work is unclear. The reaction protocol had been refined to an acceptable degree, and *n*-butyl benzene was found to be suitable as a solvent.

Table 5.2.14 Change in areas of solvent peaks A and B, in the presence of nitrobenzene

Reaction time (mins)	A (with NB) (mm^2)	B (with NB) (mm^2)	Nitrobenzene (mm^2)	Aniline (mm^2)
0	18	2	92	0
60	10	10	76	13
120	10	9	63	29
180	9	10	46	44
240	10	9	29	62
300	10	10	16	77
360	9	10	0	91

Figure 5.2.14 Change in areas of solvent peaks A and B in the presence of nitrobenzene

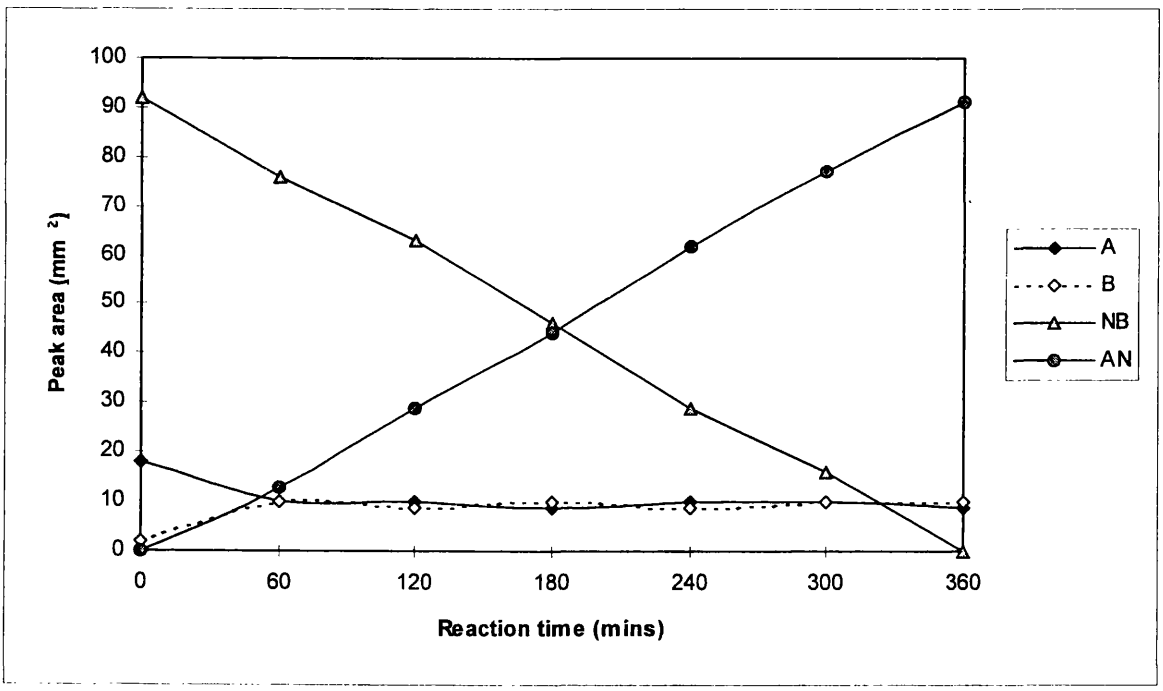

Table 5.2.15 Change in areas of solvent peaks A and B, in the presence and absence of nitrobenzene

Reaction time (mins)	A (with NB) (mm^2)	B (with NB) (mm^2)	A (no NB) (mm^2)	B (no NB) (mm^2)
0	18	2	23	2
60	10	10	19	5
120	10	9	20	4
180	9	10	20	4
240	10	9	18	4
300	10	10	19	4
360	9	10	18	5

Figure 5.2.15 Change in areas of solvent peaks A and B in the presence and absence of nitrobenzene

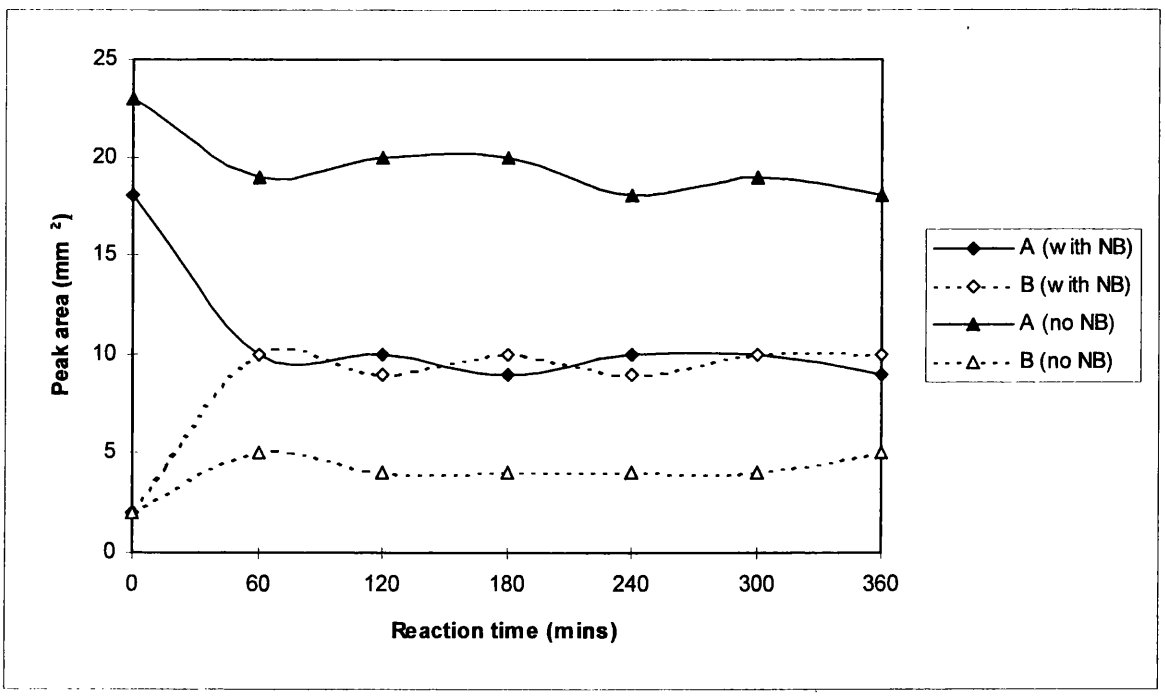

Table 5.2.16 Peak areas of aniline and N-phenylmethylenebenzenamine during a typical reaction

Reaction time (mins)	Aniline (mm^2)	N-phenylmethylenebenzenamine (mm^2)
0	0	0
30	5	2.0
60	13	4.1
90	24	4.3
120	29	4.5
150	35	4.4
180	44	4.4
210	52	4.3
240	62	5.4
270	71	5.1
300	77	4.8
330	81	4.5
360	91	4.7

Figure 5.2.16 Peak area of N-phenylmethylenebenzenamine during a typical reaction

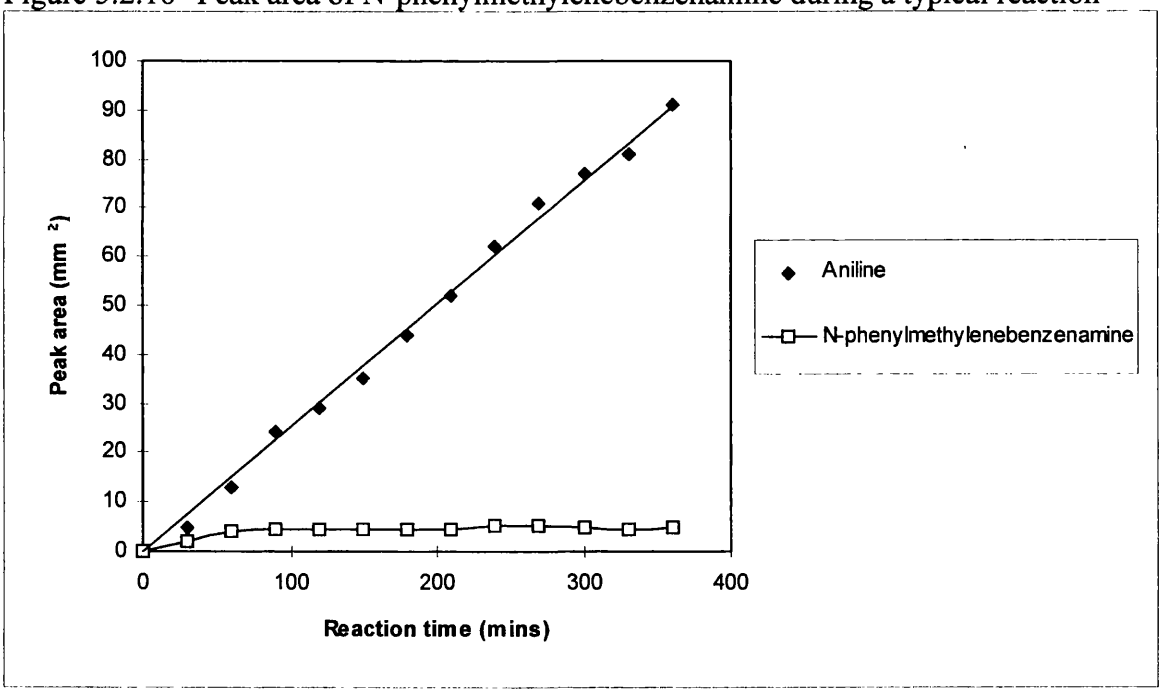

Table 5.2.17 Nitrobenzene hydrogenation and carbon laydown over Cu(N)/Cab at 110 °C

Reaction time (mins)	Nitrobenzene (mmols)	Aniline (mmols)	Carbon laydown (mmols)
0	7.87	0	0.00
30	7.55	0.717	-0.40
60	6.66	1.91	-0.70
90	4.58	3.44	-0.15
130	3.49	4.06	0.32
160	2.9	5.83	-0.86
190	1.45	6.5	-0.08
220	0	7.94	-0.07
250	0	7.56	0.31
280	0	7.17	0.70
310	0	7.17	0.70
370	0	6.79	1.08
540	0	6.41	1.46
1140	0	6.03	1.84

Figure 5.2.17 Nitrobenzene hydrogenation and carbon laydown over Cu(N)/Cab at 110 °C

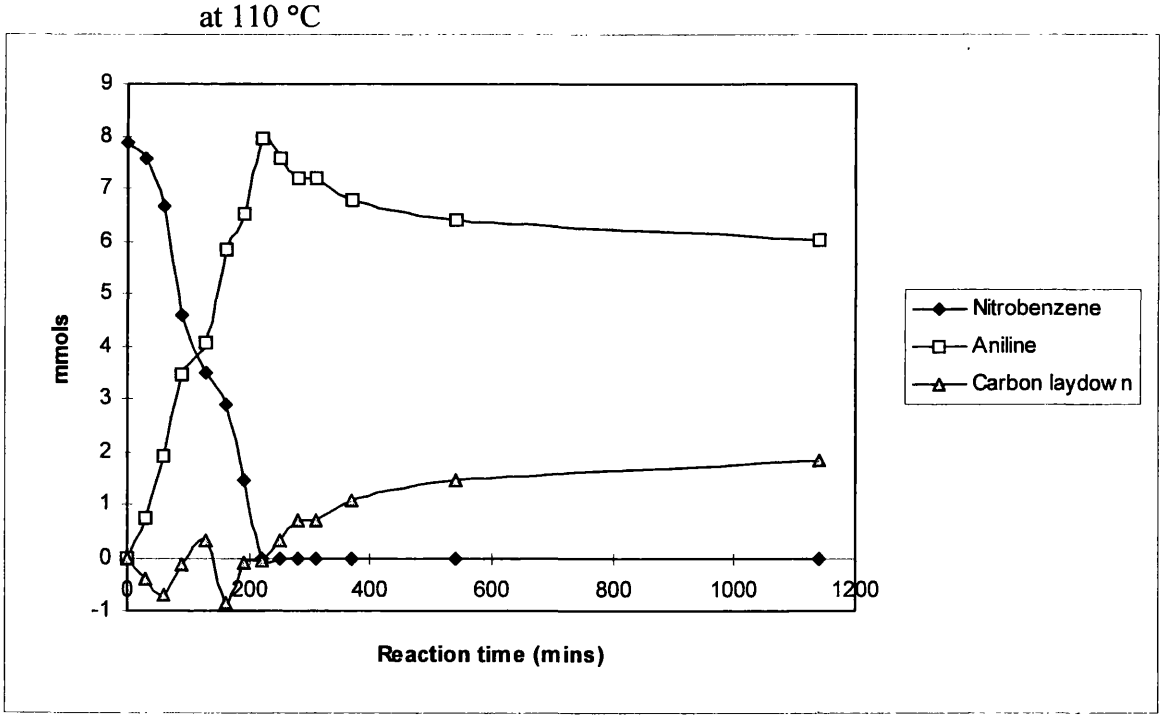

Table 5.2.18 Lifetime experiment

Reaction time (mins)	NB - 1st aliquot (mmols)	NB - 2nd aliquot (mmols)
0	8.72	9.07
60	7.50	8.37
120	6.36	7.28
180	5.66	7.16
240	4.40	
300		7.06
420		6.98
1320		5.76

Figure 5.2.19 Lifetime experiment

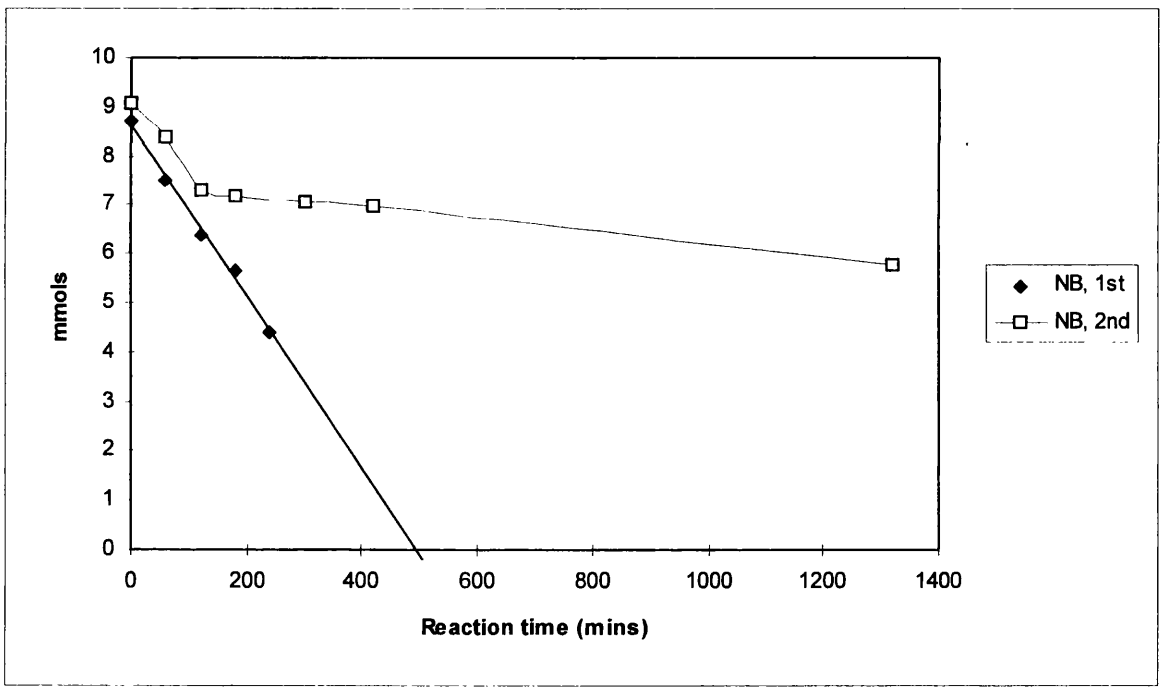

Table 5.2.19 Nitrobenzene hydrogenation and carbon laydown over Cu(N)/Cab at 158 °C

Reaction time (mins)	Nitrobenzene (mmols)	Aniline (mmols)	Carbon laydown (mmols)
0	7.63	0.00	0.00
30	6.53	0.89	0.20
60	5.42	1.90	0.31
90	4.21	3.06	0.36
120	2.91	4.16	0.56
158	1.31	5.73	0.59
179	0.31	6.65	0.67
208	0.00	7.01	0.62
222	0.00	7.02	0.61
237	0.00	6.84	0.79
268	0.00	6.90	0.73
314	0.00	6.77	0.86
416	0.00	6.46	1.17

Figure 5.2.20 Nitrobenzene hydrogenation and carbon laydown over Cu(N)/Cab at 158 °C

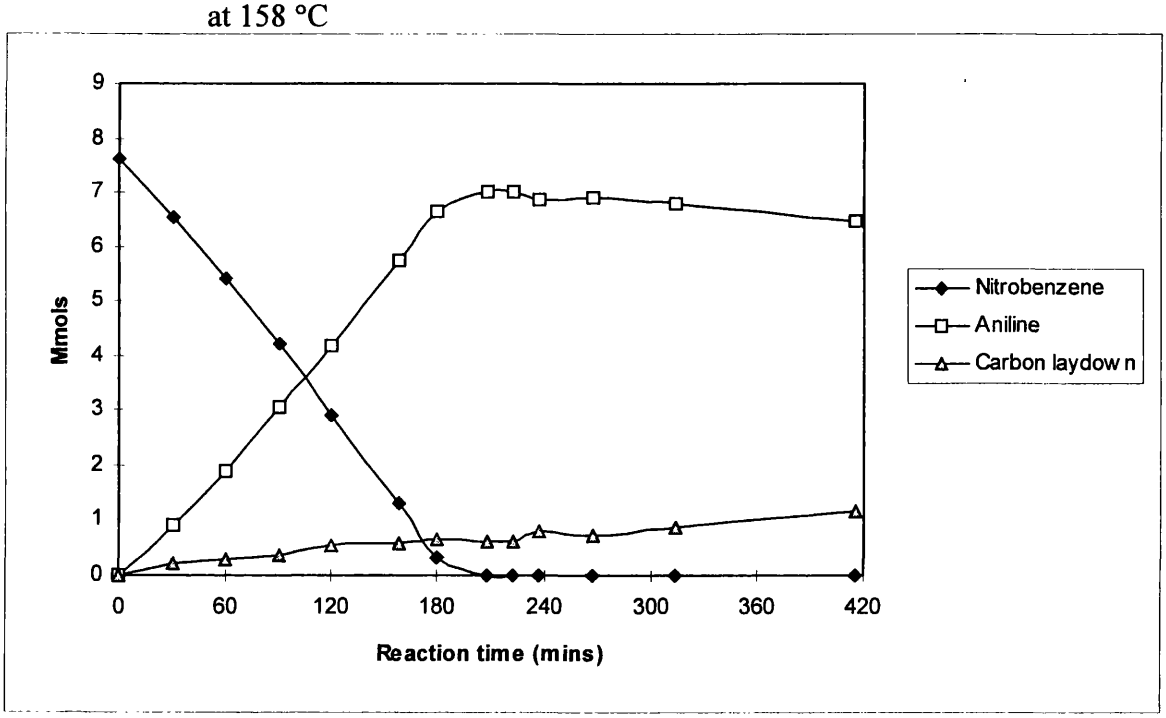

5.2.5 Alkylation of aniline

5.2.5.1 Introduction

Whilst evaluating hexan-1-ol as a solvent for nitrobenzene hydrogenation, the formation of several by-products was observed. Gas chromatography-mass spectrometry identified N-hexylenebenzenamine [$C_6H_5N{=}CH(CH_2)_4CH_3$] and N-hexylaniline [$C_6H_5NH(CH_2)_5CH_3$], revealing an alkylation reaction which occurred between the aniline product and the hexan-1-ol solvent.

Aromatic and aliphatic secondary amines are used as antioxidants in the polymer and rubber industries, and as precursors to a variety of dyes and dye intermediates [110]. N-alkylated amines are also used in the synthesis of pharmaceutical compounds [111]. The alkylation of aniline can be performed in the liquid phase using a homogeneous catalyst [112-115]. Alternatively, heterogeneous catalysts reported for use in N-alkylation of aniline include Raney nickel [53], copper chromite [116] and metal oxides such as alumina [117, 118], zeolites [119] and vanadia [120].

The reaction is usually reported with either alcohols or carbonyl compounds used as both reagent and solvent [53, 116, 120]; the use of alcohols requiring an initial dehydrogenation step to form the carbonyl group [53]. The first step of the mechanism is condensation between the aldehyde and amine to form an imine, produced via carbinolamine and iminium ion intermediates [121]. This may then be reduced to N-alkylaniline. The reaction may then in theory proceed to yield N,N-dialkylaniline, although this tertiary amine is not always observed. The reaction mechanism is shown by Figure 5.2.21 [121].

The reaction is significantly affected by steric factors. It has been shown that the percentage yield of N-alkylaniline from straight chain alcohols is approximately twice that of their equivalent branched isomers [53]. Similarly, reactivity decreases with the increasing steric hindrance of carbonyl compounds [116].

Figure 5.2.21 Mechanism of N-Alkylaniline formation

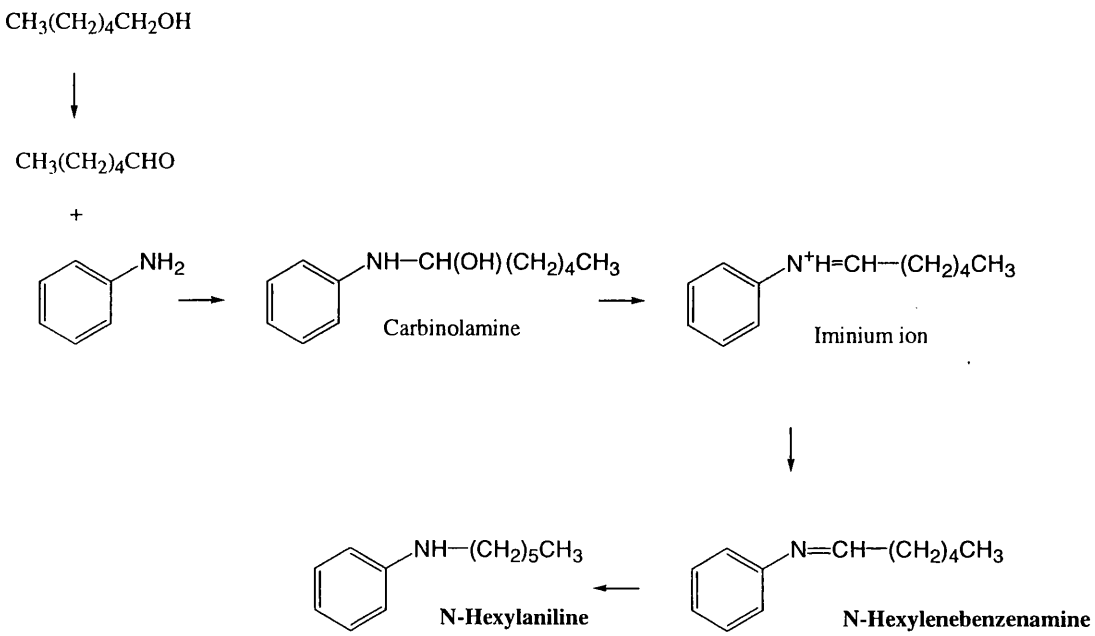

5.2.5.2 Nitrobenzene hydrogenation

Initially, the experiments using hexan-1-ol were conducted as normal, *i.e.* with 80 ml of *ca.* 0.1 M nitrobenzene in hexan-1-ol solution. Throughout the chapter N-hexylenebenzenamine and N-hexylaniline are referred to as HBA and HA respectively. The concentration of these by-products was assessed by the method described in Section 4.2. Typical results for these reactions are shown by Table 5.2.20 and Figure 5.2.22.

These results show that the nitrobenzene is consumed within ten hours, with aniline appearing as the predominant product. However, the presence of N-hexylenebenzenamine is also detected within the first sample, this species remaining in low concentration throughout the reaction. N-hexylaniline was observed after six hours, its concentration rising slowly until the complete consumption of nitrobenzene, and becoming more rapid thereafter.

5.2.5.3 Aniline alkylation

To gain further insight into the mechanism of the reaction the hydrogenation of aniline in hexan-1-ol was conducted, with the obtained data displayed in Table 5.2.21 and Figure 5.2.23. It should be noted that for these results, the sample at -20 mins corresponds to the initial reaction mixture, whilst the sample at zero minutes was taken upon the switch from helium to dihydrogen once the system was thermally equilibrated.

It is evident that the formation of N-hexylenebenzenamine can proceed under helium, but that N-hexylaniline is only produced under a reductive atmosphere. The

concentration of N-hexylenebenzenamine remains low, whilst that of N-hexylaniline rises steadily throughout the reaction, and corresponds to the observed loss of aniline.

The reaction of nitrobenzene and aniline in hexan-1-ol in the absence of catalyst was also examined. The data obtained, shown by Table 5.2.22 and Figure 5.2.24, shows fluctuations in the reagent concentrations which were within the range of experimental error at this time. No reaction was observed between nitrobenzene, aniline and the hexan-1-ol solvent. This indicates that the alkylation step does not occur homogeneously, and confirms that the reaction is catalysed by the supported copper substrate.

5.2.5.4 Overview

In view of these results several conclusions have been made. The N-hexylenebenzenamine and N-hexylaniline species observed arise through the alkylation of aniline with hexan-1-ol, and are thought to occur via the mechanism shown by Figure 5.2.21. The first intermediate stable in solution is N-hexylenebenzenamine, which is then hydrogenated to N-hexylaniline.

It has been established that such alkylation reactions are acid-catalyzed, the rate of reaction between acetone and hydroxylamine, for example, reaching a maximum at pH 4.5 [121]. It is therefore quite possible that this step could take place on the silica support, and not on the metal crystallites themselves; this could be established by conducting a reaction with just the silica support. The blank reaction, performed without catalyst or support, confirmed that it does not occur homogeneously. The subsequent hydrogenation step to N-hexylaniline, however, almost certainly occurs on the copper particles.

With regard to competition for the active sites, it is clear that the adsorption of nitrobenzene is favoured over that of the N-hexylenebenzenamine. This preference is not totally exclusive, however, as some selectivity to N-hexylaniline is evident whilst nitrobenzene is still present. The rate of N-hexylaniline formation increases markedly upon complete nitrobenzene consumption. This may indicate competitive adsorption for one type of active site. Alternatively, two types of site may be present; both of which facilitate the hydrogenation of N-hexylaniline, whilst only one allows the hydrogenation of nitrobenzene.

What is perhaps most surprising is the formation of these by-products in the first place. Alcohols are the solvents of choice for nitrobenzene hydrogenation over a wide variety of catalysts [32-34, 36, 38, 42, 46]. These catalysts are based on metals which are far more active than copper, and are generally supported on oxides which are comparable with silica, if not on silica itself. Nevertheless, only one of the papers reviewed cited the formation of N-alkylaniline, or its imine precursor, as by-products - Turek *et al* reporting the formation of N-ethylaniline over nickel/alumina catalyst when using ethanol as the reaction medium [32]. One possible explanation is that the majority of these studies were conducted around room temperature, which may be too low for a significant rate of alkylation, especially in comparison with the high rate of aniline formation over more active metals. In summary, the alkylation of aniline, via nitrobenzene, with hexan-1-ol is reported over copper/silica catalysts in the liquid phase.

Table 5.2.20 Nitrobenzene hydrogenation and subsequent aniline alkylation over 0.5459 g Cu(N)/Cab at 110 °C

Reaction time (mins)	Nitrobenzene (mmols)	Aniline (mmols)	HBA (mmols)	HA (mmols)
0	7.826	0.0	0.0	0.0
60	7.001	0.721	0.083	0.0
120	6.020	1.346	0.113	0.0
180	5.324	1.923	0.102	0.0
240	4.593	2.453	0.117	0.0
300	3.648	2.908	0.086	0.0
361	3.014	3.486	0.195	0.023
420	1.784	3.889	0.153	0.048
480	1.133	4.297	0.208	0.058
540	0.192	4.666	0.153	0.082
600	0.0	4.514	0.131	0.049
660	0.0	4.601	0.081	0.105
750	0.0	4.428	0.106	0.192
843	0.0	4.514	0.116	0.282
932	0.0	4.514	0.142	0.377
1021	0.0	4.601	0.165	0.465
1111	0.0	4.514	0.147	0.538
1200	0.0	4.297	0.091	0.625
1292	0.0	4.601	0.113	0.700
1380	0.0	4.471	0.169	0.802
1440	0.00	4.384	0.347	0.845

Figure 5.2.22 Nitrobenzene hydrogenation and subsequent aniline alkylation over 0.5459 g Cu(N)/Cab at 110 °C

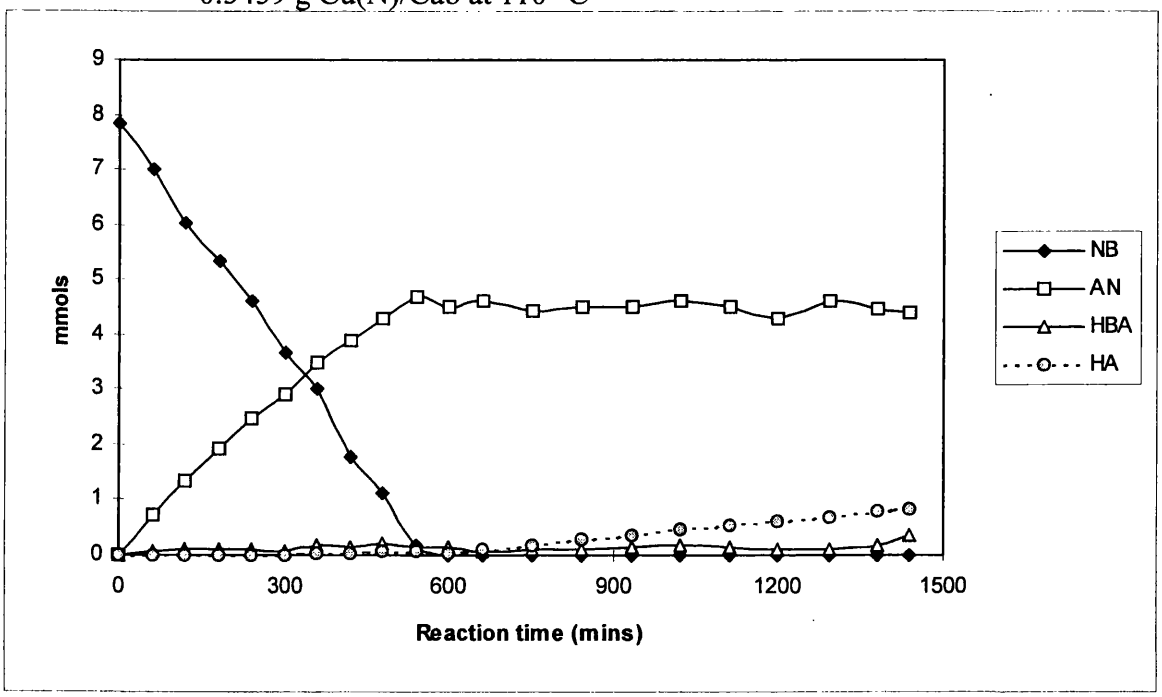

Table 5.2.21 Aniline alkylation with hexan-1-ol over 0.5491 g Cu(N)/Cab at 110 °C

Reaction time (mins)	Aniline (mmols)	HBA (mmols)	HA (mmols)
-20	8.340	0.000	0.000
0	8.288	0.096	0.000
60	7.686	0.054	0.278
121	7.529	0.052	0.419
184	7.320	0.050	0.571
259	7.163	0.056	0.726
300	7.007	0.059	0.856
361	6.954	0.052	0.992
430	6.588	0.057	1.108
480	6.745	0.047	1.169
543	6.902	0.053	1.323
651	6.536	0.050	1.485
740	6.275	0.058	1.685
840	5.856	0.061	1.808
948	5.647	0.059	1.985
1080	5.699	0.067	2.138

Figure 5.2.23 Aniline alkylation with hexan-1-ol over 0.5491 g Cu(N)/Cab at 110 °C

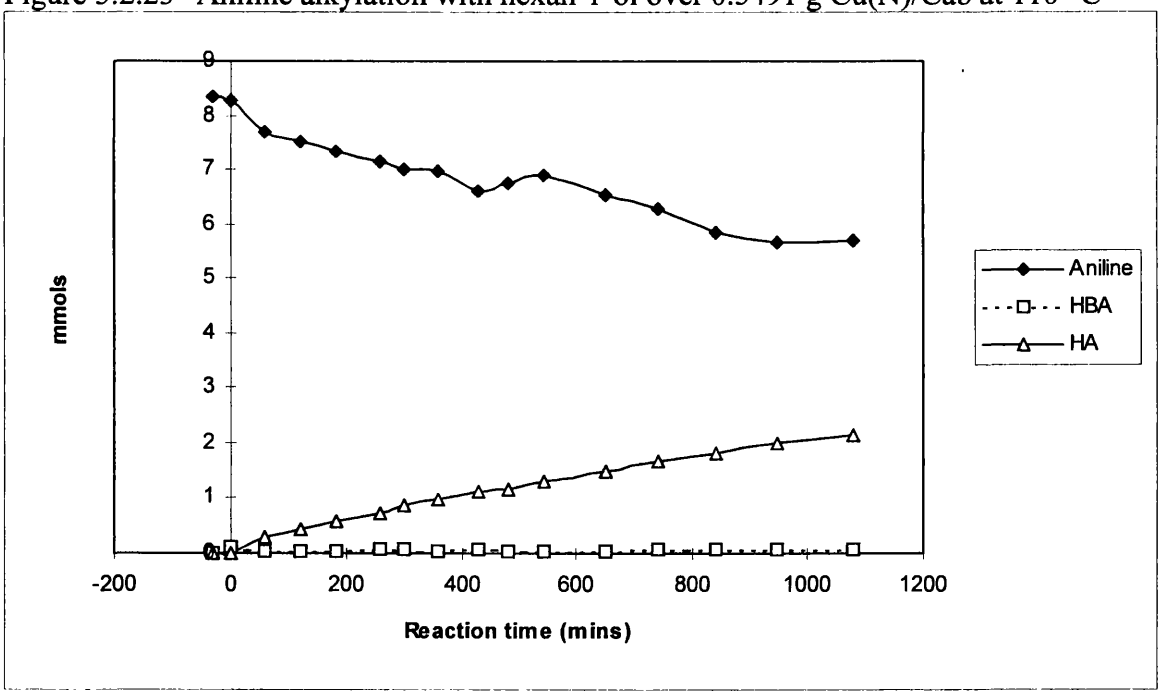

Table 5.2.22 Blank run with nitrobenzene and aniline at 133 °C

Reaction time (mins)	Nitrobenzene (mmols)	Aniline (mmols)
0	2.45	2.75
47	2.44	2.73
91	1.91	2.65
149	1.85	2.59
197	1.84	2.55
250	2.00	2.79
307	1.90	2.66

Figure 5.2.24 Blank run with nitrobenzene and aniline at 133 °C

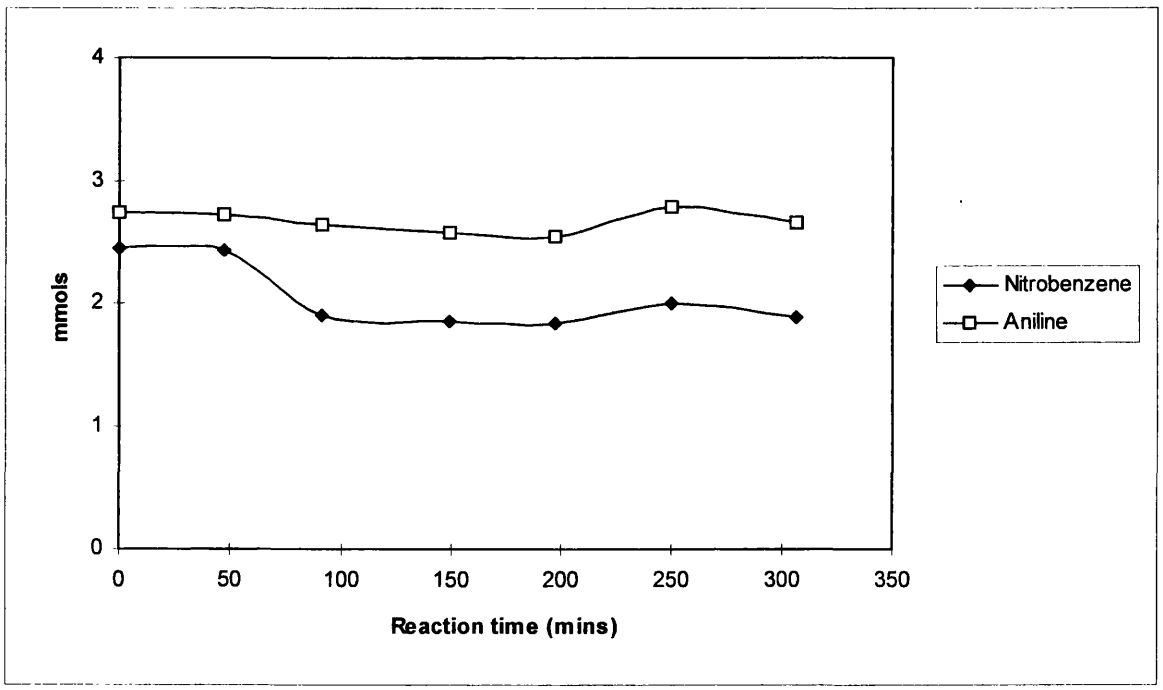

5.2.6 Sulphur effects

5.2.6.1 Introduction

The hydrogenation of nitrobenzene using *t*-butyl benzene as the reaction medium showed great variability amongst the observed rates with different batches of this solvent. The variability was eventually linked to the concentration of sulphur which was present as an impurity in the solvent (see Section 5.2.6.2). The total concentration of sulphur present in the batches of *t*-butyl benzene was established, and the presence of five sulphur-based impurities was detected. However, a full assignment of their identities was not possible. The total sulphur content of a sample of *n*-butyl benzene, the solvent used for the majority of the project, was determined. The effects of thiophene-doped *t*-butyl benzene upon catalytic performance were then investigated (see Section 5.2.6.3).

Throughout this chapter 'sulphur mixture' refers to the original blend of sulphur-containing species which were present in untreated batches of solvent, whilst 'thiophene-doped' refers to samples which were treated to contain only thiophene-derived sulphur.

Sulphur, in a variety of chemical forms, is a commonly encountered impurity in reactant mixtures. Trace quantities of sulphur can lead to rapid deactivation of a catalyst, and in such cases the sulphur is described as a catalytic poison. Poisoning of a metal catalyst can arise through chemisorption, reaction or alloying processes involving the impurity [3c]. A chemisorbed poison may act by blocking an active site, this geometrical effect then preventing adsorption of the reactant. Alternatively, the negative effect of a catalyst poison may be viewed as an electronic effect, whereby the role of the sulphur is

to change the electronic structure of the active catalyst sites and detrimentally affect reactant adsorption [3d]. The electronic effect may extend some distance from the chemisorbed species [122].

Much research has been devoted to the effects of sulphur on metal catalysts, and it has been shown that at very low levels (ppm to ppb) it can actually have a positive effect on catalyst performance [123]. Where an increase in the selectivity is observed, the adsorption of sulphur leads to a change in the product distribution, favouring the desired reaction pathway over another. Examples include the reaction of propane over platinum/alumina catalyst [124] and carbon monoxide hydrogenation over rhodium/silica [125]. This phenomena can also improve the activity of catalysts, as has been shown for platinum-catalysed reforming reactions, where the addition of sulphur decreases the amount of carbon laydown with a consequent improvement in catalyst activity [126].

Copper catalysts are extremely sensitive to the presence of catalytic poisons, in particular chlorine- and sulphur-based impurities. The presence of chlorides results in the formation of copper chlorides, which not only decrease the available reaction sites but also accelerate sintering of the metal crystallites [7e]. The reaction between sulphur-based impurities and copper metal results in the formation of copper sulphide, Cu_2S, and much effort has been devoted both to lowering the sulphur content of industrial feedgas mixtures and to the development of copper-based catalysts which are resistant to sulphur poisoning, *i.e.* methanol synthesis catalyst, $Cu/ZnO/Al_2O_3$ [7f].

However, it has been proven that the effects of low sulphur concentrations can be exploited to improve the selectivities of supported copper catalysts. The selective

hydrogenation of α,β-unsaturated aldehydes over supported copper catalysts has been studied extensively by Hutchings *et al* [127, 128]. With regard to crotonaldehyde, $CH_3CH=CHCHO$, it was found that an unmodified copper/alumina catalyst favoured the formation of the corresponding saturated alcohol, 1-butanol. Pre-dosing this catalyst with a suitable amount of thiophene shifted the product distribution towards crotyl alcohol, $CH_3CH=CHCH_2OH$, although this was accompanied by a loss of activity [127]. The adsorption of thiophene onto the catalyst was observed, which accounted for the activity loss, as the presence of the adsorbate would decrease the number of active sites available for reaction. However, the change in selectivity was found to result predominantly from the electronic effects of sulphur adsorption. Hutchings and co-workers concluded that the promotional role of thiophene over these catalysts was the creation of new Cu^+-S sites, which led to enhanced formation of the unsaturated alcohol [128].

The modification of catalysts using sulphur-based additives is not trivial, however, and it has been shown that catalytic behaviour varies greatly with the nature of such treatment, *e.g.* predosing, continuous addition to feedstock, *etc.* [124]. Nevertheless, such sulphidisation techniques are employed industrially, and are successful in enhancing the performance of catalysts used in the gas phase hydrogenation of nitrobenzene [55].

5.2.6.2 t-Butyl benzene

During the course of reaction testing using *t*-butyl benzene as the solvent, it became evident that the particular batch of *t*-butyl benzene, and its history, bore marked

effect upon catalyst performance. The adopted nomenclature and treatment of the various batches are shown in Table 5.2.3.

Table 5.2.23 Nomenclature of the batches of *t*-butyl benzene

Name	Treatment
A	Original sample of batch A
B	Original sample of batch B
C	1 : 1 Mixture of A and B
D	Recovered from reaction and reused
E	Purified by Raney nickel

To avoid ambiguity it should be pointed out that *t*-butyl benzene A and B were both supplied by Aldrich, at 99 % purity. The only difference between them is that they originated from different batches. The sample of C was an equal blend of these two batches, whilst the D sample was solvent (predominantly B) which had been recovered following use in reaction. The E sample was a volume of B which had been left stirring at room temperature with ca. 1 g of Raney nickel overnight. As nickel has a strong affinity for sulphur, forming nickel sulphide in the process, this step was undertaken to remove any sulphur-based impurities which were present in the solvent. The preparation of the Raney nickel employed is described in Section 3.2.3.

A comparison of the aniline formation using the different batches of *t*-butyl benzene is given in Table 5.2.24 and Figure 5.2.25; all other reaction conditions were identical. The aniline formation of each series is presented, as is the consumption of nitrobenzene for the reaction using A.

Table 5.2.24 Comparison of aniline formations using different batches of *t*-butyl benzene over 0.40g Cu(N)/Cab at 148 °C

		Aniline (mmols)				
Reaction time (mins)	A, NB (mmols)	A	B	C	D	E
0	7.25	0.0	0.0	0.0	0.0	0.0
26				0.0		
31	7.09	0.47				
43			0.35			
48						0.0
60	6.08	0.79				
77				0.22		
89	7.01	1.31				
91			0.46			
110					0.15	0.29
119	5.22	1.39				
130			0.68			
131				0.32		
155	5.26	1.81				
161			0.76			
165						0.36
201	5.01	2.37				
205				0.47		
212						0.41
250	4.61	2.74				
252					0.33	
272						0.43
284	4.76	3.28				
298			0.91			
342			1.05			
365						0.43
454						0.43
697				1.08		
814				1.11		
998			1.42			
1016					0.72	
1018				1.14		
1123			1.58			
1180						0.44
1195					0.81	
1328			1.43			
1398	0.62	7.03				
1445					0.94	
1468	0.50	6.99				
1841	0.0	7.12				
2000	0.0	7.37				

Figure 5.2.25 Comparison of aniline formations using different batches of *t*-butyl benzene over 0.40 ± 0.01 g Cu(N)/Cab at 148 °C

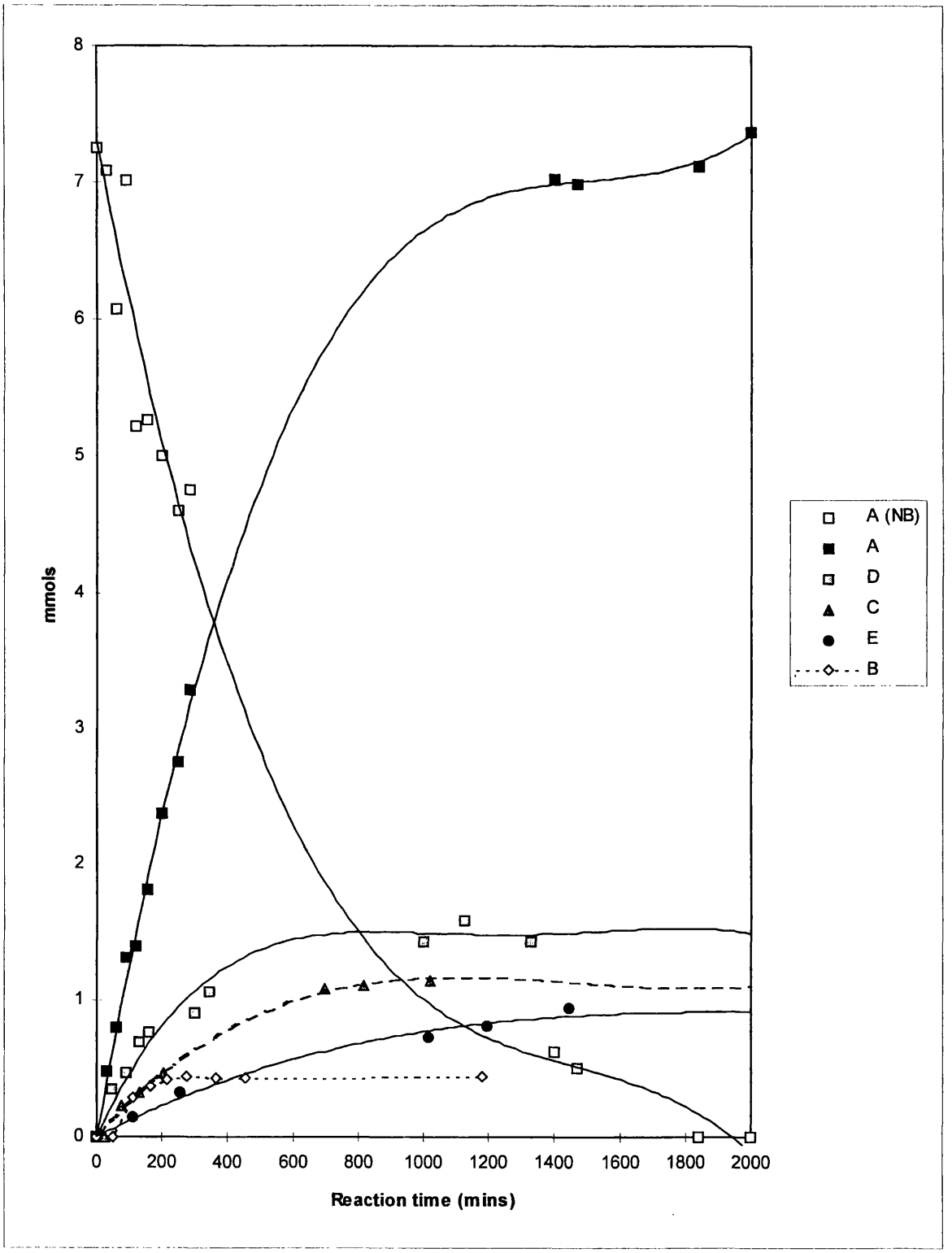

It is clear from Figure 5.2.25 and Table 5.2.24 that catalyst performance depends markedly on the nature of the *t*-butyl benzene solvent. Catalyst masses and the initial concentrations of nitrobenzene were essentially equal, and all other reaction conditions were identical. Both the rate of aniline formation and the final conversion are affected. The reaction rate is highest with A, and the hydrogenation progresses to full conversion. Reaction in B, however, proceeds far more slowly and the aniline concentration reaches a plateau far below full conversion. This pattern is repeated with the C, D and E batches, consistent with deactivation of the catalyst as the reactions progress.

The most important mechanisms of catalyst deactivation are sintering, coking and the blocking of the active metal sites by a catalytic poison. As the experimental conditions were identical for the experiments in question, any degree of metal particle agglomeration can be discounted (and is unlikely to occur so rapidly at just 148 °C). Similarly, although the formation of carbonaceous overlayers is likely [109], it would affect the various experiments equally. The cause of the huge difference in observed catalyst performance was therefore attributed to the presence of a catalytic poison, most probably a sulphur-based solvent impurity.

Conventional gas chromatography-mass spectrometry did not reveal the presence of any sulphur-containing species in the original batches A and B. However, the initial reactant mixture of each experiment was analysed for the presence of sulphur, as was the nitrobenzene, using the Houston Atlas apparatus described in Section 3.5.5 which has a high sensitivity to S-containing species. The total sulphur content determined for the five samples of *t*-butyl benzene and for nitrobenzene are shown in Table 5.2.25. This table

also includes the total sulphur content measured for a representative sample of *n*-butyl benzene, the solvent used for the majority of the project.

Table 5.2.25 Sulphur contents of *t*-butyl benzene, nitrobenzene and *n*-butyl benzene

Sample	A	B	C	D	E	NB	*n*-bb
Sulphur content (ppm)	7.74	0.10	4.20	1.00	0.07	0.26	5.51

An attempt at identifying the sulphur species present within batch A was made using the pulse flame photometric method described in Section 3.5.5. The flame photometric detector (PFD) revealed the presence of five sulphur species, two of which were identified as thiophene and benzothiophene; the remaining three are unidentified. Five sulphur-free components of the mixture were detected by the flame ionisation detector (FID). These were *t*-butyl benzene, the solvent itself, with minor peaks for secondary and normal butylbenzene, 1-methylbutylbenzene and N-pentylbenzene which were present as insignificant solvent impurities. The data obtained by the PFD and the FID is shown in Tables 5.2.26 and 5.2.27 respectively.

Table 5.2.26 Assignments of sulphur species in *t*-butyl benzene Batch A

Peak number	Retention Time (mins)	Approximate Boiling Points (°C)	Assignment and bpt (°C)
1	2.79	81	thiophene, 84.2
2	6.89	206	-
3	7.43	223	benzothiophene, 221
4	7.60	228	-
5	9.86	297	-

Table 5.2.27 Assignments of sulphur-free species in *t*-butyl benzene Batch A

Peak number	Retention Time (min)	Approximate Boiling Points (°C)	Assignment and bpt (°C)
1	6.01	179	t-Butylbenzene, 169
2	6.29	188	*sec*-butylbenzene, 173
3	6.41	191	*n*-butylbenzene, 183
4	6.74	201	1-methylbutylbenzene, 198
5	7.24	217	*n*-pentylbenzene, 205

Unfortunately it was not possible to identify the sulphur species within the other samples, as their total sulphur contents were below the reliable detection limits of the PFD apparatus. Furthermore, it should be noted that the value quoted for the sulphur content for *n*-butyl benzene in Table 5.2.25 was obtained from just one of the batches used during the course of the project. However, the reproducibility obtained with this solvent, in contrast with the variance observed when using *t*-butyl benzene, indicates that the sulphur content of the various batches of *n*-butyl benzene was approximately constant at *ca.* 5.5 ppm

5.2.6.3 Thiophene-doped *t*-butyl benzene

It was not possible to ascertain the identity of all the sulphur species, or their concentrations. However, a series of experiments were conducted using *t*-butyl benzene solvent B doped with thiophene to examine the effect of this component. In these test reactions the solvent was initially purified by the addition of Raney nickel; this mixture was left stirring overnight at ambient temperature, and the nickel catalyst was then

removed by filtration. Nitrobenzene was added to the solvent to produce the reactant mixture which was subsequently degassed under reduced pressure as normal. Thiophene was then added to the reactant mixture just before the mixture was admitted to the reaction vessel. In this way the desired concentration of thiophene was obtained, whilst the manner in which the reactant mixture was introduced to the system was comparable with the previous experiments. The results are shown by Table 5.2.28 and Figure 5.2.26.

From these results it is clear that the presence of thiophene does affect the rate of aniline formation and the final conversion obtained. The effect of thiophene, however, is less marked than that of the blend of sulphur species observed previously.

Table 5.2.28 Formation of aniline v. thiophene concentration at 148 °C

	0.10 ppm Thiophene		2.00 ppm Thiophene		7.74 ppm Thiophene	
Time (mins)	NB (mmols)	AN (mmols)	NB (mmols)	AN (mmols)	NB (mmols)	AN (mmols)
0	8.10	0.00	7.74	0.0	7.36	0.0
30					7.34	0.13
32			7.40	0.21		
48	7.32	0.00				
60			7.26	0.41		
75					7.31	0.25
90			7.16	0.54		
95					7.23	0.42
110	7.74	0.29				
120			6.88	0.67		
134					7.03	0.53
164					7.02	0.58
165	7.53	0.36	6.97	0.85		
202					7.09	0.72
210			6.69	0.95		
212	7.62	0.41				
270			6.30	1.12		
272	7.74	0.43				
285					7.01	0.71
315					7.06	0.73
330			6.25	1.27		
365	7.53	0.43				
392			6.28	1.33		
450			6.22	1.33		
454	7.83	0.43				
461					7.10	0.74
540			6.34	1.42		
544					7.00	0.72

Figure 5.2.26 Formation of aniline v. thiophene concentration at 148 °C

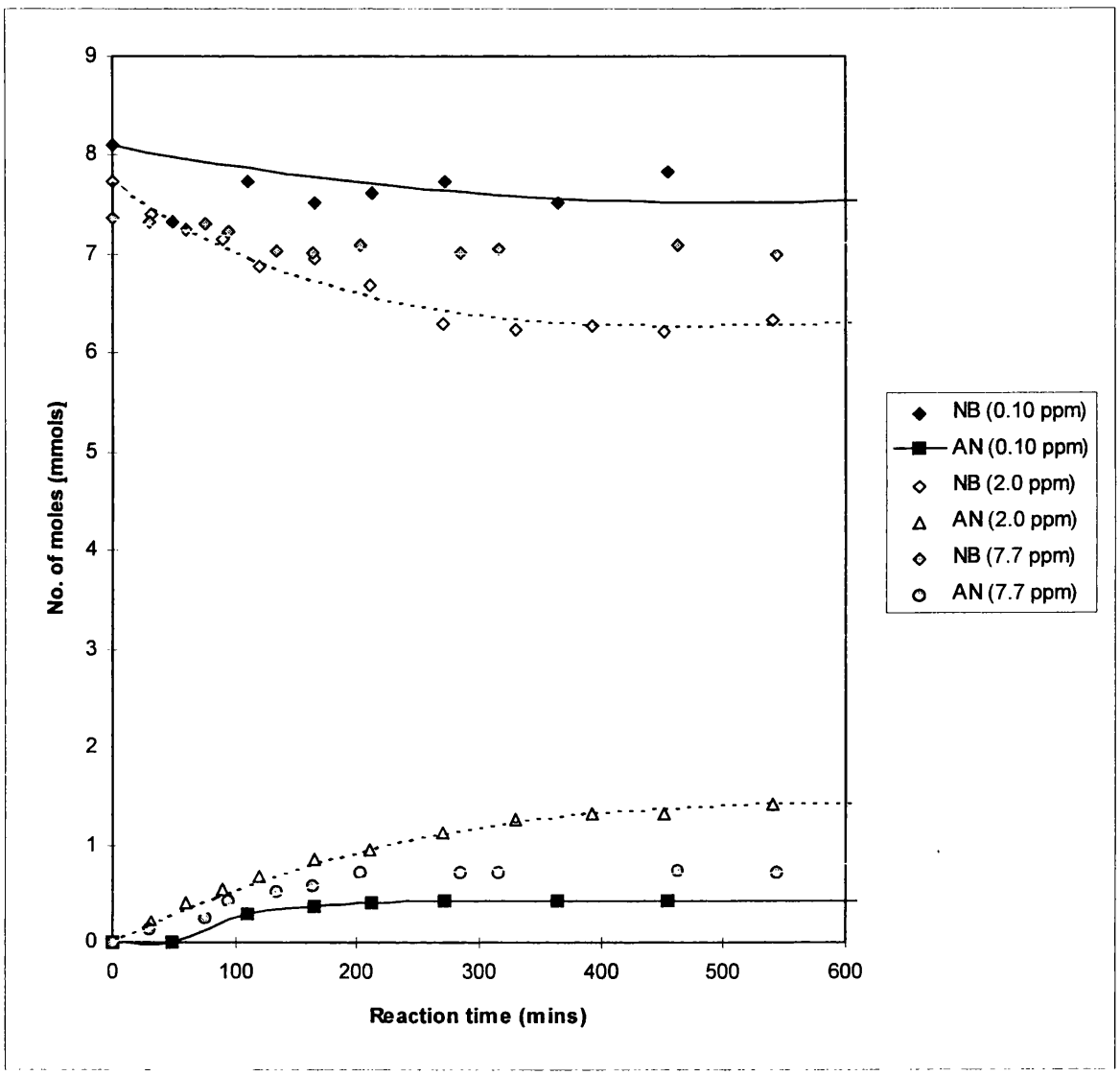

5.2.6.4 Overview

The initial catalyst activities against sulphur content, for both thiophene and the overall blend of sulphur species, are shown by Table 5.2.29 and Figure 5.2.27. It should be noted that all of these reactions were conducted at 148 °C, with the exception of that using *n*-butyl benzene as the solvent, which was conducted at 144 °C.

These results demonstrate the relationship between catalyst performance and sulphur concentration. With regard to the mixture of sulphur-based species within *t*-butyl benzene, the reaction rate rises significantly with increasing sulphur concentration, up to 7.74 ppm. The data point obtained when using *n*-butyl benzene as the solvent agrees with this general trend, with increased rates at increased sulphur concentrations, implying that the presence of the sulphur species within these different solvents affects these reactions in a similar fashion. It therefore appears that the sulphur-containing compounds function as promoters up to this level. This is in accordance with the sulphidisation techniques used in the industrial hydrogenation of nitrobenzene [55].

The effects of thiophene, however, are far less dramatic. The role that thiophene plays in the reaction is obviously complex, and the data suggests that it is the mixture of sulphur-based species which is important, rather than thiophene alone. No changes in the selectivity to aniline were observed during these experiments, with no products other than aniline detected during the reaction sequence.

To summarise the findings of this chapter, the reaction rates observed when using different batches of *t*-butyl benzene increase with higher concentrations of sulphur, up to

7.74 ppm. *t*-Butyl benzene Batch A contained a mixture of five sulphur-based species, including thiophene and benzothiophene. At lower levels of sulphur content the observed rate of reaction is considerably lower, and declines dramatically during the course of the reaction. In extreme cases the formation of aniline ceases at approximately 0.4 mmols (ca. 5 % conversion).

Reaction rate against sulphur content when using *n*-butyl benzene concurs with this general trend. This admittedly-single data point was taken from a representative sample of this solvent; since reproducibility between different batches of *n*-butyl benzene was good, it is assumed that their sulphur contents were approximately constant at *ca.* 5.5 ppm.

The dependence of catalyst performance on sulphur is evident, but it is clear that the role played by the sulphur mixture is complex; equivalent concentrations of thiophene alone do not produce equivalent effects.

Further work is needed to refine our understanding of this complex issue.

Table 5.2.29 Rate of aniline formation v. sulphur concentration

	Rate of aniline formation (g of catalyst)$^{-1}$ (moles x10^{-7} s^{-1})		
[Sulphur] (ppm)	Sulphur mixture, *t*-bb, 148 °C	Sulphur mixture, *n*-bb, 144 °C	Thiophene-doped, *t*-bb, 148 °C
0.07	0.54		
0.07	1.03		
0.10	1.02		
0.10	1.07		
0.10	1.60		
0.10	1.61		
1.00	2.18		
4.20	1.01		
5.51		3.84	
7.74	4.81		1.49
7.74			1.44
2.00			2.48
2.00			2.32

Figure 5.2.27 Rate of aniline formation v. sulphur concentration

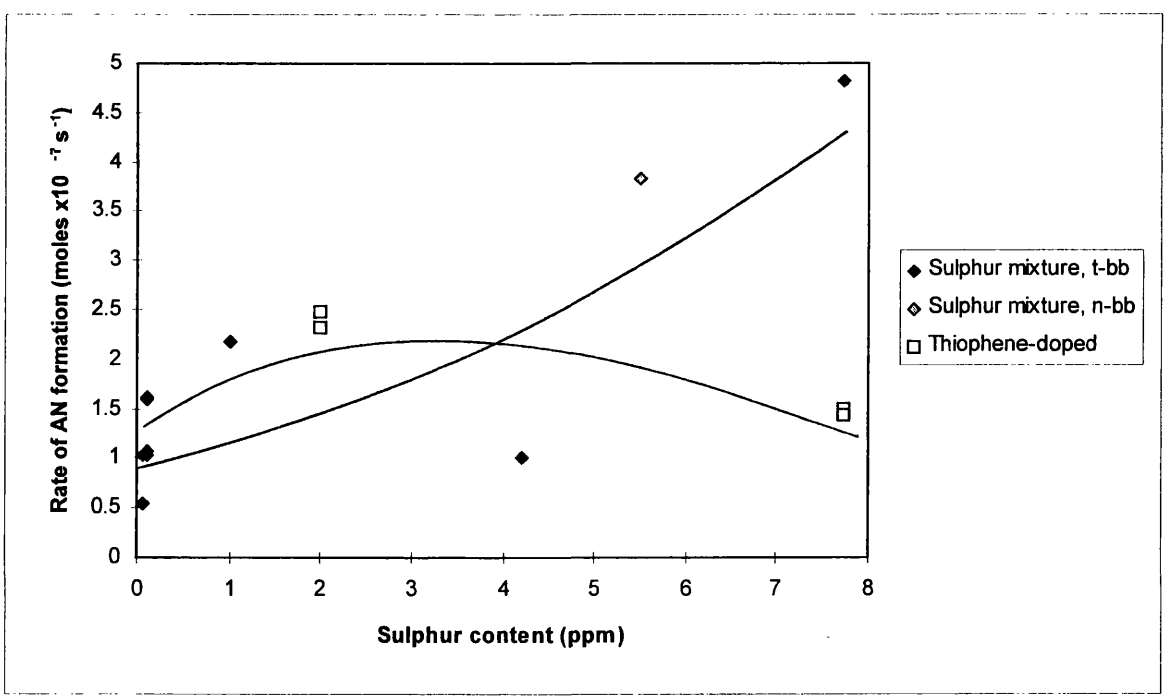

5.3 NITROBENZENE HYDROGENATION

5.3.1 Comparison of copper-based catalysts

The development of the reaction system and protocol allowed a valid evaluation of the different supported copper catalysts. The optimisation of catalyst reduction is described in Section 5.1.7. The catalysts in this section were reduced as follows. Under 10 % H_2/N_2 the temperature was ramped at 3 °C min^{-1} to 290 °C and held at this temperature for 60 minutes under the reductive gas mixture, and then for a further 30 minutes under helium.

The catalytic performance of Cu(N)/Cab, Cu(A)/Cab, Cu(C)/Cab, Cu(N)/C-10 and CuO(N)/Cab at 158 °C are displayed by Tables 5.3.1 to 5.3.5 and Figures 5.3.1 to 5.3.5 respectively. A summary of the results is presented in Table 5.3.6, where the mean particle size values and the number of active sites have been calculated from chemisorption experiments, as reported in Section 5.1.7.

Table 5.3.6 Comparison of the activity of the copper catalysts

Catalyst	Metal surface area ($m^2 g^{-1}$)	No. of active sites ($x10^{19} g^{-1}$)	Mean particle size (nm)	Reaction rate (no. of moles $x10^{-7} s^{-1}$)	Turnover frequency ($x10^{-3}$)
Cu(N)/Cab	5.47	5.27	10.6	6.455	7.37
Cu(A)/Cab	1.87	2.16	35.1	0.917	2.56
Cu(C)/Cab	2.56	3.41	16.6	1.697	2.99
Cu(N)/C-10	3.78	3.54	16.8	1.879	3.20
CuO(N)/Cab	0.97	1.34	61.6	0.124	0.56

The results in Figures 5.3.1 to 5.3.5 all display a linear consumption of nitrobenzene, with a corresponding formation of aniline as the only detected product. The reaction rates summarised in Table 5.3.6, however, vary greatly between the different catalysts. There are many factors which govern catalyst performance; in this comparison the most pertinent being the metal surface area of the catalysts, metal particle size and the potential presence of organic residues which have remained on the surface of the catalyst following the reduction of the precursor.

It is clear that the Cu(N)/Cab catalyst has the greatest activity. Whilst this is in part due to its high metal surface area, the turnover frequency reveals that its activity per surface site is also higher. This catalyst has the smallest estimated particle size. Conversely, the reaction rate and turnover frequency of the CuO(N)/Cab are the lowest of the results obtained, and this catalyst has the largest calculated metal particle size. The performance of the Cu(A)/Cab, Cu(C)/Cab and Cu(N)/C-10 catalysts again follow this trend, with activity clearly related to the surface morphology of the catalyst in question. The Cu(C)/Cab and Cu(N)/C-10 catalysts which are comparable in metal surface area have intermediate activities to those already discussed, but higher than that of the Cu(A)/Cab catalyst which has a lower number of surface sites and higher metal particle size.

The effects of metal surface area and catalyst dispersion upon catalytic activity are discussed in more detail in Section 5.3.5. In summary, the results presented in Table 5.3.6 indicate that the hydrogenation of nitrobenzene over copper catalysts is facilitated by smaller metal particles. It is therefore structure sensitive, *i.e.* the reaction rate changes

markedly with different particle sizes on the catalyst [6c]. However, the validity of this conclusion was questioned by further investigation (see Section 5.3.5).

The situation is further complicated by the presence of residues which remain on the surface of the catalysts following reduction. As discussed in Section 5.1.7 the nitrate precursor is the 'cleanest' catalyst post-activation, although the presence of some copper nitride on the metal surface cannot be discounted [129]. The reduction of the carbon-derived catalysts, without prior calcination, is more likely to result in the presence of residues which may well block some of the surface copper atoms. Whilst metal surface areas have been measured by nitrous oxide decomposition for the Cu(A)/Cab and Cu(C)/Cab catalysts, and their catalytic activities have been established, the effect of these deposits on the hydrogenation reaction is unknown. The nitrate-derived catalysts exhibit higher turnover frequencies than those prepared from carbon-based salts. The copper oxide catalyst, CuO(N)/Cab, which can be regarded as having the 'cleanest' metal surface, displays the lowest activity both per gram of catalyst and per surface metal atom. The residues left on the catalyst surfaces, following reduction without prior calcination, therefore appear to exercise a positive effect on catalyst performance. The nature of this apparent promotional effect is unknown.

In summary, there is a relationship between catalyst activity for the hydrogenation of nitrobenzene and metal surface area. The results imply that nitrobenzene hydrogenation is structure sensitive, the reaction being enhanced over smaller metal particles, but subsequent findings raise doubt over this theory. The nature of the residues

remaining on the catalyst surface following reduction is believed to affect the rate of reaction. The Cu(N)/Cab catalyst was found to be the most active of the catalysts examined, which is attributed largely to its high metal surface area.

Table 5.3.1 Nitrobenzene hydrogenation over 0.5473 g Cu(N)/Cab at 158 °C

Reaction Time (mins)	Nitrobenzene (mmols)	Aniline (mmols)	Selectivity to aniline (%)
0	7.45	0.00	0.0
31	6.55	0.64	71.3
66	6.07	1.43	103.8
90	5.10	1.90	80.8
120	4.53	2.51	86.1
150	3.87	3.22	89.9
180	3.25	3.84	91.5

Rate of aniline formation $(g \text{ of catalyst})^{-1} = 6.455 \text{ moles } x10^{-7} \text{ s}^{-1}$

Figure 5.3.1 Nitrobenzene hydrogenation over 0.5473 g Cu(N)/Cab at 158 °C

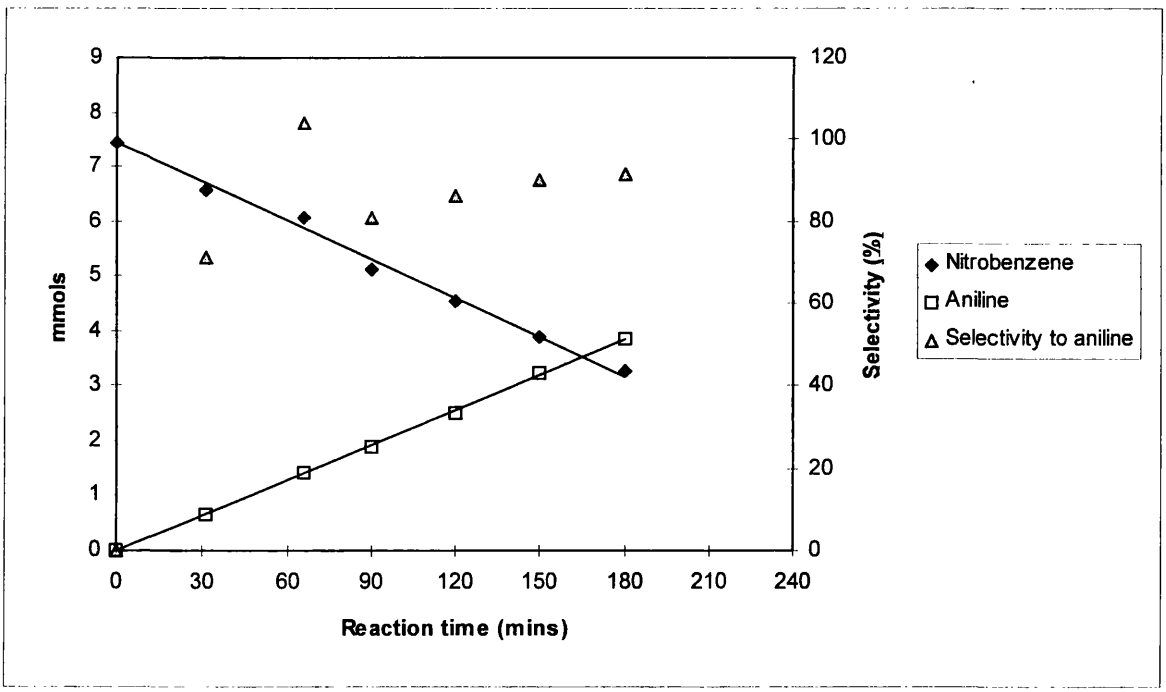

Table 5.3.2 Nitrobenzene hydrogenation over 0.7998 g Cu(A)/Cab at 158 °C

Reaction Time (mins)	Nitrobenzene (mmols)	Aniline (mmols)	Selectivity to aniline (%)
0	8.02	0.00	0.0
30	7.98	0.14	376.5
60	7.97	0.32	679.2
90	7.65	0.41	112.8
128	7.45	0.49	86.6
150	7.40	0.53	85.2
185	7.63	0.87	224.7
210	7.42	0.99	165.3

Rate of aniline formation (g of catalyst)$^{-1}$ = 0.917 moles x10^{-7} s^{-1}

Figure 5.3.2 Nitrobenzene hydrogenation over 0.7998 g Cu(A)/Cab at 158 °C

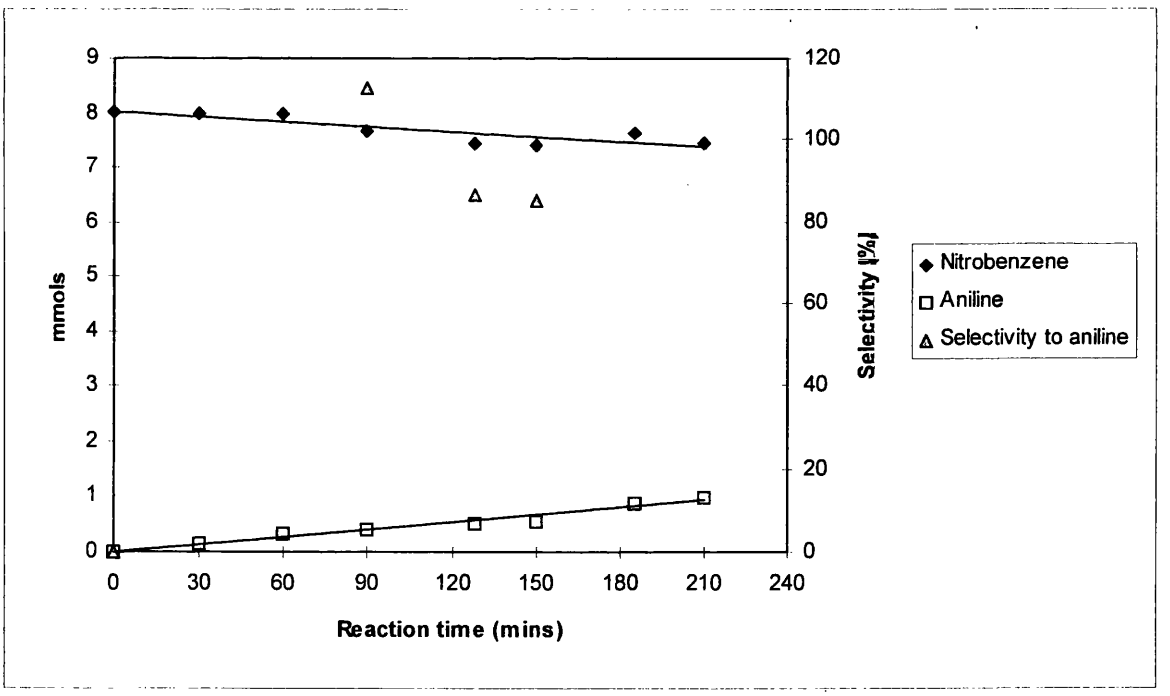

Table 5.3.3 Nitrobenzene hydrogenation over 0.5484 g Cu(C)/Cab at 158 °C

Reaction Time (mins)	Nitrobenzene (mmols)	Aniline (mmols)	Selectivity to aniline (%)
0	8.37	0.00	0.0
30	8.03	0.14	41.5
60	8.12	0.32	126.6
90	8.06	0.51	165.0
121	7.32	0.69	66.1
152	7.29	0.86	79.1
180	7.01	0.98	72.2

Rate of aniline formation (g of catalyst)$^{-1}$ = 1.697 moles x10^{-7} s^{-1}

Figure 5.3.3 Nitrobenzene hydrogenation over 0.5484 g Cu(C)/Cab at 158 °C

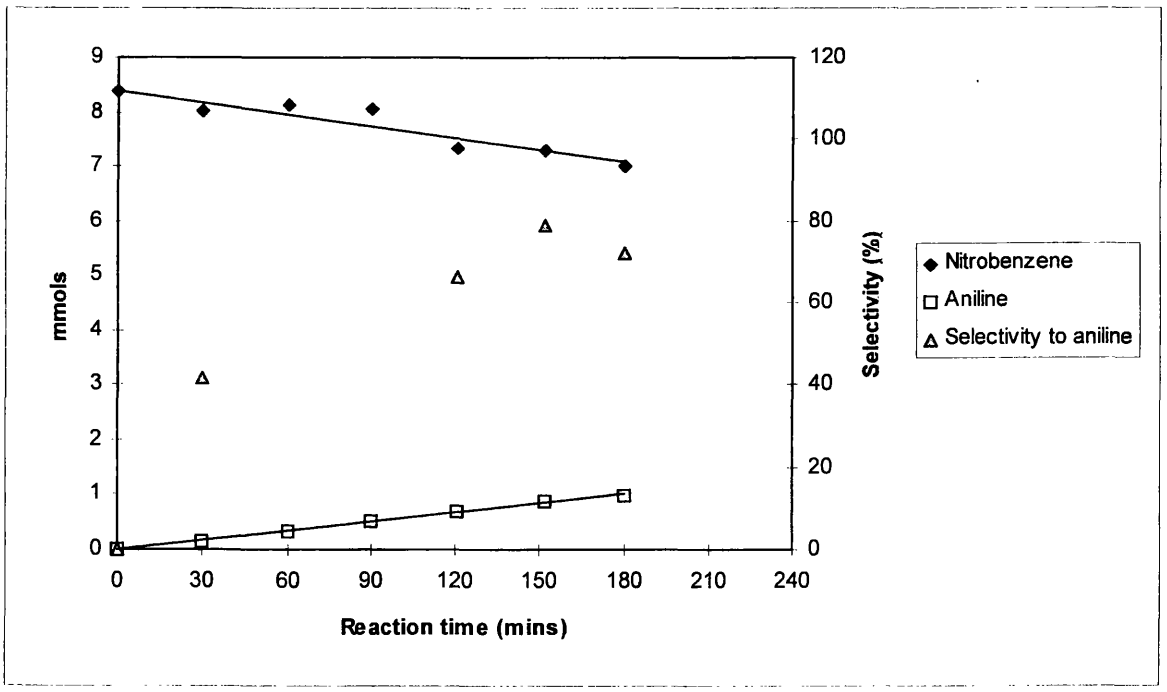

Table 5.3.4 Nitrobenzene hydrogenation over 0.5480 g Cu(N)/C-10 at 158 °C

Reaction Time (mins)	Nitrobenzene (mmols)	Aniline (mmols)	Selectivity to aniline (%)
0	8.09	0.00	0.0
30	7.67	0.10	22.6
60	7.86	0.27	120.1
90	7.89	0.47	237.3
120	7.35	0.69	92.9
152	6.90	0.88	73.4
180	6.68	1.09	77.8

Rate of aniline formation (g of catalyst)$^{-1}$ = 1.879 moles x10^{-7} s^{-1}

Figure 5.3.4 Nitrobenzene hydrogenation over 0.5480 g Cu(N)/C-10 at 158 °C

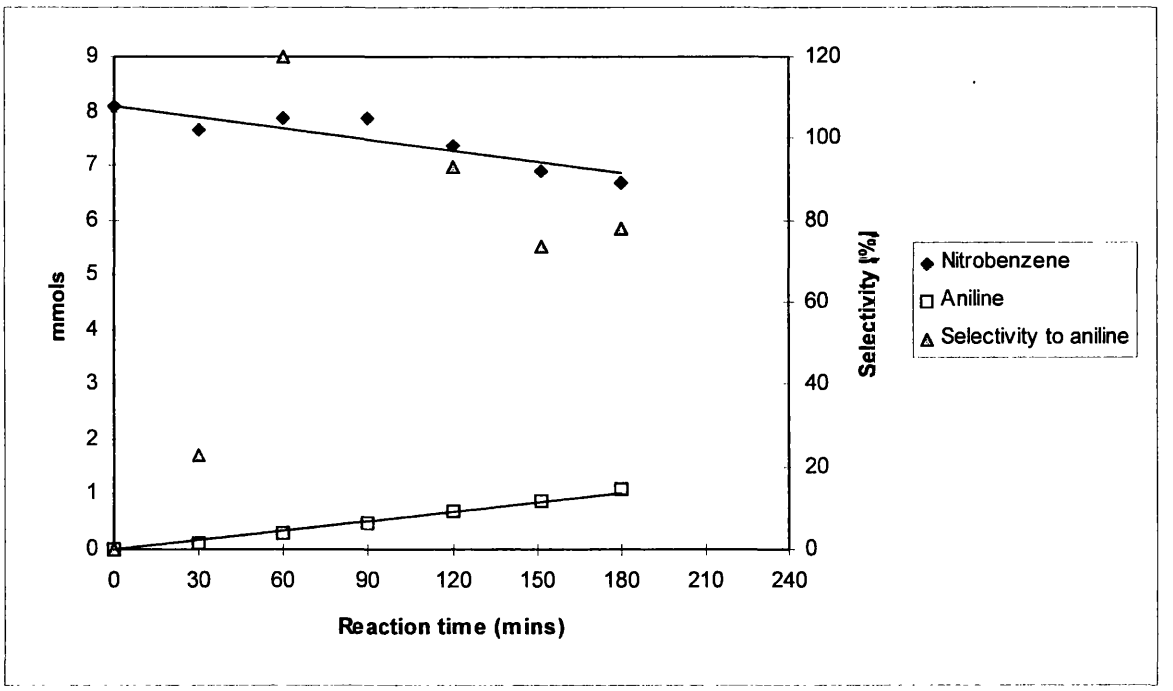

Figure 5.3.5 Nitrobenzene hydrogenation over 0.5555 g CuO(N)/Cab at 158 °C

Reaction Time (mins)	Nitrobenzene (mmols)	Aniline (mmols)	Selectivity to aniline (%)
0	8.05	0.00	0.0
30	8.32	0.01	-3.4
58	8.32	0.03	-10.2
88	8.18	0.03	-25.8
120	8.36	0.06	-19.4
162	7.11	0.06	6.6
180	6.05	0.07	3.7

Rate of aniline formation (g of catalyst)$^{-1}$ = 0.124 moles x10^{-7} s^{-1}

Figure 5.3.5 Nitrobenzene hydrogenation over 0.5555 g CuO(N)/Cab at 158 °C

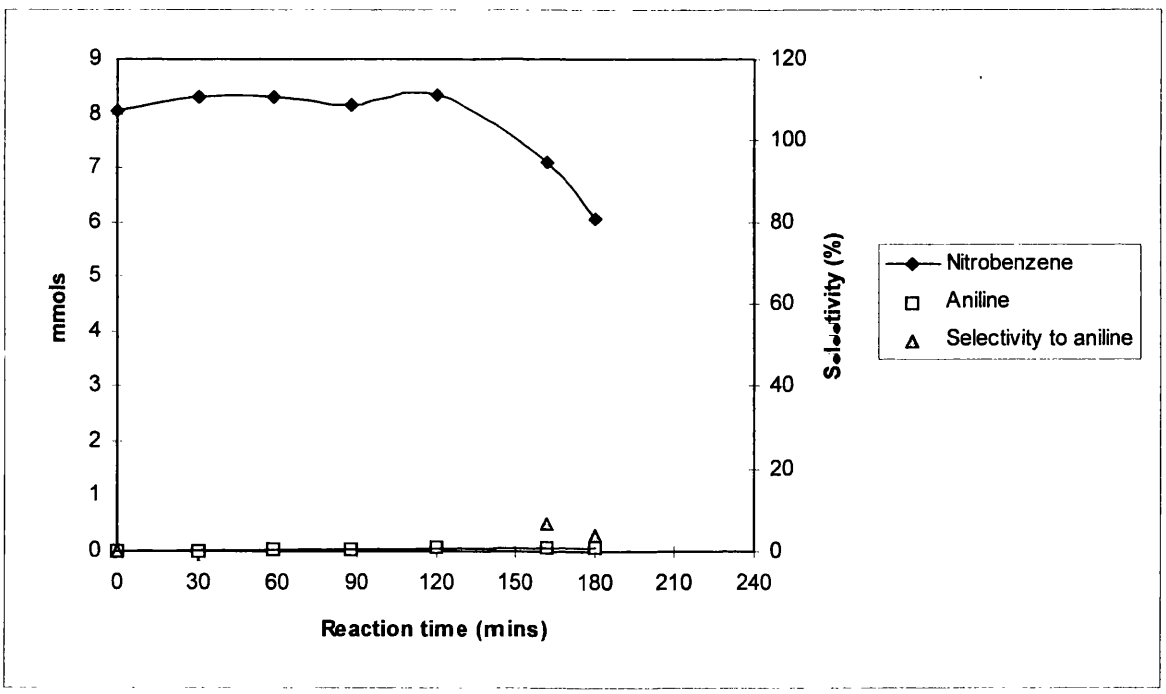

5.3.2 Reaction orders of nitrobenzene, aniline and catalyst mass

Nitrobenzene hydrogenation has been studied over a variety of catalysts, and is generally found to be zero order in nitrobenzene [16, 21, 32, 33, 35-37, 39, 41, 43-45]. Peureux *et al* however, found this order to be slightly positive [24], whilst Metcalfe & Rowden found that the rate of hydrogenation decreased with increasing nitrobenzene concentration, and that this 'self-poisoning' phenomenon commenced above 0.15M [42]. Petrov and co-workers similarly found nitrobenzene to act as poison [28].

Less published data is available on the effect of aniline upon nitrobenzene hydrogenation. Tsutsumi *et al* affirmed that aniline did retard the reaction rate [130], whilst Petrov *et al* found that the reaction products, aniline and water, were not detrimental to the performance of copper catalysts when used in the gas phase [28].

The reaction order in dihydrogen is overwhelmingly reported as being first order [16, 24, 33, 35, 37, 41, 42, 45], although Collins, Smith and Davis found that the order in dihydrogen appeared to be second order or higher [33].

This section of the report outlines the effects of catalyst mass, nitrobenzene and aniline concentrations upon the observed reaction rate. On the basis of overwhelming evidence [16, 24, 33, 35, 37, 41, 42, 45] it is assumed that the reaction is first order with respect to hydrogen. The Cu(N)/Cab catalyst used throughout this chapter was reduced at 3 °C min^{-1} to 290 °C. This $T_{red.}$ was maintained for 60 minutes under 10 % H_2/N_2 and 30 minutes under helium for the series of experiments varying the nitrobenzene concentration and the mass of catalyst. For the series examining the effect of aniline concentration, the $T_{red.}$ time under the reductive gas was limited to 30 minutes.

Table 5.3.7 and Figure 5.3.6 display the rate of aniline formation against mass of active catalyst. Table 5.3.7 also shows the numbers of copper metal atoms which are equivalent to these catalyst masses, and the ratios of nitrobenzene molecules to surface copper atoms for these experiments.

The results show a linear dependence between reaction rate and the mass of catalyst. As illustrated by Bond [131a], a non-linear dependence of the reaction rate on catalyst mass, at a given stirring speed of agitation, indicates that an experimental system is limited by diffusion. The linearity of the relationship between observed reaction rate and catalyst mass, shown by Figure 5.3.6, therefore indicates that the reaction testing conducted over this range of catalyst mass is not diffusion limited. In consequence the measured rates are dictated by the rate of reaction on the catalyst surface, and not by the rate of diffusion of reactants and products through the reaction medium [131b].

The masses of catalyst used during these experiments is considerable. However, the activity of copper-based catalysts are low when compared to other metal systems, *e.g.* nickel, palladium or platinum, and relatively high weights of catalyst were required to ensure a reasonable experimental period. To ensure that the reaction testing was not limited by diffusion, the mass of catalyst used in subsequent experiments was selected at approximately 0.55 g, well within the range of linearity (Figure 5.3.6), with the ratio of nitrobenzene molecules to surface copper atoms of *ca.* 164 : 1.

Table 5.3.8 and Figure 5.3.7 display the rates of reaction at different concentrations of nitrobenzene. The individual experiments themselves showed a linear

consumption of nitrobenzene, with the corresponding formation of aniline. The data in Table 5.3.8 and Figure 5.3.7 show that the rate of hydrogenation is effectively constant over the range 0.005 to 0.98 M nitrobenzene. The data point at 0.0098 M nitrobenzene is regarded as anomalous.

A mathematical definition of the reaction order with respect to the concentration of one particular substance is shown by Equation 5.3.1 [132].

$$\text{Order with respect to reagent } X = \frac{\delta \log_{10} \text{rate}}{\delta \log_{10} [X]} \qquad \text{Equation 5.3.1}$$

where the reaction rate is evaluated under conditions such that the reaction variables are held constant [132]. In essence, the gradient of the plot of log rate versus the log of a concentration of a particular species equals the reaction order.

The data shown by Table 5.3.8 was processed in accordance with Equation 5.3.1; the results are given by Table 5.3.9 and Figure 5.3.8. These results show a near-zero reaction order in nitrobenzene, the gradient of the line being -0.0165. Considering the range of experimental error, and the pattern shown during individual experiments, the order with respect to nitrobenzene is found to be zero order. This is in agreement with the literature [16, 21, 32, 33, 35-37, 39, 41, 43-45].

The effect of aniline upon the reaction rate was studied up to a concentration of 1.37 M, which gave a maximum ratio of 14 : 1 between aniline and nitrobenzene. It should be noted that due to the high concentrations of aniline present in this series of

experiments, it was deemed to be more accurate to determine the rates of reaction via the consumption of the nitrobenzene. The results are shown in Table 5.3.10 and Figure 5.3.9. This data was then processed according to Equation 5.3.1 (Table 5.3.11 and Figure 5.3.10).

It is evident that aniline does exhibit a marginally detrimental effect on the hydrogenation of nitrobenzene, in agreement with Tsutsumi *et al* [130]. The effect increases linearly with aniline concentration, and is attributed to the relative adsorption strengths of the nitrobenzene and aniline species. Whilst the nitro compound is preferentially adsorbed before the amine, as would be expected, there is a degree of competition for the active sites, and at high ratios of aniline to nitrobenzene the major reaction is retarded. From Figure 5.3.11 the reaction order with respect to aniline is calculated at -0.316.

In summary of the results discussed in this section, the hydrogenation of nitrobenzene over copper catalysts is found to be zero order with respect to nitrobenzene. The order in aniline is fractional and negative, and the effect of aniline in retarding the reaction is attributed to competitive adsorption between the substrate and the product for the active sites of the catalyst. Finally, reaction rates increase linearly with the mass of catalyst, and the system was found to operate under kinetic control, *i.e.* not limited by diffusion. This indicates the validity of the current experimental system as a means of evaluating different catalysts.

Table 5.3.7 Rate of aniline formation v. mass of catalyst at 158 °C

Mass of catalyst (g)	No. of surface metal atoms ($x10^{19}$)	NB : $Cu^0_{surf.}$	Rate of aniline formation (moles $x10^{-7}$ s^{-1})
0.0	0.0	-	0.0
0.137	0.72	654	0.77
0.204	1.08	436	1.17
0.273	1.44	327	1.39
0.342	1.80	262	2.15
0.547	2.88	164	3.75
0.545	2.88	164	3.43
0.546	2.88	164	3.96
0.800	4.22	112	5.86
0.801	4.22	112	6.23
0.801	4.22	112	5.54
1.201	6.33	74	8.64

Figure 5.3.6 Rate of aniline formation v. mass of catalyst at 158 °C

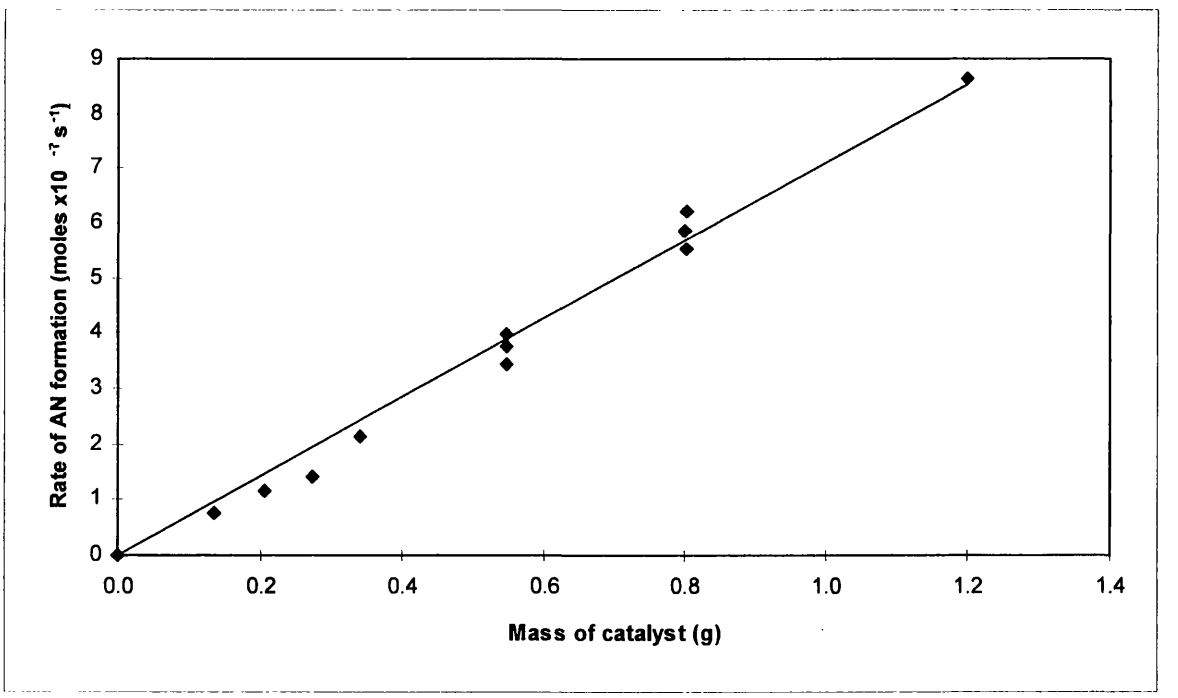

Table 5.3.8 Rate of aniline formation v. initial nitrobenzene concentration at 158 °C over 0.55 g Cu(N)/Cab

Initial nitrobenzene concentration (mol l^{-1})	Rate of aniline formation (moles $x10^{-7}$ s^{-1})
0.0049	3.85
0.0098	2.13
0.0978	3.75
0.0978	3.43
0.0978	3.96
0.9777	3.52

Figure 5.3.7 Rate of aniline formation v. initial nitrobenzene concentration at 158 °C over 0.55 g Cu(N)/Cab

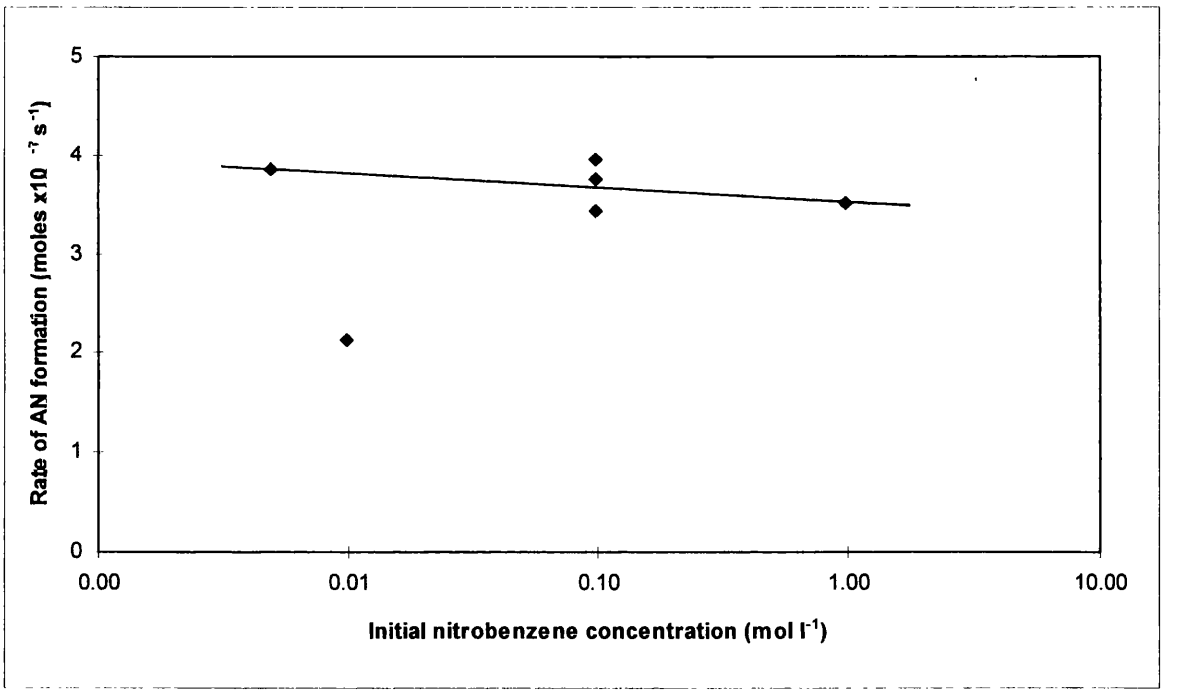

Table 5.3.9 Log (reaction rate) v. log (nitrobenzene concentration)

Log (nitrobenzene concentration)	Log (reaction rate)
-2.3098	0.585461
-1.00966	0.574031
-1.00966	0.535294
-1.00966	0.597695
-0.00979	0.546543

Figure 5.3.8 Log (reaction rate) v. log (nitrobenzene concentration)

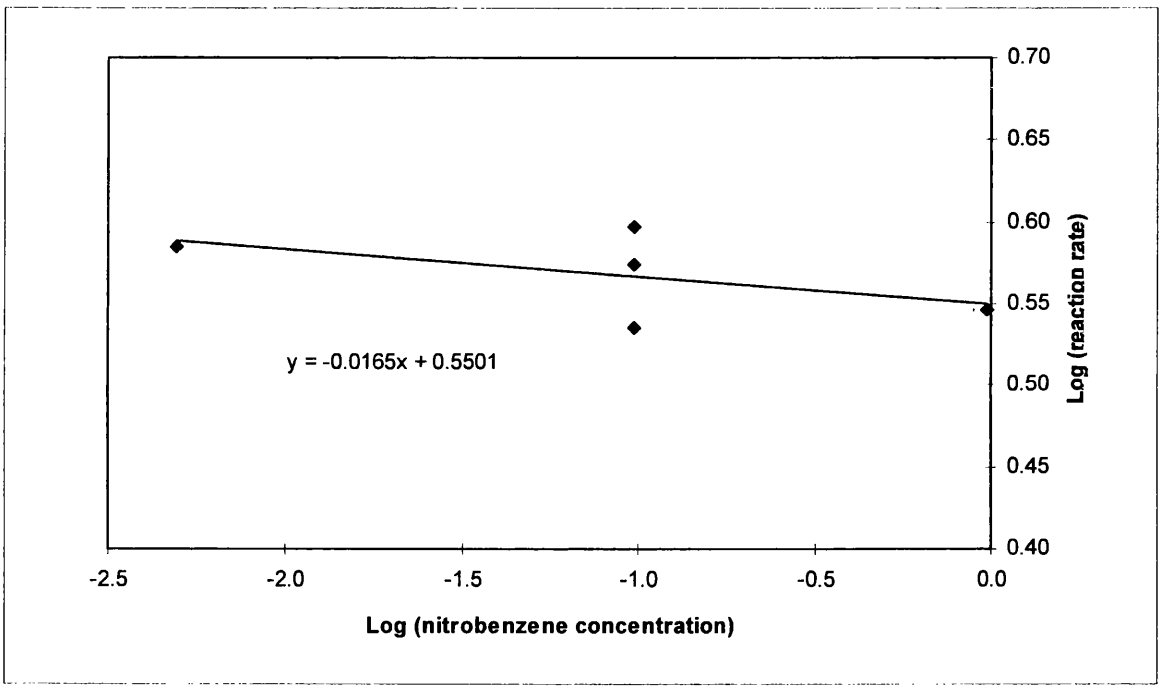

Table 5.3.10 Rate of nitrobenzene consumption v. initial aniline concentration at 158 °C over 0.55 g Cu(N)/Cab

Aniline concentration (mol l^{-1})	Rate of NB consumption (moles $x10^{-7}$ s^{-1})
0.000	7.88
0.110	9.33
0.274	6.79
0.549	5.39
0.960	4.27
1.371	4.45

Figure 5.3.9 Rate of nitrobenzene consumption v. initial aniline concentration at 158 °C over 0.55 g Cu(N)/Cab

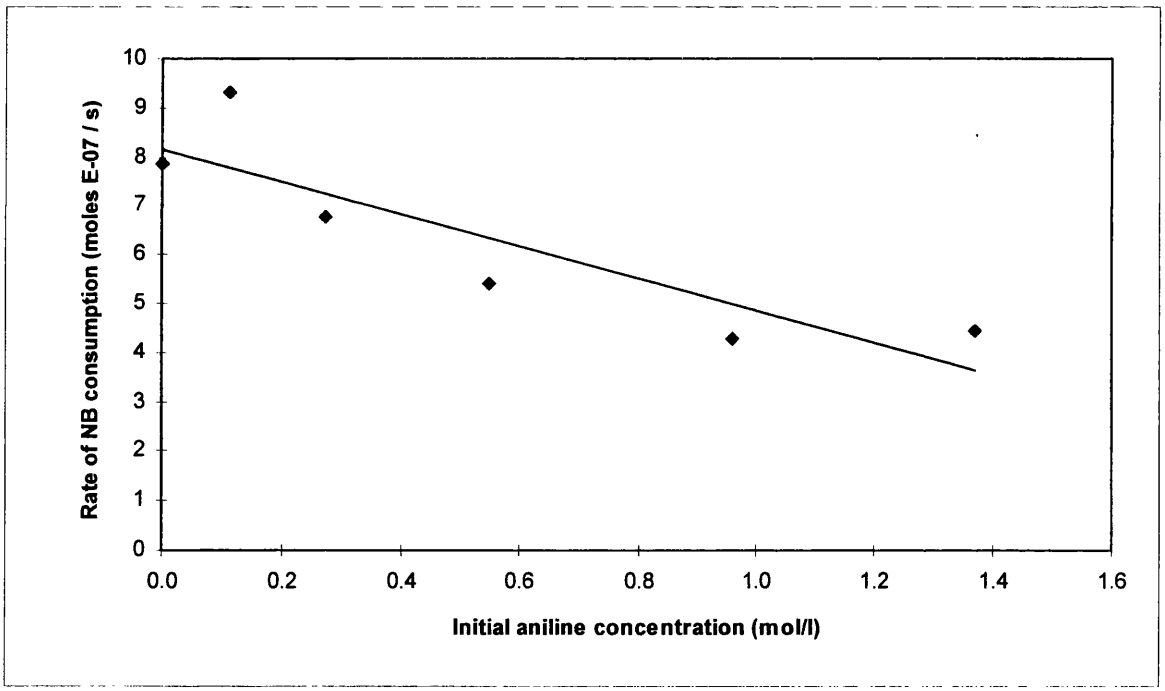

Table 5.3.11 Log (reaction rate) v. log (aniline concentration)

Log (aniline concentration)	Log (reaction rate)
-0.95861	0.969882
-0.56225	0.83187
-0.26043	0.731589
-0.01773	0.630428
0.137037	0.64836

Figure 5.3.10 Log (reaction rate) v. log (aniline concentration)

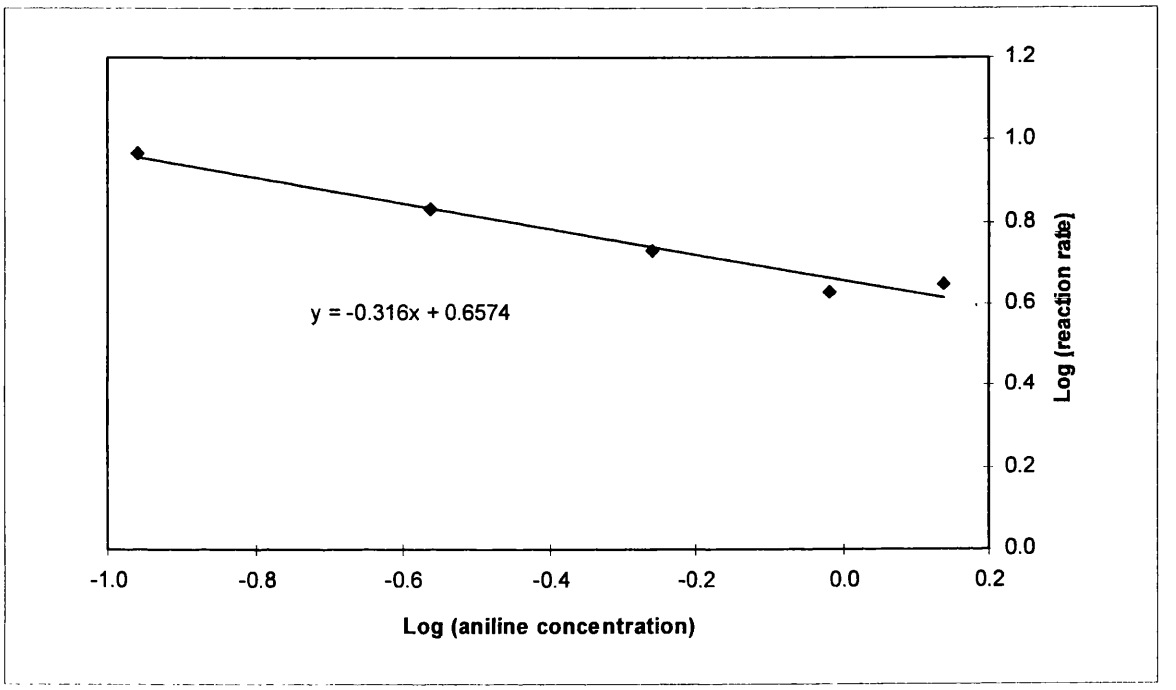

5.3.3 Determination of the activation energy

The function of a catalyst is to decrease the activation energy of a reaction, E_a, in relation to that which could be expected for the equivalent homogeneous process. This chapter outlines the determination of the apparent activation energy of nitrobenzene hydrogenation over copper catalysts.

Nitrobenzene hydrogenation has been studied over a variety of catalysts. Over palladium/alumina catalysts Peureux *et al* calculated the activation energy at 45 kJ mol^{-1} [24], whilst Wisniak and Klein found the value to be 40.6 kJ mol^{-1} over palladium/carbon catalysts and 59.0 kJ mol^{-1} when using Raney nickel [16]. Metcalfe and Rowden, however, determined the activation energy as between 21 and 105 kJ mol^{-1} over palladium/silver alloys, the higher and lower extents of the range being observed from silver-rich and palladium-rich alloys respectively [42]. With perhaps the most relevance to this project, were the findings of Rihani and co-workers who calculated the value of 69 kJ mol^{-1} over copper and nickel catalysts in the gas phase hydrogenation of nitrobenzene [30].

The rate of nitrobenzene hydrogenation was studied between the range 60 to 170 °C. The data is shown in Table 5.3.12 and Figure 5.3.11. These results show that the reaction rate increases with higher temperatures. This rate increase does not reach a maximum over the range studied. It is also apparent that a certain critical temperature must be reached before hydrogenation commences. Extrapolation of the curve in Figure 5.3.11 places this value at 87 °C.

The activation energy was calculated from these results, with the omission of the reaction results at 60 °C, via the Arrhenius equation:-

$$k = Ae^{-Ea/RT}$$

where k is the observed rate, A is the pre-exponential factor, E_a is the activation energy, R is the gas constant and T is the absolute temperature. Values for E_a and A were calculated by rearranging this equation, and plotting the data as ln (k) against 1000/(temperature, K). The results are shown by Table 5.3.13 and Figure 5.3.12. The data has been divided into two regions, A and B, for reasons which are explained below.

A catalytic reaction may be broken down into five stages, as described by Bond [131b]:-

i) Transport of the reactants to the catalyst surface

ii) Adsorption of the reactants on the catalyst

iii) Reaction of the reactants on the catalyst

iv) Desorption of the products from the catalyst surface

v) Transport of the products away from the catalyst

These five steps may be grouped into two categories; ii), iii) and iv) which are chemical in nature, and steps i) and v) which are the physical transfer of the reactants/products through the reaction medium. The latter do not involve any chemical change and are mass transport phenomena, or diffusion processes. When the diffusional

steps are slower than the catalytic rate itself the reaction is diffusion limited, *i.e.* the observed rate does not depend solely on the activity of the catalyst, but is governed by the rate at which the reactant/product molecules can reach/leave the catalyst surface.

Since the rates of the chemical steps are far more sensitive to temperature than those of mass transfer, it is possible to observe two regions when plotting ln(k) against 1/T, as is exhibited by Figure 5.3.12. At lower temperatures the overall rate is determined by catalytic processes, denoted as region A in Table 5.3.13 and Figure 5.3.12, whilst in region B it is the rates of diffusion which govern the observed rate of reaction. These may be described as the kinetic and diffusion regions respectively.

The apparent activation energy has therefore been derived from the gradient of region A, indicating that E_a equals 57.1 ± 10.5 kJ mol^{-1}. This value is consistent with the literature. When calculated from the curve through region B, the activation energy equals 14.8 kJ mol^{-1}, which is consistent with diffusion control.

In summary, the plot of ln(k) against 1/T reveals two distinct regions. Above 125 °C the reaction is diffusion limited, whilst below this temperature it is the catalytic steps which govern the observed reaction rates. What is perhaps most surprising is that the reaction is diffusion limited at 158 °C with 0.55 g of catalyst. This is contrary to the observation in Section 5.3.2 where the reaction rate at this temperature varied linearly with catalyst mass up to 1.2 g. This implies that previous experiments conducted above 125 °C were limited by mass transfer phenomena. This is of relevance primarily to

Sections 5.3.1, the evaluation of the different copper catalysts, and Section 5.3.2, the determination of the reaction orders in nitrobenzene and aniline.

In view of the conflicting evidence of Section 5.3.2 and the current chapter, subsequent testing was conducted at 110 °C with 0.55 g catalyst to ensure that the reaction lay within the kinetic region.

Table 5.3.12 Rate of aniline formation v. reaction temperature

Reaction temperature (°C)	Rate of aniline formation (moles $x10^{-7}$ s^{-1})
60	0
95	1.24
110	2.61
110	3.47
125	5.01
144	7.04
158	8.28
170	9.03

Figure 5.3.11 Rate of aniline formation v. reaction temperature

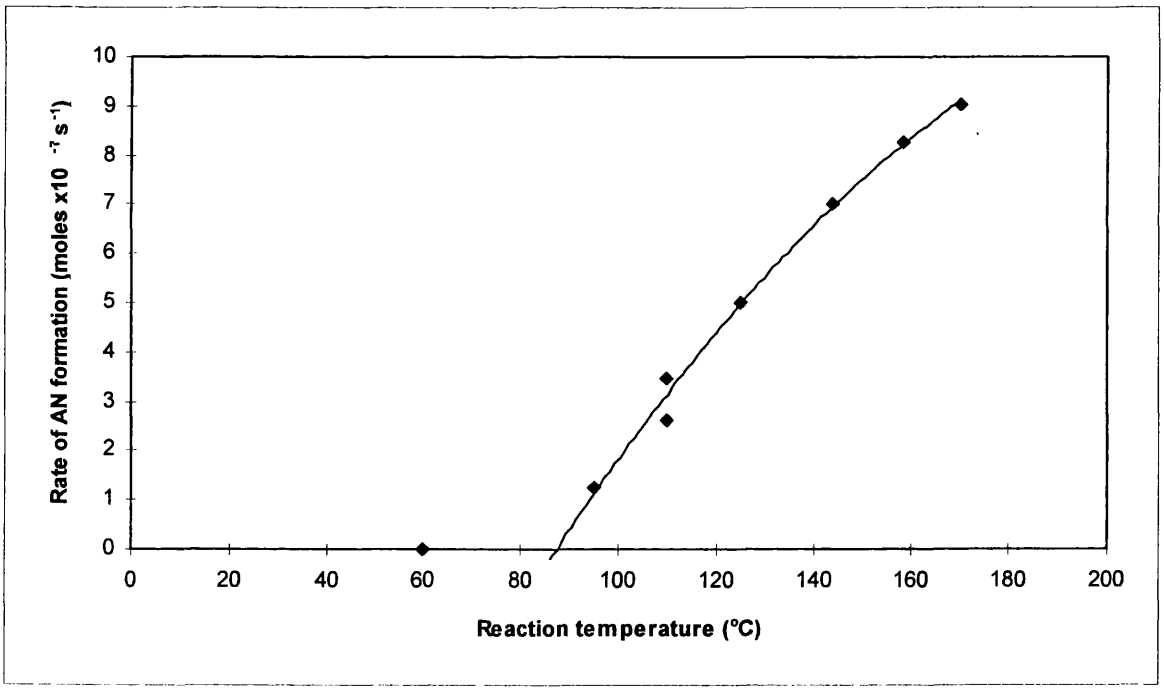

Table 5.3.13 Ln (k) v. 1000 / T (K)

	Ln (k)	
1000/T(K)	Region A	Region B
2.716	-15.91	
2.610	-15.16	
2.610	-14.87	
2.512	-14.51	
2.397		-14.17
2.319		-14.00
2.257		-13.92

Figure 5.3.12 Ln (k) v. 1000 / T (K)

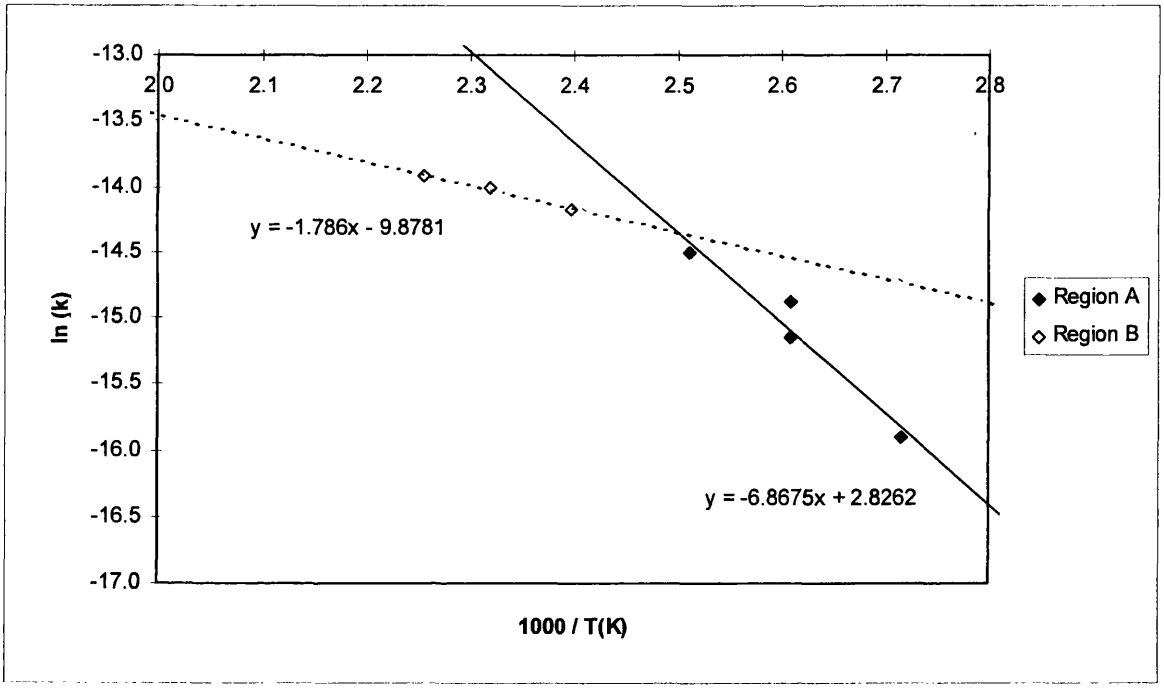

5.3.4 Reaction of nitrosobenzene

The accepted reaction scheme (shown by Figure 1.1, Section 1.2.1, p5) indicates that nitrosobenzene is the primary intermediate of nitrobenzene hydrogenation. The nitrobenzene molecule is not stable on metal surfaces [133-135], and it has been shown that upon adsorption of nitrobenzene on nickel and iron catalysts the nitro group of the substrate undergoes a stepwise dissociation [135]. This latter study found that at low temperatures (below ambient) nitrosobenzene was the predominant species on the metal surface, whilst an increase in temperature results in further dissociation to form an anionic species [$C_6H_5N_{(ads.)}$]. Chen and co-workers examined the decomposition of nitrobenzene on a Cu (110) surface using Auger and high resolution electron energy loss spectroscopies, concluding that the dissociation products on this metal surface were atomic oxygen and phenyl groups [133].

Many authors have reported the hydrogenation of nitrobenzene to aniline without observing the presence of nitrosobenzene [28, 32, 33, 41]. Li *et al* [37], in agreement with Metcalfe and Rowden [42] and Aramendia and co-workers [41] found that the rate determining step of nitrobenzene hydrogenation was the surface reaction between nitrobenzene and atomic hydrogen. In addition, Carturan *et al* observed that the rate of nitrosobenzene hydrogenation at 25 °C was about 100 times faster than that of nitrobenzene hydrogenation at 90 °C, irrespective of substrate concentration [39].

Conversely, Galvagno *et al* [36] in agreement with other studies [34, 38], did observe the presence of nitrosobenzene during the hydrogenation of nitrobenzene. It therefore seems that one reason why nitrosobenzene may not always be detected in

solution, is that the relative rates of reaction for nitrosobenzene formation and nitrosobenzene reduction are such that nitrosobenzene concentration is kept below the limits of detection.

This section details the hydrogenation of nitrosobenzene in n-butyl benzene over the Cu(N)/Cab catalyst at 110 °C. Due to the nature of the reaction, the experimental protocol was modified as follows. The catalyst was reduced as normal, and 70 ml of degassed solvent was admitted. This mixture was brought to the desired reaction temperature under flowing dihydrogen. Once thermally stable, 10 ml of a nitrosobenzene/n-butyl benzene solution was added, to give the desired overall concentration of nitrosobenzene in the 80 ml of reactant mixture. The point of this addition was regarded as 'time zero', and the reaction conducted as normal. The concentrations of nitrosobenzene and aniline reported from 0.5 minutes onwards were therefore determined quantitatively from calibration lines of their detector response factors, whilst the amount of nitrosobenzene present at 0 minutes was calculated from the concentration of the standard solution added. Table 5.3.14 and Figure 5.3.13 show the observed results.

These results show the rapid loss of the nitrosobenzene substrate from the solution. Furthermore, after just thirty seconds it appears that one third of the amount of nitrosobenzene added has disappeared. In comparison, the formation of aniline is not rapid to begin with, and slows even further during the course of the reaction. No other products were detected, and the data shows a considerable negative carbon mass balance.

It is evident that nitrosobenzene can be reduced to aniline. The rate of this hydrogenation, however, is far slower than that of nitrobenzene hydrogenation to aniline; the rates of these two hydrogenations under equivalent conditions are as shown:-

Nitrobenzene (i)	Rate of aniline formation (g of catalyst)$^{-1}$ = 2.61 moles x10^{-7} s^{-1}
Nitrobenzene (ii)	Rate of aniline formation (g of catalyst)$^{-1}$ = 3.47 moles x10^{-7} s^{-1}
Nitrosobenzene	Rate of aniline formation (g of catalyst)$^{-1}$ = 0.435 moles x10^{-7} s^{-1}

These results are in contrast with the observations of Carturan *et al* [39], which suggest that nitrosobenzene is rapidly hydrogenated to form the thermodynamically stable product aniline, given a sufficient supply of hydrogen. The findings of the present study imply that nitrosobenzene is not one of the intermediates in this reaction. Nevertheless, the literature overwhelming supports the formation of aniline from nitrobenzene via nitrosobenzene and phenylhydroxylamine intermediates. In view of this evidence it seems that the adsorption strength of nitrosobenzene, and its rate of adsorption, are sufficient to saturate the catalytic sites under the experimental conditions adopted. Molecules of dihydrogen are therefore denied access to the catalyst surface, and subsequently cannot dissociate to provide the hydrogen atoms which are active towards hydrogenation. This would severely hamper the hydrogenation reaction, although some degree of reaction would still be possible, as is evident in Figure 5.3.13. This hypothesis remains speculative, but essentially 'the nitrosobenzene goes in, comes into contact with the

catalyst, and disappears', with a minimal formation of aniline, the only observed reaction product.

Clearly, the role of nitrosobenzene in the postulated reaction mechanism is not simple. Its detection during the current study was possible, and its presence could be quantified down to low concentrations, yet under normal operating conditions no nitrosobenzene is observed in solution. This shows that this species does not exist in equilibrium with the solution, although it could still exist on the catalyst surface. It is possible that introduction in the manner described above, allows the nitrosobenzene to dominate the adsorption rates, possibly decompose in the presence of a restricted hydrogen supply, and hence ultimately poison the catalyst.

Table 5.3.14 Nitrosobenzene hydrogenation over 0.5458 g Cu(N)/Cab at 110 °C

Reaction time (mins)	Nitrosobenzene (mmols)	Aniline (mmols)	Selectivity to aniline (%)
0	7.53	0.00	0.0
0.5	5.03	0.00	0.0
30	4.73	0.04	1.4
60	4.46	0.07	2.3
120	3.60	0.17	4.4
180	3.04	0.23	5.1
240	1.66	0.26	4.4
795	0.19	0.32	4.4
1230	0.00	0.43	5.7
1290	0.00	0.44	5.8

Figure 5.3.13 Nitrosobenzene hydrogenation over 0.5458 g Cu(N)/Cab at 110 °C

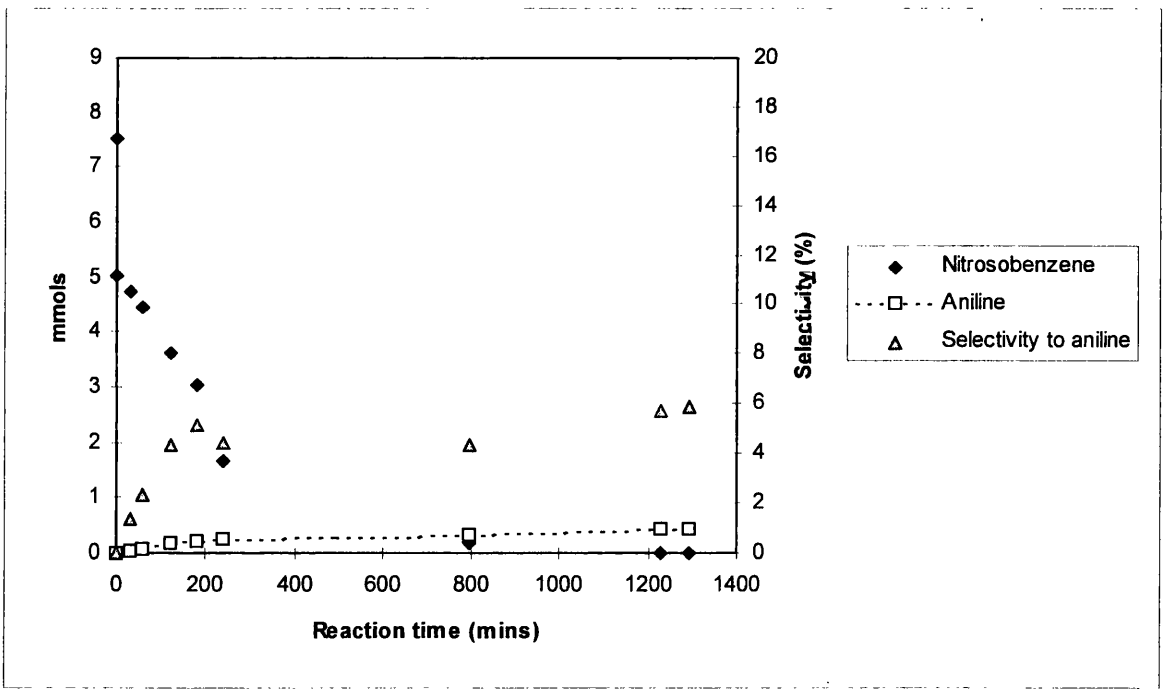

5.3.5 Effect of copper metal surface area upon the reaction

The activity of a catalyst is related, *ceterus paribus*, to its metal surface area. The greater the area of the metal particles, the more surface metal atoms which are available for the adsorption and reaction of the reactant(s). Catalyst surfaces, however, are far from homogeneous, and can assume structures which differ greatly from those of the bulk metal. Steps, kinks, terraces and different crystal planes are all features of a metal surface [6d], as are defects in the crystal structure. Since the different types of metal atoms on the surface have different physical and electronic environments, their catalytic behaviours will vary. This led to the concept of *active sites* by Taylor in 1948 [136], whereby the reaction occurs only on specific locations on the catalyst.

Since the ratio of steps, terraces, *etc.* generally vary with changes in the size of the metal crystallite, the overall rate of reactions may vary over different sizes of metal particles. A catalytic reaction is defined as *structure sensitive* if its rate changes significantly as the particle size of a particular catalyst is changed; this behaviour is exhibited, for example, by the hydrogenolysis of ethane over different faces of single Ni crystals [6c]. The alternative situation is termed *structure insensitive* and is most clearly established for relatively simple hydrogenation reactions such as the hydrogenation of benzene to cyclohexane over palladium- or nickel-based catalysts [3e]. Within this context, the activity of the catalyst is usually expressed as the *specific rate* per surface site, or turnover frequency. Similarly, the selectivity of a catalyst may vary with different sizes of metal particle. Such behaviour is exhibited in the hydrogenation of

cinnamaldehyde, the selectivity to cinnamyl alcohol increasing with larger metal particle sizes [137-139].

There is conflicting evidence regarding the behaviour of nitrobenzene hydrogenation in this respect. Macías Pérez and co-workers conducted the reaction in the liquid phase over carbon-supported platinum catalysts [38]. They found a linear relationship between catalytic activity and the number of surface platinum atoms, concluding that nitrobenzene hydrogenation was structure insensitive over the range of dispersion studied. This was in agreement with the results of Blakely and Somorjai who reported that using platinum catalysts in the gas phase the reaction takes place on one Pt surface atom [140]. In contrast were the findings of Carturan *et al*, who observed a dramatic increase in the catalytic specific activity as the metal dispersion was decreased, their work focussing on liquid phase nitrobenzene hydrogenation over supported palladium catalysts [39].

This section of the report outlines the results regarding catalytic activity and the metal surface areas of the copper catalysts. The turnover frequency against mean metal particle size is then examined to assess the nature of nitrobenzene hydrogenation over copper metal particles. The study of structure sensitive/insensitive reactions requires a great deal of careful experimentation. The causes of this phenomena are not always clear; there are a large number of variables which will affect adsorption and reaction on the catalyst surface at the molecular scale *e.g.* particle size distribution, range over which metal particle size varies, influence of carbonaceous overlayers, *etc.* A conclusive

investigation into this matter was beyond the scope of the current work. Nevertheless, the variation of turnover frequency against mean particle size provides an indication of whether nitrobenzene hydrogenation tends toward structure sensitivity or not.

Metal surface areas were measured via nitrous oxide decomposition experiments and this data used to calculate the mean copper particle sizes (see Section 5.1.7). Turnover frequencies were calculated as described in Section 4.2.

The performances of the different copper catalysts described in Section 5.3.1, and those of the Cu(N)/Cab catalyst under different reduction conditions are shown in Table 5.3.15 and Figure 5.3.14. The reduction treatments employed are outlined in Section 5.1.7; the reactions were conducted at 158 °C with ca. 0.55g of catalyst. Turnover number versus mean particle size is illustrated by Table 5.3.16 and Figure 5.3.15

From Figure 5.3.14 it is clear that catalyst activity is related to metal surface area, but that the relationship is not linear. Figure 5.3.15 exhibits a trend where smaller metal particles lead to an increased turnover frequency. This is a somewhat surprising result given the observations of Pérez *et al* [38] and Blakely and Somorjai [140], who found that nitrobenzene hydrogenation was structure insensitive. Furthermore, the data is in direct contrast to the findings of Carturan *et al* [39]. However, considering the results presented in Section 5.3.3 it is noted that at 158 °C the reaction is not under kinetic control, making meaningful comparisons difficult.

In order to circumvent the problems of diffusion limitation a similar set of experiments were conducted at 110 °C. The reduction treatments applied to Cu(N)/Cab samples were varied to control the metal surface areas of the reduced catalysts. This

series also incorporates two different samples of CuO(A)/Cab. The treatment of this precursor is detailed in Section 5.4; in this context it is the metal surface areas and particle sizes of the catalysts which are of relevance. The relationship between catalyst activity and metal surface area at 110 °C is shown by Table 5.3.17 and Figure 5.3.16.

The rate of aniline formation with respect to metal surface area under these conditions is described well by a straight line (Figure 5.3.16). Furthermore, within the limits of experimental error, the activity of the copper catalysts studied is found to be independent of the metal particle size (Figure 5.3.17). This agrees with the observations of Pérez *et al* [38] and Blakely and Somorjai [140]. It is also consistent with the fact that hydrogenation reactions over supported metal catalysts are, in general, structure insensitive [3e]. On this basis, Figure 5.3.15 is considered to be anomalous, and reflects diffusion limitation issues rather than a genuine particle size dependency.

In conclusion, nitrobenzene hydrogenation over the copper catalysts is structure insensitive over the range studied. The principal factor in controlling catalyst activity is the available metal surface area. Comparable trends for copper catalysts have been reported for methanol synthesis [7g]. After combining the results presented in this chapter and Section 5.3.2, and the dependence on hydrogen concentration [16, 24, 33, 35, 37, 41, 42, 45], the reaction can be described by Equation 5.3.2.

$$\text{rate} = \frac{d[A]}{dt} = \frac{k\,[NB]^0\,[H_2]^1\,[Cu^0_{surf.}]^1}{[AN]^{0.3}} \qquad \text{Equation 5.3.2}$$

where k is a rate coefficient

Table 5.3.15 Rate of aniline formation v. metal surface area at 158 °C

Catalyst	Metal surface area ($m^2 g^{-1}$)	Rate of aniline formation (g of catalyst)$^{-1}$ (moles x10^{-7} s^{-1})
CuO(N)/Cab	0.97	0.124
Cu(A)/Cab	1.87	0.917
Cu(C)/Cab	2.56	1.697
Cu(N)/Cab	3.61	6.636
Cu(N)/C-10	3.78	1.879
Cu(N)/Cab	5.47	6.455
Cu(N)/Cab	6.62	8.212

Figure 5.3.14 Rate of aniline formation v. metal surface area at 158 °C

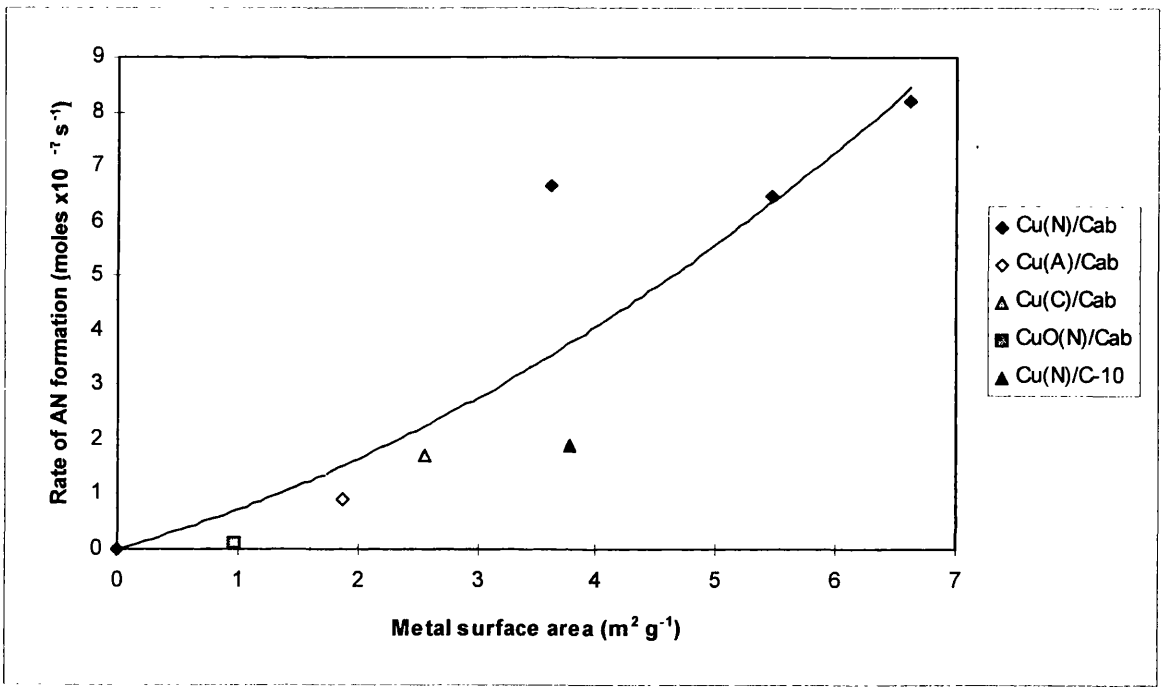

Table 5.3.16 Turnover frequency versus mean particle size at 158 °C

Catalyst	Metal surface area ($m^2 g^{-1}$)	No. of surface sites ($x10^{19}$)	Mean particle size (nm)	Turnover frequency ($x10^{-3}$)
CuO(N)/Cab	0.97	1.37	61.6	0.55
Cu(A)/Cab	1.87	2.64	35.1	2.09
Cu(C)/Cab	2.56	3.61	16.6	2.83
Cu(N)/Cab	3.61	5.09	16.1	7.85
Cu(N)/C-10	3.78	5.33	16.8	2.12
Cu(N)/Cab	5.47	7.71	10.6	5.04
Cu(N)/Cab	6.62	9.33	8.8	5.30

Figure 5.3.15 Turnover frequency versus mean particle size at 158 °C

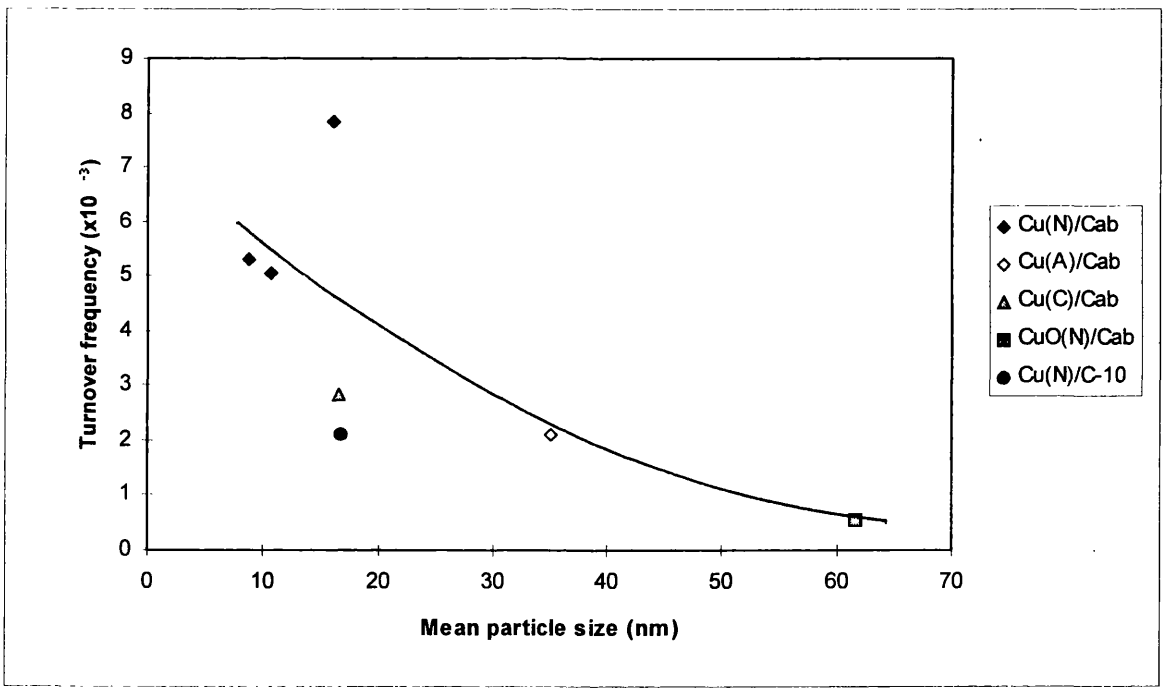

Table 5.3.17 Rate of aniline formation versus metal surface area at 110 °C

Catalyst	Metal surface area ($m^2 g^{-1}$)	Rate of aniline formation (g of catalyst)$^{-1}$ (moles x10^{-7} s^{-1})
Cu(N)/Cab	3.61	2.703
Cu(N)/Cab	5.47	3.091
Cu(N)/Cab	6.62	2.594
Cu(N)/Cab	6.62	3.455
Cu(N)/Cab	7.39	2.797
CuO(A)/Cab	2.91	1.427
CuO(A)/Cab	4.98	3.212

Figure 5.3.16 Rate of aniline formation versus metal surface area at 110 °C

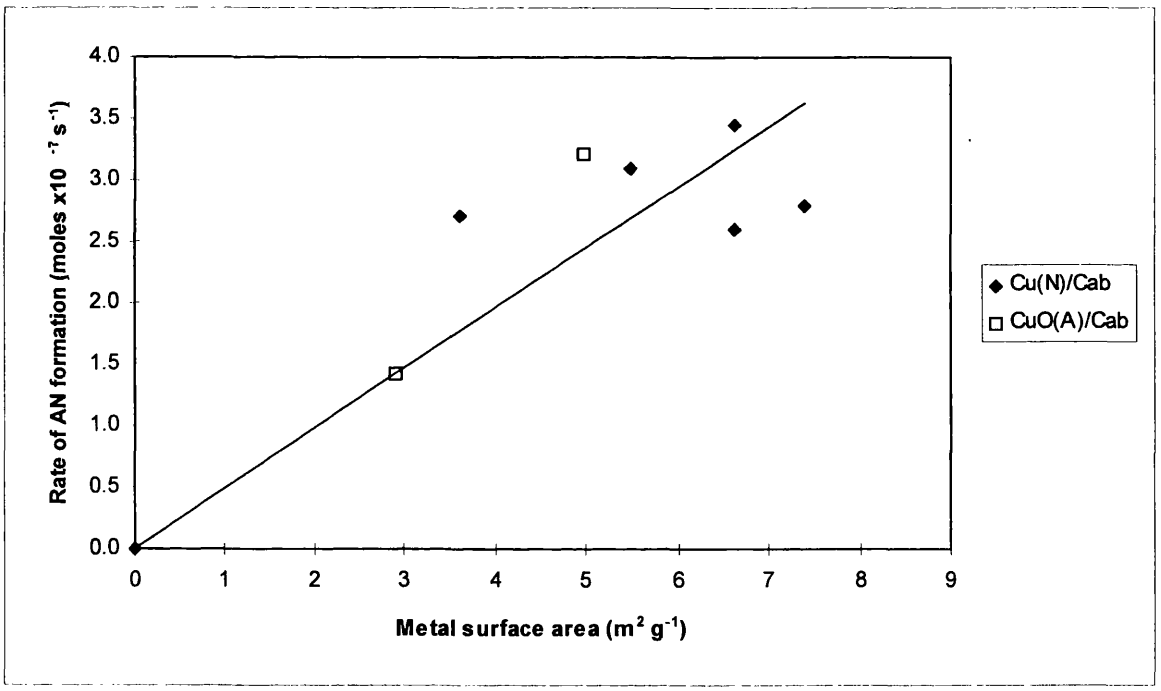

Table 5.3.18 Turnover frequency versus mean particle size at 110 °C

Catalyst	Metal surface area (m^2 g^{-1})	No. of surface sites ($x10^{19}$)	Mean particle size (nm)	Turnover frequency ($x10^{-3}$)
Cu(N)/Cab	3.61	5.09	16.1	3.20
Cu(N)/Cab	5.47	7.71	10.6	2.41
Cu(N)/Cab	6.62	9.33	8.8	1.67
Cu(N)/Cab	6.62	9.33	8.8	2.23
Cu(N)/Cab	7.39	10.40	7.9	1.62
CuO(A)/Cab	2.91	4.10	22.6	2.09
CuO(A)/Cab	4.98	7.02	13.1	2.75

Figure 5.3.17 Turnover frequency versus mean particle size at 110 °C

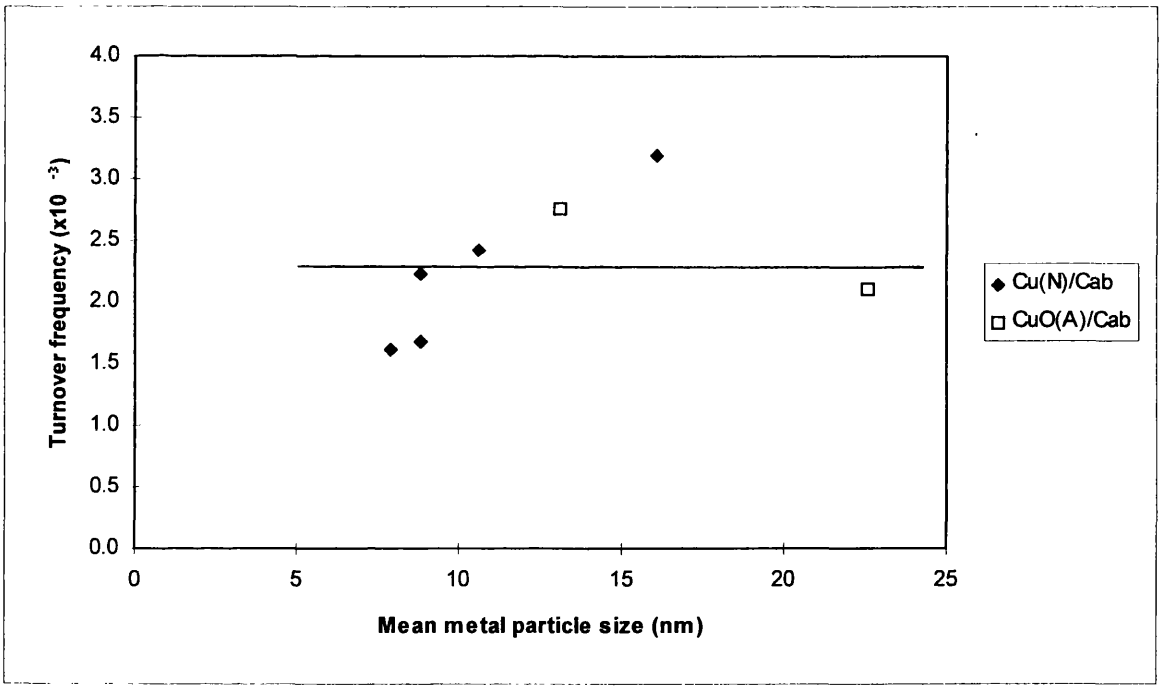

5.3.6 Evaluation of nickel-based catalysts

5.3.6.1 Introduction

The use of nickel-based catalysts towards nitrobenzene hydrogenation has been proven since at least 1898 [15]. Since that time numerous forms of nickel catalyst have been studied, including Raney nickel [16, 34, 35, 51], nickel/alumina [32], nickel boride [33] and nickel powder [35]. Bayer and Allied conduct the industrial hydrogenation of nitrobenzene in the gas phase using nickel sulphide catalysts [55].

The mechanism of the reaction is complex, however, and is still poorly understood. The original mechanism proposed by Haber [15] (shown by Figure 1.1 in Section 1.2.1) is still used today. The formation of azoxybenzene [$C_6H_5(NO)NC_6H_5$] and azobenzene [$C_6H_5NNC_6H_5$] as unwelcome side-products is generally observed [16, 33-35, 42]. Turek *et al* using a nickel/alumina catalyst, however, did not observe these by-products [32].

This chapter outlines the results obtained when using a Raney nickel and an industrial nickel/silica catalyst. Details on these catalysts are provided in Section 3.2.3.

5.3.6.2 Raney nickel

The results of reaction testing using Raney nickel are shown in Table 5.3.19 and Figure 5.3.18. The rate of formation of aniline declines through time. It should be noted that this reaction was performed in the early stages of catalyst testing using *t*-butyl benzene as the solvent. The apparent gradual loss of catalyst activity was a feature of the reactions conducted in *t*-butyl benzene at this time. Whilst similar losses of activity have

been observed with other nickel catalysts [32], it is more likely that this phenomena arose as a consequence of the unoptimised experimental protocol which was employed in these earlier stages of the project.

Although the rate of reaction appears to be relatively slow, the low mass of catalyst should be borne in mind. The activity of Raney nickel towards nitrobenzene hydrogenation is not in doubt; indeed, following the use of Raney nickel to remove catalytic poisons from batches of reactant mixture (described in Section 5.2.6), it was observed that some hydrogenation of the nitrobenzene had been converted to aniline. This occurred at room temperature, with the Raney nickel itself furnishing the only source of dihydrogen.

The formation of azoxybenzene, azobenzene or other by-products was not observed. This is probably due to the relatively low conversion levels achieved in the experimental period. Collins *et al* [33], using a nickel boride catalyst reported that the concentration of the intermediates never comprised more than 2 % of the mixture, and at this percentage, with the low conversions observed in the present study, the by-products may have remained below the detection limits of the analysis.

Table 5.3.19 Nitrobenzene hydrogenation over 0.0669 g Raney Ni at 148 °C

Reaction time (mins)	Nitrobenzene (mmols)	Aniline (mmols)	Selectivity to aniline (%)
0	12.76	0.0	0.0
0	12.28	0.0	0.0
21	12.46	0.0	0.0
67	13.83	0.36	-33.9
125	13.01	0.63	-255.3
184	11.64	0.80	71.5
444	11.01	1.62	92.1
999	11.10	2.75	165.1
1197	11.64	3.08	276.0
1487	9.55	3.41	106.3
2429	10.01	4.58	166.3
2641	8.21	4.53	99.7

Rate of aniline formation (g of catalyst)$^{-1}$ = 12.01 moles x10^{-7} s^{-1}

Figure 5.3.18 Nitrobenzene hydrogenation over 0.0669 g Raney Ni at 148 °C

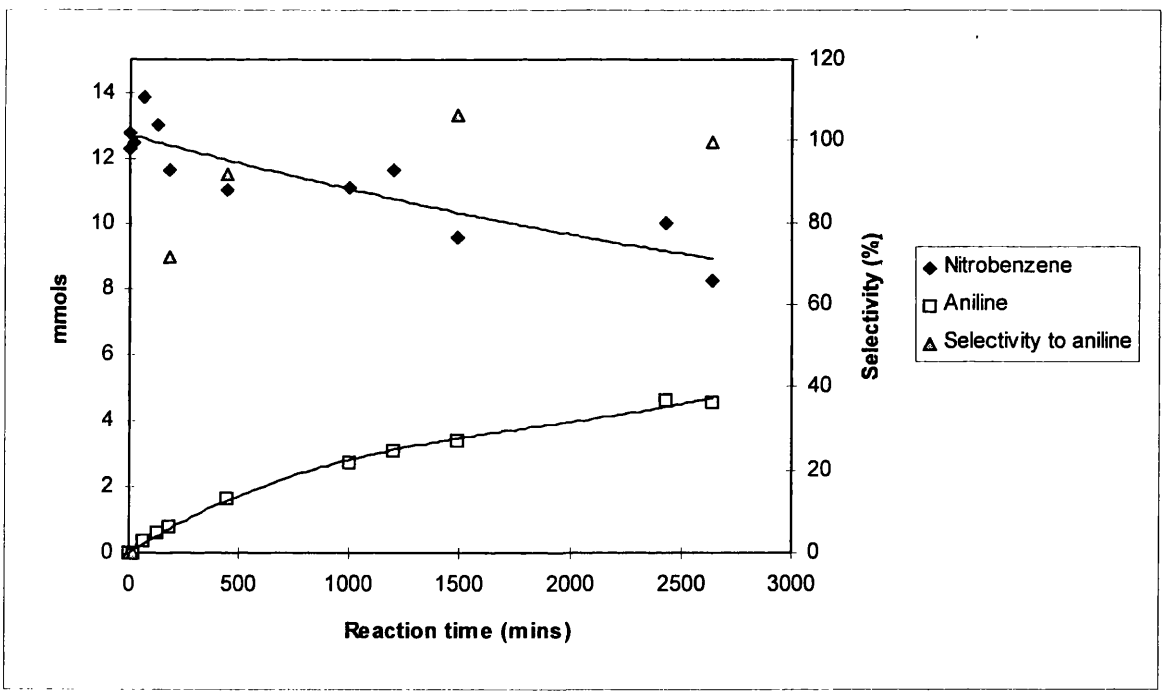

5.3.6.3 Nickel/silica

As discussed in Section 3.2.3 this catalyst was supplied by ICI Synetix. It has a metal loading of 55 wt% and a metal surface area of 39 $m^2 g^{-1}$. Assuming a site density of 1.5 $x10^{19}$ nickel atoms per m^2, based on an equal partition of the three lowest index planes of nickel (fcc) [141], relates to 5.85 $x10^{20}$ surface nickel atoms per gram of catalyst. Detailed information on the catalyst's preparation, characterisation and catalytic behaviour is the domain of the industrial company. During the current work, an activation procedure for the catalyst was established, and its behaviour towards nitrobenzene hydrogenation under the developed experimental protocol assessed.

Approximately 0.1 g of the nickel catalyst were placed in the slurry reactor with a batch of typical reaction mixture (80 ml of 0.1 M nitrobenzene in n-butyl benzene). The vessel was raised to the desired reaction temperature (110 °C) under helium, and once thermally stable the gas was switched to dihydrogen. The results shown in Table 5.3.20 and Figure 5.3.19 reveal no catalyst activity at this temperature, as 110 °C is insufficient to reduce the oxide layer on the catalyst particles. The gas was switched to helium and the applied temperature raised. Upon reaching 174 °C the gas flow was reverted back to dihydrogen.

Complete consumption of the nitrobenzene is achieved within 180 minutes of this point, with aniline as the predominant reaction product. The formation of by-products was detected in small quantities; this is discussed later in greater detail. The aniline concentration passes through a maximum at approximately 320 minutes into the experiment, and then drops significantly. In conclusion the catalyst could be activated

under this experimental system around 170 °C, and the reduced catalyst had considerable activity.

For further reaction testing the mass of catalyst used was dropped to approximately 0.03 g, whilst the reaction system was raised to 170 °C before the addition of dihydrogen. Results obtained are shown by Table 5.3.21 and Figure 5.3.20. These results show a steady loss of nitrobenzene in the first 90 minutes of the experiment, but with little aniline formation during this time. The rate of reaction then increases dramatically, with complete conversion of the nitrobenzene occurring by 345 minutes, at which point the aniline concentration peaks with a selectivity value of 90.5 %. The concentration of aniline subsequently drops over the following ninety minutes, reaching a plateau thereafter.

It is presumed that catalyst activation occurs during the first ninety minutes of the experiment, and that the reduction is complete after this time. This correlates with the reaction results, the rate of nitrobenzene consumption exhibiting two distinct phases. The activity of the reduced catalyst is remarkable, and corresponds to a turnover frequency of 1.71×10^{-2} molecules aniline formed / $Ni_{(surf.)}$ / second.

In addition to aniline, three minor products were detected, N-phenylmethylene-benzenamine [$C_6H_5(CH)=NC_6H_5$], N-benzylaniline [$C_6H_5CH_2NHC_6H_5$] and N-phenylbenzenebutanamine [$C_6H_5CH(C_3H_7)NHC_6H_5$] (see Figure 5.3.22). Calibration lines were not prepared for these minor species, but Table 5.3.22 and Figure 5.3.21 show their peak areas throughout the reaction. The secondary axis of this figure also indicates the percentage conversion which is equivalent to these peak areas (assuming the

calibration line of nitrobenzene). This measure is intended as a guide only. As the specific relative atomic masses of each of the three by-products are roughly twice that of nitrobenzene, their actual concentrations will be approximately 50 % lower, assuming a direct correlation between carbon number and FID response.

Figure 5.3.22

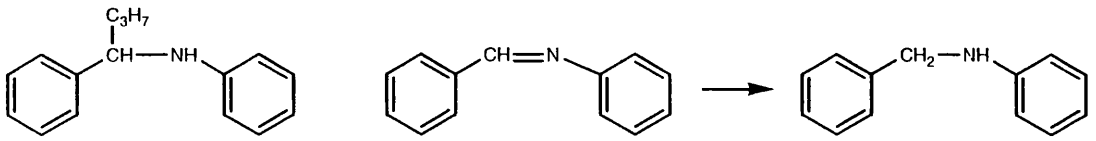

N-Phenylbenzenebutanamine N-Phenylmethylenebenzenamine N-Benzylaniline

In view of the structure of these species it is believed that the N-phenylmethylenebenzenamine and N-phenylbenzenebutanamine compounds are formed via reactions between solvent impurities and the organic substrate (although these side-reactions most likely incorporate aniline, the involvement of nitrobenzene or the reaction intermediates cannot be discounted). It is interesting to note that the formation of these molecules occurs during the early stage of the reaction, at which time nitrobenzene loss exceeds the formation of aniline. Perhaps the partially-reduced catalyst favours their formation over nitrobenzene hydrogenation to aniline. Alternatively the reaction between the nitrobenzene/aniline and the impurity molecules is preferred to nitrobenzene hydrogenation, and proceeds until the supply of impurity is exhausted, at which point aniline formation predominates. The production of N-phenylmethylenebenzeneamine has also been observed when using the copper catalysts, as described in Section 5.2.4. The

concentration of the N-phenylmethylenebenzenamine species reaches a maximum after 165 minutes and remains roughly constant until the nitrobenzene has been completely consumed. Hydrogenation of N-phenylmethylenebenzenamine to N-benzylaniline then occurs, indicating that in terms of competition for the active sites of the catalyst, nitrobenzene is favoured over N-phenylmethylenebenzenamine. The sum total of the three components roughly accounts for the deficit observed between the sum of the nitrobenzene and aniline up until the exhaustion of the nitrobenzene.

Considering again the formation of the aniline it is obvious that this is the major product. The cause of its concentration decrease following the completion of nitrobenzene hydrogenation is uncertain, but it is believed that this occurs due to hydrogenolysis of the aniline molecule to form benzene and ammonia. This concept, whereby the benzene species then goes on to form polyaromatic carbon layers on the catalyst surface is outlined in Section 5.2.4.

5.3.6.4 Conclusions

The Raney nickel and nickel/silica catalysts both displayed activity towards nitrobenzene hydrogenation in the liquid phase. The activation of the nickel/silica catalyst was achievable *in situ* at 170 °C in the presence of dihydrogen. Any by-products or intermediates formed when using the Raney nickel catalyst were below the detection limits of the analytical technique. Use of the nickel/silica catalyst resulted in the formation of a series of minor by-products, which are believed to originate from reactions involving impurities within the *n*-butyl benzene solvent.

Table 5.3.20 Nitrobenzene hydrogenation over 0.0999 g industrial Ni catalyst

Reaction Time (mins)	Nitrobenzene (mmols)	Aniline (mmols)	Temperature (°C)
0	7.49	0.00	112
15	6.94	0.00	110
30	7.31	0.00	110
45	7.12	0.00	111
60	6.80	0.00	111
100	6.89	0.00	110
147	6.85	0.00	110
200	6.85	0.00	174
230	5.75	0.62	173
260	4.25	2.08	175
291	2.42	3.79	174
321	0.42	5.82	174
382	0.00	5.42	167

Figure 5.3.19 Nitrobenzene hydrogenation over 0.0999 g industrial Ni catalyst

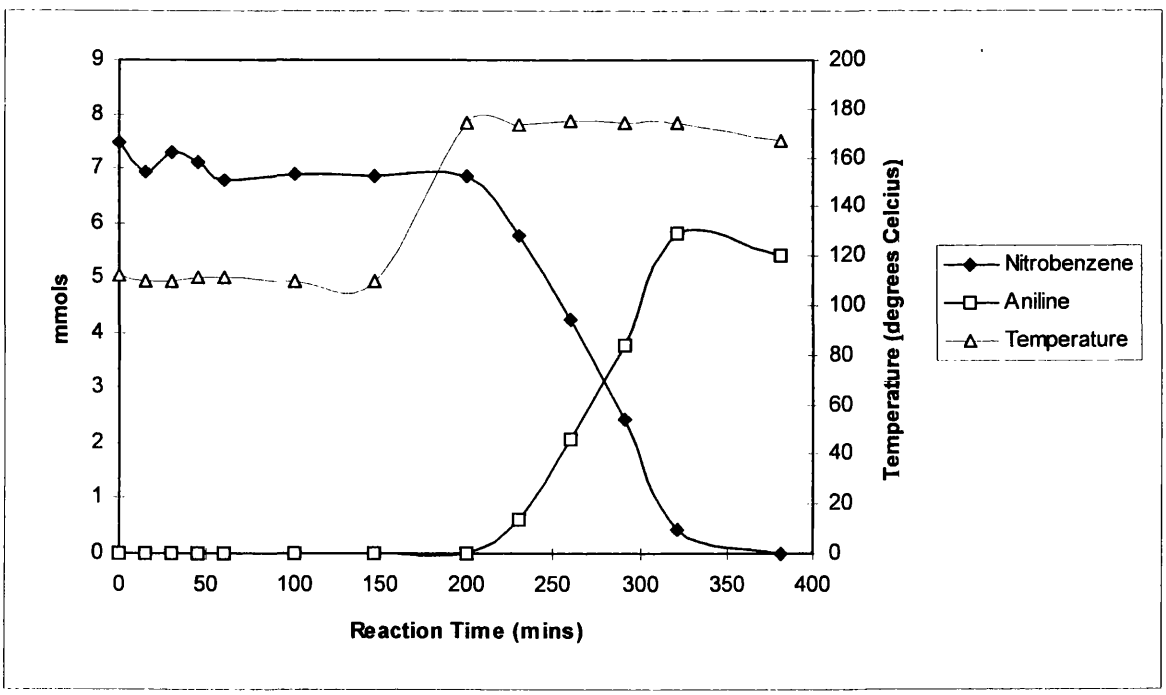

Table 5.3.21 Nitrobenzene hydrogenation over 0.0316 g industrial Ni catalyst at 170 °C

Reaction time (mins)	Nitrobenzene (mmols)	Aniline (mmols)	Selectivity to aniline (%)
0	8.21	0.00	0.0
30	7.93	0.00	0.0
60	7.81	0.16	38.7
90	7.62	0.50	85.0
120	6.54	1.08	64.7
165	5.04	2.26	71.4
210	3.96	3.94	92.7
255	2.46	5.71	99.3
300	0.83	6.72	91.1
345	0.00	7.43	90.5
390	0.00	7.17	87.4
435	0.00	6.72	81.9
495	0.00	6.59	80.3
555	0.00	6.66	81.1
660	0.00	6.72	81.9

Rate of aniline formation (g of catalyst)$^{-1}$ = 166.1 moles x10^{-7} s^{-1}

Figure 5.3.20 Nitrobenzene hydrogenation over 0.0316 g industrial Ni catalyst at 170 °C

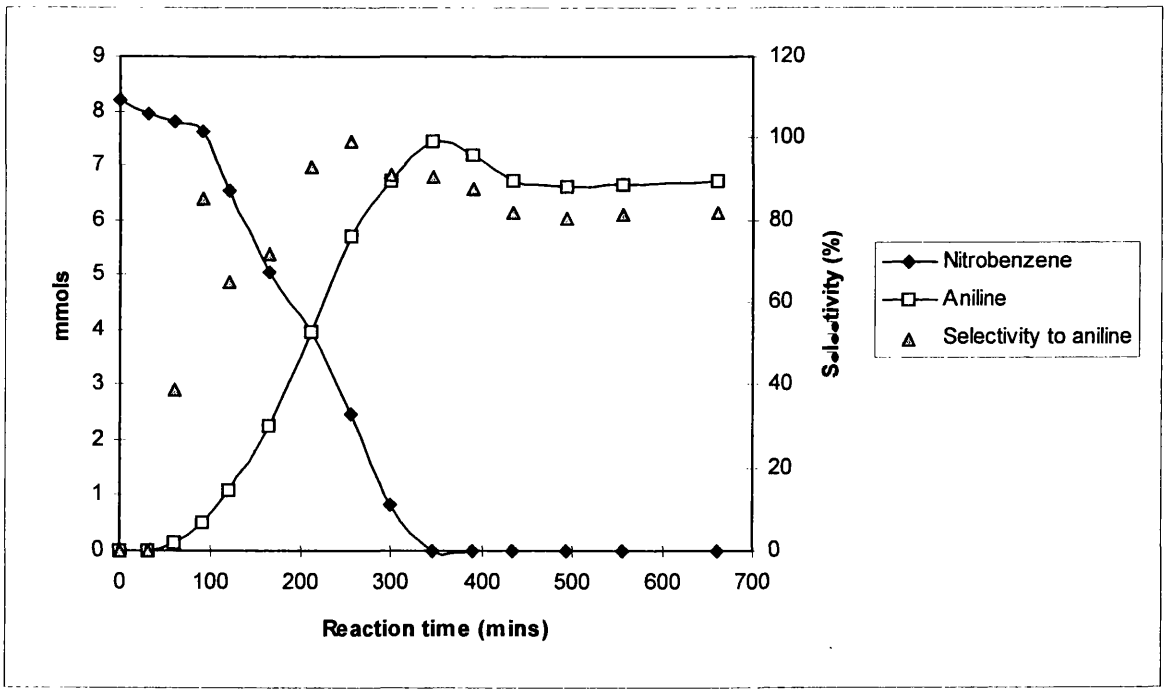

Table 5.3.22 By-products formed during nitrobenzene hydrogenation over 0.0316 g industrial nickel/silica catalyst at 170 °C

	Peak area (mm^2)		
Reaction time (mins)	N-Phenylmethylene-benzenamine	N-Benzyl aniline	N-Phenylbenzene-butanamine
0	0.00	0.00	0.00
30	0.30	0.08	3.97
60	1.27	0.13	5.19
90	5.25	0.16	5.69
120	8.06	0.16	5.94
165	10.25	0.16	6.25
210	10.06	0.16	6.13
255	10.19	0.16	6.38
300	10.06	0.16	6.25
345	8.13	0.53	6.88
390	5.83	1.25	6.50
435	4.99	2.03	6.75
495	3.26	2.75	6.75
555	1.38	3.08	6.56
660	0.51	3.53	7.00

Figure 5.3.21 By-products formed during nitrobenzene hydrogenation over 0.0316 g industrial nickel/silica catalyst at 170 °C

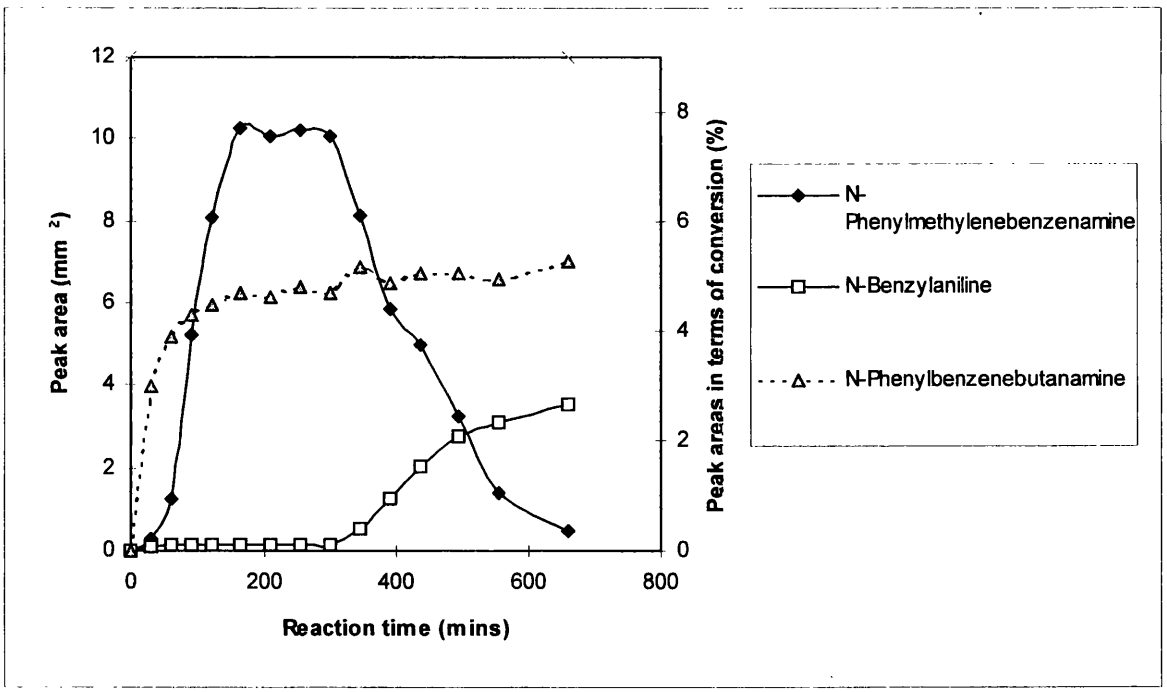

5.4 FLUIDISED BED PRETREATMENT

5.4.1 Introduction

The experimental technique and development of the apparatus for this work are discussed in Section 3.4. The apparatus shown by Figures 3.4 and 3.5 of this section was used for three different calcination experiments using the Cu(A)/Cab precursor. Samples of this catalyst were calcined as fixed and fluidised beds, with flow rates of 50 and 500 ml min^{-1} respectively. The critical differences in the characteristics of these two methods are the gas flow rate and the nature of the bed itself. An additional 'intermediate' treatment was therefore attempted, whereby the high flow rate of the fluidised bed procedure was employed, but directed down through the catalyst against the sinter. This produced the behaviour of a fixed bed at the higher flow rate, to allow the two features to be assessed independently.

The calcined samples are referred to as CuO(A)/Cab (fixed50), CuO(A)/Cab (fl.bed500) and CuO(A)/Cab (fixed500). The temperatures of the various beds were monitored throughout each experiment, as were the temperatures applied by the furnace. The metal surface areas of the catalysts following the calcination and subsequent reduction were determined by nitrous oxide decomposition, and the metal particle sizes of the CuO(A)/Cab (fixed50) and CuO(A)/Cab (fl.bed500) samples were assessed using transmission electron microscopy. These latter samples were also tested for their catalytic behaviour towards nitrobenzene hydrogenation. The overall effects of the different calcination methods are discussed with reference to the differential scanning calorimetry, variable temperature x-ray diffraction and TEM results reported previously.

5.4.2 Calcination treatment

For all three experiments, 1.2 g samples of the Cu(A)/Cab were calcined at 3 °C min^{-1} to 300 °C, and this temperature was held for 60 minutes before the system was allowed to cool. Some carry-over of fines was observed during the experiments, this material being pressed against the sinter of the disengagement section. Agitation by the mechanical vibrator kept this to a minimum. Any material which was removed from the bed and pressed against the sinter remained distinct from the bed proper. This was carefully seperated from the bulk of the sample at the end of the experiment.

The temperature profiles for the CuO(A)/Cab (fixed50), CuO(A)/Cab (fl.bed500) and CuO(A)/Cab (fixed500) experiments are shown by Tables 5.4.1, 5.4.2 and 5.4.3 and Figures 5.4.1, 5.4.2 and 5.4.3 respectively.

The most striking feature amongst these results is the dramatic rise in temperature observed when calcining the catalyst as a fixed bed at 50 ml min^{-1} (Table and Figure 5.4.1). This commences around 190 °C and at its maximum raises the temperature of the bed to 279 °C, roughly 86 °C above its preprogrammed value. This is attributed to the exothermic nature of the calcination process. Figure 5.1.2, in the chapter discussing the results of DSC on the Cu(A)/Cab catalyst (Section 5.1.4, p63), illustrates the thermodynamics of its combustion. From the results obtained using VTXRD it is concluded that this exotherm arises from the oxidation of copper acetate [$Cu(CH_3COO)_2$] to tenorite [CuO]. Once this step is initiated the heat evolved provides the energy for complete oxidation of the organic material, and consequently a substantial increase in the

temperature of the sample is noted. This has important implications regarding the size of the metal particles.

The heat produced during this reaction was sufficient to raise the temperature of the air flow, and the catalyst bed and its immediate environ; the thermocouple controlling the temperature programmed was placed just outside the reactor in the thermocouple pocket, but shows an equivalent rise in measured temperature. Such a rapid temperature rise has a detrimental effect on the catalyst dispersion. Repeat runs of this experiment confirmed that this exothermic event was reproducible, and not caused by the 'misbehaviour' of the temperature programmer.

The temperature programmer (TP) is based on a proportional, integral, derivative facility (PID), that has been previously tuned to the temperature characteristics of the furnace. This minimises fluctuations in the temperature control. However, the second sharp exotherm, which is observed at 63 minutes, was caused by the temperature programmer. That is, following the initial exotherm the TP perceives that the system is cooling rapidly and consequently increases the power output to the furnace, which leads to the second observed rise in temperature, with the TP adjusting and stabilising thereafter.

Calcinations conducted as fluidised bed at an air flow of 500 ml min^{-1} showed no such exotherm, with the temperature ramping smoothly as programmed (Table and Figure 5.4.2). It was concluded that up until 190 °C the two techniques and the calcination treatments are essentially similar. However, whereas the fixed bed calcination results in a self-propagating reaction, this is prevented by the characteristics of the fluidised bed. The

strong flow of gas acts to dissipate and remove the heat evolved by the oxidation of the copper acetate and the resultant water molecules which are formed in the process. The calcination can therefore proceed gradually at the desired ramp rate.

The last experiment of this series conducted as a fixed bed with the flow rate of 500 ml min^{-1} (Table and Figure 5.4.3). It is clear that the exotherm produced by the calcination of copper acettate is not observed macroscopically. However, it is believed that the copper crystallites experience the exotherm locally, which leads to metal particle agglomeration. This is supported by the metal surface area measured for this sample in comparison with that obtained via the fluidised bed treatment. These results are presented below (Section 5.4.3). The fluidised bed method is clearly more efficient at dissipating the heat of calcination evenly throughout the sample.

The deviation of the temperature shown in Table and Figure 5.4.3 reflects the difficulty the PID temperature programmer had in maintaining a linear ramp during this experiment. This apparently cyclical fluctuation was not observed in other calcination experiments, and is thought to have occurred as a result of the different positioning of the temperature programmer's thermocouple in the reactor.

Figure 5.4.1 Temperature of fixed bed at 50 ml min^{-1} during calcination

Time (mins)	Thermocouple pocket (°C)	Catalyst bed (°C)	Time (mins)	Thermocouple pocket (°C)	Catalyst bed (°C)
0.0	31	30	58.25	248	239
3.0	44	41	58.5	261	264
6.0	56	53	58.75	263	280
9.0	58	56	59.0	279	278
12.0	68	65	59.25	277	262
15.0	76	73	59.5	262	250
18.0	85	81	59.75	244	239
21.0	94	89	60.0	230	229
24.0	103	97	60.25	220	222
27.0	112	107	60.5	215	217
30.0	121	116	60.75	213	214
33.0	130	124	61.0	215	213
37.0	142	136	63.0	234	233
39.0	148	142	66.0	219	215
42.0	157	151	70.0	223	220
45.0	167	165	72.0	229	225
48.0	177	176	75.0	236	231
51.0	185	179	78.0	245	240
52.0	186	179	81.0	254	249
53.0	190	183	84.0	263	258
54.0	198	190	87.0	272	266
55.0	191	189	90.0	281	275
56.0	213	205	93.0	290	283
57.0	224	217	96.0	299	292
57.25	225	218	108.0	300	293
57.5	230	220	112.0	307	300
57.75	237	226	130.0	307	300
58.0	241	228	140.0	307	300

Figure 5.4.2 Temperature of fluidised bed at 500 ml min^{-1} during calcination

Time (mins)	Thermocouple pocket (°C)	Catalyst bed (°C)	Time (mins)	Thermocouple pocket (°C)	Catalyst bed (°C)
0.0	20	19	67.0	220	221
3.0	28	26	67.5	223	223
6.0	41	40	68.0	224	225
9.0	47	45	68.5	226	228
12.0	57	55	69.0	228	230
15.0	66	64	69.5	231	233
18.0	75	73	70.0	234	236
21.0	84	82	70.5	233	236
24.0	93	91	71.0	234	236
27.0	102	100	72.0	242	244
30.0	111	109	73.0	245	247
33.0	120	118	74.0	242	242
36.0	129	128	75.0	248	249
39.0	138	137	76.0	252	253
42.0	147	147	77.0	253	254
47.0	161	161	78.0	255	257
48.0	165	164	78.5	259	261
51.0	174	174	79.0	260	262
54.0	183	183	80.0	260	263
56.0	189	189	81.0	265	267
58.0	193	192	82.0	262	265
59.0	197	197	83.0	266	268
60.0	200	200	84.0	273	275
60.5	202	202	85.0	276	277
61.0	204	204	86.0	279	281
61.5	206	206	87.0	283	284
62.0	206	206	88.0	284	286
62.5	207	207	89.0	288	289
63.0	210	210	90.0	291	292
63.5	211	211	92.0	297	298
64.0	212	212	93.0	300	301
64.5	213	213	95.0	302	302
65.0	214	214	100.0	301	302
65.5	215	216	109.0	300	301
66.0	217	217	124.0	301	306
66.5	218	219	133.0	293	295

Figure 5.4.1 Temperature of fixed bed at 50 ml min^{-1} during calcination

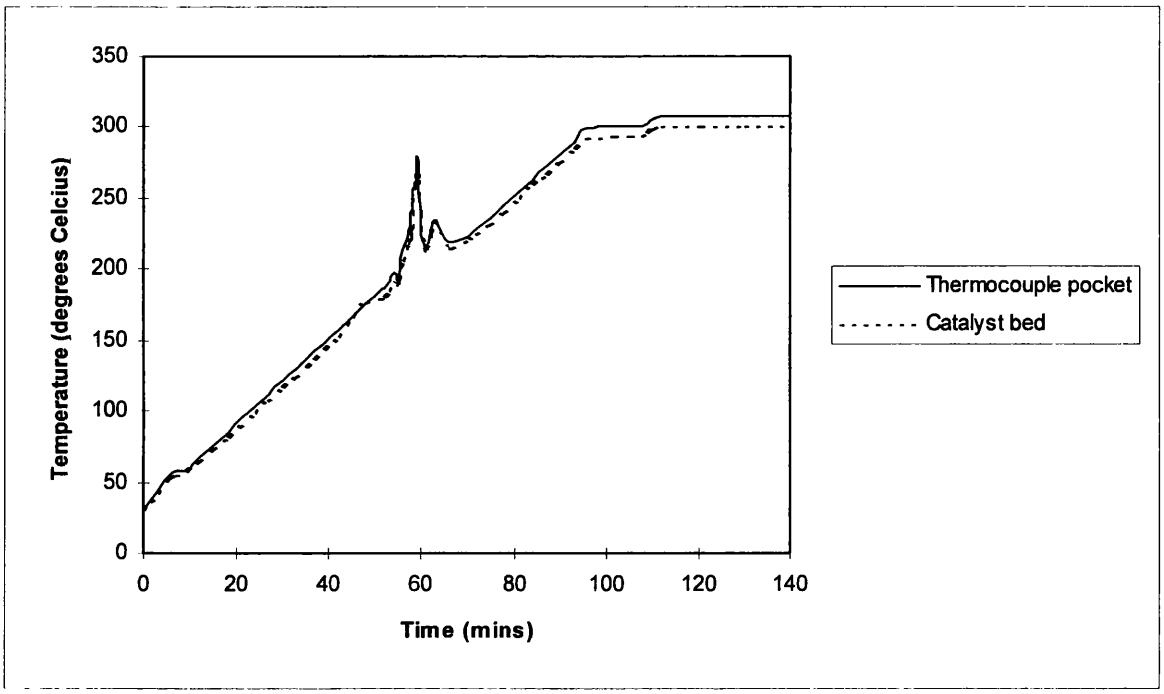

Figure 5.4.2 Temperature of fluidised bed at 500 ml min^{-1} during calcination

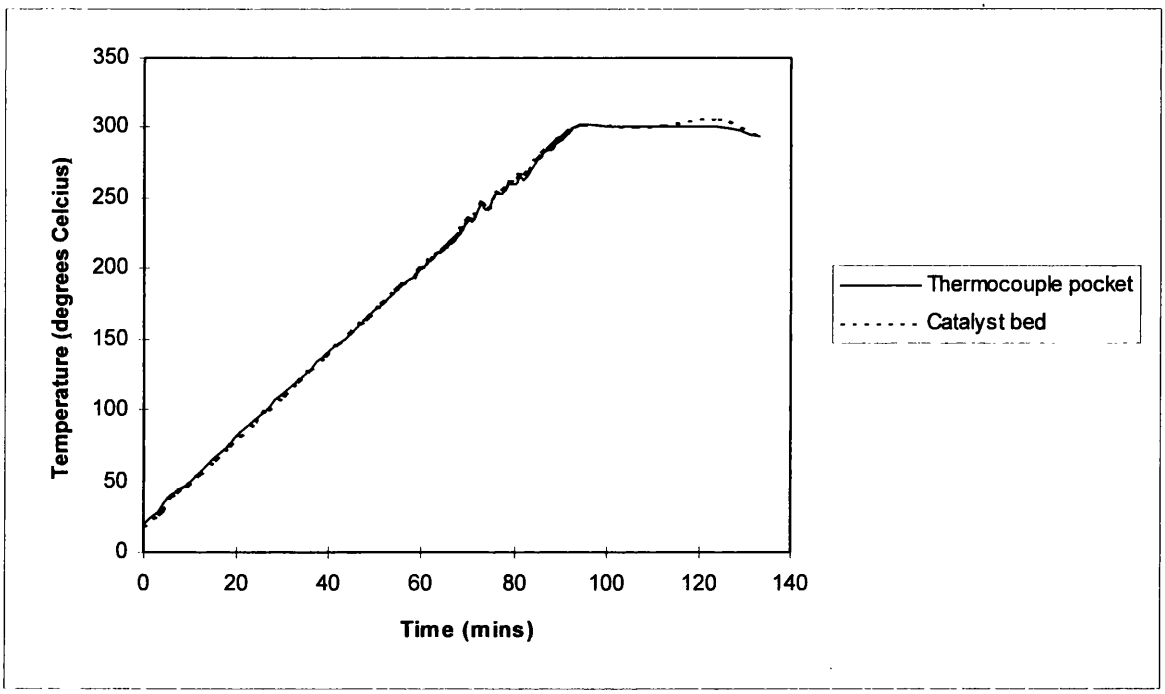

Figure 5.4.3 Temperature of fixed bed at 500 ml min^{-1} during calcination

Time (mins)	Thermocouple pocket (°C)	Catalyst bed (°C)	Time (mins)	Thermocouple pocket (°C)	Catalyst bed (°C)
0.0	23	23	60.0	205	192
3.0	42	42	61.0	212	198
6.0	43	42	62.0	221	206
9.0	65	68	63.0	222	209
12.0	69	80	64.0	219	206
15.0	71	81	65.0	219	207
18.0	84	93	66.0	224	209
21.0	90	102	67.0	234	216
26.0	109	117	68.0	237	223
29.0	111	117	69.0	235	223
32.0	127	127	70.0	235	222
35.0	132	131	71.0	238	224
38.0	145	140	72.0	248	231
41.0	151	145	73.0	252	238
44.0	168	161	74.0	249	236
47.0	168	162	75.0	250	236
50.0	185	172	76.0	255	240
51.0	188	177	77.0	263	246
52.0	187	178	78.0	266	252
53.0	186	177	79.0	264	250
54.0	187	177	80.0	263	250
55.0	194	181	83.0	280	266
56.0	199	189	86.0	293	274
57.0	204	193	89.0	293	280
58.0	204	194	91.0	300	282
59.0	201	191	97.0	300	289

Figure 5.4.3 Temperature of fixed bed at 500 ml min^{-1} during calcination

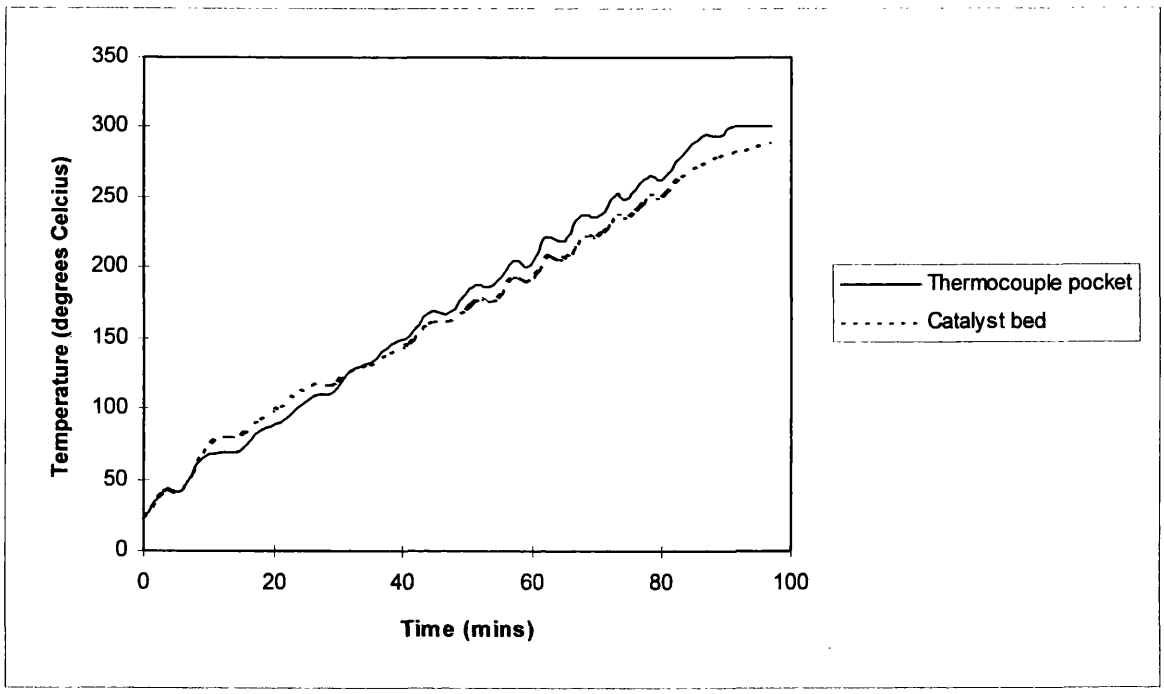

5.4.3 Post-calcination testing

All catalyst activation steps performed for this chapter of the report were conducted at 3 °C min^{-1} to 290 °C, and this temperature was held for 60 minutes under 10 % H_2/N_2 and 30 minutes under helium. The metal surface areas of the three samples, CuO(A)/Cab (fixed50), CuO(A)/Cab (fl.bed500) and CuO(A)/Cab (fixed500) were determined by nitrous oxide decomposition experiments as described in Section 5.1.7. The results obtained are shown in Table 5.4.7, which also includes the metal surface area measured for the uncalcined/directly reduced form of this catalyst, Cu(A)/Cab.

Table 5.4.7 Metal surface areas of the CuO(A)/Cab and Cu(A)/Cab catalysts

Catalyst	Dispersion (%)	Metal surface area (m^2 g^{-1})	Mean particle size (nm)
CuO(A)/Cab (fixed50)	4.47	2.91	22.6
CuO(A)/Cab (fl.bed500)	7.64	4.98	13.1
CuO(A)/Cab (fixed500)	1.63	1.06	6.17
Cu(A)/Cab	6.12	1.87	16.8

The Cu(A)/Cab catalyst has a relatively low metal surface area of 1.87 m^2 g^{-1}, but this is improved when the calcination is conducted as a fixed bed with a gas flow of 50 ml min^{-1}. Furthermore, it should be remembered that the Cu(A)/Cab retains organic material on the catalyst surface when reduced without prior calcination, indicating that any loss of surface area through sintering of the metal particles during the calcination step is more than offset by the removal of the carbon-based salt. The function of the calcination stage to remove any residues is revealed by VTXRD studies (Section 5.1.5).

The CuO(A)/Cab (fl.bed500) catalyst presents a metal surface area of 4.98 $m^2 g^{-1}$, and shows that calcination as a fluidised bed ultimately optimises the final metal surface area. The lowest metal surface area is displayed by the CuO(A)/Cab (fixed500) catalyst.

The lower dispersion and metal surface area values of the CuO(A)/Cab (fixed50) catalyst, when compared to the CuO(A)/Cab (fl.bed500) sample are attributed to sintering of the metal crystallites. This is illustrated by the TEM work reported in Section 5.1.8. The particle dimensions measured for the CuO(A)/Cab (fixed50) catalyst are significantly higher, and micrographs show signs that these comparatively large particles have been formed via the agglomeration of several smaller crystallites (see Figure 5.1.23 in Section 5.1.8, p99).

In retrospect, the calcination conducted as a fixed bed at the higher flow rate of 500 ml min^{-1} was not without value. It indicates that exploitation of the benefits of fluidised bed techniques during such pretreatment requires the appropriate equipment; it is ineffective to simply use fixed bed apparatus at increased air flows.

The CuO(A)/Cab (fixed50) and CuO(A)/Cab (fl.bed500) catalysts were screened for activity during nitrobenzene hydrogenation, at 110 °C with *n*-butyl benzene as the solvent. The results of the former are presented by Table and Figure 5.4.4, whilst those obtained using the latter are shown by Table and Figure 5.4.5.

Both catalysts show the linear consumption of nitrobenzene, with the corresponding formation of aniline. As reported with the other copper-based catalysts aniline was the only product detected. The difference in the activity of the two catalysts, however, is marked, with the sample calcined as a fluidised bed displaying much higher

activity. There is a definite correlation between their measured metal surface areas and their catalytic activity. The relationships between activity and metal surface area, and turnover frequency versus metal particle size, have been presented in Section 5.3.5.

The two catalysts have also been directly compared against the Cu(N)/Cab catalyst, at equivalent reaction conditions. The results, shown by Table and Figure 5.4.6, have been normalised to one gram of catalyst and plotted in terms of conversion, assuming an initial 8.0 mmols of nitrobenzene. Since the formation of aniline mirrors the consumption of the nitrobenzene, only the production of aniline has been presented to simplify the comparison.

Cu(N)/Cab displayed the greatest activity of the directly-reduced copper/silica precursors studied, and remains more active than CuO(A)/Cab (fixed50). Nevertheless, these results show that the most active form of the catalysts is CuO(A)/Cab (fl.bed500). This is considered a conclusive demonstration of the merits of fluidised bed techniques when applied to the pretreatment of supported catalysts.

Table 5.4.4 Nitrobenzene hydrogenation over 0.5867 g CuO(A)/Cab (fixed[50])

Reaction time (mins)	Nitrobenzene (mmols)	Aniline (mmols)	Selectivity to aniline (%)
0	8.01	0.00	0.0
58	7.65	0.14	38.1
122	7.08	0.62	66.5
180	6.55	0.92	62.7
225	6.01	1.20	60.4
Rate of aniline formation (g of catalyst)$^{-1}$ = 1.427 moles x10^{-7} s^{-1}			

Figure 5.4.4 Nitrobenzene hydrogenation over 0.5867 g CuO(A)/Cab (fixed[50])

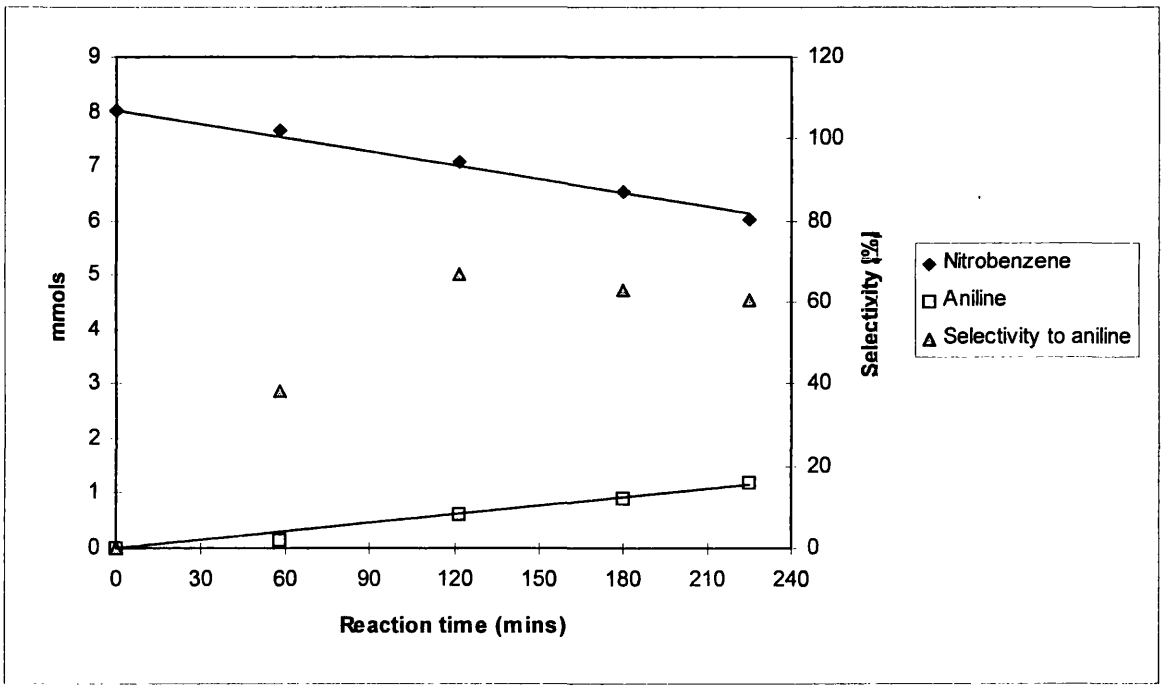

Table 5.4.5 Nitrobenzene hydrogenation over 0.5844 g CuO(A)/Cab (fl.bed^{500})

Reaction time (mins)	Nitrobenzene (mmols)	Aniline (mmols)	Selectivity to aniline (%)
0	7.57	0.00	0.0
31	7.21	0.15	42.6
64	7.13	0.60	136.3
90	7.00	0.97	169.8
124	6.44	1.35	119.8
157	6.01	1.78	114.3
180	5.85	2.20	128.4
225	4.84	2.60	95.5

Rate of aniline formation (g of catalyst)$^{-1}$ = 3.212 moles x10^{-7} s^{-1}

Figure 5.4.5 Nitrobenzene hydrogenation over 0.5844 g CuO(A)/Cab (fl.bed^{500})

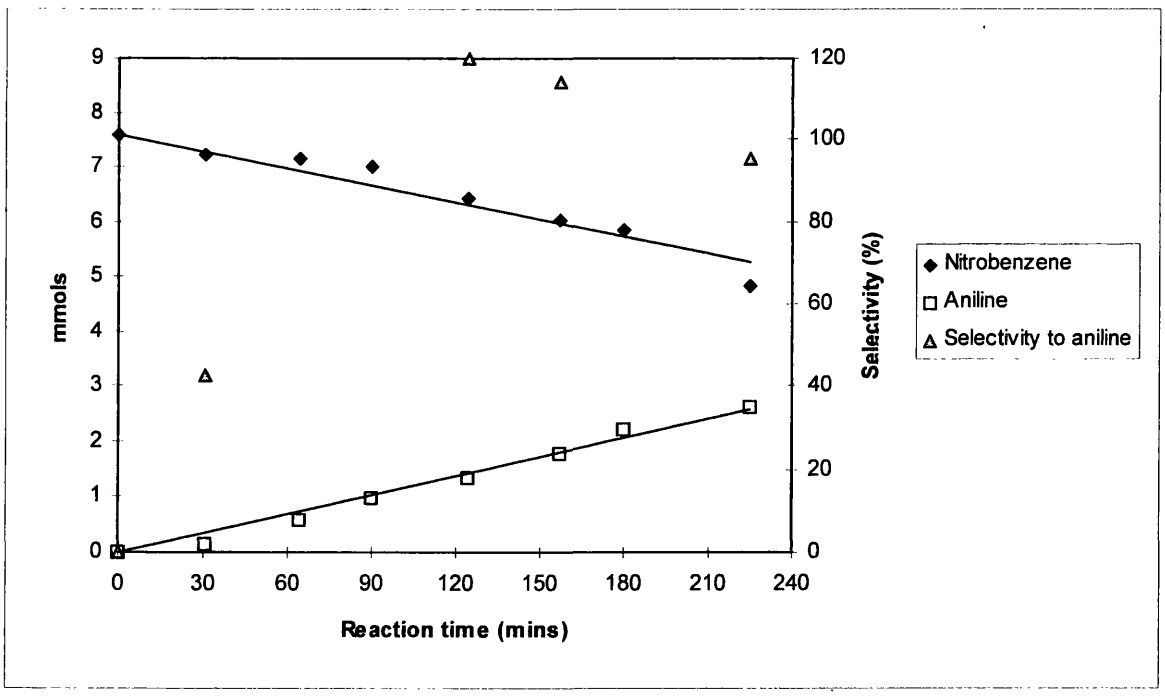

Table 5.4.6 Comparison of activities of Cu(N)/Cab, CuO(A)/Cab (fixed^{50}) and CuO(A)/Cab (fl.bed^{500})

	Conversion (%)		
Reaction time (mins)	CuO(A)/Cab (fl.bed500)	Cu(N)/Cab	CuO(A)/Cab (fixed50)
0	0.0	0.0	0.00
30		2.74	
31	3.31		
58			2.98
60		9.14	
64	12.76		
90	20.73	17.37	
120		24.45	
122			13.21
124	28.95		
150		31.99	
157	38.03		
180	47.10	40.68	19.60
225	55.69		25.57
Rate of aniline formation (moles x10^{-7} s^{-1})	3.212	1.427	3.091

Figure 5.4.6 Comparison of activities of Cu(N)/Cab, CuO(A)/Cab (fixed^{50}) and CuO(A)/Cab (fl.bed^{500})

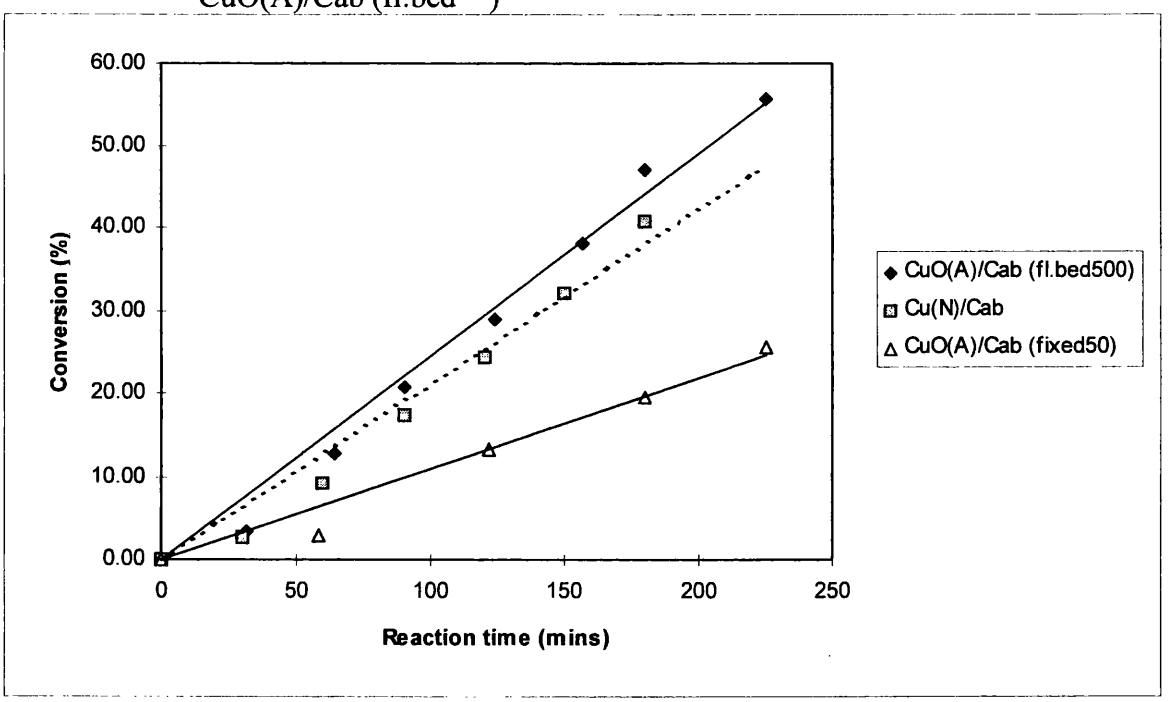

5.4.4 Conclusions

Overall, calcination is a beneficial step in the pretreatment of catalysts which have been derived from carbon-based salts. The exothermic nature of this step, however, produces a significant output of heat, which provides the energy for further oxidation of the organic material. If this is not controlled then it can result in a 'chain reaction', whereby the calcination proceeds to completion in a short period of time. When the calcination procedure is conducted as a fixed bed, as is conventionally employed, the resultant exotherm promotes the sintering of the metal particles. The catalyst's metal surface area and subsequent activity are consequently decreased.

However, the use of a fluidised bed during the calcination procedure provides a means to control the rate of oxidation. No such exotherm is observed during the process, and the calcination of organic material is allowed to progress gradually. Whilst some particle agglomeration will inevitably occur at elevated temperatures, it is to a lesser degree than occurs within fixed catalyst beds. The fluidised bed approach offers efficient heat transfer, thereby minimising the rise in temperature experienced by the copper crystallites that results from the oxidation of the copper acetate to the tenorite. Upon reduction the catalyst calcined by the fluidised bed technique shows a higher metal surface area than that calcined as a fixed bed, with a corresponding improvement in its activity. No differences in selectivity arising from the two techniques were observed.

It has also been shown that simply increasing the flow rate of air through a fixed bed of catalyst is ineffective during this pretreatment.

Various methods are used to control the exothermic nature of catalyst reduction. Low ramp rates and multi-level ramps allow the reduction to proceed in a gradual and controlled manner, preventing the production of a detrimental exotherm. This is obviously not possible during the calcination procedure; once a critical temperature is reached, and an adequate supply of oxygen is present, the reaction is essentially self-propagating. Dilution of the reductant gas with an inert carrier to inhibit the rate of catalyst reduction is also possible. Whilst this measure may be feasible for the calcination stage, it is also possible that organic material containing sufficient oxygen could still produce the damaging exotherm. The calcination reactor could be actively cooled during the critical juncture of the procedure, but this would no doubt be expensive at the industrial scale. In summary, it seems that the use of a fluidised bed technique could be the most satisfactory means of controlling the rate of calcination.

Finally, it would be worthwhile to assess the effect of catalyst reduction conducted as a fluidised bed. This was not possible with the existing apparatus. Substantial redesign of the reactor vessel would be required, and hence was not pursued further during the current work.

Chapter Six

Conclusions

6.1 THE NATURE OF THE COPPER CATALYSTS

i) UV-vis spectroscopy of samples of condensate collected during the drying stage of catalyst preparation show that solid material, *i.e.* copper salt and silica, is removed from the slurry mixture.

ii) The actual metal loadings of the catalysts are lower than nominal, as is usually observed in catalyst preparation. This may be partly attributed to the findings of i).

iii) BET studies revealed that the total surface areas of the catalysts change little from the original support, with the exception of the Cu(C)/Cab sample.

iv) The results of AAS and BET studies indicate that precipitation of the metal salt from solution, and some reconstruction of the silica support, both occurred during the preparation of the Cu(C)/Cab catalyst.

v) TGA studies showed that considerable loss of mass is experienced by the catalysts at elevated temperatures in a reductive atmosphere. This varies between 5.5 and 33.6 % for the uncalcined samples, but is approximately constant around 2 % for the calcined samples.

vi) VTXRD revealed that the reduction of the Cu(N)/Cab catalyst proceeds as shown:-

$Cu(NO_3)_2.xH_2O$		$Cu_2(NO_3)(OH)_3$		CuO		Cu^0 + [CuO]
	→		→		→	
Ambient		190 °C		215 °C		240 °C +

Similarly, the calcination of Cu(A)/Cab proceeds as shown:-

$Cu(CH_3COO)_2.H_2O$		$Cu(CH_3COO)_2$		$Cu(CH_3COO)_2$ + [CuO]		CuO
	→		→		→	
Ambient		150 °C		200 °C		225 °C +

vii) The reduction of the Cu(N)/Cab catalyst was found by TPR to proceed over a narrow temperature range, centred around 245 °C, and indicated that reduction of the deposited copper nitrate was complete upon reaching 290 °C. Significant uptake of hydrogen by the other catalysts was similarly found to have ceased around this higher temperature.

viii) TEM studies on the reduced catalysts, however, displayed the presence of metal complex material, which indicated that the reduction does not proceed to completion under the applied treatments. Micrographs revealed that the metal salt was not deposited homogeneously over the silica support during the preparation stage. The particle size distribution measured for the Cu(N)/Cab catalyst had a modal value of approximately 4 nm, which remained constant regardless of the reduction treatments tested.

ix) The metal surface areas of the catalysts were determined by nitrous oxide decomposition, and this technique was employed to optimise catalyst dispersion with respect to the Cu(N)/Cab precursor. The metal surface areas thereby obtained were sufficient to allow reasonable rates of reaction, but were somewhat limited by incomplete dispersion of the metal salts during the catalyst preparation stage. The

dispersions of the nitrate-derived catalysts were found superior to those of the carbon-based catalysts, which is attributed to the difficulty in removing carbon from the catalyst surface without prior calcination. Calcination of the Cu(N)/Cab catalyst, however, resulted in a dramatic loss of metal surface area.

6.2 ASSESSMENT OF THE REACTION PROTOCOL

i) A slurry batch reactor was found suitable for nitrobenzene hydrogenation in the liquid phase. A modified Liebig condensor was sufficient to ensure a closed system. Catalyst activation could be conducted *in situ* immediately prior to the reaction. The progress of the reaction could be analysed quantitatively by GLC.

ii) After a series of tests, *n*-butyl benzene was chosen as the reaction medium.

iii) The apparatus allows control over different reaction variables.

iv) Conditions were determined whereby the reaction is not limited by diffusion processes.

v) The developed protocol was successfully used to assess the activity and selectivity of a series of copper catalysts, as well as nickel and platinum catalysts. This system could therefore be applied to evaluate the catalytic performance of different catalysts in the liquid phase hydrogenation of nitrobenzene.

6.3 NITROBENZENE HYDROGENATION

i) The reaction is zero order in nitrobenzene, and -0.3 with respect to aniline.

ii) The major determinant affecting catalyst activity is the available copper metal surface area, and it can be assumed with reference to the literature that the reaction is first order in dihydrogen. The reaction may therefore be expressed thus:-

$$\text{rate} = d[A]/dt = k\,[NB]^0\,[H_2]^1\,[Cu^0_{surf.}]^1\,[AN]^{-0.3}$$ where k is a rate coefficient

iii) The value of the activation energy of nitrobenzene hydrogenation over copper catalysts was found to be 57.1 ± 10.5 kJ mol^{-1}.

iv) The rate of aniline formation varies linearly with metal surface area, and the reaction was found to be structure insensitive.

v) The hydrogenation of nitrososbenzene, the prime intermediate of nitrobenzene hydrogenation, is not easily converted to aniline. A considerable negative carbon mass balance is observed during its reaction, as the dramatic disappearance of nitrosobenzene from solution is not accounted for by a minimal formation of aniline. Although it is observable in solution it was not detected during sampling of typical reactions, and it was concluded that the nitrosobenzene strongly adsorbs on the catalyst surface, thereby preventing the supply of dissociated hydrogen which is active in hydrogenation reactions.

vi) The use of an alcohol solvent during the hydrogenation of nitrobenzene results in a subsequent alkylation reaction between the reaction product aniline and the solvent. In this study the reaction between aniline and hexan-1-ol resulted in the formation of N-hexylenebenzenamine, which was then hydrogenated to N-hexylaniline.

6.4 FLUIDISED BED PRETREATMENT

i) An exotherm was observed during calcination of the Cu(A)/Cab catalyst as a fixed bed. The magnitude of this heat output was sufficient to raise the catalyst bed temperature by 86 °C, whilst the origin of the exotherm was confirmed by DSC as the combustion of copper acetate to copper oxide.

ii) The exotherm was not observed during calcination as a fluidised bed, which was attributed to the superior heat transfer of this system compared to a fixed bed.

iii) Particle size distributions obtained via TEM for the two different batches of CuO(A)/Cab revealed that the modal values were approximately 2 and 8 nm for samples calcined as fluidised and fixed beds respectively. Whilst both samples exhibited large particles up to 700 nm the proportion of crystallites measured at 50 nm or above was significantly higher for the fixed bed sample (18.0 % versus 13.3 %). Furthermore, the structure of the larger particles observed on the micrographs indicated that they were formed via the agglomeration of smaller

crystallites, which suggests the occurrence of sintering of the metal particles.

iv) Nitrous oxide decomposition experiments determined the metal surface areas of the CuO(A)/Cab Fixed^{50} and CuO(A)/Cab Fl.Bed^{500} samples to be 2.91 and 4.98 $m^2 g^{-1}$ respectively, and the metal surface areas of the catalysts were shown to be proportional to their catalytic activity towards nitrobenzene hydrogenation.

v) In conclusion, the heat and mass transfer properties of a fluidised bed facillitated the rapid dissispation of heat which was evolved during the calcination step, thereby allowing the oxidation of the metal salt to proceed gradually. The degree of sintering which the catalyst underwent during this stage of pretreatment is subsequently reduced, which ultimately results in improved metal dispersion. Catalyst calcination as a fluidised bed could therefore be used as a means of enhancing catalyst performance, *i.e.* activity and lifetime.

6.5 EVALUATION OF COPPER, NICKEL AND PLATINUM CATALYSTS

The catalytic performance of the platinum/silica and copper/silica, *i.e.* Cu(N)/Cab, catalysts at comparable reaction temperatures (148 and 144 °C respectively) is shown by Table and Figure 6.1. The results have been normalised as aniline formation per gram of catalyst, and per surface metal atom. This format has been repeated for a comparison of the nickel- and copper-based catalysts at 170 °C (Table and Figure 6.2), where the rates calculated for the nickel catalyst are derived from the linear region of the graph.

Table 6.1 Comparison of platinum/silica and copper/silica catalysts

	AN formation (mmols / g of catalyst)		AN formation (moles x10^{-22} / surface metal atom)	
Reaction time (mins)	Platinum/silica 148 °C	Copper/silica 144 °C	Platinum/silica 148 °C	Copper/silica 144 °C
0	0.00	0.00	0.00	0.00
4	1.55		0.75	
9	3.38		1.64	
14	5.66		2.75	
19	7.86		3.82	
25	10.67		5.18	
29	12.57		6.10	
34	14.92		7.24	
39	17.75		8.62	
43	18.93		9.19	
30		1.04		0.11
60		2.71		0.29
90		4.11		0.44
120		5.68		0.61
145		6.38		0.68
180		7.16		0.77

Figure 6.1 Comparison of platinum/silica and copper/silica catalysts

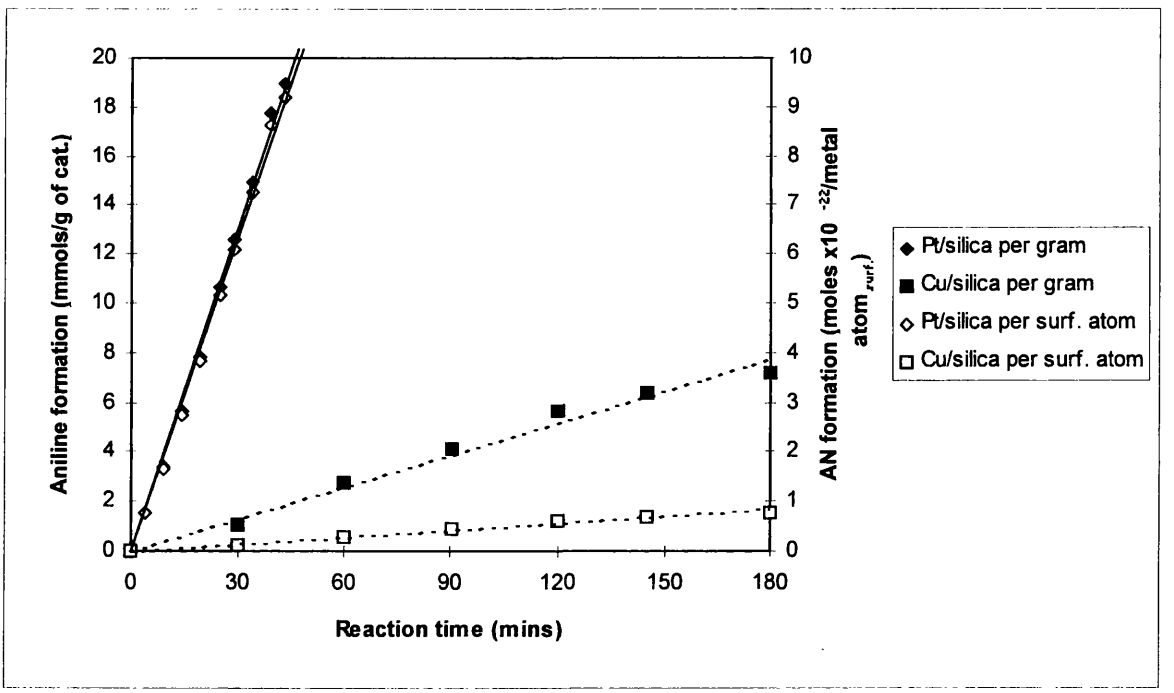

Table 6.2 Comparison of nickel/silica and copper/silica catalysts

	AN formation (mmols / g of catalyst)		AN formation (moles $x10^{-22}$ / surface metal atom)	
Reaction time (mins)	Nickel/silica 170 °C	Copper/silica 170 °C	Nickel/silica 170 °C	Copper/silica 170 °C
0	0.00	0.00	0.00	0.00
30	0.00		0.00	
60	5.06		0.09	
90	15.82		0.27	
120	34.18		0.58	
165	71.52		1.22	
210	124.68		2.13	
255	180.70		3.09	
300	212.66		3.64	
345	235.13		4.02	
30		1.74		0.19
60		3.69		0.40
90		5.34		0.57
120		7.76		0.83
150		9.70		1.04
180		12.33		1.32

Figure 6.2 Comparison of nickel/silica and copper/silica catalysts

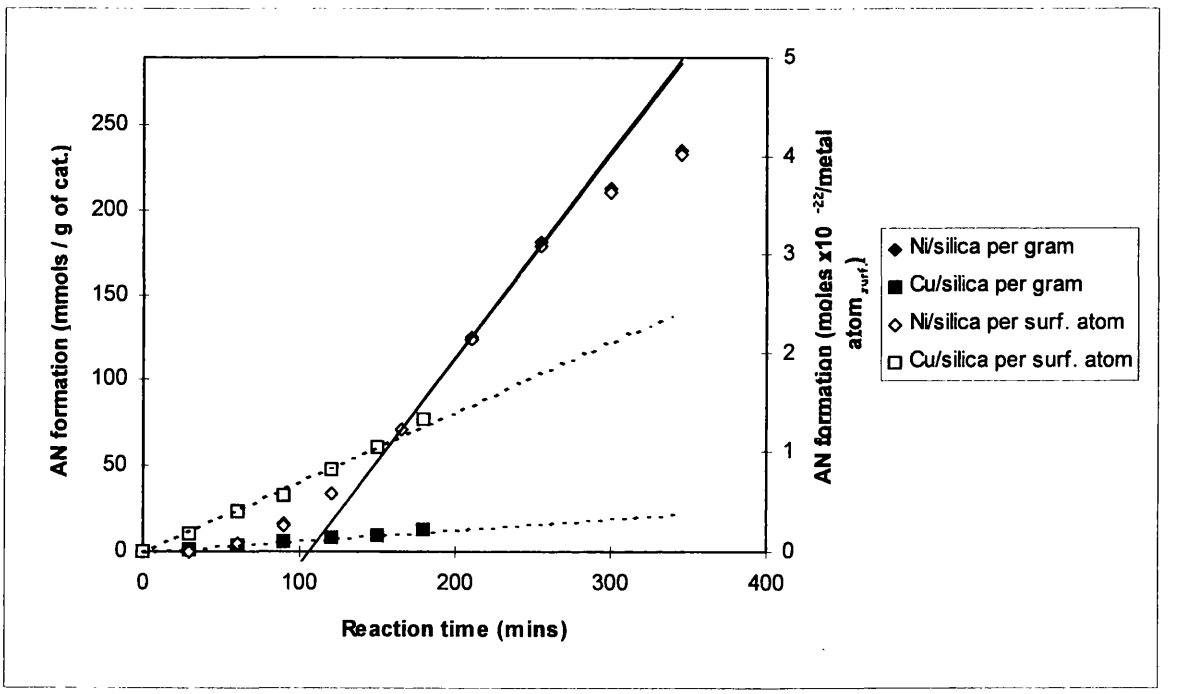

A summary of the catalysts, temperatures, rates and turnover frequencies is presented by Table 6.3.

Table 6.3 Summary of catalyst activities

	Pt/SiO_2 (148 °C)	Cu/SiO_2 (144 °C)	Cu/SiO_2 (170 °C)	Ni/SiO_2 (170 °C)
Metal loading (wt%)	1.14	8.59	8.59	55
No. of surface metal atoms per g ($x10^{19}$)	2.06	9.33	9.33	58.5
Rate of aniline formation (g of catalyst)$^{-1}$ (moles $x10^{-7}$ s^{-1})	73.0	7.04	9.03	166.1
Turnover frequency ($x10^{-3}$)	213.18	4.55	5.83	17.10

It is clear that the nickel/silica catalyst has the highest activity per gram, but it is noted that as the reaction conditions differ, it is not possible to obtain a quantitative comparison. Furthermore, as the metal loadings of the catalysts vary by such a degree, it is more appropriate to compare the turnover frequencies. In this way the activity of the platinum/silica catalyst is undoubtedly the highest, and the activity of one platinum atom is equivalent to roughly that of 47 copper atoms. Similarly, the activity of one nickel atom is equivalent to roughly 3 copper atoms. A qualitative order of reactivity may therefore be established as shown:-

$$Pt >> Ni > Cu$$

However, the reverse of this trend is observed when comparing the selectivities of the catalysts, although it is acknowledged that there is some arbitrariness in deciding where in the reaction profile to determine this parameter. Use of the platinum catalyst resulted in the sequential formation of N-cyclohexylaniline and N-dicyclohexylamine, following the consumption of the nitrobenzene (see Section 5.2.4). Use of the nickel catalyst resulted in the formation of three by-products, N-phenylmethylenebenzenamine, N-benzylaniline and N-phenyl-benzenebutanamine, which involved solvent impurities (see Section 5.3.6). The only by-product observed using the copper catalysts was N-phenylmethylenebenzenamine, which arose via an effect of the solvent. Consequently, a qualitative order of selectivity may be presented:-

$$Cu > Ni >> Pt$$

Given these relative orders of activity and selectivity of the catalysts examined using the reaction protocol developed in this study, how applicable are copper-based catalysts to the industrial environment?

- Firstly, the modest activity of the supported copper catalysts can be improved upon by recognising that the reaction is first order with respect to dihydrogen, and so the rate of aniline formation can be increased at elevated pressures. In fact, due to the large exotherm associated with this reaction (-550 kJ/mol), high catalytic activities mean that large quantities of heat have to be efficiently removed from the system, requiring

substantial engineering resource. Therefore, the modest catalytic activity associated with the copper catalysts can be managed by controlling dihydrogen pressure, thereby allowing the possibility of effective and manageable control over the rate of reaction and of the thermal output of the chemical system.

- Up to 100 % conversion, the copper catalysts demonstrate excellent selectivity to aniline formation (selectivity ~ 100 %). However, once the nitrobenzene is consumed within the batch reactor deactivation issues become apparent, and aniline is lost from the system. This problem can clearly be circumvented by conducting the reaction at fixed conversion, whereby the nitrobenzene is added continously at a comparable rate to that of its consumption. Under these conditions, and given a suitable solvent, the aniline product could be removed by distillation. Whilst this approach is applicable to any of the metal-based catalysts studied, the copper catalysts, with their associated reaction rate and excellent selectivity, would be more 'forgiving' to the occasional imbalances in the nitrobenzene and hydrogen feedstocks which inevitably occur in an industrial environment.

- One factor which disadvantages the copper-based catalysts is the process of catalyst activation. Whilst the nickel/silica catalyst can be activated in solution at 170 °C, temperatures of *ca.* 300 °C are necessary to fully reduce the copper catalysts. However, this work has demonstrated that the gas phase activation of copper catalysts, applied to

liquid phase hydrogenations, can be successfully implemented and it should be possible to reconfigure existing larger scale reactors to include this facility.

Overall, given some limitations, it is thought that the copper-based catalysts offer some significant advantages when applied to the large scale manufacture of aniline. Moreover, the reaction protocol presented in this work enables the efficiency of new copper catalysts preparations, that could be applied to a wide range of liquid phase hydrogenation reactions, to be evaluated.

6.6 FUTURE WORK

The dispersions of the copper/silica catalysts prepared in this study are somewhat modest, and the results of Section 5.3.5 show the linear relationship between catalyst activity and the available metal surface area. The activity of copper catalysts for nitrobenzene hydrogenation could therefore be increased by improving their metal surface areas, whilst maintaining their selectivity towards aniline. The use of catalyst promoters provides another route to optimise such catalysts, such as sulphur-containing molecules, as is currently employed for the gas phase hydrogenation of nitrobenzene [55]. In summary, whilst the potential of supported copper catalysts has been successfully demonstrated, it should not be considered as a definitive evaluation.

Finally, a second 120 g batch of copper/silica, comparable with the original Cu(N)/Cab catalyst, has been prepared, characterised and tested for nitrobenzene

hydrogenation. The results for the two batches were essentially identical, indicating that the preparation of this catalyst is reproducible. Catalyst evaluation of this precursor is currently underway at the laboratories of the industrial sponsor of this project.

References

1 J.W. Dobereiner, J.Chem.Phys., **38** (1823) 321

2 S.J. Gregg and K.S.W.Sing, 'Adsorption, Surface Area and Porosity', Academic Press, New York, 1967, references therein

3 C.N. Satterfield, 'Heterogeneous Catalysis in Industrial Practice', McGraw-Hill Inc., New York 1991 (a, p8), (b, p101), (c, p198), (d, p199), (e, p178)

4 B.C. Gates, 'Catalytic Chemistry', John Wiley & Sons, New York, 1992

5 Paul N. Rylander, 'Hydrogenation Methods', Academic Press, London, 1985, p1

6 G.A. Somorjai, 'Introduction to Surface Chemistry and Catalysis', Wiley-Interscience, New York, 1994, (a, p460), (b, p455), (c, 453), (d, Chap.2)

7 M.V. Twigg, 'Catalyst Handbook', 2nd Ed., Manson Publishing, London, 1996 (a, p23), (b, p314), (c, p172), (d, p455), (e, p83), (f, p326), (g, p464)

8 K. Klier, Adv.Catal., **31** (1982) 243

9 H.H. Kung, Catal.Rev.-Sci.Eng., **22** (1980) 235

10 G.C. Chinchen, P.J. Denny, J.R. Jennings, M.S. Spencer and K.C. Waugh, Appl.Catal., **36** (1988) 1

11 J. Jenck and J.E. Germain, J.Catal., **65** (1980) 141

12 R. Hubaut, J.P. Bonnelle and M. Daage, J.Mol.Catal., **55** (1989) 170

13 P. Rylander, 'Catalytic Hydrogenation over Platinum Metals', Academic Press, New York, 1967

14 J.A. Dean, 'Lange's Handbook of Chemistry', McGraw-Hill Book Co., New York 1973, Chapter 9

15 F. Haber, Z.Elektrochem, **22** (1898) 506

16 J. Wisniak and M. Klein, Ind.Eng.Chem.Prod.Res.Dev., **23** (1984) 44

17 F. l'Eplattenier, P. Matthys and F.Calderazzo, Inorg.Chem., **9** (1970) 342

18 J.N. Shah and R.N. Ram, J.Mol.Catal., **77** (1992) 235

19 D.R. Patel, M.K. Dalal and R.N. Ram, J.Mol.Catal., A: Chemical, **109** (1996) 141

20 F. Ragaini, Organometallics, **15** (1996) 3572

21 D.J. Collins, R.P. Schneider and M.C.Wolf, J.Mol.Catal., **62** (1990) 57

22 M. Arai, A. Obata and Y. Nishiyama, React.Kinet.Catal.Lett., **61**, No.2 (1997) 275

23 M.S. Hoogenraad, M.F. Onwezen, A.J.van Dillen, J.W.Geus, J.W. Hightower, W.N. Delgass, E. Iglesia and A.T. Bell (Eds), 11th International Congress on Catalysis - 40th Anniversary, Studies in Surface Science and Catalysis, Vol 101, 1996 Elsevier Science B.V.

24 J. Peureux, M. Torres, H. Mozzanega, A. Giroir-Fendler and J.A. Dalmon, Catalysis Today, **25** (1995) 409

25 M. Torres, J. Sanchez, J.A. Dalmon, B. Bernauer and J. Lieto, Ind.Eng.Chem.Res., **33** (1994) 2421

26 S.R. de Miguel, G. Torres, A.A. Castro and O.A. Scelza, React.Kinet.Catal.Lett., **51** (1993) 443

27 L.A. Petrov, N.V. Kirkov and D.M. Shopov, Kinet. Catal., **26**, No.4 (1985) 775

28 L. Petrov, K. Kumbilieva and N. Kirkov, Appl. Catal., **59** (1990) 31

29 L. Petrov, C.H. Vladov, A. Eliyas, N. Kirkov, K. Tenchev, CH. Bonev, D. Filkova and L. Prahov, J. Mol. Catal., **54** (1989) 237

30 D.N. Rihani, T.K. Narayanan and L.K. Doraiswamy, Ind.Eng.Chem., **4**, No.4 (1965) 403

31 X. Fang, S. Yao, Z. Qing and F. Li, Appl.Catal., A:General, **161** (1997) 129

32 F. Turek, R. Geike and R. Lange, Chem.Eng.Proc., **20**(4) (1986) 213

33 D.J. Collins, A.D. Smith and B.H. Davis, Ind.Eng.Chem.Prod.Res.Dev., **21** (1982) 279

34 J. Maestro, J. Aracil and M. Martinez, Afinidad, **43** (1986) 60

35 H.C. Yao and P.H. Emmett, J.Am.Chem.Soc., **84** (1962) 1086

36 S. Galvagno, A. Donato, G. Neri and R. Pietropaolo, J.Mol.Catal., **42** (1987) 379

37 C. Li, Y. Chen and W. Wang, Appl.Catal., A: General, **119** (1994) 185

38 M.C. Macias Perez, C. Salinas Martinez de Lecea and A. Linares Solano, Appl.Catal., A:General, **151** (1997) 461

39 G. Carturan, G. Facchin, G. Cocco, G. Navazio and G. Gubitosa, J.Catal., **82** (1983) 56

40 M.A. Aramendia, V. Borau, C. Jimenez, J.M. Marinas and J.A. Pajares, J.Catal., **78** (1982) 188

41 M.A. Aramendia, V. Borau, J. Gomez, C. Jimenez and J.M.Marinas, Appl.Catal., **10** (1984) 347

42 A. Metcalfe and M.W. Rowden, J.Catal., **22** (1971) 30

43 P.B. Kalautri and S.B. Chandalla, Ind.Eng.Chem.,Process Des. Dev., **21** (1982) 186

44 M.Mejstrikova, Collect.Czech.Chem.Commun., **39** (1974) 2740

45 H.C.Yao and P.H.Emmett, J.Am.Chem.Soc., **81** (1959) 4125

46 G.C. Torres, E.L. Jablonski, G.T. Baronetti, A.A. Castro, S.R. de Miguel, O.A. Scelza, M.D. Blanco, M.A. Pena jimenez and J.L.G. Fierro, Appl.Catal. A:General, **161** (1997) 213

47 N.J. Jebarathinam, M. Eswaramoorthy and V. Krishnasamy, React.Kinet.Catal.Lett., **58**, No.2 (1996) 291

48 N.J. Jebarathinam, M. Eswaramoorthy and V. Krishnasamy in 'Studies in Surface Science and Catalysis', T.S.R. Prasada and G. Murali Dhar (Eds.), Vol.113, 1998 Elevier Science, p1039

49 V. Krishnasamy and V.S. Balasubramanian, Indian Journal of Chemistry, **23A** (1984) 589

50 D.J. Collins, R.P. Schneider, M.C. Wolf and B.H. Davis, J.Mol.Catal., **62** (1990) 57

51 G.S. Samuelsen, V.L. Garik and G.B.L. Smith, J.Am.Chem.Soc., **72** (1950) 3872

52 R.S. Downing, P.J. Kunkeler and H. van Bekkum, Catalysis Today, **37** (1997) 121

53 R.G. Rice and E.J. Kohn, J.Am.Chem.Soc., **77** (1955) 4052

54 H. Beckhaus, E. Waldau and H. Witt, Ger. Offen. DE 3 611 677 (1987) to Bayer AG

55 K. Weissermel and H.-J. Arpe, 'Industrial Organic Chemistry', 3rd Ed., VCH, Weinheim 1997 p374-377

56 C.S. Rohrer, J.Phys.Chem., **56** (1952) 662

57 H. Keki, S. Iharada and C. Sliepcevich, Ind.Eng.Chem., **52** (1960) 137

58 T. Nagata, K. Watanabe, Y. Kono, A. Tamaki and T.Kobayashi, US Pat 5 283 365 (1994) to Mitsui Toatsu Chemicals

59 'Handbook of Heterogeneous Catalysis', G. Ertl, H. Knözinger, J. Weitkamp (Eds.), VCH, Weinheim, 1997, Vol. 3, (a, p1399), (b, p1405), (c, p1426), (d, p1436), (e, p1438), (f, p1427), (g, p1429), (h, p1433), (i, p1442)

60 M. Suvanto, J. Raty and T.A. Pakkanen, Appl.Catal., **181**, No.1 (1999) 189

61 M. Suvanto, T.A. Pakkanen and L. Backman, Appl.Catal., A:General, **177**, No.1 (1999) 25

62 S. Myllyoja and T.A. Pakkanen, J.Mol.Catal., A:Chemical, **136**, No.2 (1998) 153

63 H. Schonfelder, M. Kammerer and W. deLange, Studies in Surface Science, **122** (1999) 255

64 S.S. Zabrodsky, 'Hydrodynamics and Heat Transfer in Fluidised Beds', MIT Press, Massachusetts, 1966, p145

65 A. Chambers, S.D. Jackson, D. Stirling and G.Webb, J.Catal., **168** (1997) 301

66 D.R. Kennedy, Ph.D. Thesis, University of Glasgow, 1997

67 N. Young, Ph.D. Thesis, University of Glasgow, 1995

68 B.S. Furniss, A.J. Hannaford, P.W.G. Smith and A.R. Tatchell, 'Vogel's Textbook of Practical Organic Chemistry' (5th Ed.), Longman Scientific & Technical, Harlow (England), 1989

69 S.D. Jackson, J. Willis, G.D. McLellan, G. Webb, M.B.T. Keegan, R.B. Mayes, S. Simpson, P.B. Wells and R. Whyman, J. Catal., **139** (1993) 191

70 S.D. Robertson, B.D. McNicol, J.H. de Baas, S.C. Kloet and J.W.Jenkins, J.Catal., **37** (1975) 424

71 J.W. Jenkins, B.D. McNicol and S.D. Robertson, Chem.Tech., **7** (1977) 316

72 A. Jones, B.D. McNicol, 'Temperature-programmed Reduction for Solid Materials Characterisation', Marcel Dekker, New York, 1986

73 P.H. Emmett and N. Skau, J.Am.Chem.Soc., **65** (1943) 1029

74 J.H. Sinfelt, W.F. Taylor and D.J.C.Yates, J.Phys.Chem., **69** (1965) 95

75 G.E. Parris and K. Klier, J.Catal., **97** (1986) 374

76 J.A. Allen and J.W. Mitchell, Discuss.Faraday Soc., **8** (1950) 1815

77 B. Denise, R.P.A. Sneeden, B. Beguin and O. Cherifi, Appl.Catal., **30** (1987) 353

78 K.J. Soerensen and N.W. Cant, Catalysis Letters, **33** (1995) 117

79 G.C. Bond and S.N. Namijo, J.Catal., **118** (1989) 507

80 E. Giamello, B. Fubini, P. Lauro and A. Bossi, J.Catal., **87** (1984) 443

81 J.W. Evans, M.S. Wainwright, A.J. Bridgewater and D.J.Young, Appl.Catal., **7** (1983) 75

82 H. Berndt, V. Briehn and S.Evert, J.Mol.Catal., **73** (1992) 203

83 J.J.F. Scholten and J.A. Konvalinka, Trans.Faraday Soc., **65** (1965) 2465

84 G. Sengupta, D.K. Gupta, M.L. Kundu and S.P. Sens, J.Catal., **67** (1983) 223

85 T.J. Osinga, B.G. Linsen and W.P. van Beet, J.Catal., **7** (1967) 277

86 K. Narita, N. Takeyawa, H. Kobayashi and I. Toyoshima, React.Kinet.Catal.Lett., **19** (1982) 91

87 E. Giamello, B. Fubini, P. Lauro and A. Bossi, J.Catal., **18** (1970) 108

88 G.C. Chinchen, C.M. Hay, H.D. Vandervell and K.C. Waugh, J.Catal., **103** (1987) 79

89 D.B. Williams, C. Barry Carter, 'Transmission Electron Microscopy', Plenum Press, New York, 1996, Vol.1, p142

90 S.D. Jackson, F.J. Robertson and J. Willis, J. Mol. Catal., **63** (1990) 255

91 J.L. Lemaitre, P.G. Menon and F. Delannay (F.Del Ed.), 'Characterisation of Heterogeneous Catalysts', Chemical Industries/15, Marcel Dekker, New York (1984) p299-365

92 J.S. Smith, P.A. Thrower and M.A. Vannice, J.Catal., **56** (1979) 236

93 D.W. Grant, 'Gas-Liquid Chromatography', Van Nostrand Reinhold Company, London, 1971, (a, p96), (b, p123)

94 R.K. Iler, 'The Chemistry of Silica', Wiley-Interscience, New York, 1979, p47

95 G.C. Bond, S.N. Namijo and J.S. Wakeman, J. Mol. Catal., **64** (1991) 305

96 M.A. Kohler, H.E. Curry-Hyde, A.E. Hughes, B.A. Sexton and N.W. Cant, J. Catal., **108** (1987) 323

97 F.S. Delk II and A. Vavere, J.Catal., **85** (1984) 380

98 S.J. Gentry and P.T. Walsh, J.Chem.Soc.,Faraday Trans I, **78** (1982) 1515

99 H. Kobayashi, N. Takezawa, M. Shimokawabe and K. Takahashi in 'Preparation of Catalysts III', G. Poncelet, P. Grange and P.A. Jacobs (Eds.), Elsevier, Amsterdam, 1983, p697

100 M. Shimokawabe, N. Takezawa and H.Kobayashi, Appl.Catal., **2** (1982) 379

101 D.B. Clarke, I. Suzuki and A.T. Bell, J. Catal., **142** (1993) 27

102 M.A. Kohler, J.C. Lee, D.L. Trimm, N.W. Cant and M.S. Wainwright, Appl. Catal., **31** (1987) 309

103 R.A. Koeppel, J.T. Wehrli, M.S. Wainwright, D.L. Trimm and N.W.Cant, Appl.Catalysis A:General, **120** (1994) 163

104 B.G. Cox, 'Modern Liquid Phase Kinetics', Oxford Chemistry Primers Series, Oxford University Press, Oxford, 1994, p19

105 G. Mestroni, G. Zassinovich, C. Del Bianco and A. Camus, J.Mol.Catal., **18** (1983) 33

106 H. Greenfield, J.Org.Chem., **29** (1964) 3082

107 J.M. Devereux, K.R. Payne and E.R.A. Peeling, J.Chem.Soc., (1957) 2845

108 V. Vishwanathan and S. Narayanan, J.Chem.Soc., Chem.Commun., (1990) 78

109 G. Webb, Catalysis Today, **7** (1990) 139

110 A.K. Bhattcharyya and D.K. Nandi, Ind.Eng.Chem.Pro.Res.Dev., **14** (1975) 162

111 M. Sharma, J.R. Moniot, 'Isoquinoline Alkaloid Research', Plenum Press, New York, 1978

112 G.H. Posner, Angew.Chem., Int.Ed.Engl., **17** (1978) 847

113 R. Grigg, T.R.B. Mitchell, S. Sathixaigukit and N. Tongpengai, J.Chem.Soc., Chem.Commun., (1981) 611

114 Y. Watanabe, Y. Tsuji, H. Ige, Y. Ohsugi and T. Ohta, J.Org.Chem., **49** (1984) 3359

115 M. Onaka, K. Ishikawa and Y. Izunin, J.Inclusion Phenom., **2** (1984) 359

116 R.B.C. Pillai, J.Mol.Catal., **84** (1993) 125

117 A.G. Hill, J.H. Shipp and A.J. Hill, Ind.Eng.Chem., **43** (1951) 1579

118 L.K. Doraiswamy, G.R. Venkatakrishnan and S.P. Mukerjee, Chem.Eng., **88** (1981) 78

119 P.Y. Chen, M.C. Chen, H.Y. Chen, N.S. Chang and T.K.Chuang in Y.Murakami, A.Lizima and W.C.Ward (Eds.), Proc. 7th Int. Zeolite Conf., Tokyo, Elsevier, Amsterdam, 1986, p739

120 S. Narayanan and B.P. Prasad, J.Mol.Catal. A:Chemical, **96** (1995) 57

121 J.McMurry, 'Organic Chemistry', 3rd Ed., Brook/Cole Publishing Co., California, 1992, p725

122 R.W. Joyner and J. Pendry, J.Catal.Lett., **1** (1988) 1

123 C.H. Bartholomew, P.K. Agrawal and J.R. Katzer, Adv.Catal., **31** (1982) 135

124 S.D. Jackson, P. Leeming and J. Grenfell, J.Catal., **150** (1994) 170

125 S.D. Jackson, B.J. Brandreth and D. Winstanley, J.Catal., **129** (1991) 540

126 V.K. Shum, J.B. Butt and W.M.H. Sachtler, J.Catal., **96** (1985) 371

127 G.J. Hutchings, F. King, I.P. Okoye and C.H. Rochester, Appl.Catalysis A:General, **83** (1992) L7

128 G.J. Hutchings, F. King, I.P. Okoye, M.B. Padley and C.H. Rochester, J.Catal., **148** (1994) 453

129 V. Higgs and J. Pritchard, Appl.Catal., **25** (1986) 149

130 S. Tsutsumi and H. Ferada, J.Chem.Soc.Jap.Ind.Chem.Sect., **54** (1951) 527

131 G.C. Bond, 'Heterogeneous Catalysis: Principles & Applications', Clarendon Press, Oxford, 1974, (a, p82), (b, p49)

132 J.H. Espenson, 'Chemical Kinetics and Reaction Mechanisms', McGraw-Hill Book Company, New York, 1981, p5

133 Q. Chen, B.G. Frederick and N.V. Richardson, Surf.Sci., **436** (1999) 160

134 J.M. Meyers and A.J. Gellman, Surf.Sci., **337** (1995) 40

135 K. Kishi, K. Chinomi, Y. Inoue and S. Ikeda, J.Catal., **60** (1979) 228

136 H.S. Taylor, Adv.Catal., **1** (1948) 1

137 S. Galvagno, G. Capanneli, G. Neri, A. Donato and R. Pietropaolo, J.Mol.Catal., **64** (1991) 237

138 P. Gallezot, A. Giroir-Fendler, D. Richard, 'Heterogeneous Catalysis and Fine Chemicals', Elsevier Amsterdam, 1988, p171

139 P. Gallezot, D. Richard, P. Fouilloux, Proc. 9th Int.Cong.Catal., Calgary, 1074 (1988)

140 D.W. Blakely and G.A. Somorjai, J.Catal., **42** (1976) 181

141 C. Hoang-Van, Y. Kachaya, S.J. Teichner, Y. Arnaud and J.A.Dalmon, Appl.Catal., **46** (1989) 281

'There is one more thing. It's been emotional.'

Big Chris

Lock, Stock & Two Smoking Barrels (1998)